



HAL
open science

Dynamics and Photodynamics of Acetylacetone in para-Hydrogen matrices

Rolando Lozada-Garcia

► **To cite this version:**

Rolando Lozada-Garcia. Dynamics and Photodynamics of Acetylacetone in para-Hydrogen matrices. Other [cond-mat.other]. Université Paris Sud - Paris XI; Instituto superior de Tecnologias Y Ciencias Aplicadas de Cuba, 2012. English. NNT : 2012PA112380 . tel-00780495

HAL Id: tel-00780495

<https://theses.hal.science/tel-00780495>

Submitted on 24 Jan 2013

HAL is a multi-disciplinary open access archive for the deposit and dissemination of scientific research documents, whether they are published or not. The documents may come from teaching and research institutions in France or abroad, or from public or private research centers.

L'archive ouverte pluridisciplinaire **HAL**, est destinée au dépôt et à la diffusion de documents scientifiques de niveau recherche, publiés ou non, émanant des établissements d'enseignement et de recherche français ou étrangers, des laboratoires publics ou privés.

UNIVERSITE PARIS-SUD

ÉCOLE DOCTORALE : Ondes et Matière
Institut des Sciences Moléculaires d'Orsay

DISCIPLINE Physique

THÈSE DE DOCTORAT

soutenue le 12/12/2012

par

Rolando Rafael LOZADA GARCÍA

Dynamics and Photodynamics of Acetylacetone in
para-Hydrogen matrices

Directeur de thèse : Claudine CREPIN
Co-directeur de thèse : Germán Alfredo ROJAS LORENZO

Directeur de recherche au CNRS. (ISMO, UPS, France)
Full Professor. (InSTEC, Cuba)

Composition du jury :

Président du jury : Jean-Pierre GALAUP
Rapporteurs : Jesús RUBAYO SONEIRA
Robert KOŁOS
Examineurs : Pascal LARREGARAY
Oscar Edgar RODRIGUEZ HOYOS
Michèle CHEVALIER

Directeur de recherche au CNRS. (LAC, UPS, France)
Full Professor. (InSTEC, Cuba)
Professor. (IChF, Poland)
Chargé de recherche au CNRS. (ISM, UB, France)
Full Professor. (InSTEC, Cuba)
Maître de conférences. (ISMO, UPS, France)

Abstract

Acetylacetone (AcAc) exists as a mixture of enol and keto tautomers. Besides providing a good example for the study of tautomerization, it is a model system for investigating intramolecular hydrogen bonds in its enol form. Trapping AcAc in the soft para-Hydrogen (pH₂) environment brings out new opportunities to investigate its properties. Infrared spectra of the samples give a good characterization of the two stable enol and keto tautomers. The keto/enol ratio in solid pH₂ is found to be higher than in other matrices. While vibrational bands of keto are narrow, those of enol are broad, reflecting the intrinsic properties of the enol which exhibits three entangled large amplitude motions (two methyl torsions and the intramolecular hydrogen transfer). Surprisingly, narrowing of some of these bands is observed in a slow time evolution. This effect is interpreted as a consequence of nuclear spin conversion in the hydrogen atoms of the methyl groups, giving access to AcAc species differing by their nuclear spin symmetry. This offers new pertinent investigations on the large amplitude motions, especially on the intramolecular hydrogen transfer. AcAc/pH₂ samples have been irradiated by UV laser beams. Irradiation at 266 nm induces isomerization from the stable chelated enol form to non chelated conformers, similarly to the case of other matrices. A clear IR signature of the conformers is obtained thanks to the pH₂ host. Irradiation at 248 nm induces the enol/keto tautomerization. The kinetics of this interconversion highlights a non-direct process. Fragmentation is clearly observed under irradiation at 193 nm, followed by chemical reaction with the hydrogen host.

Keywords: acetylacetone, solid parahydrogen, matrix isolation, infrared spectroscopy, large amplitude motion, isomerization, photochemistry in matrices.

Résumé

L'acétylacétone (AcAc) existe sous deux formes tautomères énol et kéto. Sous sa forme énol chélaté, c'est une des molécules les plus simples présentant une liaison hydrogène intramoléculaire. Nous l'avons isolée dans la matrice « quantique » de parahydrogène (pH_2) pour étudier ses propriétés en bénéficiant des avantages spécifiques de ce solide cryogénique. Les spectres infrarouges apportent une caractérisation claire des formes énol et kéto. Le rapport kéto/énol est plus important en matrice de pH_2 que dans les autres matrices. Les bandes du kéto sont fines alors que certaines bandes de l'énol sont très larges à cause de la présence de la liaison hydrogène. Plusieurs bandes s'affinent très lentement avec le temps. Cet effet surprenant a été interprété en terme de conversion nucléaire de spin dans un groupement méthyle d'AcAc, donnant accès aux spectres de niveaux de torsion différents. Les résultats offrent alors un nouveau moyen d'investigation des mouvements de grande amplitude de la molécule (mouvements couplés de torsion des méthyles et du transfert d'hydrogène interne). La photolyse UV des matrices AcAc/ pH_2 a été étudiée. Une irradiation à 266 nm conduit à l'isomérisation de l'énol sous différentes formes non chélatées ; des spectres très bien résolus de ces formes sont obtenus grâce aux propriétés du pH_2 solide. En irradiant à 248 nm, on observe la tautomérisation vers la forme kéto, l'étude cinétique démontrant que le processus n'est pas direct à partir de l'énol chélaté. Enfin, une irradiation à 193 nm provoque la fragmentation de la molécule, processus qui peut être suivi de réactions avec l'hydrogène de la matrice.

Mots-clés : acétylacétone, parahydrogène solide, isolation en matrice, spectroscopie infrarouge, mouvements de grande amplitude, isomérisation, photochimie en matrice.

Acknowledgements

I would like to acknowledge to all people that make possible this work. In a first place to my family, my parents, my grandparents especially my grandmother. I would like to especially thanks to Norka Camacho Pérez who was next to me these long four years supporting many hours of studies and distance. To my friends Ernesto Quintas Sánchez and Acel Garcia Ríos for been always available to my calls. My acknowledgements to Jesus Rubayo Soneira the head of our group and the people of my department in Cuba for covering my teaching time and supporting me all these years. I want to thanks to my supervisors Mme. Claudine Crepin and German Alfredo Rojas Lorenzo for believe in me in the first place and bring me the opportunity of this investigation. Thanks to Justinas Ceponkus from Vilnius University for been my teacher not only in experimental science but in English language. I want to thanks all people from ISMO in Paris, especially Michèle Chevalier, Wutharath Chin and Raphael Thon who, jointly to Claudine and Jean-Pierre Galaup from LAC, were my family in France. The technical service of ISMO who attended very quickly to our call for repairing or building things necessary for making the experiments. I would like to acknowledge to the institutions who bring the financial support for this work: The embassy of France in Cuba, the University of Paris SUD XI, EGIDE, and ANR Gouttelium.

Contents

Abstract	i
Résumé	iii
Acknowledgements	v
List of Figures	xiii
List of Tables	xvii
Glossary	xix
Introduction	1
1 Molecule of Acetylacetone	7
1.1 Acetylacetone	7
1.1.1 General physicochemical properties	7
1.1.2 β -diketones compounds	8
1.1.3 Main Characteristics of Acetylacetone related to this study	8
1.2 Acetylacetone enol/keto tautomers	9
1.3 Enol forms of AcAc	11
1.3.1 Hydrogen bonds and proton transfer	11
1.3.2 Chelated enol form of AcAc	12
1.3.3 Non Chelated enols	14
1.4 Photochemistry of AcAc	15

CONTENTS

2	Experimental Techniques	19
2.1	Infrared radiation	19
2.1.1	Historical overview	19
2.1.2	Infrared spectroscopy Theory	21
2.1.2.1	Pure rotation spectra	23
2.1.2.2	Pure vibrational spectra	26
2.1.2.3	Polyatomic molecules	28
2.1.2.4	Vibration-rotation spectra	29
2.1.2.5	The intensities of spectral bands	30
2.1.2.6	Line width	31
2.1.3	Infrared interferometers:	
	The Fourier-transform spectroscopy	33
2.1.4	Application of Infrared spectroscopy	37
2.2	Low temperature spectroscopy	38
2.2.1	Advantages of low temperature spectroscopy	38
2.2.2	Matrix isolation technique	39
2.2.3	Molecular hydrogen matrices	42
3	Experimental SetUp.	47
3.1	Chemical products	47
3.2	The para-hydrogen conversion.	48
3.3	Matrix deposition.	51
3.4	IR absorption spectroscopic technique.	53
3.5	UV sources for irradiation of the sample	54
4	Computational methods	55
4.1	General features	55
4.2	Hartree-Fock (HF) calculation	58
4.3	Density functional theory (DFT)	61
4.4	Basis sets	63
4.5	Harmonic/anharmonic vibrational frequencies	67

5	Acetylacetone Infrared spectra	69
5.1	Acetylacetone Infrared spectra	69
5.2	Chelated enol form	70
5.2.1	Bands assignments: comparison with simulated infrared spectra	71
5.2.2	Keto form	73
5.2.3	Keto/enol ratio	76
6	Coupling between spin states and torsional levels	79
6.1	Experimental evidence of NSC	79
6.2	Nuclear Spin Conversion (NSC)	83
6.2.1	Theoretical calculation	84
6.3	Bandwidths matrices dependent	89
6.3.1	Anharmonic calculations	91
6.4	summary	92
7	UV laser irradiation at 266 nm	93
7.1	General overview	93
7.2	Theoretical calculations	95
7.3	Spectroscopic analysis	95
7.3.1	Assignment of the First Group	95
7.3.2	Assignment of the second group	97
7.3.3	Combinations bands	101
7.4	Relaxation process	102
7.4.1	Kinetic study	102
7.4.2	Mechanism	106
7.5	Fragmentation	108
7.5.1	In pure solid parahydrogen	108
7.5.2	O ₂ doping	109
8	UV laser irradiation at 248 nm	111
8.1	Keto IR spectrum	111
8.2	Fragments	115
8.3	Kinetics	116

CONTENTS

9 UV laser irradiation at 193 nm	119
9.1 IR Spectra	119
9.2 Assigned products	121
9.2.1 “First” products	122
9.2.2 “Second” products	125
9.2.3 Formation of C ₂ H ₂ , C ₂ H ₄ , C ₂ H ₆ and C ₃	129
9.2.4 HCO radical and Formaldehyde	133
9.3 Unassigned bands	135
9.4 Summary	138
Conclusions	141
References	145
A Isomerization Kinetics	151
A.1 Approximations	152
A.2 Homogeneous problem:	153
A.3 Solution of inhomogeneous equation	154
A.4 First and second derivate	156
A.5 Evaluation in (t=0)	159
A.6 Values of the constants rates	159
A.6.1 Calculation of relatively absorbance factors	160
B Tables of Theoretical frequencies of AcAc isomers	163
B.1 CCC	164
B.2 Keto	165
B.3 CCT	166
B.4 CTC	167
B.5 CTT	168
B.6 TCC	169
B.7 TCT	170
B.8 TTC	171
B.9 TTT	172

C IR spectra of AcAc in pH₂ matrix under UV 193nm irradiation	173
700-1100 cm ⁻¹	174
1000-1300 cm ⁻¹	175
1250-1350 cm ⁻¹	176
1330-1410 cm ⁻¹	177
1410-1540 cm ⁻¹	178
1520-1800 cm ⁻¹	179
1750-2150 cm ⁻¹	180
2110-2160 cm ⁻¹	181
2190-2800 cm ⁻¹	182
2790-3000 cm ⁻¹	183
3000-3100 cm ⁻¹	184
3080-3600 cm ⁻¹	185
3550-4000 cm ⁻¹	186
I Resumen en Español	187
Introducción	187
I.1 Dispositivo experimental	191
I.2 Espectro infrarrojo del AcAc	191
I.3 Irradiación Ultra violeta	194
I.3.1 Irradiación con una longitud de onda de 266nm	194
I.3.2 Irradiación con una longitud de onda de 248nm	197
I.3.3 Irradiación con una longitud de onda de 193nm	199
Conclusiones	202
II Résumé en Français	207
Introduction	207
II.1 Dispositif expérimental	210
II.2 Spectroscopie infrarouge de l'acétylacétone	211
II.3 Irradiation dans l'ultra-violet	214
II.3.1 Irradiation avec une longueur d'onde de 266nm	214
II.3.2 Irradiation avec une longueur d'onde de 248 nm	217
II.3.3 Irradiation avec une longueur d'onde de 193 nm	219
Conclusions	221

CONTENTS

List of Figures

1.1	Schema of Ketone and β -diketone species	8
1.2	The enol and keto stable forms of Acetylacetone	9
1.3	Resonance-assisted hydrogen bonding in β -diketones enolates	11
1.4	Structure and dynamics in enolic acetylacetone.	14
1.5	Eight possible isomers of enol AcAc.	15
1.6	Schematic diagram of the most possible pathways upon photoexcitation of AcAc in the UV regions.	17
2.1	The components of a typical absorption experiment	33
2.2	Michelson interferometer	34
2.3	An interference record $F(x)$	35
2.4	The electronic charge density of the hydrogen molecule.	43
2.5	The molecular rotational energy levels for an isolated H_2 molecule.	44
2.6	Equilibrium ortho-para of hydrogen as a function of temperature.	46
3.1	Schematics representation of the converter system.	48
3.2	Fundamental bands of Hydrogen matrices.	49
3.3	Simplified scheme of the cryostat used for matrix deposition.	52
3.4	Drawing of the real experimental setup.	52
5.1	IR spectra of acetylacetone isolated in different matrices.	70
5.2	Selected regions of the infrared spectra of acetylacetone isolated in different matrices.	71
5.3	IR spectra of AcAc: Experimental compared with simulated C_{2v} and C_s symmetries.	72
5.4	IR spectra of AcAc: Experimental compared with simulated harmonic and anharmonic approach.	72
5.5	IR spectra of AcAc: Experimental compared with simulated keto.	75

LIST OF FIGURES

6.1	Selected regions of the spectrum of AcAc in different matrices.	80
6.2	Time evolution of the spectra of AcAc in pH ₂ when the sample is kept in dark.	81
6.3	Spectra of the “ms” and “ls” species of AcAc.	82
6.4	Time evolution of the “ms” and “ls” species of AcAc.	82
6.5	Calculated structures and energies of AcAc conformers.	84
6.6	Section of the threefold PES of m _{CO} rotation.	86
6.7	Dispersion the ratio between experimental calculated frequencies.	91
7.1	IR spectra of AcAc isolated in pH ₂ matrix at different UV irradiation times.	94
7.2	Irradiated AcAc in different matrices.	95
7.3	IR spectra of the first group of isomers.	96
7.4	IR spectra of the second group of isomers.	98
7.5	Second group bands in different matrices.	100
7.6	Comparison between experimental an theoretical IR spectrum of the second group. . .	101
7.7	Time evolution of isomers.	103
7.8	Simplified kinetics’ diagram of isomerization processes.	105
7.9	IR spectra in selected regions after strong and prolonged irradiation at 266 nm.	109
8.1	IR spectra of AcAc before and after UV irradiation at 248 nm	112
8.2	Comparison of IR spectra of irradiated AcAc in pH ₂ with 266 nm and 248 nm	113
8.3	Spectra of several hours irradiated AcAc in different matrices compared with simulated spectra.	114
8.4	UV irradiation kinetics of AcAc irradiated with 248 nm in pH ₂ matrix	117
8.5	Time evolution under UV 248 nm laser irradiation of AcAc in pH ₂ matrix.	118
9.1	Several infrared spectra of irradiated (193 nm) AcAc in pH ₂ matrix	121
9.2	Bands assigned to propyne after UV (193nm) laser irradiation of AcAc in pH ₂	122
9.3	Water bands and pH ₂ absorption induced by close water molecule.	128
9.4	IR spectra of C ₃ clusters in pH ₂ solid	132
9.5	IR spectra and time evolution of HCO radical in pH ₂	133
9.6	IR spectra and time evolution of HCCO radical in pH ₂	135
9.7	IR spectra and time evolution of fist group of unassigned bands	136
9.8	IR spectra and time evolution of first subgroup of growing unassigned bands	137
9.9	IR spectra and time evolution of second subgroup of growing unassigned bands	138
A.1	Time evolution of the normalized intensities of the four enol isomers of AcAc	153

A.2	Time evolution of the integrated absorbance A_{bi} of isomers.	157
A.3	Plots for obtaining the n_i and m_i coefficients	159
A.4	Plots for obtaining the relative absorbance coefficients	160
I.1	<i>Formas enólica y cetónica de la AcAc</i>	188
I.2	Espectros de AcAc en diferentes matrices	192
I.3	Evolución temporal del espectro de AcAc en pH_2	193
I.4	Espectros tomados durante el proceso de irradiación del AcAc en matrices de pH_2	195
I.5	<i>Comparación de espectros del AcAc aislada en diferentes matrices después de la irradiación con laser a 266nm. (a) pH_2, (b) nH_2, (c) nD_2 y (d) Ne. Las bandas asignadas al isómero TCT están marcadas con un (+).</i>	196
I.6	<i>Diagrama de reacción de la AcAc aislada en pH_2 bajo la acción de un laser UV a 266nm. K_{ij} son las constantes de reacción. Las energías están dadas en kJ/mol</i>	197
I.7	<i>Comparación de espectros IR luego de la irradiación de la AcAc aislada en matrices de pH_2 (a) Luego de algunos minutos (~ 40 min) usando una longitud de onda de 266 nm; (b) Luego de algo minutos (~ 10 min) usando una longitud de onda de 248 nm y (c) luego de algunas horas (~ 6 heure) usando una longitud de onda de 248 nm. La contribución de la forma CCC se han sustraídos en todos los espectros para facilitar la comparación. Las posiciones de las bandas de la forma cetónica de la AcAc están marcadas con líneas de puntos verticales. El símbolo (+) designa a las bandas que se encuentran el el primer grupo de isómeros y el símbolo (*) designa las bandas del segundo grupo de isómeros</i>	198
I.8	<i>Espectros infrarojos de la molécula de AcAc aislada en matrices de pH_2 luego de un largo período de irradiación con una longitud de onda de 193 nm. Algunas de las moléculas encontradas después de la irradiación se representan con su imagen sobre las posiciones de sus bandas más intensas.</i>	201
II.1	<i>Formes énol et cétone de AcAc.</i>	208
II.2	Spectres de AcAc dans différentes matrices	212
II.3	Evolution temporelle du spectre de AcAc isolée dans pH_2	212
II.4	Spectres IR de AcAc pris à différents temps d'irradiation laser à 266 nm	214
II.5	<i>Comparaison des spectres de AcAc isolée dans différentes matrices après irradiation avec un laser à 266nm. (a) pH_2, (b) nH_2, (c) et nD_2 (d) Ne. Les bandes attribuées à l'isomère TCT sont marquées d'un (+)</i>	215
II.6	<i>Diagramme cinétique simplifié du processus d'isomérisation. ΔH [kJ/mol] représente la différence entre l'énergie calculée d'un isomère et la forme CCC de AcAc, en utilisant une méthode DFT(B3LYP/6-311++G(3df, 3pd)). Les valeurs estimées des constantes de vitesse de k_{ij} [min^{-1}] sont données pour nos conditions expérimentales (intensité laser constante à 10 Hz, quelques mJ/impulsion).</i>	216

LIST OF FIGURES

- II.7 *Comparaison des spectres IR après irradiation de AcAc dans pH_2 (a) après quelques minutes (~ 40 min) à 266nm; (b) après quelques minutes (~ 10 min) à 248nm et (c) après quelques heures (~ 6 heure) à 248 nm. La contribution de la forme CCC a été soustraite dans tous les spectres pour faciliter la comparaison. Les positions des bandes de la forme cétone sont repérées par des lignes pointillées verticales. (+) Désigne le premier groupe d'isomères et (*) désigne le second groupe d'isomères. . . . 217*
- II.8 *Spectre infrarouge de la molécule AcAc isolée dans une matrice pH_2 après une très longue période d'irradiation UV à 193 nm. Certaines molécules obtenues par irradiation sont représentées sur la position de leurs bandes les plus intenses. Les (?) sont les bandes encore non attribuées 220*

List of Tables

1.1	Physical-chemical properties of Acetylacetone molecule.	7
1.2	Percentage of the chelated enol form for different solvents.	10
1.3	Selected structural parameters for Acetylacetone.	12
3.1	Windows characteristics	53
4.1	Density Functionals	64
5.1	Experimental and theoretical frequencies of the chelated enol form of AcAc.	74
5.2	Experimental and theoretical frequencies of the keto enol form of AcAc.	76
6.1	IR frequencies of the “ms” and “ls” species of AcAc.	88
6.2	Comparison between experimental and calculated frequencies and bandwidths of CCC.	90
7.1	Experimental vibrational frequencies of CTC in different matrices.	97
7.2	Experimental vibrational frequencies of the second group of isomers in different matrices.	99
7.3	Calculated values of the rate constants k_{ij}	105
8.1	Experimental and theoretical frequencies of the keto form of AcAc	115
9.1	Propyne	123
9.2	Carbon Monoxide	124
9.3	Radicals	125
9.4	Methane in $p\text{H}_2$	126
9.5	Methane isotopes in $n\text{D}_2$	127
9.6	Water	127
9.7	Acetylene	129
9.8	Ethylene	130
9.9	Carbon Clusters	131

LIST OF TABLES

9.10	Ethane	132
9.11	Formaldehyde	134
9.12	Unassigned bands	138
A.1	Integrated absorbance of each isomer detected in the infrared spectra	156
A.2	Values of the parameters of equations A.15	157
A.3	Values of the parameters of equations A.16 and A.17	158
A.4	Values of the parameter of equations A.24	161
B.1	Theoretical IR frequencies of CCC form	164
B.2	Theoretical IR frequencies of Keto form	165
B.3	Theoretical IR frequencies of CCT form	166
B.4	Theoretical IR frequencies of CTC form	167
B.5	Theoretical IR frequencies of CTT form	168
B.6	Theoretical IR frequencies of TCC form	169
B.7	Theoretical IR frequencies of TCT form	170
B.8	Theoretical IR frequencies of TTC form	171
B.9	Theoretical IR frequencies of TTT form	172

Glossary

- ls** less stable. 80, 81, 83, 86–88, 143
- ms** most stable. 80, 81, 83, 86–89, 143
- AcAc** Acetylacetone. i, xix, xx, 2–5, 7–11, 13–17, 47, 69–73, 75–77, 79–81, 83, 85, 87, 89–96, 101–103, 106–113, 115, 117–120, 122, 124–126, 129, 130, 132–134, 139, 141–143, 145, 146, 152
- AO** atomic orbitals. 64
- CASSCF** Complete active space self-consistent field. 16
- CCC** Refers to the chelated enol form of AcAc. It is the most stable isomer of AcAc. The three letters in the name XYZ means *Cis* or *Trans* configuration of the bonds in the central ring of AcAc molecule. 93, 94, 102–109, 120, 141, 145, 146, 152
- CTC** Refers to isomer of AcAc in which the C=C bond of the central ring of AcAc is in *Trans* configuration.. 95–97, 101–107, 141, 145, 146, 149, 152
- CTT** Refers to isomer of AcAc in which both C=C and C-O bonds of the central ring of AcAc are in *Trans* configuration.. 95, 96, 101
- DFT** Density Functional Theory. 16, 55, 57, 61–63, 67, 89, 92, 95, 111, 113
- FC** Frank-Condon. 16
- FIR** far-infrared. 20, 21
- FT** Fourier transform. 33, 34, 36, 37
- FT-IR** Fourier transform infrared. 19, 37, 38
- FTS** Fourier transform spectroscopy. 34, 36, 37
- FWHM** full width measured at half high. 37, 40, 42
- GTO** Gaussian-type orbitals. 64, 65
- H₂** hydrogen molecule. 2, 3, 5, 43, 45, 142, 143
- H_{int}** intramolecular hydrogen. 2, 13, 14, 83–85, 87, 89, 91, 92, 141–143
- HB** hydrogen bond. 1, 2, 8, 9, 11–14, 16
- hcp** hexagonal close packed. 44
- HF** Hartree-Fock. 55, 57–64
- IR** infrared. 2, 4, 20, 21, 37–40, 49, 141, 143
- LCAO** linear combination of atomic orbitals. 58
- LDA** local density approximation. 63
- LSDA** local spin density approximation. 63
- m_{CO}** Refers to the methyl group in the C=O side of AcAc. 84–87, 92
- m_{OH}** Refers to the methyl group in the C-O-H side of AcAc. 84–86, 88
- MIR** middle-infrared. 20, 21
- MIS** Matrix Isolation Spectroscopy. 1, 2, 19
- MO** Molecular Orbital. 16, 58, 62, 120
- nD₂** normal-Deuterium. 4, 47, 52, 69, 70, 73, 74, 76, 77, 93, 94, 98, 100, 101, 111–113, 122, 125–127, 130, 131, 133, 141, 142
- Ne** Neon. 47, 52, 53, 69, 70, 73, 74, 76, 77, 93, 94, 98, 100–102, 107–111
- nH₂** normal-Hydrogen. 4, 47, 49, 50, 52, 69, 70, 73, 74, 76, 77, 82, 83, 89, 90, 93, 94, 97–101, 111, 141, 143
- NIR** near-infrared. 20, 21
- NSC** nuclear spin conversion. 81–83, 89, 92, 143
- oH₂** ortho-Hydrogen. 3, 4, 43–45, 50, 81–83, 89, 128
- PES** potential energy surface. 14, 60, 88, 95, 120

Glossary

- pH₂** para-Hydrogen. i, 1–5, 19, 42–47, 49–53, 69–77, 79–83, 89, 91–102, 106–114, 116, 117, 119, 120, 122–136, 138, 141–143
- pH₂O** Refers to the water molecule with both hydrogen atoms in antiparallel spin configuration. 127, 128
- R_{ke}** keto/enol ratio. 69, 76, 77, 141
- RMS** root-mean-square. 45
- SCF** self-consistent field. 58, 65
- STO** Slater-type orbitals. 64, 65
- TCC** Refers to isomer of AcAc in which the C-C bond of the central ring of AcAc is in Trans configuration.. 98, 100–105, 107, 141, 145, 146, 149
- TCT** Refers to isomer of AcAc in which both C-C and C-O bonds of the central ring of AcAc are in Trans configuration.. 100, 101, 141
- TTC** Refers to isomer of AcAc in which both C-C and C=C bonds of the central ring of AcAc are in Trans configuration.. 98, 100–105, 107, 141, 145, 146, 149
- ZPM** zero point motion. 44

Introduction

Investigation of molecular dynamics and photodynamics gives access to the key points of elementary steps in very important molecular processes such as energy transfers or chemical reactivity. Photochemistry, a peculiar case of photodynamics, consists in the study of chemical reactions that occur only when a molecule reaches the necessary "activation energy" by means of photons. Absorption of photons by a reactant molecule may also change the symmetry of the molecule's electronic configuration, enabling an otherwise inaccessible reaction path. If a laser excitation is used, it is possible to selectively excite a molecule to a desired electronic and vibrational state. Equally, the emission from a particular state may be selectively monitored, providing a measure of the population of that state. If the chemical system is in gas phase at low pressure, this enables to observe the energy distribution of the products before the differences in energy have been smeared out and averaged by repeated collisions. On the other hand, the photo-products flow away then do not stay in the interaction zone. In consequence, recombinations are not possible and secondary reactions are very improbable. Moreover, reactants and products in the observation zone are in a limited amount, giving very weak signals in the case of inefficient processes. Then, it is interesting to use cryogenics matrix environments to have higher concentrations of molecules of interest and the possibility to investigate various processes during long time.

Matrix Isolation Spectroscopy (MIS) technique is a well-known tool to investigate the molecular properties such as geometry and reactivity of trapped species, especially in the case of unstable species or reactive intermediates. MIS technique has been used since 1954 for trapping reactive molecules in a frozen inert media.¹ Many molecules such as CO, CO₂, N₂, H₂, O₂, Cl₂, CCl₄ as well as noble gas have been used as hosts in which a small guest molecule is isolated for further spectroscopic studies. The use of H₂ as a matrix host brings new advantages due to the "quantum" properties of the solid, particularly with para-Hydrogen (pH₂) solids. Guest-host interactions are very weak and species embedded in such solids keep molecular characteristics close to those of the gas phase. In order to benefit from these specific properties, photochemical studies in pH₂ solid with molecules and complexes involving hydrogen bonds (HBs) were performed.

INTRODUCTION

HBs are molecular interactions weak in their strength but very important in their chemical impact on reactivity. It is expected that HBs would not be too much disturbed in $p\text{H}_2$ host. Dynamics and especially photodynamics of HB species in $p\text{H}_2$ solid will thus give pertinent insights on wide molecular problems such as the relation between solvation and chemical reactivity, at the molecular scale.

This work is devoted to the study of a small organic molecule showing an internal HB: Acetylacetone (AcAc). AcAc is a β -Diketone which belongs to the well-known class of tautomeric compounds that are widely used in organic and inorganic chemistry. Over the years the structure of both keto and enol forms, and the nature of the strong intramolecular hydrogen (H_{int}) bond $\text{O}-\text{H}\cdots\text{O}$ in the enol form of AcAc were subject of intensive studies using a large variety of different methods, including IR, Raman, microwave, and NMR spectroscopies, X-ray and neutron diffraction measurements, quantum-chemical calculations, and some other techniques.²⁻¹⁰

An increased interest in compounds with the short (strong) hydrogen bonds including chelated enol forms of β -diketones is related to the study of transfer of a proton from one oxygen atom to another along the hydrogen bond. This phenomena is one of the most important and general reactions in chemistry. Proton transfer plays a crucial role in many processes such as acid-base neutralization reactions, electrophilic addition, and many others.¹¹ It has also a great importance in catalysis and in several biochemical processes, ranging from enzymatic reactions to tautomeric interconversion in DNA bases.¹² AcAc is one of the simplest β -diketones which presents intramolecular proton transfer between two oxygen atoms,² so it is a good prototype to study this phenomena.¹³

Special attention has been paid to the structural characteristics of AcAc tautomers and tautomerization process itself between two forms observed in nature: the enol and the keto forms. The keto/enol equilibrium of AcAc in different media has been subject of study for many years resulting that the keto/enol ratio is really depending of the characteristics and conditions of the surrounding media.¹⁴⁻¹⁷ It is generally accepted that at moderate temperatures the enol form predominates in both gas and liquid phases.¹⁷⁻¹⁹

Processes taking place in the AcAc under UV light irradiation such as isomerization, tautomerization and fragmentation have also been studied from both experimental and theoretical works.^{2,20,21} Gas phase irradiation leads to a fragmentation of the molecules giving as primary product the OH radical.²⁰ When the AcAc molecule is trapped in the low temperature inert solids as Ne, Ar, Kr and N_2 open enol isomers are found as a result of irradiation.^{2,22,23}

Infrared (IR) spectroscopy is very convenient when using MIS technique. Due to the very low temperature ($< 70\text{ K}$) only the lowest vibrational and rotational levels are populated in most of the cases. In a matrix isolated media, controlled chemical reaction can also take place.²⁴⁻²⁶

The Hydrogen matrices and specifically the $p\text{H}_2$ are an interesting media to use in the MIS technique.²⁷ Because of the symmetry requirement of the total wavefunction of hydrogen molecule (H_2),

there are two possibilities for hydrogen molecules in nature.²⁸ H_2 having the total molecular spin $I=0$ are called pH_2 and have a rotational quantum number J even, and those having $I=1$ are called ortho-Hydrogen (oH_2) and have an odd J . At room temperatures, the equilibrium population ratio between oH_2 and pH_2 is 3:1. The interconversion between the $I=0$ and $I=1$ nuclear spin states for isolated H_2 molecule is forbidden. Due to the very large splittings of the rotational levels (354.38 cm^{-1} for $J=0 \rightarrow J=2$ and 587.06 cm^{-1} for $J=1 \rightarrow J=3$), at low temperatures ($\leq 20 \text{ K}$), only the $J=0$ and $J=1$ levels are thermally populated. A $J=1$ molecule will remain metastably in that level, as conversion to the $J=0$ level is very slow in absence of external magnetic field.^{28,29}

Since rotational wavefunction of H_2 at $J=0$ state has a completely spherical character, pH_2 molecule in this state has no permanent electric moments of any order. Thus, the crystal of pH_2 ($T = 6\text{K}$) provides a homogeneous environment for a guest molecule embedded therein. The large zero point lattice vibration, almost 20% of lattice constant (3.78\AA) make of pH_2 solid a very soft crystal. Then, the softness of pH_2 crystal makes the imperfection of the crystal structure around the dopant molecules very small.³⁰

By virtue of the above very special features of solid pH_2 , infrared spectra of small molecules trapped in this solid show surprisingly sharp linewidths associated with well quantized, rotation-vibration states.^{11,31-33} In addition pH_2 solid is useful for the study of chemical reactions at cryogenic temperature, as mentioned previously; the cage effect is minimized and, for example, the primary products of a chemical reaction are expected to be closer to those of the gas phase reaction than in other matrices. It is advantageous for studying photochemical reactions in condensed phase.^{30,34,35} In rare gas matrices, *in situ* photolysis is greatly influenced by the lattice of the matrix, because, in most of the cases, the photolyzed species may not escape from the trapping site due to the cage effect. In contrast, the photo-fragment in the solid pH_2 crystal can be separated more easily utilizing the excess energy of photo-dissociation because the cage effect is weaker. The recombination *in-situ* of photofragments is not favored. It allows a secondary reaction of photo-fragment which could occur during or after the photolysis. In all cases, a spectral measurement can be done after the photolysis for a long period of time, which is favorable for observation of slow reaction after photolysis, and for detection of weak amount of photoproducts.³⁰

The present work studies the photodynamic of AcAc molecule isolated in pH_2 matrices. The molecule is characterized by the infrared spectra recorded in the region of $700\text{-}5000 \text{ cm}^{-1}$. Bands assigned to the chelated enol form as well as the keto form of AcAc can be found in the spectra. The photochemistry of these molecules is studied by using three different UV lasers, fourth harmonic of Nd:YAG laser providing 266 nm radiation, excimer KrF laser at 248 nm and excimer ArF laser at 193 nm, probing excitation to different electronic states of the molecule.

INTRODUCTION

This thesis is organized as follows: introduction, nine chapters, conclusions and two appendixes. The Chapter “**Molecule of Acetylacetone**” has a detailed description of the Acetylacetone (AcAc) molecule. General chemical features of this molecule are presented followed by a discussion about its most interesting and contradictory properties.(1) The tautomerization processes linked with the keto/enol ratio and its dependence on the solvent properties.(2) The geometric parameters and their corresponding symmetry (C_{2v} or C_s). (3) The electronic excitation due to the $\pi \rightarrow \pi^*$ transition or Rydberg excitation leading to fragmentation in the gas phase or isomerization in a matrix. The chapter “**Experimental Techniques**” has an extensive historical introduction to the infrared spectroscopy. The fundamental principles of infrared spectroscopy theory are also presented. Working principles of infrared spectrometer are explained based on the Michelson interferometer the most commonly used in the Fourier Transform Infrared Spectroscopy (FTIR). Some applications are summarized.

Chapter “**Experimental Setup**” explains all details of the experimental setup used for the performed experiments. The $oH_2 \rightarrow pH_2$ conversion apparatus as well as the method for normal-Hydrogen (nH_2) to 99.9 % of pH_2 conversion are explained. Details of the liquid-He SMC flow cryostat used for matrix deposition and the deposition parameters are presented. Finally the UV and IR sources are also described in this chapter. The next chapter is “**Computational methods**”. This chapter outlines some general features for the computational methods used to simulated molecular systems. Hartree-Fock (HF) and Density Functional Theory (DFT) computational methods are summarized. The explanation of some basis sets used by those methods and the anharmonic approximation are also presented.

The results of this study are reported in the following five chapters. Chapter “**Acetylacetone Infrared spectra**” summarizes all results from as deposited sample, i.e. all the information extracted from the infrared spectra of AcAc in pH_2 matrices just right after deposition of the matrix. The assignment of infrared absorption bands of chelated enol and keto tautomers of AcAc in pH_2 compared with the results obtained using others matrices such as Ne and normal-Deuterium (nD_2) and the performed theoretical simulations are discussed. The keto/enol ratio is also estimated. Chapter “**Spin Conformers**” analyzes the behavior of the infrared spectra of AcAc isolated in pH_2 kept in dark. It shows the changing in the intensity of some bands in the IR spectra connected to the interconversion of at least two species. Due to the kinetic analysis of the process and the relatively long interconversion characteristic time (τ), these species are assigned to two different spin states of the chelated enol form of AcAc.

The chapter “**UV laser irradiation at 266 nm**” explains the changes in the infrared spectra of AcAc in pH_2 matrices after UV (266 nm) laser irradiation. The appearance of new bands in the spectra are assigned to three open enol isomers of AcAc. The frequency values of isomers are listed and compared with the corresponding values in other matrices and theoretical values. The evidence

of a new isomer is presented. The kinetic study of the appearance of those isomers is discussed and the mathematical details are summarized in the appendix. A reaction mechanism is proposed for the formation of isomers. Chapter “ **UV laser UV irradiation at 248 nm**” presents the infrared spectra of AcAc in pH₂ matrices after UV (248 nm) laser irradiation. The changes in the infrared spectra due to the UV irradiation are analyzed. The full bands assignment of keto tautomer of AcAc is presented and compared with other matrices. The evidence of photofragments is supported by appearance of new bands in the spectra. The last chapter “**UV laser irradiation at 193 nm**” discusses the photolysis of AcAc in pH₂ matrices upon UV (193 nm) laser irradiation. Infrared spectra of photofragments in pH₂ matrices are presented. Some fragmentation mechanisms are proposed as well as the reactions between fragments or reactions of fragments with the H₂ molecule of the matrix. In the Conclusions, fundamental results are summarized. Perspective and future experiments are proposed for further understanding of some processes.

INTRODUCTION

Chapter 1

Molecule of Acetylacetone

1.1 Acetylacetone

1.1.1 General physicochemical properties

Acetylacetone (AcAc) ($C_5H_8O_2$) is a relatively small molecule from the family of diketones. Under normal gas phase conditions, AcAc coexists as two tautomers: enol and keto but the concentration of enol tautomer is largely predominant in the gas phase.³⁶ At ambient temperature and pressure, AcAc is a colorless stable product. It is a commercial product that for this research was provided by Sigma-Aldrich (purity ≥ 99.5 %). *Table 1.1* presents the major physical-chemical properties of this molecule.

Formule	$C_5H_8O_2$
Molar mass ($g\ mol^{-1}$)	100,12
Boiling point ($^{\circ}C$)	140 ³⁷
Melting point ($^{\circ}C$)	23 ³⁷
Density ($g\ mL^{-1}$)	0,975 at 25 $^{\circ}C$ ³⁷
Vapor pressure (mbar)	8 at 20 $^{\circ}C$ ³⁷
Dipole moment of the enol form (D)	3,0 ¹⁴

Table 1.1: *Physical-chemical properties of Acetylacetone molecule.*

1. MOLECULE OF ACETYLACETONE

1.1.2 β -diketones compounds

In the picture 1.1 are shown the graphical representation of a) ketone, β -diketone species in both b) keto and c) enol forms. According to IUPAC Gold Book, the ketones are compounds in which a carbonyl group is bonded to two carbon atoms $RR'C=O$ (neither R may be H).³⁸ Meanwhile, a β -diketone are two ketones arranged in such way that the second one is in the β carbon position, counting from the first, as is shown in figure 1.1 (b) and (c).

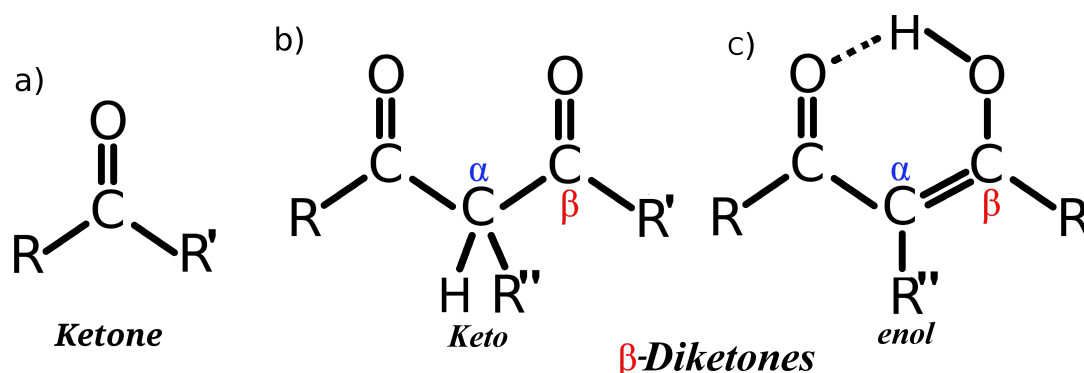


Figure 1.1: Schema of a) Ketone, β -diketone species in both b) keto and c) enol forms

The structure and reactivity of many β -diketones compounds have been important issues in several fields of science as organic chemistry,³⁹ since the beginning of the twenty century.^{39–42}

Most ketones exist predominantly in the keto structures (figure 1.1b) as they are energetically more stable than the enols (figure 1.1c). However, stable enol diketones have been observed. These enol diketones contain a strong intramolecular hydrogen-bonds $O-H \cdots O$ which is reinforced by the electron delocalization that provides an additional stabilization.⁴³ For this reason, these hydrogen bonds (HBs) are sometimes called hydrogen bond assisted by resonance. Molecules having these types of HB often called enol resonant or chelated enol (From Greek *khélé*, “crab’s claw” because the molecule looks like pinching the hydrogen atom as a pincer),

1.1.3 Main Characteristics of Acetylacetonone related to this study

AcAc is the simplest β -diketone. It can be found in both, chelated enol and keto form (see figure 1.2), in gas, liquid, and solid phase, predominantly as a chelated enolic form in the gas phase due to highly acidic nature of the H atom in $(-CO-CH_2-CO-)$ group and the formation of a relatively strong intramolecular HB.⁴⁴ The keto-enol tautomerization of AcAc has been extensively studied experimentally.^{8,45–47} In solution, the relative amount of enol and keto forms depends of the solvent properties and AcAc is a good prototype to study tautomerization mechanisms (As described later).

AcAc chelated enol form has an internal HB that can exhibit a proton transfer between two oxygen atoms. The stabilization energy of the hydrogen bonding in this molecule has been calculated theoretically to be 12.5 kcal/mol,⁴⁴ much higher than the usual H-bonding, which is $\approx 3 - 5$ kcal/mol. The proton transfer mechanisms and its relationship with the enolic structure of AcAc have been the principal subject of several experimental and theoretical studies showing different viewpoints.

The photochemistry of AcAc had been studied as well. The UV^{4,14} studies have shown that in the gas phase, the enolic AcAc at room temperature has a broad structureless absorption band around 270 nm, which is attributed to the allowed (π, π^*) transition. Gas phase and supersonic jet studies show that under UV irradiation only fragmentation of the AcAc takes place by separation of OH radical.^{20,48,49} In matrices, meanwhile, isomerization process is more efficient and open enol forms appear.⁵⁰ Fragmentation and isomerization have been extensively studied, nevertheless open questions about photoreaction pathway intermediate and final products still remain.

1.2 Acetylacetonone enol/keto tautomers

Acetylacetonone is a good prototype to study tautomerization mechanisms. The enol chelated form (*Z-4-hydroxy-3-penten-2-one*) can coexist with the β -diketone tautomer (*2,4-pentanedione also called keto*) in the gas phase and the liquid phase.¹⁴ Both structures are presented in *figure 1.2*. For this system, tautomerization consists in a displacement of the proton of the OH group to the central carbon, which requires an electronic rearrangement.

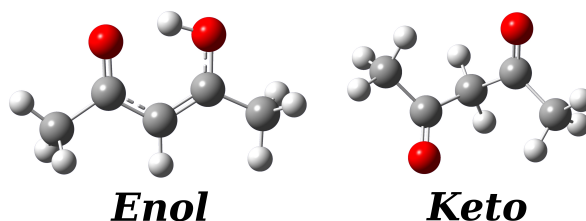


Figure 1.2: The enol (left) and keto (right) stable forms of Acetylacetonone: the optimized geometries of chelated enol and keto tautomers are obtained at the B3LYP/6-311++G(3df, 3pd) level of theory (See chapter 5)

The keto/enol ratio of AcAc had been the subject of study of many work and it is known that the keto \rightleftharpoons enol equilibrium is influenced by a variety of different factors, such as temperature, solvent, presence of other species which are capable of hydrogen bonding.^{15-17,45-47,51,52}

The study done by Spencer *et al.*¹⁷ of AcAc in different solvents shows that the enol/keto ratio depends on the solvent properties (See table 1.2). The usual rule that is applied to rationalize the effect of solvent on the percentage of enol in a β -diketone is that the enol tautomer is less polar than

1. MOLECULE OF ACETYLACETONE

the keto tautomer and therefore polar solvents stabilize the keto tautomer over the corresponding enol tautomer.¹⁷

Solvent	ϵ	% enol (278K)
C_6H_6	2,3	97
CCl_4	2,2	95
CH_3OH	32,6	74
$(CH_3)_2NH$	37,8	66
$(CH_3)_2SO$	46,6	62
H_2O	78,5	16

Table 1.2: Percentage of the chelated enol form for different solvents. ϵ : solvent's dielectric constant.

According to various Nuclear Magnetic Resonance (NMR) studies^{18,51} the enol tautomer prevails in liquid and gas phase. Temprado *et al.*¹⁶ point out that the enol tautomer is more volatile and therefore its concentration in the gas phase should be even higher than that in the liquid. Meanwhile, Irving and Wadso⁵³ derived the tautomeric composition of AcAc in the gas phase: (liquid; 81.4% enol)¹⁸ \rightleftharpoons (gas; 93.3% enol). The temperature dependence had been showed also by photoelectron spectroscopic studies.⁵⁴ Belova *et al.*¹⁵ derived enol concentrations of 73% at 25 °C, 60% at 100 °C and about 50% at 175 °C by using the values of the keto \rightleftharpoons enol equilibrium constant reported by Schweig *et al.*⁵⁴ This value of enol concentration of 73% at 25°C obtained by Belova and co-workers¹⁵ is in clear disagreement with 93.3 % reported by Irving and Wadso⁵³ for the gas phase AcAc.

The gas electron diffraction (GED) techniques show slightly conflicting results.^{3,8-10} Experimental intensities recorded at room temperature^{3,9} have been interpreted in terms of the presence of the enol form only. A study performed at 105 °C resulted in an enol contribution of $66 \pm 5\%$.⁸ This value is in a good agreement with one derived from the photoelectron spectra at 100 °C.⁵⁴ In a recent GED investigation¹⁰ an enol contribution of $78 \pm 4\%$ at 155 °C was reported. According to quantum chemical calculations the keto \rightleftharpoons enol equilibrium should be shifted strongly towards enol. CBS-4 calculations⁵⁵ lead to a value of only 1.1% of keto at 298 K. DFT/B3LYP calculations⁵⁶ predict even stronger predominance of the enol tautomer (only 0.1% of diketo). Studies in cryogenic matrices showed a large amount of enol form as in the gas phase at room temperature.^{50,57,58}

1.3 Enol forms of AcAc

1.3.1 Hydrogen bonds and proton transfer

As said before, chelated enol form of AcAc exhibits a strong interacting hydrogen bond (HB). The HB is the most important of all directional intermolecular interactions. It was discovered in the beginning of the 20th century, but still is a topic of vital scientific research. The reason for this long-lasting interest lies in the eminent importance of HBs for the structure, function, and dynamics of a vast number of chemical systems, which range from inorganic to biological chemistry.

At the beginning the HBs had a “classical” interpretation and the directional interaction between water molecules was considered as the prototype of all HBs. Today, it is known that the HB is a much broader phenomenon than this one called the “Classical HB” which is just one among many. While the strength of this “Classical HB” is around (3-5) kcal/mol, some HBs are so strong that they resemble covalent bonds in most of their properties, and some others that are so weak that they can hardly be distinguished from Van der Waals interactions. Hydrogen-bond strengths span more than 2 orders of magnitude (0.2 - 40) kcal/mol. The nature of those HB varies as a function of their electrostatic, dispersion, charge-transfer and covalent contributions. In general an X–H \cdots Y interaction is called “HB”, if 1. it constitutes a local bond, and 2. X–H acts as proton donor to Y.⁵⁹ In the extreme limit, for symmetric HBs (X–H–X), the H-atom is equally shared; no distinction can then be made between the donor and acceptor, or the “covalent” X–H and “noncovalent” H \cdots X bond.⁶⁰

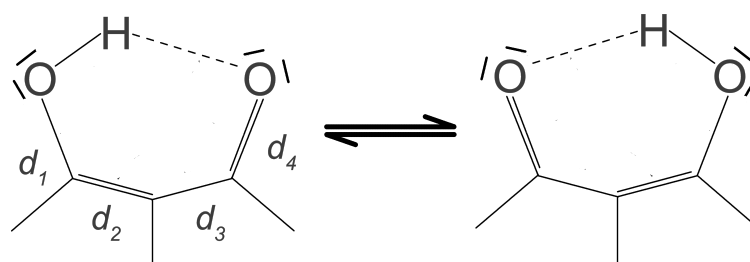
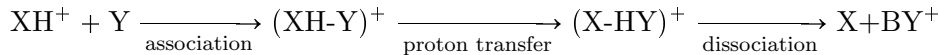


Figure 1.3: Resonance-assisted hydrogen bonding (RAHB) in β -diketones enolates

The enol tautomers of β -diketones, contain two neutral donor and acceptor oxygen atoms connected by a system of conjugated double bonds (*figure 1.3*); the consequent synergistic reinforcement of H-bonding and π -delocalization can lead to strong intramolecular “resonance-assisted hydrogen bonding” (RAHB).^{5,61} Increasing delocalization may transform the HB from an asymmetric O–H \cdots O interaction to a symmetric O–H–O bond. In the limit of complete delocalization, the C–C and C=C bonds as well as the C–O and C=O distances become very close to each other, the O \cdots O distance becomes shorter, and the H-atom lies midway between the two oxygens.

1. MOLECULE OF ACETYLACETONE

A very important way of looking at HBs is to regard them as incipient proton-transfer reactions. The reaction typically studied by the gas phase experiments may be characterized as⁶²



From this viewpoint, a stable HB $\text{X-H} \cdots \text{Y}$ is a “frozen” stage of the previous reaction. This means that a partial bond $\text{H} \cdots \text{Y}$ is already established and the X-H bond is concomitantly weakened. Strong HBs represents an advanced stage proton-transfer reaction.⁵⁹

Particular systems are those which have HBs involving oxygen atoms as a proton donor and proton acceptor. The manifestations of proton dynamics in these systems is a broadening of the OH stretching band in vibrational spectra. From the shape of the vibrational spectrum one can draw conclusions about the strength of the HB and the shape of the proton potentials. A broad band is characteristic of strong HBs ($\text{O-H} \cdots \text{O}$) and can be assigned to OH stretching. The half-width of this band often exceeds 200 cm^{-1} . On the other hand, weak HBs are associated with a high proton potential barrier, which is typically associated with a high degree of asymmetry and a much less pronounced broadening of the OH band that appears at higher frequency.¹³

Source		$\text{O}_1 \cdots \text{O}_2$	$\text{O}_1\text{-H}_1$	$\text{O}_2\text{-H}_1$	$\text{C}_1\text{-O}_1$	$\text{C}_2\text{-O}_2$	$\angle \text{O}_1\text{H}_1\text{O}_2$
1971 Karle ⁸ [C_{2v}]	(elec- tron diffraction)	2.381	1.192	1.1920	1.315	1.315	186.0 ^g
1972 Bauer ⁹ [C_{2v}]	(electron diffraction)	2.519	1.259	1.2595	1.287	1.287	181.5 ^g
1987 Shibata ³ [C_1]	(electron diffraction)	2.512	1.049	1.6400	1.319	1.243	137.0
1994 Dannenberg ⁴⁴ [C_s]	(MP2/D95++**)	2.549	1.004	1.7800	1.291	1.291	155.0
2004 Zewail ¹⁰ [C_s]	(electron diffraction)	2.592	1.003 ^h	1.683 ^h	1.321	1.262	148.4 ^h
2007 Vaccaro ⁶³ [C_s]	(CCSD(T)/aug-cc-pVDZ)	2.575	0.998	1.6653	1.344	1.256	149.3

Table 1.3: Selected structural parameters for Acetylacetonone. The subscripts appearing on atomic symbols follow from the labeling scheme introduced in Fig. 1, where O_1 and O_2 denote the hydroxyl and carbonyl oxygen atoms, respectively. ^g Reported structures indicate shuttling hydrogen is located below the axis connecting the two oxygen atoms. To maintain consistency, tabulated values are the conjugate angles of those given by the authors. ^h Due to the weak scattering of electrons by the hydrogen atom, these parameters were held at calculated DFT values.

1.3.2 Chelated enol form of AcAc

Acetylacetonone is postulated to have unusually strong HB in its cyclic, conjugated enolic form. Conjugated enols of this kind contain 6π electrons within a ring. This delocalization provides additional

stabilization through electron resonance: they are quasi-aromatic systems.

The structure of the enol has been somewhat controversial see Table 1.3. On the basis of two separate gas-phase electron diffraction studies, Karle and coworkers⁸ determined that at 100-110 °C only $66 \pm 5\%$ was chelated enol form with a symmetrical structure C_{2v} and short $O \cdots O$ distance (2.381 Å) and the HB in the plane of the ring; each methyl group has a C–H bond in the molecular plane that eclipses the C–O bonds. This assertion of local C_{2v} geometry was confirmed by subsequent electron diffraction work done by Andreassen and Bauer,⁹ which reported a much longer $O \cdots O$ distance (2.519 Å). Shibata and coworkers,³ on the other hand, reported an unsymmetrical chelated enol form with $O \cdots O$ distance (2.512 Å) and the HB out of the ring plane. The methyl groups have a C–H bond 30° out of the molecular plane.

Dannenbergh and Rios⁴⁴ made a theoretical work by calculation of the structural parameters of several configuration. They focus on the comparison between these two configurations (C_s and C_{2v}). They report the C_s as the most stable and C_{2v} as transition state configuration. The C_s structure has a relatively large $O \cdots O$ distance (2.549 Å) and the H-bond in the plane of the ring. It has also one of these methyl groups with the C–H bond eclipsed with the C–O bond and another anti to the C=O bond. Zewail and coworkers¹⁰ made experiment to explain the nature of the intramolecular $O-H \cdots O$ HB in enolic AcAc using electron diffraction technique. As a result the enolic structure clearly indicates that AcAc does exhibit some π -delocalization, leading to shorter C–C, C–O and longer C=C, C=O bonds compared to “unperturbed” distances in enols.^{5,61} However, this delocalization is not strong enough to give a symmetric skeletal geometry. The resulting long $O \cdots O$ distance (2.592 Å) is significant in making the homonuclear $O-H \cdots O$ HB localized and asymmetric. In a newer experimental endeavors, Caminati and Grabow⁶⁴ have employed high-resolution rotational spectroscopy to probe the parent AcAc species and its singly ^{13}C -substituted isotopolog under supersonic free-jet expansion conditions. They conclude that AcAc has a symmetric C_{2v} equilibrium configuration that has the shuttling proton localized midway between the two oxygen atom centers.

More recently, Vaccaro and coworkers⁶³ used various quantum chemical methods such as Hartree–Fock(HF), density functional(DFT/B3LYP), Møller-Plesset perturbation (MP2), and coupled-cluster [CCSD, CCSD(T), CC3] with correlation-consistent basis sets to elucidate equilibrium structure of ground-state AcAc. The geometry optimizations performed at the CCSD(T)/aug-cc-pVDZ level of theory predict of a global minimum-energy configuration that exhibits C_s symmetry, while the higher-lying C_{2v} arrangement of nuclei is found to represent the transition-state for proton transfer reaction(see figure 1.4).

Enolic AcAc has three large amplitude motions, one intramolecular hydrogen transfer and two methyl torsions. Therefore, the C_s structure has 18 ($3 \times 3 \times 2$) equivalent equilibrium molecular frameworks, nine (3×3) of them are from the two methyl torsions, and two are from the intramolecular

1. MOLECULE OF ACETYLACETONE

hydrogen (H_{int}) transfer. The H_{int} transfer induces a rearrangement of the CC, CO single and double bonds, and then triggers two additional 60° internal rotations, one in each of the two methyl groups. This interaction further complicates the tunneling splitting patterns and increases the difficulty of spectral analysis.⁶⁵

It is possible that the symmetry C_{2v} found in some experiments⁶⁴ only reflects the complications incurred by the action of methyl group dynamics. The uncorrelated internal rotation of the two $-\text{CH}_3$ moieties will perturb the symmetric nature of the double-minimum well along the $\text{O}\cdots\text{H}\cdots\text{O}$ coordinate. In addition the strong coupling among three large amplitude degrees of freedom (dual $-\text{CH}_3$ torsion and $\text{O}\cdots\text{H}\cdots\text{O}$ displacement) can be expected to reduce the overall efficiency of hydrogen migration and to partially quench the usual signatures of such intramolecular processes (e.g. tunneling-induced spectral bifurcations).⁶³

1.3.3 Non Chelated enols

When the O-H, CH_3CO , and CH_3COH groups (see figure 1.5) rotate around the C-O, C-C, and C=C bonds of the chelated enol form, respectively, and these rotations are proceeded in turn, seven more conformers could be obtained, namely, CCT, TCC, CTC, TCT, CTT, TTC, and TTT, according to the relative position (T for trans and C for cis).

The seven conformers have been confirmed to be local minimum on potential energy surface (PES) by several theoretical calculations.²¹⁻²³ Intensive experimental^{2,7,23,50,57,58} studies have been conducted to study the UV and IR photoisomerisation of AcAc. It was observed that upon UV irradiation in cryogenic matrices such as nitrogen and rare gas matrices, the intramolecular HB was broken, leading to formation of nonchelated isomers.^{2,7,23,50,57,58} They have higher relative energy than the chelated isomer and have never been observed in the gas or liquid phase.²²

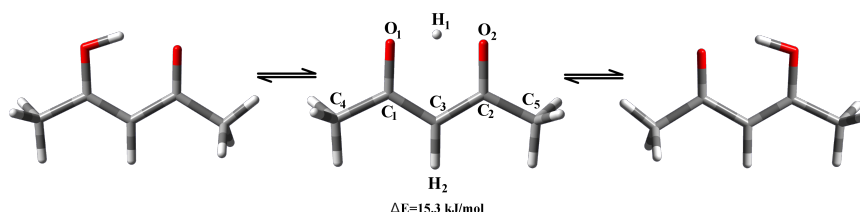


Figure 1.4: Structure and dynamics in enolic acetylacetone. The proton-transfer process taking place in the enolic tautomer of acetylacetone is depicted schematically, illustrating how the shuttling hydron (H_1) mediates the interconversion of two equivalent and asymmetric (C_s) conformers through a symmetric (C_{2v}) transition state.⁶³

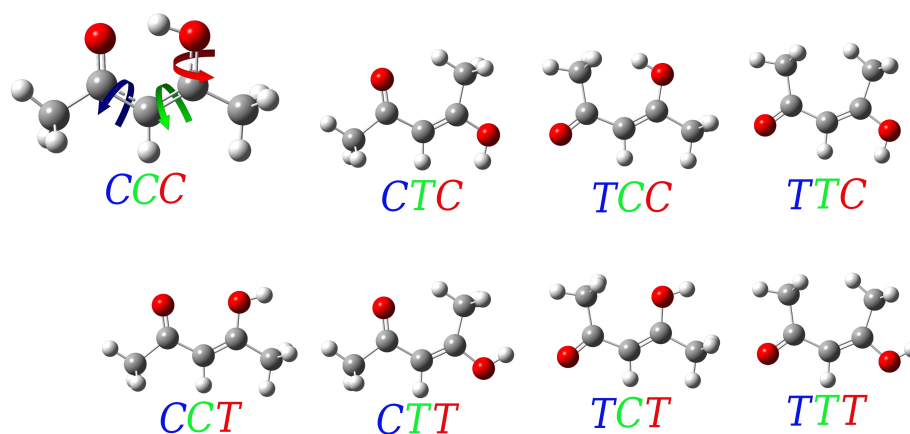


Figure 1.5: Eight possible isomers of enol AcAc. Labels in terms of three letters (C or T) based on the cis or trans configuration around the C-C, C=C or C-O bonds respectively.

1.4 Photochemistry of AcAc

The excited states of AcAc and their reactions are another open field on the understanding of this molecule. Nakanishi *et al.*¹⁴ measured the near and vacuum UV absorption spectra of acetylacetone in the gas phase and in several organic solvents at various temperatures. A broad structureless absorption band is observed at 263 nm for the enol form which corresponds to a $\pi - \pi^*$ transition. A weak band observed at 294 nm for the keto form was assigned to the first $n - \pi^*$ transition. They also could assign the Rydberg excitation bands observed at 212 nm and 188 nm for the enol form, and 192 nm for the keto form. Meanwhile Walz *et al.*⁴ in their electron-impact spectroscopic studies showed a very strong band with a maximum at ~ 264 nm which is identified with the lowest spin-allowed $\pi - \pi^*$ transition in the enol molecule. A weak band was observed with the maximum at 307 nm due to the first spin-allowed $n - \pi^*$ band in the keto form.

Yoon *et al.*^{48,49} used a laser-induced fluorescence (LIF) technique at the excitation wavelengths of 291 and 266 nm to study the AcAc in supersonic jet. After the $\pi - \pi^*$ transition induced by the UV absorption the OH fragment was detected. The pump-probe experiment (*ns*) allowed them to study the population of the OH fragment and estimate the dissociation energy of the molecule to 90.3 kcal mol⁻¹ (378.07 kJ mol⁻¹). No fluorescence from the excited AcAc was observed even in the energy region near the origin, suggesting ultrafast nonradiative processes from the excited state.

Upadhyaya *et al.*²⁰ studied the photodissociation dynamics of enolic-acetylacetone at 266, 248 and 193 nm in gas phase. They also indicated that the dissociation of the molecule requires about 90 kcal mol⁻¹ (376.81 kJ mol⁻¹) but their subject of study was the reaction mechanism that leads to fragmentation after excitation of the $\pi \rightarrow \pi^*$ transition that takes place between S₀ and S₂ states.

1. MOLECULE OF ACETYLACETONE

Subsequent to excitation they did not observe fluorescence of the parent molecule even with a time resolution of $\sim 10^{-8}$ seconds (pump-probe experiment). This suggests the importance of fast non-radiative processes in this region of excitation. Due to fast non-radiative processes, the S_2 state crosses over to any of the lower states, namely S_1 , T_2 , and T_1 from which fragmentation takes place. Ab initio Molecular Orbital (MO) calculations were performed to investigate the potential energy surface (PES) of the ground and excited electronic states of AcAc. In accord with this experimental result, the dissociation to OH is possible only from the T_1 triple state.

Zewail and co-workers⁶⁶ documented the real-time dissociation dynamics of AcAc, following excitation to the S_2 state. The electron diffraction technique was used as a probe, indicating that the loss of OH was achieved with a time constant of 247 ± 34 ps. This time was assigned to the lifetime of the S_1 state of AcAc, assuming that it decays through the intersystems crossing $T_1 \leftarrow S_1$. According to J.M. Mestdagh and coworkers,⁶⁷ S_1 was populated from S_2 through an ultrafast non-adiabatic process that could not be resolved, apparently because the S_2 and S_0 states have geometries that can hardly be separated in the diffraction peaks on the electron diffraction techniques. However they use femtochemistry technique to study the dynamics of AcAc in molecular beam under UV 266 nm irradiation. This experiment has highlighted the existence of two characteristic times during the electronic relaxation. First, the departure from the Frank-Condon (FC) region is found in the time frame of 70 ± 10 fs in which initial deformation is likely the H-atom transfer from one oxygen atom to the other. More complex deformations are certainly involved in this initial step as well. Then the system moves to a region of important coupling between the S_2 and S_1 surfaces, the full transfer of the wavepacket from one surface to the other taking 1.4 ± 0.2 ps. The dynamics after the transfer to the S_1 surface appears as a slow decay, which is consistent with the time scale of 247 ± 34 ps found by Zewail and co-workers⁶⁶ for the decay of this state toward triplet states.

From a theoretical point of view Chen *et al.*²¹ performed in the Complete active space self-consistent field (CASSCF) and Density Functional Theory (DFT) formalisms to study the ultrafast non-radiative relaxation between the lowest five electronic states of S_0 , T_1 , T_2 , S_1 , and S_2 . These processes are summarized in Figure 1.6. The AcAc molecule is initially promoted to the FC region of the S_2 state by UV excitation (vertical excitation). Decay to the S_1 state takes place in a short period via a vibronic interaction, and finally it relaxes to the T_1 minimum through the $S_1/T_1/T_2$ three-surface intersection. Rotational isomerization proceeds easily on the T_1 state. But the predominant decomposition process, in gas phase, on the T_1 state is the C-OH cleavage, forming the fragments of $\text{CH}_3\text{COCHCCH}_3$ and OH. Since rotational isomerization processes involve a breakage of the intramolecular O-H \cdots O HB and breaking the C=C π bond, these processes could not proceed in the ground state.

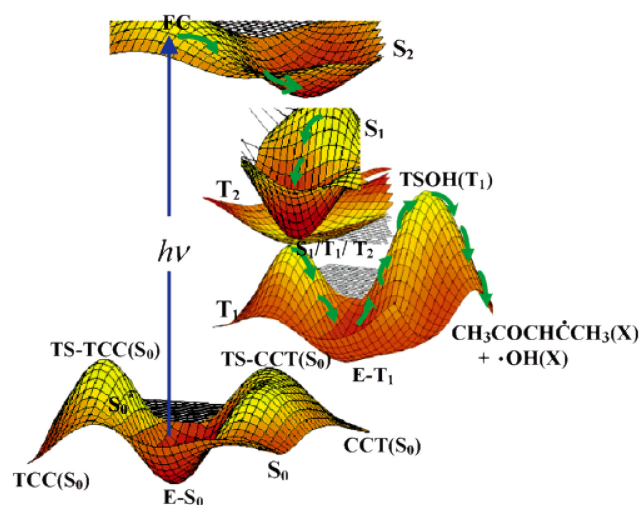


Figure 1.6: Schematic diagram of the most possible pathways upon photoexcitation of AcAc in the UV regions.²¹

In matrices,^{7,22,23,50,58} the trend is somewhat different. Upon UV irradiation in the 230–300 nm range, the intramolecular HB is broken, leading to formation of “open forms” (non-chelated enol see figure 1.5). The reaction pathway proposed to interpret isomerisation follows the picture provided by the gas phase studies²¹ for the first steps but after relaxation to the triplet state (T₁) it seems that the matrix quenches the dissociation of AcAc, thereby allowing the molecule to relax to the different isomers. When using broadband UV excitation source, little fragmentation leading to the formation of CO was found to occur in matrices.⁵⁰ This fragmentation could be increased by adding molecular oxygen in the solid to trap radical species. Coussan and co-workers showed a larger fragmentation yield in Ne or Xe than in Ar or N₂ matrices which are more rigid media favoring a larger confinement of the fragments and thus a more efficient recombination.⁵⁰

1. MOLECULE OF ACETYLACETONE

Chapter 2

Experimental Techniques

This chapter is split in two main subjects: first, the infrared radiation and the second the spectroscopical techniques at low temperatures. The infrared radiation topic starts with a historical overview about the discovering of the infrared region and the first steps for measuring one spectrum. Then, a basic explanation of the formalism of the infrared spectroscopy and its relation with the vibrational and rotational states of molecular systems. The influence in the bands width of different factors are also explained. Next the Michelson interferometer is presented as a precursor of the Fourier transform infrared (FT-IR) spectroscopy. The advantages of FT-IR spectroscopy over dispersive spectroscopy presented. At the end, some applications of the infrared spectroscopy are discussed.

In the second part, the advantage of low temperature spectroscopy are presented followed by a description of the matrix isolation technique and its utility in the low temperature spectroscopy. Finally, the hydrogen matrices and particularly the para-Hydrogen ($p\text{H}_2$) matrices are detailed and its advantages as a host matrix for Matrix Isolation Spectroscopy (MIS)

2.1 Infrared radiation

2.1.1 Historical overview

The first non-visible region of the electromagnetic spectrum was discovered by the astronomer Sir William Herschel in 1800.⁶⁸ He investigated the distribution of heat in the visible solar spectrum obtained by placing a glass prism in front of a slit cut in a window blind. The heat associated with different positions in the well-dispersed spectrum displayed on a horizontal surface was measured by mercury-in-glass thermometers with blackened bulbs. Herschel found that the temperature maximum shown by the thermometers occurred just beyond the red end of the spectrum, i.e. at a very different

2. EXPERIMENTAL TECHNIQUES

position from that of maximum luminosity, and that heating extended well beyond there. Herschel's glass prism transmitted only the very beginnings of the infrared (IR) range, what we now term the near-infrared (NIR) region.

John Tyndall at the Royal Institution in London, starting in the 1850s, used the thermopile and cells with rock salt windows to make systematic measurements of the reduced transparency to undispersed IR radiation of a wide variety of gases and liquids.⁶⁸ He was a pioneer in speculating in terms of molecules, and vibrations within molecules, as the origin of IR absorption.

The first measurements of NIR absorption bands were made by Sir John Herschel, Sir William's son, in 1840 using solar radiation, a glass prism and the visually perceived evaporation of alcohol on a blackened sheet of paper as the detector.⁶⁹ Melloni seemingly first observed absorption bands in what we now term the middle-infrared (MIR) region using a prism made from a large natural crystal of rock salt for dispersion experiments.⁶⁸ He showed that hotter sources gave stronger radiation that was of higher mean refractivity, i.e. what we would now express as shorter mean wavelength. After several refinements, Melloni had by 1850 designed a spectrometer with a slit, a rock salt lens to provide an image of the slit, and provision for moving a slit-shaped thermopile across the spectrum generated by the fixed-position prism.

Samuel P. Langley has constructed a bolometer and was also responsible for a second fundamental advance in the IR region. He was the first to calibrate spectra in terms of wavelength by measuring the refractive-index-versus-wavelength dispersion curve for rock salt.⁶⁸

After their first use by E. Pringsheim in 1883, surface-metallized concave mirrors gradually replaced the non-achromatic rock salt lenses of the Melloni/Langley spectrometers but a quartz lens found specific use in the far-infrared (FIR) region because of its capacity to transmit and focus radiation of wavelengths below 250 cm^{-1} but to absorb strongly much radiation of shorter wavelengths.

While progress was being made in the techniques of the MIR and FIR regions, an important development also occurred in the NIR region. This was the discovery in 1880 by William Abney, who worked in the Chatham School of Military Engineering in England, that photographic silver bromide films treated with nitric acid could be prepared in such a way that they were sensitive to the NIR radiation transmitted by a glass prism. In 1881 Abney and R.E. Festing⁷⁰ published the NIR spectra of some 50 liquids, mostly organic compounds, between 13300 and 9100 cm^{-1} using the required long pathlengths of up to 60 cm.

William Weber Coblentz, in 1903, built his infrared spectrometer based on rock salt prism and investigated the spectra of hundreds of substances, both organic and inorganic. His work was so accurate that most spectra were used for more than 50 years as a reference. Ending result of Coblentz works was the recognition that each compound has a unique IR spectra and that certain groups, even when they were in different molecules, gave absorption bands that were found approximately at the

same wavelength. This work established infrared spectroscopy as a diagnostic tool for recognition of unknown chemical substances.⁷¹

It was not until the advent of quantum theory in the first few decades of the twentieth century that a general understanding of the origins of molecular spectra – in the visible, ultraviolet (UV) or IR regions – could be achieved. Towards the end of the nineteenth century a general view was that absorption or emission bands in the visible region related to resonances involving oscillatory charges within a molecule, perhaps of a bond-vibrational nature. However this could not account for the emission spectra of atoms, even although these gave line spectra that were simpler than the band spectra of molecules.

As quantum theory developed, the Schrödinger wave equation was applied to a series of models that accounted with great success for the features of MIR (600-4000 cm^{-1}) spectra as corresponding to transitions between vibrational and more closely spaced rotational energy levels, the latter giving rise to the fine structure associated with a rotational absorption in the gas phase; NIR (4000-12500 cm^{-1}) spectra as originating in overtones or combinations of the vibrational fundamentals; and FIR (10-600 cm^{-1}) spectra as originating in low-frequency vibrational fundamentals, e.g. the lattice modes of crystalline solids, or in pure rotational spectra in the gas phase.

A quantum-theoretical analysis shows that there must be a change in dipole moment for absorption of the radiation may occur. Now the forces and nuclear masses within molecules are such that the vibrational frequencies lie within the range 10^{12} – 10^{14} Hz. Such frequencies lie within the IR portion of the spectrum. Because instruments used to measure IR radiation measure wavelength, rather than frequencies, it is normal to describe IR radiation by its inverse wavelength (wavenumber). The usual unit is cm^{-1} . In such terms, fundamental vibrational wavenumbers fall below 3700 cm^{-1} . A lower practical limit is usually 200 cm^{-1} , although there are modes that involve such weak forces that the wavenumbers tend towards zero.

2.1.2 Infrared spectroscopy Theory

Absorption of the infrared radiation in matter can be described by classical electromagnetic theory. It can be shown that periodically oscillating electrical dipoles absorb or emit radiation. Frequency of absorbed (or emitted) radiation is equal to the frequency of dipole oscillation. In order to estimate the intensity of spectral band one should calculate square of transition moment, which means that one should estimate the change of dipole moment (μ_{fi}). The transition dipole moment can be obtained from⁷²:

$$\mu_{fi} = \langle \psi_f | \hat{\mu} | \psi_i \rangle \quad (2.1)$$

where ψ_i and ψ_f are the wavefunction of the initial and final states.

2. EXPERIMENTAL TECHNIQUES

Einstein identified three contributions to the transitions between states.⁷²

1. *Absorption* is the transition from a low energy state to one of higher energy that is driven by the electromagnetic field oscillating at the transition frequency ν .
2. *Stimulated emission*. Consider that the radiation is also able to induce the molecule in the upper state to undergo a transition to the lower state. Only radiation of the same frequency as the transition can stimulate an excited state to fall to a lower state.
3. *Spontaneous emission*. Excited state could undergo spontaneous emission at a rate that was independent of the intensity of the radiation that is already present.

Einstein was able to show that the two coefficients of absorption and stimulated emission are equal, and that the coefficient of spontaneous emission is related to them by⁷²:

$$\mathcal{A} = \left(\frac{8\pi h\nu^3}{c^3} \right) \mathcal{B} \quad (2.2)$$

where \mathcal{A} and \mathcal{B} are the Einstein coefficient of spontaneous emission and stimulated emission respectively.

Spontaneous emission can be largely ignored at the relatively low frequencies of rotational and vibrational transitions, and the intensities of these transitions can be discussed in terms of stimulated emission and absorption. Then the net rate of absorption for non-degenerate levels is given by:

$$W_{\text{net}} = (N_i - N_f)\mathcal{B}\rho \quad (2.3)$$

where N_i and N_f are the population of the lower and upper states involved in the transition and ρ is the energy density of radiation in the frequency range ν to $\nu + d\nu$.

From time-dependent perturbation theory, it can be shown that the transition rate is proportional to $|\boldsymbol{\mu}_{fi}|^2$ and is proportional to Einstein coefficient:

$$\mathcal{B} = \frac{|\boldsymbol{\mu}_{fi}|^2}{6\epsilon_0\hbar^2} \quad (2.4)$$

From here one can form a rule for the occurrence of infrared radiation absorption in the matter. Dipole moment of the molecular system should change when atoms vibrate in order to make absorption possible. This is not always the case. Good example are diatomic homonucleus molecules (e.g. N_2 , O_2 etc.), such molecules possess only one vibrational motion along the axis uniting two atoms. Atoms forming such molecule are identical therefore the change of the distance between them do not change dipole moment of the system. Therefore such molecules do not absorb infrared radiation. Another case when vibrations of atoms in the molecule occur without infrared absorption in high symmetry molecules. In such molecules some vibrations (ones whose symmetry is the same as of the molecules) also do not change the moment of whole system.⁷¹

2.1.2.1 Pure rotation spectra

The key molecular parameter we shall need is the moment of inertia, \vec{I} , of the molecule related to an axis α

$$I_\alpha = \sum_i m_i r_i^2 \quad (2.5)$$

where r_i is the perpendicular distance of the atom i from the axis of rotation. The moment of inertia depends on the masses of the atoms present and on the molecular geometry.⁷²

We shall suppose initially that molecules are rigid rotors, bodies that do not distort under the stress of rotation. Rigid rotors can be classified into four types:

1. *Asymmetric rotors* have three different moments of inertia.
2. *Symmetric rotors* have two equal moments of inertia.
3. *Linear rotors* have one moment of inertia (the one about the molecular axis) equal to zero.
4. *Spherical rotors* have three equal moments of inertia.

The rotational energy levels of a rigid rotor may be obtained by solving the appropriate Schrödinger equation. Fortunately, however, there is a much less onerous short cut. Using the classical expression for the energy of a rotating body in terms of the angular momentum, and then importing the quantum mechanical properties of angular momentum into the equations.⁷²

In general, the rotational properties of any molecule can be expressed in terms of the moments of inertia about three perpendicular axes set in the molecule. The convention is to label the moments of inertia I_a , I_b and I_c with the axis chosen so that $I_c \geq I_b \geq I_a$

The classical expression for the energy of a body rotating around an axis α is:

$$E_\alpha = \frac{1}{2} I_\alpha \omega_\alpha^2 \quad (2.6)$$

where ($\alpha = a, b, c$) and ω_α is the angular velocity around that axis and I_α is the corresponding moment of inertia. A body free to rotate about three axes has an energy⁷²:

$$E = \frac{1}{2} \sum_\alpha I_\alpha \omega_\alpha^2 = \frac{1}{2} \sum_\alpha \frac{J_\alpha^2}{I_\alpha} \quad (2.7)$$

where $J_\alpha = I_\alpha \omega_\alpha$ is the classical angular momentum around the axis α .

With this equation we can describe the quantum mechanical properties of angular momentum and obtain the rotational energy levels.

Symmetric rotors.

2. EXPERIMENTAL TECHNIQUES

Two moments of inertia are equal but different from the third; the third axis of the molecule is its principal axis. Writing the moment of inertia (that about the principal axis) as I_{\parallel} and the other two as I_{\perp} (1) If $I_{\parallel} > I_{\perp}$, the rotor is classified as *oblate* (2) If $I_{\parallel} < I_{\perp}$ it is classified as *prolate*. The classical expression for the energy becomes:

$$E = \frac{\mathcal{J}^2}{2I_{\perp}} + \left(\frac{1}{2I_{\parallel}} - \frac{1}{2I_{\perp}} \right) J_{\parallel}^2 \quad (2.8)$$

where $\mathcal{J}^2 = \sum_{\alpha} J_{\alpha}^2$ is the square of the magnitude of the angular momentum. We can immediately find the quantum expression by making the replacement:

$$\mathcal{J}^2 \rightarrow J(J+1)\hbar^2 \quad J = 0, 1, 2, \dots \quad (2.9)$$

where J is the angular momentum quantum number.⁷² We also know from the quantum theory of angular momentum that the component of angular momentum about any axis is restricted to the values $K\hbar$, with $K = 0, \pm 1, \dots, \pm J$ (K is the quantum number used to signify a component on the principal axis.) Therefore, we also replace J_{\parallel}^2 by $K^2\hbar^2$. The energy is confined to the values:

$$E_{J,K} = hcBJ(J+1) + hc(A-B)K^2 \quad (2.10)$$

with rotational constants A and B

$$A = \frac{\hbar}{4\pi c I_{\parallel}} \quad B = \frac{\hbar}{4\pi c I_{\perp}} \quad (2.11)$$

The energy of a rotational state is normally reported as the rotational term $F(J, K) = E_{J,K}/hc$. Then:

$$F(J, K) = BJ(J+1) + (A-B)K^2 \quad (2.12)$$

Spherical rotors

All three moments of inertia are equal to some value I then $A = B$ and the expression for the rotational term is⁷²:

$$F(J) = BJ(J+1) \quad J = 0, 1, 2, \dots \quad (2.13)$$

Linear rotors.

The nuclei are regarded as mass points, the rotation occurs only about an axis perpendicular to the line of atoms and there is zero angular momentum around the line. Therefore, the component of

angular momentum around the figure axis of a linear rotor is identically zero, and $K = 0$ in equation 2.12. The rotational terms of a linear molecule are therefore:

$$F(J) = BJ(J + 1) \quad J = 0, 1, 2, \dots \quad (2.14)$$

This expression is the same as for spherical rotors, but derived at it in a significantly different way: here $K = 0$ but for a spherical rotor $A = B$.

The energy of a symmetric rotor depends on J and K , and each level except those with $K = 0$ is doubly degenerate: the states with K and $-K$ have the same energy. However, the angular momentum of the molecule has a component on an external, laboratory-fixed axis. This component is quantized, and its permitted values are $M_J\hbar$, with $M_J = 0, \pm 1, \dots, \pm J$, giving $2J + 1$ values in all. The quantum number M_J does not appear in the expression for the energy, but it is necessary for a complete specification of the state of the rotor. Consequently, all $2J + 1$ orientations of the rotating molecule have the same energy. The degeneracy associated with the quantum number M_J (the orientation of the rotation in space) is partly removed when an electric field is applied to a polar molecule. The splitting of states by an electric field is called the *Stark effect*.⁷²

The total wavefunction for a molecule, which can be written as:

$$\psi_{total} = \psi_{c.m.}\psi \quad (2.15)$$

where $\psi_{c.m.}$ describes the motion of the center of mass and ψ describes the internal motion of the molecule. If we neglect the effect of electron spin, the Born-Oppenheimer approximation allows us to write ψ as the product of an electronic part, $|\varepsilon\rangle$, a vibrational part, $|v\rangle$, and a rotational part, which for a diatomic molecule can be represented by the spherical harmonics $Y_{J,M_J}(\theta, \phi)$. The transition dipole moment for a spectroscopic transition can now be written as⁷²:

$$\boldsymbol{\mu}_{fi} = \langle \varepsilon_f v_f Y_{J,f,M_{J,f}} | \hat{\boldsymbol{\mu}} | \varepsilon_i v_i Y_{J,i,M_{J,i}} \rangle \quad (2.16)$$

During a pure rotational transition the molecule does not change electronic or vibrational states, so that $|\varepsilon_f v_f\rangle = |\varepsilon_i v_i\rangle = |\varepsilon v\rangle$ and $\boldsymbol{\mu}_{\varepsilon v} = \langle \varepsilon v | \hat{\boldsymbol{\mu}} | \varepsilon v \rangle$ is the permanent electric dipole moment of the molecule in the state εv . The general selection rule for the observation of a pure rotational spectrum is that a molecule must have a permanent electric dipole moment ($\boldsymbol{\mu}$). That is, for a molecule to give a pure rotational spectrum, it must be polar.⁷² Equation 2.16 becomes:

$$\boldsymbol{\mu}_{fi} = \langle Y_{J,f,M_{J,f}} | \hat{\boldsymbol{\mu}}_{\varepsilon v} | Y_{J,i,M_{J,i}} \rangle \quad (2.17)$$

The electric dipole moment has components $\mu_{\varepsilon v,x}$, $\mu_{\varepsilon v,y}$ and $\mu_{\varepsilon v,z}$ which, in spherical polar coordinates, are written in terms of μ_0 the magnitude of the vector, and the angles θ and ϕ . According to the properties of the spherical harmonics this integral vanishes unless⁷²:

$$\Delta J = \pm 1 \quad \Delta M_J = 0, \pm 1 \quad (2.18)$$

2. EXPERIMENTAL TECHNIQUES

2.1.2.2 Pure vibrational spectra

Harmonic approach

The most simplest molecular vibration is the motion of a diatomic system. In regions close to the minimum of the potential energy the curve can be approximated by a parabola, so we can write:

$$V(x) = \frac{1}{2}kx^2 \quad (2.19)$$

where k is the force constant of the bond and:

$$k = \left(\frac{d^2V(x)}{dx^2} \right)_{x_0} \quad (2.20)$$

and x_0 is the equilibrium position.⁷²

The Schrödinger equation for the relative motion of two atoms of masses m_1 and m_2 with a parabolic potential energy is:

$$-\frac{\hbar^2}{2m_{red}} \frac{d^2\psi}{dx^2} + \frac{1}{2}kx^2\psi = E\psi \quad (2.21)$$

where m_{red} is the reduced mass:

$$m_{red} = \frac{m_1m_2}{m_1 + m_2} \quad (2.22)$$

By solving the equation 2.21, the vibrational energy levels can be obtained:

$$E_v = \left(v + \frac{1}{2} \right) \hbar\omega \quad \omega = \left(\frac{k}{m_{red}} \right)^{\frac{1}{2}} \quad v = 0, 1, 2, \dots \quad (2.23)$$

The vibrational terms of a molecule $G(v) = E_v/hc$ are so:

$$G(v) = \left(v + \frac{1}{2} \right) \tilde{\nu} \quad \tilde{\nu} = \frac{1}{2\pi c} \left(\frac{k}{m_{red}} \right)^{\frac{1}{2}} \quad (2.24)$$

Returning to the analysis of the transition dipole moment, but in this case the molecule does not change electronic or rotational state. From the equation 2.16, the only important is $\langle v_f | \hat{\mu} | v_i \rangle$. If the dipole moment arises from two partial charges $\pm\delta q$ separated by a distance $R = R_e + x$, then its variation with displacement from the equilibrium separation, x , can be written as:

$$\mu = R\delta q = R_e\delta q + x\delta q = \mu_0 + x\delta q \quad (2.25)$$

where μ_0 is the electric dipole moment operator when the nuclei have their equilibrium separation. It then follows that, with $f \neq i$:

$$\langle v_f | \hat{\mu} | v_i \rangle = \mu_0 \langle v_f | v_i \rangle + \delta q \langle v_f | x | v_i \rangle = \langle v_f | x | v_i \rangle \delta q \quad (2.26)$$

Because:

$$\delta q = \frac{d\mu}{dx} \quad (2.27)$$

we can write the transition dipole moment more generally as:

$$\langle v_f | \hat{\mu} | v_i \rangle = \langle v_f | x | v_i \rangle \left(\frac{d\mu}{dx} \right) \quad (2.28)$$

and the right-hand side is zero unless the dipole moment varies with displacement. This is the general selection rule for infrared spectroscopy. The specific selection rule is determined by considering the value of $\langle v_f | x | v_i \rangle$. The wavefunctions for diatomic system can be written in terms of the Hermite polynomials and then it is possible to use their properties to evaluate the integral.

$$\langle v_f | x | v_i \rangle = \alpha^2 N_{v_f} N_{v_i} \left\{ v_i \int_{-\infty}^{\infty} H_{v_f} H_{v_i-1} e^{-y^2} dy + \frac{1}{2} \int_{-\infty}^{\infty} H_{v_f} H_{v_i+1} e^{-y^2} dy \right\} \quad (2.29)$$

where $x = \alpha y$ and $\alpha = (\hbar^2/m_{\text{eff}}k)^{1/4}$. It follows that the transition dipole moment is zero unless $\Delta v = \pm 1$. Transitions for which $\Delta v = +1$ correspond to absorption and those with $\Delta v = -1$ correspond to emission.

It follows from the Boltzmann distribution that almost all molecules will be in their vibrational ground states at room temperatures and at lower temperature. Hence, the dominant spectral transition will be the *fundamental transition*, $1 \leftarrow 0$. As a result, the spectrum is expected to consist of a single absorption line. If the molecules are in a vibrationally excited state, transitions between higher levels ‘hot bands’, for instance $5 \leftarrow 4$, $4 \leftarrow 3$, ... may also appear. In the harmonic approximation, all these bands lie at the same frequency, and the spectrum is also a single line. Moreover harmonic approximation cannot be correct at all extensions because it does not allow a bond to dissociate and all energy levels are equidistant.

Anharmonic approach

However the breakdown of the harmonic approximation causes the transitions to lie at slightly different frequencies, so several bands are observed and the energy levels become less widely spaced at high excitations.

If we span the potential V in Taylor series around the its minimum ($x_0 = 0$):

$$V(x) = V(0) + \left(\frac{dV}{dx} \right)_0 x + \frac{1}{2!} \left(\frac{d^2V}{dx^2} \right)_0 x^2 + \frac{1}{3!} \left(\frac{d^3V}{dx^3} \right)_0 x^3 + \dots + \frac{1}{n!} \left(\frac{d^nV}{dx^n} \right)_0 x^n \quad (2.30)$$

The term $V(0)$ can be set arbitrarily to zero. The first derivative of V is 0 at the minimum. Therefore, the first surviving term is the parabolic approximation. At high vibrational excitations the spread of the vibrational wavefunction allows the molecule to explore regions of the potential energy

2. EXPERIMENTAL TECHNIQUES

curve where the parabolic approximation is poor and additional terms in the Taylor expansion of V must be retained. The motion then becomes *anharmonic*, in the sense that the restoring force is no longer proportional to the displacement.

One approach to the calculation of the energy levels in the presence of anharmonicity is to use a function that resembles the true potential energy more closely, for instance the Morse function.

$$V(r) = D_e \left(1 - e^{-a(r-r_e)}\right)^2 \quad (2.31)$$

were r is the distance between the atoms, r_e is the equilibrium bond distance, D_e is the well depth, and a controls the 'width' of the potential. Anharmonicity also accounts for the appearance of additional weak absorption bands corresponding to the transitions $2 \leftarrow 0, 3 \leftarrow 0, \dots$, even though these first, second, ... overtones are forbidden by the selection rule $\Delta v = \pm 1$. The reason for the appearance of overtones is that the selection rule is derived from the properties of harmonic oscillator wave functions, which are only approximately valid when anharmonicity is present. Therefore, the selection rule is also only an approximation. For an anharmonic oscillator, all values of Δv are allowed, but transitions with $\Delta v > 1$ are allowed only weakly and if the anharmonicity is small.

2.1.2.3 Polyatomic molecules

A diatomic molecule have only one mode of vibration, the bond stretch. On the other hand the polyatomic molecules have several modes of vibration because all the bond lengths and angles may change and the vibrational spectra are very complex. For a nonlinear molecule that consists of N atoms, there are $3N-6$ independent modes of vibration. If the molecule is linear, there are $3N-5$ independent vibrational modes.⁷³ The active modes are subject to the specific selection rule $\Delta v_q = \pm 1$ in the harmonic approximation.⁷²

Normally, the description of the vibrational movement of the molecule is based on *normal modes* of vibration. One normal mode can be a linear combination of several vibrational coordinates. In the harmonic approach a normal mode is an independent, synchronous motion of atoms or groups of atoms that may be excited without leading to the excitation of any other normal mode.⁷²

Then the general selection rule for infrared activity is that the motion corresponding to a normal mode should be accompanied by a change of dipole moment. Using the same approximation than before, the eigenfunction is the product of electronic, a vibrational, and a rotational eigenfunction; then the transition dipole moment is represented as^{72,73}:

$$\boldsymbol{\mu}_{v_f v_i} = \langle v_f | \hat{\boldsymbol{\mu}} | v_i \rangle \quad (2.32)$$

This is the general vibrational selection rule for the infrared, which is valid as long as the interaction with rotation and electronic motion is neglected. In particular it is independent of whether or not the vibration is harmonic.⁷³

It is best to use group theory to judge the activities of more complex modes of vibration. This is easily done by checking the character table of the molecular point group for the symmetry species of the irreducible representations covered by x, y, and z, for their species are also the symmetry species of the components of the electric dipole moment.⁷² In order to ascertain whether a certain transition $v_f \leftarrow v_i$ is active in the infrared, therefore, it is only necessary to see whether the species of $v_f v_i$ is the same as at least one component of the dipole moment μ for the particular point group.⁷³

2.1.2.4 Vibration-rotation spectra

Each band of the high resolution vibrational spectrum of a gas-phase heteronuclear diatomic molecule is found to consist of a large number of closely spaced components. The separation between the components is less than 10 cm^{-1} , which suggests that the structure is due to rotational transitions accompanying the vibrational transition.

A detailed analysis of the quantum mechanics of simultaneous vibrational and rotational changes shows that the rotational quantum number J changes by ± 1 during the vibrational transition of a diatomic molecule. If the molecule also possesses angular momentum about its axis then the selection rules also allow $\Delta J = 0$.

The appearance of the vibration-rotation spectrum of a diatomic molecule can be discussed in terms of the combined vibration-rotation terms, S :

$$S(v, J) = G(v) + F(J) \quad (2.33)$$

If we ignore anharmonicity and centrifugal distortion,

$$S(v, J) = \left(v + \frac{1}{2}\right)\tilde{\nu} + BJ(J + 1) \quad (2.34)$$

When the vibrational transition $v + 1 \leftarrow v$ occurs, J changes by ± 1 and in some cases by 0 (when $\Delta J = 0$ is allowed). The absorptions then fall into three groups called *branches* of the spectrum. The *P branch* consists of all transitions with $\Delta J = -1$:

$$\tilde{\nu}_P(J) = S(v + 1, J - 1) - S(v, J) = \tilde{\nu} - 2BJ \quad (2.35)$$

This branch consists of bands at $\tilde{\nu} - 2B, \tilde{\nu} - 4B, \dots$ with an intensity distribution reflecting both the populations of the rotational levels and the magnitude of the $J - 1 \leftarrow J$ transition moment. The *Q branch* consists of all bands with $\Delta J = 0$, and its wavenumbers are all

$$\tilde{\nu}_Q(J) = S(v + 1, J) - S(v, J) = \tilde{\nu} \quad (2.36)$$

2. EXPERIMENTAL TECHNIQUES

for all values of J . This branch, when it is allowed, appears at the vibrational transition wavenumber. The R branch consists of bands with $\Delta J = +1$:

$$\tilde{\nu}_R(J) = S(v+1, J+1) - S(v, J) = \tilde{\nu} + 2B(J+1) \quad (2.37)$$

This branch consists of bands displaced from $\tilde{\nu}$ to high wavenumber by $2B, 4B, \dots$. The separation between the bands in the P and R branches of a vibrational transition gives the value of B .

The rotational constant of the vibrationally excited state, B_v is in fact slightly smaller than that of the ground vibrational state, B_0 , because the anharmonicity of the vibration results in a slightly extended bond in the upper state. As a result, the Q branch (if it exists) consists of a series of closely spaced bands. The bands of the R branch converge slightly as J increases; and those of the P branch diverge.⁷²

$$\tilde{\nu}_P(J) = \tilde{\nu} - (B_1 + B_0)J - (B_0 - B_1)J^2 \quad (2.38)$$

$$\tilde{\nu}_Q(J) = \tilde{\nu} + (B_1 - B_0)J(J+1) \quad (2.39)$$

$$\tilde{\nu}_R(J) = \tilde{\nu} + (B_1 + B_0)(J+1) - (B_0 - B_1)(J+1)^2 \quad (2.40)$$

2.1.2.5 The intensities of spectral bands

It is an important point that in the infrared spectroscopy, selection rules tell only whether a transition may occur but tell nothing about the intensities, which may be very low or even zero.⁷¹

It is noted from the experimental observation that infrared radiation intensity decrease is proportional to the distance l it travels in the matter:

$$-\frac{\delta I}{I} = b\delta l \quad (2.41)$$

where b is absorption coefficient. After solving this differential equation we get relation known as Lambert-Bouguer law:

$$\ln \frac{I_0}{I} = bl \quad (2.42)$$

Often this relation is written in decimal logarithmic form, where a is decimal absorption coefficient:

$$\log_{10} \frac{I_0}{I} = al \quad (2.43)$$

Relation $I/I_0 = T$ is called transmittance and usually presented in percents. It is related to another spectral quantity absorbance as: $A = -\log T$.

It was shown experimentally by A. Beer,⁷¹ that a radiation of intensity I_0 falls on the absorption cell of length l containing absorbing material of concentration c in the liquid phase. The radiation emerges with intensity I , and scanning the radiation through an appropriate wavenumber range of the

absorption, say $\tilde{\nu}_1$ to $\tilde{\nu}_2$, and measuring I_0/I produces the absorption spectrum typically measured as absorbance A which is proportional to c and l ; so that:

$$A(\tilde{\nu}) = \log_{10} \frac{I_0}{I} = \varepsilon(\tilde{\nu})cl \quad (2.44)$$

where ε is a function of $\tilde{\nu}$ and is the molar absorption coefficient or molar absorptivity or molar extinction coefficient. Since A is dimensionless, ε has dimensions of $(\text{concentration} \times \text{length})^{-1}$. By integration $\tilde{\nu}_1$ to $\tilde{\nu}_2$ the absorbance is possible to calculate the Einstein coefficient \mathcal{B} from⁷¹:

$$\int_{\tilde{\nu}_1}^{\tilde{\nu}_2} \varepsilon(\tilde{\nu}) d\tilde{\nu} = \frac{N_A h \tilde{\nu}_m \mathcal{B}}{\ln 10} \quad (2.45)$$

where $\tilde{\nu}_m$ is the average wavenumber of the absorption and N_A is the Avogadro constant.

2.1.2.6 Line width

The ubiquitous use of the word ‘line’ to describe an experimentally observed transition goes back to the early days of observations of visible spectra with spectroscopes in which the bands observed in, say, the spectrum of a sodium flame are images, formed at various wavelengths, of the entrance slit. The line is not infinitely narrow even if we assume that the instrument used for observation has not imposed any broadening of its own. We shall consider three important factors that may contribute to the line width and shape.⁷¹

1. *Natural line broadening.* This broadening is due to quantum mechanical effects. Specifically, when the Schrodinger equation is solved for a system that is changing with time, it is found that it is impossible to specify the energy levels exactly. If on average a system survives in a state for a time τ , the lifetime of the state, then its energy levels are blurred to an extent of order ΔE .

$$\Delta E \approx \frac{\hbar}{\tau} \quad (2.46)$$

This expression is reminiscent of the Heisenberg uncertainty principle, and consequently this lifetime broadening is often called ‘uncertainty broadening’. No excited state has an infinite lifetime; therefore, all states are subject to some lifetime broadening and, the shorter the lifetimes of the states involved in a transition, the broader the corresponding spectral bands.⁷²

If a state n is populated in excess of its Boltzmann population by absorption, the species M^* in this state will decay to the lower state until the Boltzmann population is regained. The decay is a first-order process, so that

$$-\frac{dN_n}{dt} = kN_n \quad (2.47)$$

2. EXPERIMENTAL TECHNIQUES

where k is the first-order rate constant and

$$\frac{1}{k} = \tau \quad (2.48)$$

Here, τ is the time taken for N_n to fall to $1/e$ of its initial value (where e is the base of natural logarithms) and is referred to as the lifetime of state n . If spontaneous emission is the only process by which M^* decays then k is the Einstein coefficient for spontaneous emission,⁷¹ i.e. $k = \mathcal{A}$ and:

$$\Delta E \approx \hbar \mathcal{A} \quad \text{or} \quad \Delta \nu \approx \frac{\mathcal{A}}{2\pi} \quad (2.49)$$

2. *Doppler broadening.* Whether radiation is being absorbed or emitted the frequency at which it takes place depends on the velocity of the atom or molecule relative to the detector. When a source emitting electromagnetic radiation of frequency ν moves with a speed v_a relative to an observer, for nonrelativistic speeds ($v_a \ll c$), the frequency ν_a at which a transition is observed to occur is related to the actual transition frequency ν in a stationary atom or molecule by:

$$\nu_a = \nu \left(1 - \frac{v_a}{c}\right)^{-1} \quad (2.50)$$

where c is the speed of light. Due to the usual Maxwell velocity distribution there is a spread of values of v_a and a characteristic line broadening given by:⁷¹

$$\Delta \nu = \frac{\nu}{c} \left(\frac{2kT \ln 2}{m}\right)^{1/2} \quad (2.51)$$

where m is the mass of the atom or molecule; this $\Delta \nu$ is normally far greater than the natural line width. The broadening is inhomogeneous, since not all atoms or molecules in a particular sample behave in the same way, and results in a line shape known as gaussian.

3. *Pressure broadening.* When collisions occur between gas phase atoms or molecules there is an exchange of energy, which leads effectively to a broadening of energy levels. If τ is the mean time between collisions and each collision results in a transition between two states there is a line broadening $\Delta \nu$ of the transition, where:

$$\Delta \nu = (2\pi\tau)^{-1} \quad (2.52)$$

derived from the uncertainty principle. This broadening is, like natural line broadening, homogeneous and usually produces a lorentzian line shape except for transitions at low frequencies, when an unsymmetrical line shape results.⁷¹

2.1.3 Infrared interferometers:

The Fourier-transform spectroscopy

The first instruments for measuring infrared absorption in the matter were based on dispersing light. The Figure 2.1 shows schematically the four main components – source, cell, dispersing element and detector – of an absorption experiment. The source is ideally a continuum in which radiation is emitted over a wide wavelength range with uniform intensity. The absorption cell containing the sample must have windows made from a material which transmits the radiation and it must also be long enough for the absorbance to be sufficiently high. After, the light is dispersed by a prism and intensity at each wavelength is measured by some detector. Latter prism based spectrometers were replaced by grating ones. The principle of operation of such instruments was very similar.

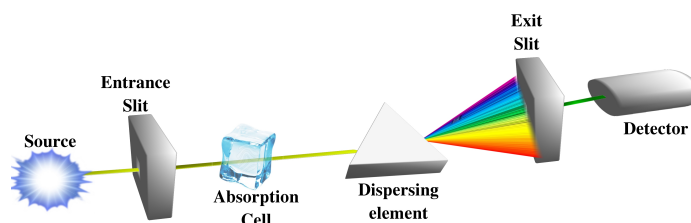


Figure 2.1: *The components of a typical absorption experiment*

Basic draw back of such instruments was very long measuring time. To obtain spectrum covering all middle infrared region with not very high (e.g. 0.5 cm^{-1}) spectral resolution one needed several hours.⁶⁸

The work of A. Michelson, who used interferometry to give very high resolution in atomic line spectra, is very well known. It was pointed out in 1952 by P.B. Fellgett,⁷⁴ that in principle interferometry also provides multiple advantage using broad-band sources in that an interferogram records the superimposed signals from all the different wavelengths presented to the detector. The separate signals at each wavelength can again be recovered from the combined interferogram by Fourier-transform mathematical analysis.

If an interferogram is measured over the same period of time as is required to record a dispersion spectrum with N resolution elements, then any single element will be recorded for an N -times longer period in the interferogram, giving a signal/noise advantage of \sqrt{N} .⁷⁵ Furthermore Jacquinot⁷⁶ emphasized the additional energy-throughput advantage of interferometers over dispersion spectrometers based on their circular apertures in comparison with the entrance slits of the former. In dispersive instruments resolution strongly depends on the slit width and in Fourier transform (FT) instruments mainly from the interferometer pass length. Spectral resolution in interferometry is determined by the reciprocal of the extreme path differences between the two beams. The main drawback of Fourier

2. EXPERIMENTAL TECHNIQUES

spectrometers, is the complicated mathematical procedure for obtaining absorption spectrum from interferogram.

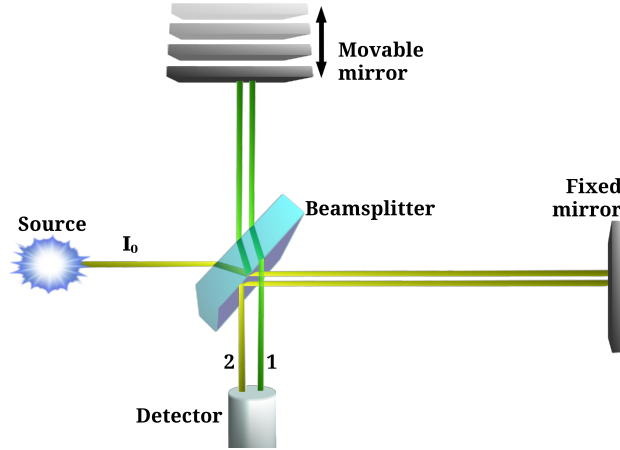


Figure 2.2: *Michelson interferometer*

Fourier transform mathematical analysis of the interferogram requires high computing power. It was not until the early 1970s when the development and incorporation of computers within spectrometers enabled the multiplex and energy-throughput advantages of interferometry to be exploited. Then, Fourier transform spectroscopy (FTS) was used to derive conventional intensity versus frequency spectra. Nowadays, with continued advances in computing speed, a 1000-point interferogram can be analyzed to give a normal intensity versus wavenumber spectrum in a fraction of a second.⁶⁸

As it is mentioned above working principle of FT spectrometers is based on interference of light. Main optical component in such instruments is Michelson interferometer figure 2.2. In the ideal Michelson interferometer, radiation coming from the source is collimated and then by the beamsplitter divided in two beams (or wave fronts). One beam is reflected by fixed mirror and another from moving mirror, in such a way creating the pathlength difference " δ " (often called retardation). The reflected beams are combined by the beamsplitter and then focused on the detector. The detected signal is the result of interference of two beams, and its intensity depends on the retardation $I(\delta)$.

If the interferometer is illuminated with a monochromatic radiation and if the beamsplitter is perfect, it divides the beam into two parts with equal intensity $I_0/2$, the output intensity of the interferometer is

$$I(\delta) = I_0(1 + \cos \delta) \quad (2.53)$$

where

$$\delta = \frac{2\pi x}{\lambda} = 2\pi\nu x \quad (2.54)$$

where x is the displacement of the moving mirror. The intensity in the optical axis of the interferometer follows a cosine function as:

$$F = I_0 [1 + \cos(2\pi\nu x)] \quad (2.55)$$

Let us now assume that the spectrum of the light source is continuous (often referred as “white light” indicating broad spectral region covered) and consists of a wide band of wavenumbers, so that the spectrum of the beams in both branches of the interferometer is $E(\nu)$. At a given optical path difference x , the interference signal from the infinitesimal spectral element between ν and $\nu + \delta\nu$ is

$$dF(x, \nu) = 2E(\nu) [1 + \cos(2\pi\nu x)] d\nu \quad (2.56)$$

Consequently, the total signal from the whole spectral band is

$$F(x) = 2 \int_0^{\infty} E(\nu) [1 + \cos(2\pi\nu x)] d\nu \quad (2.57)$$

$F(x)$ is called an *interference record*. An interference record is the total interference signal of the whole spectral band, measured as the function of the optical path difference x . A typical interference record is shown in Figure 2.3.

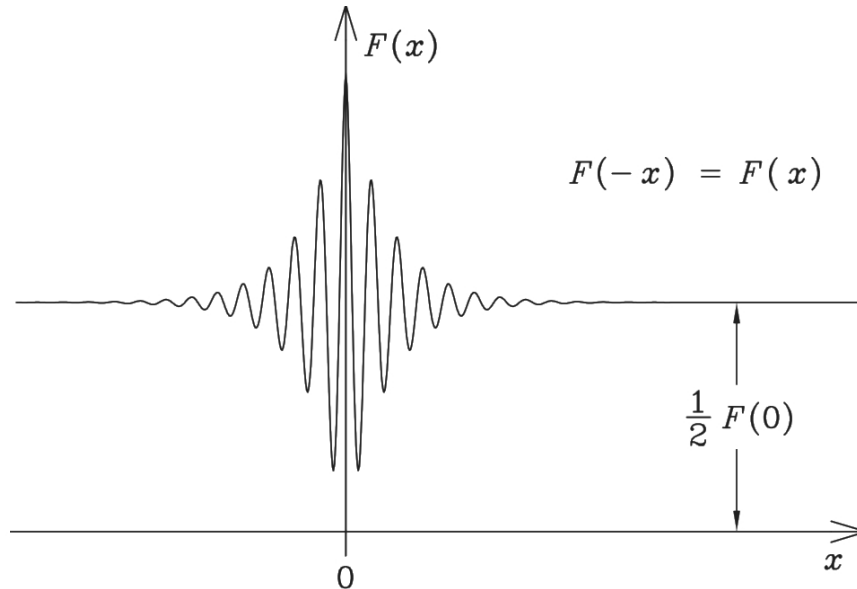


Figure 2.3: An interference record $F(x)$ ⁷⁷

If we subtract the constant term

$$\frac{1}{2}F(0) = 2 \int_0^{\infty} E(\nu) d\nu \quad (2.58)$$

2. EXPERIMENTAL TECHNIQUES

from the interference record $F(x)$, we obtain

$$I(x) = F(x) - \frac{1}{2}F(0) = 2 \int_0^{\infty} E(\nu) \cos(2\pi\nu x) d\nu \quad (2.59)$$

$I(x)$ is called an interferogram.

If we define $E(-\nu) = E(\nu)$, the computation is simplified, and we obtain

$$I(x) = \int_{-\infty}^{\infty} E(\nu) \cos(2\pi\nu x) d\nu = \int_{-\infty}^{\infty} E(\nu) e^{i2\pi\nu x} d\nu = \mathcal{F}\{E(\nu)\} \quad (2.60)$$

where \mathcal{F} is the FT. Hence, $I(x)$ and $E(\nu)$ form a FT pair, and they can be written as:

$$\begin{aligned} I(x) &= \int_{-\infty}^{\infty} E(\nu) e^{i2\pi\nu x} d\nu = \mathcal{F}\{E(\nu)\} \\ E(\nu) &= \int_{-\infty}^{\infty} I(x) e^{-i2\pi\nu x} dx = \mathcal{F}^{-1}\{I(x)\} \end{aligned} \quad (2.61)$$

In FTS, the output of a measurement is generally a signal in x -domain, and the most interesting information is obtained from the spectrum in ν -domain, which is calculated from the signal by inverse FT.

In practice, we compute the spectrum by Equation 2.61 at a set of discrete point with a sampling interval Δx . The data are collected only in the finite region from $x = -L$ to $x = L$, where $L = N\Delta x$. This construction results in loss of some spectral information when Fourier transform is performed and calculated spectra is somewhat corrupted. In order to solve this problem additional function in the Fourier integral is included. These are so called apodization functions.

Then, the Fourier integral is written as:

$$E_A(\nu) = \mathcal{F}^{-1}\{A(x)I(x)\} = \mathcal{F}^{-1}\{A(x)\} \otimes E(\nu) = W_A(\nu) \otimes E(\nu) \quad (2.62)$$

where $A(x)$ is the "apodization function", which equals unity at $x = 0$ and approaches zero smoothly at large values of $|x|$. There is a number of such functions applied in modern Fourier spectroscopy and particular function usually is chosen depending on experimental conditions.⁷⁷ In a particular case that the apodication function is the boxcar function:

$$A(x) = \begin{cases} 1 & \rightarrow |x| \leq L \\ 0 & \rightarrow |x| \geq L \end{cases} \quad (2.63)$$

then the $W_A(\nu)$ from equation 2.62 can be calculated as:

$$W_A(\nu) = \int_{-\infty}^{\infty} A(x) \cos(2\pi\nu x) dx = 2L \frac{\sin(2\pi\nu L)}{2\pi\nu L} = 2L \operatorname{sinc}(2\pi\nu L) \quad (2.64)$$

The sinc function has a full width measured at half high (FWHM) of $0.603/L$. Then the spectral resolution of Fourier spectrometers is also limited by the distance which moving mirror can travel. Spectral $\delta\tilde{\nu}$ resolution given by⁷¹:

$$\delta\tilde{\nu} \approx \frac{1}{2L} \quad (2.65)$$

In order to calculate Fourier integral correctly, one has to measure interferogram with a very high precision. The step between two points of the interferogram should fulfill condition:

$$\Delta x \leq \frac{1}{2} \lambda_{max} \quad (2.66)$$

In the infrared region this condition is achieved by using interference from He-Ne lasers ($\lambda_{max}=632.8$ nm) for the positioning of moving mirror.

2.1.4 Application of Infrared spectroscopy

Fourier transform spectroscopy (FTS) is frequently used in many various practical and scientific applications. The most important practical application of FT spectrometers is the qualitative and quantitative analysis of unknown samples. Conventionally, the analysis of a sample has taken place so that the user records the IR spectrum of the sample using some commercial instrument with its maximum resolution. Then, looking at the spectrum with the naked eye, or using some commercial search program based on the correlation between the observed and a library spectrum, the user tries to identify the unknown compound. The multicomponent analysis of a sample has usually taken place by the so-called subtraction technique: the library spectrum multiplied by a constant is subtracted from the observed mixture spectrum. The constant, which gives the desired concentration of the component, is determined in such a way that the corresponding component just disappears after subtraction. This analysis method, however, requires high resolution and is slow and laborious to carry out. It requires an experienced user, and it is very difficult to automatize.⁷⁷

An important scientific application of FTS is molecular spectroscopy. In this application, infrared FT spectrometers are used to study geometric structures of molecules, and the behavior of molecules in rotations and vibrations as well as the determination of the molecular potentials. The high resolution and accuracy in the wavenumber scale of the FT-IR spectrometer reveal quantum mechanical phenomena and interactions in an effective way.

2. EXPERIMENTAL TECHNIQUES

FT-IR spectroscopy is one of the most used method to study molecular complexes. It is known that under formation of intermolecular complexes certain bonds between atoms in the molecule are changed. Bond length between atom, participating in the intermolecular complex formation, and the rest of molecule is prolonged, as well additional constrain on the vibration of such atom is added. These effects can be observed from spectral band shifts in the infrared spectrum. Studies of the far infrared region of spectra can be even more informative. In this spectral region spectral bands associated with intermolecular vibrations are observed. Far infrared spectra of molecular complexes give detailed information on the shape of intermolecular potential energy function of the molecular complexes.⁷⁸

The infrared spectroscopy is, in general, a non destructive method of investigation. Probing the sample with infrared radiation does not change its properties, as well does not have any residual effects on it. The infrared spectroscopy can not only be used to measure IR spectra of the type of samples that have been classically investigated by IR spectrometers for decades, i.e. gases, liquids, bulk and powdered solids in milligram quantities, but interfacial species, microsamples, low temperature matrix isolation, low temperature low pressure gas phase cells, molecular beam techniques and trace analytes can now be characterized routinely. Nowadays Fourier transform spectrometers are fully controlled by computer. Measurement times have been reduced from minutes to a second; using special technique (step scan for example), reactions taking place in less than a microsecond can be followed. The physical properties of materials can be correlated to the molecular structure by vibrational spectroscopy better than by any other analytical technique.^{68,71,77}

2.2 Low temperature spectroscopy

2.2.1 Advantages of low temperature spectroscopy

Infrared spectroscopy of samples often faces some limitations. Spectral bands usually are broad therefore close laying spectral bands associated with the similar vibrations of different molecular structures may be partially or even completely overlapped and some important spectral data may be lost. In the very low pressure gas phase, the molecules can be observed unhindered by the environment, and very high-resolution spectra can be used to determine the physical properties of a molecular system. In practice this is nontrivial and requires knowledge of the approximate vibrational frequencies in advance. In this case, an absorption band consists of bands arising from a large number of transitions arising from rovibrational transitions, sometimes from excited vibrational states as well as the ground state. In high-density liquid states the interaction between different molecules will affect the spectrum

by causing perturbations of the rovibrational energy states and by reducing the lifetimes of the excited states through energy transfer processes.^{68,79}

At high temperatures not only the lowest vibrational levels are populated. Transitions from higher vibrational levels results in appearance of so called “hot” bands. Potential function is not harmonic, and transitions from zero to the first and from the first to the second levels have not the same energy. Another temperature dependent broadening reason is that at high temperatures, high rotational levels are populated. Transitions from different rotational levels result in broadening of not resolved rotational-vibrational bands. If the rotational structure is resolved (for the gas phase sample), high population of rotational levels results in very complicated rotational structure of the vibrational band.⁷¹

The number of rotational bands is significantly decreased when gases are cooled down. Population of rotational energy levels is given by Boltzmann distribution:

$$N_i = N_0 e^{-\frac{E_i - E_0}{kT}} \quad (2.67)$$

where N_i is number of particles in the current state, E_i is the energy of the state i , T temperature, and k is Boltzmann constant. At low temperature only transitions from low levels are possible. This results in much simpler and easier to interpret gas phase rotational spectra.⁷⁹ Most important advantages of low-temperature spectroscopic studies are: the elimination of hot transitions from the thermally populated vibrational states, sharpness and a significantly reduced overlap of the spectral bands.⁶⁸ Several techniques for low temperature spectroscopy have been developed, such as Liquefied Gases as Solvents for Vibrational Spectroscopy, supersonic jet, collisional cooling techniques, low temperature matrix isolation, etc.

2.2.2 Matrix isolation technique

In matrix isolation technique, a guest molecule is trapped at high dilution in a frozen solid (rare gas, N_2 , H_2 , O_2 , CO_2 , Cl_2 , CCl_4 and more) then, the IR spectrum of the guest molecules trapped in the host matrix can then be recorded. First of all, reaction between two separated species is quenched by isolation in a solid host, which enables the survival of transient species for extended time periods. This method was introduced by G. C. Pimentel and coworkers back in 1954.¹ In the first experiments matrix isolation technique was used for the isolation and stabilization of the free radicals.

Matrix samples are prepared by vapor co-deposition of a matrix gas (host) and the vapor of the guest molecule on a low temperature target (optical window or mirror), usually at temperatures between 20 and 4 K.⁸⁰ Population of vibrational and rotational level is given by Boltzmann distribution. Because the temperature of the sample is very low, therefore only the lowest vibrational energy level

2. EXPERIMENTAL TECHNIQUES

is populated. This means that the “hot” bands are not present in the low temperature spectrum. For the molecules isolated in the matrices the rotational motions are blocked except for very small molecules for which only lower rotational energy levels are populated. All these conditions results in simplification of the spectra.⁸¹

If the guest molecules comes into contact with each other, some physical and chemical changes can result. In matrices, the critical concentration for disappearance of guest-guest effects is not so well defined. Its depends on the relative size of guest and host molecules. It also depends on diffusion, i.e., the sample temperature, because a matrix is not an equilibrium solution, if the guests can diffuse through the matrix then they can aggregate irreversibly. It is generally assumed that in the matrix with matrix to guest (or radical) ratio (M/R) of 1000:1 the most of the guest is present as a monomer, but dimer and polymer spectra can be present up to an M/R ratio 100000:1 depending on the guest molecule. In absorption, guest-guest interaction influences fine details of the spectrum at M/R ratio of 1000:1 or smaller. It results in line broadening and frequency shifts, shoulders, and fine structure due to site distortion or dimer formation. In emission studies, guest-guest interaction can occur even at an M/R of 10000:1. It can result in sensitized fluorescence, depolarization, and changes of decay times.⁸⁰

The sample thickness depends on the oscillator strength of the optical transition that is to be observed. Any material that vaporizes without decomposition can be easily embedded in a matrix. Other molecules can be synthesized *in situ* by diffusion, controlled chemical reaction, or by laser ablation technique or photolysis of any vaporizable reagent.⁸⁰

Molecules which are isolated in a noble gas matrix can be characterized by a wide range of spectroscopic techniques. However, the most common and most powerful tool is vibrational spectroscopy. Similarity of infrared absorption spectra of matrix isolated samples to the spectra of gas phase samples is confirmed by experimental evidences. Although there is little interaction between host and matrix (Van der Waals interaction), environmental effects shift the IR absorptions of trapped species relative to those of unperturbed molecules in the gas phase (in general, $\delta\nu/\nu$ is on the order of 0.005).⁸² This change is often called the “matrix shift”. The matrix cage affects the vibrational coordinates of the trapped molecule, with the low force-constant coordinates experiencing a stronger influence than the high force-constant coordinates. Normal matrix effect is that all frequencies are red shifted with exception of special case where cage effect to the vibration is very important and overweight interactive effect. In comparison with bands in liquid or solid phase, the FWHM of infrared absorptions of matrix-isolated molecules are small (0.1 to 2 cm^{-1}), because intermolecular interactions, and hot transitions are prevented. Hence it is possible to resolve close lying vibrations of similar molecular structures such as conformers, and isomers; and to study weakly bound molecular complexes which are hard to study under normal temperature and pressure conditions.⁸²

Often spectral bands of matrix isolated samples are split, indicating different environments near the isolated molecules under study. The matrix shift and bands splitting can be caused by presence of some impurities, such as water or nitrogen and other atmospheric gases. It is also notable that in some cases the splitting is due to the existence of distinct trapping sites (*Site effects*) that differ only in the interaction of the guest with the matrix.⁸¹ The site effects is due to the fact that isolated particles occupy different substitutional lattice sites (which differ slightly in energy). Since this effect is connected with the geometry of guest and host species, the impact of a site effect depends on the matrix material (Ne, Ar, Kr, N₂, etc.)⁸² Different trapping sites in the matrix occur because of non-equilibrium process of matrix formation during sample deposition on cold substrate. The necessity of non-equilibrium deposition comes from Gibbs free energy condition. For the spontaneous mixing of substances under equilibrium conditions, change of free Gibbs energy should be negative:

$$\Delta G = \Delta H - T\Delta S < 0 \quad (2.68)$$

where G is the Gibbs energy, H is the enthalpy, T is temperature, and S is entropy.⁸³ Assuming that the matrix is ideally inert and do not interacts with substance under study, the enthalpy of mixing is positive ($\Delta H > 0$), because energy for the separation of individual molecules of substance under study is needed. Term $T\Delta S$ is always positive, but is small especially in the low temperature region. Therefore as it follows from 2.68 effective mixing can not be achieved under equilibrium conditions.⁸³ The resulting non-equilibrium matrices always exhibit some degree of disorder, which can be lowered by annealing process. However annealing procedure favors complex formation.⁸³

It should be noted, that it may be difficult in practice to determine whether a splitting of spectral bands is due to different chemical species (particularly different conformers) or to different trapping sites. Changing the matrix host is a common method for distinguishing between these options since spectral bands arising from different sites are usually much more sensitive to the nature of the matrix than the conformers relative population. Another conclusive method is changing the temperature of the gaseous mixture before deposition: a change in the relative gas phase population of conformers follows, leading to a corresponding change in the intensity of the spectral bands in the matrix.⁸¹

Matrix environmental influence to the substance under study is being evaluated both theoretically and experimentally. Generally it is hard to construct good theoretical model which would take into account all phenomena occurring in the process of matrix formation. Quality of the sample is very dependent on the conditions of individual experiment therefore only very general evaluation can be applied. From the empirical observations it is noted that matrix influence on the sample is very dependent on the polarizability of the molecules of matrix. Frequency shifts of the spectral bands from the gas phase values for the substances isolated in neon matrices are very small.⁷⁸

2. EXPERIMENTAL TECHNIQUES

Nature provides several examples of matrix isolation. Traces of H_2O_2 , for instance, formed photochemically in the atmosphere are trapped in Greenland's glaciers. The variation of the H_2O_2 concentration with the depth makes it possible to draw conclusions about the activity of the sun over the past 20000 years. Another interesting case of a prehistoric matrix is *Lapis lazuli*. The blue color of this mineral is due to S_3^- radical anions, isolated in a lattice of aluminosilicate. In solution, the S_3^- ion is short-lived. However, science has extended nature's possibilities in stabilizing especially short-lived species by using frozen noble gases at low temperature as host materials.⁸² Their inherent simplicity may actually make them ideal models also for more complex unconventional environments, which appear to be of crucial importance in biological and many industrial applications.⁸¹

2.2.3 Molecular hydrogen matrices

Noble gases are the most often used as matrix host because of their chemical inertness and simplicity of physical properties when compared with molecular matrices such as H_2 , N_2 , CO , CO_2 and others. However due to homogeneous and inhomogeneous line broadening, the resolution of matrix isolation spectroscopy is limited. For the long time it was considered that high resolution spectroscopy comparable to the gas phase is not possible.²⁷

Molecular hydrogen is used as a matrix host almost since the beginning of matrix isolation history.⁸⁴ Strommen and coworkers studied water dimer isolated in D_2 matrices.⁸⁴ Solid molecular matrices were not very extensively used because of somewhat complicated experimental technique. In order to prepare such matrices one should use temperatures of the order of 4 K and below. Additional argument usually used against solid hydrogen is that similar results on guest substances (dopant) can be obtained by using simpler experimental techniques and such an available matrix host as nitrogen.

It is since 1989 that the use of molecular hydrogen matrices in the infrared spectroscopy experiments increased. The works of Okumura, Chan and Oka in 1989⁸⁵ discovered that the bandwidth of rotational transition in solid pH_2 was 0.006 cm^{-1} at FWHM. This work was followed by finding the stimulated Raman transition of solid pH_2 .²⁷ The bandwidth of rotational-vibrational transition of deuterated hydrogen is even narrower, exceeding Doppler-limited bandwidth of the transition in the gas phase by one order of magnitude.⁸⁶

In the solid state, molecular hydrogen has a number of features which distinguish it from other (molecular) solids. Most important and simplifying is that, even in the solid, the free rotor states that describe the rotational motions of an isolated molecule are almost undistorted by the interactions with neighbors. Thus the solid can be visualized as an assembly of molecules all translationally localized at lattice sites but freely rotating even at $T=0 \text{ K}$!. This remarkable state is a consequence of the large molecular rotational constant (small moment of inertia) and the weak anisotropic forces which are

a result of the almost spherical molecular charge distribution and the relatively large intermolecular nearest neighbor distances ($\sim 3.79 \text{ \AA}$) in the zero pressure solid. The figure 2.4 shows a plot, proposed by Silvera,²⁸ of the radial distribution of the electronic charge density of the hydrogen molecule in the ground electronic state.

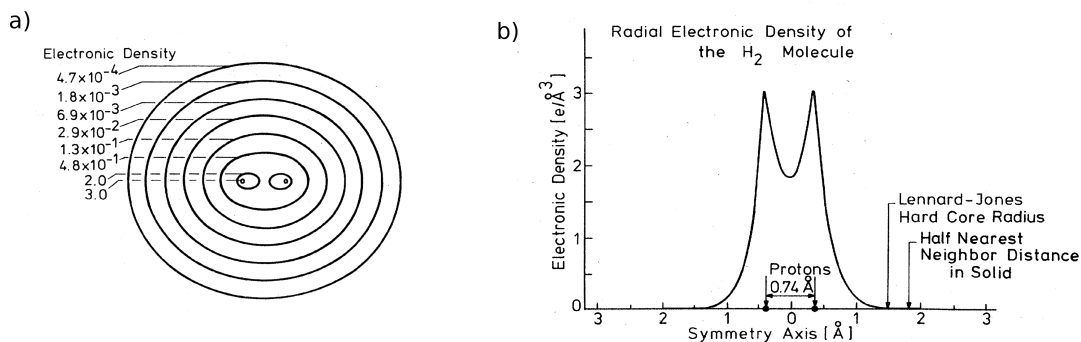


Figure 2.4: The electronic charge density of the hydrogen molecule. (a) Contours of equal density. (b) Density along the symmetry axis.²⁸

The nuclear spin state of diatomic hydrogen is antisymmetric (antiparallel, singlet state) or symmetric (parallel, triplet state) then hydrogen molecule has two species, para and ortho, which are associated with rotational states of even and odd quantum numbers respectively. Transitions between these states are forbidden for isolated molecule and as a result samples of almost pure para or ortho species can be prepared. If out-of-equilibrium samples are prepared they will remain metastably for long enough periods of time to allow detailed studies. The ground-state para species are spherical whereas the ortho are anisotropic in charge distribution. By varying the concentration of these species one can easily "turn the anisotropic interactions on and off." At room temperature hydrogen gas consists of three quarters of ortho-Hydrogen ($o\text{H}_2$) and one quarter of $p\text{H}_2$. This mixture is often referred as normal hydrogen (n-hydrogen).²⁷

Hydrogen molecule (H_2) is the smallest stable molecule, therefore it possess very large rotational constant ($\sim 60.8 \text{ cm}^{-1}$).²⁷ In figure, 2.5 Silvera shows the rotational levels of H_2 molecule and its energy gaps. The reason for the large physical distinction between the species can be seen from considering the rotational energy levels for H_2 . Due to the very large splittings of the rotational levels (354.38 cm^{-1} for $J=0 \rightarrow J=2$ and 587.06 cm^{-1} for $J=1 \rightarrow J=3$), at the low temperatures of the solid hydrogens ($\lesssim 20 \text{ K}$), only the $J=0$ and 1 levels are thermally populated (a $J=1$ molecule will remain metastably in that level, as conversion to the $J=0$ level is very slow in the solid). Since the single molecule rotational wave functions are the spherical harmonics, $Y_{jm}(\theta, \phi)$, all $p\text{H}_2$ molecules will be in the spherically symmetric Y_{00} states, and all $o\text{H}_2$ molecules will be in the p -like states Y_{1m} .

2. EXPERIMENTAL TECHNIQUES

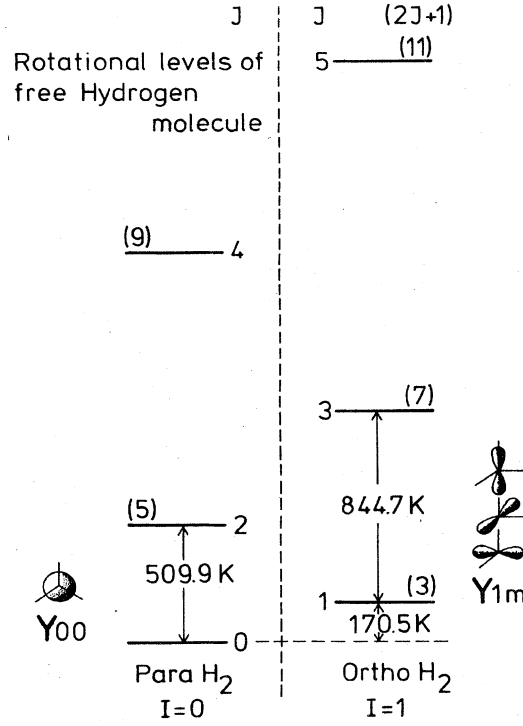


Figure 2.5: The molecular rotational energy levels for an isolated H₂ molecule. The angular distribution of the two lowest rotational states are also indicated (Y₁₀ and Y₁₁±Y₁₋₁ are actually shown). I is the total nuclear spin. Numbers in parenthesis are the m degeneracies²⁸

One would expect solid pH₂ to behave somewhat like solid helium, interacting isotropically, whereas anisotropic interactions between molecules should be important in solid oH₂.²⁸ Thus, although pH₂ is a diatomic molecule, its electrostatic character is spherical as rare gas atoms. An interaction between pH₂ molecules is extremely weak.

Para-Hydrogen (pH₂) crystals have a hexagonal close packed (hcp) structure, which is described using symmetry point group D_{3h}. It is a translational quantum solid. In such solids, at T=0, the particles are not sharply localized at lattice sites due to the large zero point motion (ZPM). This large ZPM is a result of the weak isotropic intermolecular potential and the light mass. The ground state of a solid is determined by hamiltonian²⁸:

$$H = -\frac{1}{2}\lambda^2 \sum_i \nabla_i^2 + \frac{1}{2} \sum_{i \neq j} V(i, j) \quad (2.69)$$

where, ∇^2 is Laplace operator, and λ is the Boer quantum parameter given by:

$$\lambda = \frac{\hbar}{\sigma \sqrt{m\varepsilon}} \quad (2.70)$$

λ is a measure of the relative contributions of kinetic versus potential energies, approximated by a sum over all pair-wise interactions. Parameters σ and ε are the core radius and potential well depth, from the Lenard-Jones (6-12) pair potential²⁸:

$$V = \varepsilon \left[\left(\frac{\sigma}{r} \right)^{12} - \left(\frac{\sigma}{r} \right)^6 \right] \quad (2.71)$$

The lighter the particle and shallower the potential (smaller ε), the larger is λ . For example $\lambda^2(\text{H}_2)=0.076$, $\lambda^2(\text{Ne})=0.0049$ and $\lambda^2(\text{Ar})=0.0027$.

Large contribution of zero-point vibration kinetic energy in the hydrogen crystal causes repulsion between molecules to result in the large lattice constant. The distance between hydrogen molecules in crystal is between 10-20% larger than the distance of $\text{H}_2\text{-H}_2$ cluster in the gas phase. Localization of the particles in the crystal to their equilibrium positions is given by the ratio of the root-mean-square (RMS) vibration amplitude relative to the lattice constant.²⁸ RMS amplitude is the linear function of λ . Localization parameter calculated for H_2 , Ne and Ar at 0 K respectively is 0.18, 0.09 and 0.05.⁸⁷ As it is seen from these results argon atoms are almost localized at they equilibrium position in the crystal while H_2 amplitude is 18 % of the lattice constant. Therefore solid pH_2 is considered as a spacious and “soft” medium compared with ordinary rigid, non-quantum solids such as noble gases.

As stated above, all averaged permanent multipole of pH_2 are zero, while oH_2 has a quadrupole moment as the lowest multipole moment. The existence of oH_2 in solid pH_2 causes inhomogeneities of internal electrostatic field which leads to spectral line broadening in spectroscopic measurements when solid pH_2 is used as a matrix. Therefore, for spectroscopic applications the concentration of oH_2 should be reduced as much as possible. In the figure 2.6 Silvera plots the ortho-para concentration dependence with the temperature. At thermal equilibrium, the concentration of oH_2 is 75% at room temperature, approximately 0.4% at the boiling point of liquid hydrogen (20.28 K at 1 atm), and approximately 0.0045% at the triple point (13.80 K). Therefore, the conversion should be carried out at temperatures as low as possible.²⁷

For isolated or noninteracting molecules, transition between para and ortho states is forbidden. As the temperature is varied, the population of the respective even or odd states varies due to interactions between molecules which can cause conversion.. If a H_2 molecule is converted by the magnetic field gradient due to the magnetic dipole moment on another H_2 molecule, then the conversion is intrinsic or homogeneous. In the solid state at zero pressure intrinsic conversion towards equilibrium takes place with a rate constant of 1.90%/h. For hydrogen, a magnetic field gradient can catalyze the transition.²⁸

In addition to the above structural features, the energy density of solid pH_2 is exceptionally sparse for a molecular solid because of the rotational constant of 60.853 cm^{-1} , the fundamental vibrational frequency of 4401.2 cm^{-1} , and the first excited electronic energy of 91700 cm^{-1} all exceed the corresponding parameters of other molecules. Furthermore, the Debye temperature, which characterizes

2. EXPERIMENTAL TECHNIQUES

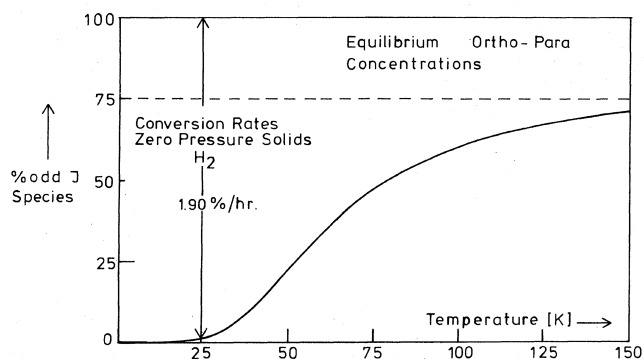


Figure 2.6: *Equilibrium ortho-para concentration of noninteracting hydrogen as a function of temperature*²⁸

the lattice motion in term of temperature, amounts to approximately 100 K ($\cong 70 \text{ cm}^{-1}$).²⁸ All this features imply that the relaxation of excited molecules in solid pH_2 is extraordinary slow, which means that bands are thinner than classical matrices. Moreover, small molecules such as CH_4 can rotate in a cryogenic pH_2 environment and the infrared spectra in this the matrix resemble the infrared spectra of the gas phase. Thus, the solid pH_2 can be superb medium for high-resolution matrix isolation spectroscopy.²⁷

Chapter 3

Experimental SetUp.

As outlined in Chapter 2, the matrix-isolation technique involves co-condensing a gaseous mixture of matrix atoms or molecules (host) and molecules under study (guest) onto a cold window. In this project the atomic rare gas was Neon (Ne) while molecular host used were para-Hydrogen ($p\text{H}_2$), normal-Hydrogen ($n\text{H}_2$), normal-Deuterium ($n\text{D}_2$) and the guest molecule was the acetylacetone (AcAc). The following sections present and describe the experimental set-up and techniques used to form matrix isolated samples of acetylacetone in these hosts and the apparatus employed to spectrally characterize samples and photo-reaction products. The chemical products used in the experiments are listed as well as the purity and supplier. After, the setup used for ortho/para conversion of hydrogen molecules is detailed followed by a brief explanation of the infrared spectra of hydrogen matrices. Next, the matrix-isolation equipment used to attain low sample temperatures is described together with the description of the matrix isolation sample preparation procedure and the UV laser system for irradiation of the sample is detailed. Finally, the infrared spectroscopic setups and detection methods are presented.

3.1 Chemical products

Normal-Hydrogen ($n\text{H}_2$) gaseous (99.9996%, Messer)(ortho/para ratio: 75/25).

Neon (Ne) gaseous (Ne 4,0 (99,99%) Messer).

Normal-Deuterium ($n\text{D}_2$) gaseous (D_2) (99,90 % Alpha Gaz).

Paramagnetic catalyst powder (Fe_2O_3 , powder, 5 micron diameter = 99% Sigma-Aldrich Company).

Liquid Acetylacetone (AcAc) (99.5% Sigma-Aldrich).

The Liquid AcAc, for the experiments, is maintained in a stainless-steel reservoir. Before experiments, AcAc is degassed in the vacuum (10^{-5} mbar). To degas AcAc liquid nitrogen is used to cool down the reservoir. At liquid nitrogen temperature the AcAc is solid and one can pump out the

3. EXPERIMENTAL SETUP.

impurities which remain in gas phase. When the pressure above the solid AcAc is again 10^{-5} mbar the liquid nitrogen is removed and the sample warms up to the room temperature. During the warming up, because of the vapor pressure of the liquid AcAc, the pressure starts to grow and the valve connecting the AcAc reservoir to the pump should be closed. Sample degassing procedure is repeated for 5-6 times, until there is not excess gas pressure above AcAc at liquid nitrogen temperature.

3.2 The para-hydrogen conversion.

The ortho/para conversion was done by following the description of Tam *et al.*^{88,89} A flow system using a catalyst bed maintained in a helium closed cycle cryostat (*Air Products Displex DF 202 S*) is used for the preparation of parahydrogen (pH_2). The figure 3.1 shows a schematic representation of the converter system.

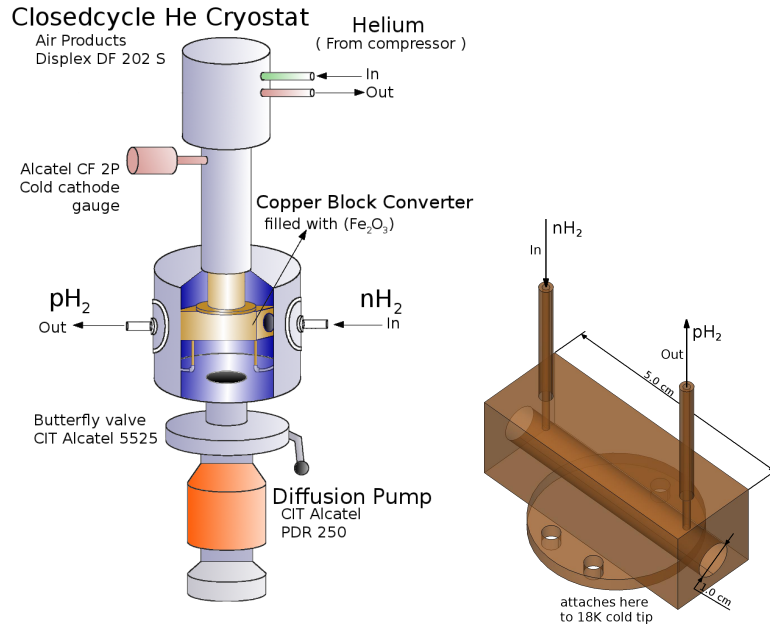


Figure 3.1: Schematics representation of the converter system. Copper block attached to the head of the converter cryostat (right)

A copper block converter (inner-diameter: 1 cm; length: 5 cm homemade) filled with a paramagnetic catalyst powder (Fe_2O_3) is attached to the heat exchanger of the cryostat which can reach a temperature close to 19 K. Lens cleaning paper (Kodak) are inserted into the inlet and outlet tubes of the converter in order to prevent catalyst from escaping from the converter. The inside of the cryostat is maintained under vacuum (10^{-6} mbar) by a diffusion pump *CIT Alcatel PDR 250* attached to the

system. The vacuum is monitored using a cold cathode gauge *Alcatel CF 2P* connected to a pressure reading unit *CIT-Alcatel-Annecy FA101*.

The inlet tube of the converter is connected to a 2.25 L reservoir filled with normal hydrogen. The flow rate of the hydrogen into converter is regulated by a needle valve. One pressure gauge is connected between the needle valve and the reservoir in order to control the pressure inside the reservoir (P_r). In normal experiments $P_r \approx 1.0$ bar. Between the needle valve and the converter another pressure gauge is connected to measure the pressure inside the converter (P_c). In order to fill the converter the needle valve is opened until $P_c \approx 0.5$ bar. Higher P_c may warm up the converter and no condensation of nH_2 will occur. When $\Delta P_r \approx -0.4$ bar about 40 mmol of nH_2 gas is condensed into the converter. The purity of para-Hydrogen (pH_2) is checked by infrared (IR) spectrum.

In figure 3.2, spectra of hydrogen matrices are shown. (a) nH_2 is deposited without conversion, (b) hydrogen is deposited after 60 min in the converter and (c) hydrogen is deposited after 90 min in the converter.

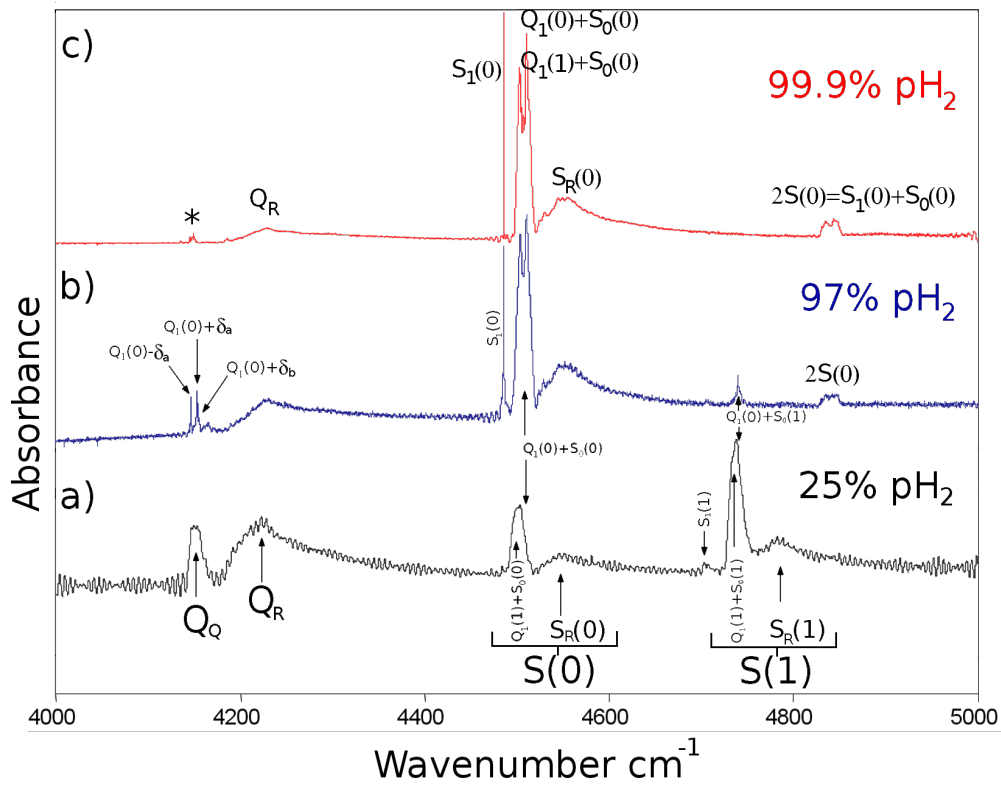


Figure 3.2: Fundamental bands of Hydrogen matrices. a) normal hydrogen (nH_2). b) 60 min in the converter (97% pure pH_2). c) 90 min in the converter (99.9% pH_2). (*) impurities induced pH_2 infrared bands.⁹⁰ Assignment of bands was done following Gush et al.⁹¹

Homonuclear diatomic molecules in gas phase do not absorb infrared radiation, as there is not

3. EXPERIMENTAL SETUP.

dipole moment change when the molecule vibrates. Nevertheless, because of the collisions between molecules, the distortion of the electron distribution induces infrared spectral bands. The theory of pressure-induced absorption in gaseous hydrogen⁹² shows that quadrupole interaction are responsible for most of the intensity of the S bands and a small part of the intensity of the Q branches; the greater part of the intensity of the Q branch is due to the overlap interaction of the colliding molecules. The fundamental bands assignment of hydrogen matrices was done carefully by Gush *et al.*⁹¹

1. The spectrum of solid hydrogen, see figure 3.2a, shows comparatively Q , $S(0)$, and $S(1)$ bands due to the quadrupolar interaction. Both rotational transitions groups, the $S(0)$ ($J = 0 \rightarrow J = 2$) transition for $p\text{H}_2$ and $S(1)$ ($J = 1 \rightarrow J = 3$) transition for $n\text{H}_2$, show weak single transition, $S_1(0)$ and $S_1(1)$, and much stronger double transition of the type $Q_1(J_1) + S_0(J_2)$, $J_{1,2} = 0, 1$. When the concentration of $p\text{H}_2$ increases (ortho-Hydrogen ($o\text{H}_2$) decreases), bands associated to rotational and double transitions involving ortho molecules decrease rapidly in intensity. The quadrupolar Q branch shows a structure which is interpreted as a double transition of the type $Q \pm \delta_i$, where δ_i are the small changes in the energy due to the orientational transitions of two ortho-molecules surrounding a para-molecule. In solid $p\text{H}_2$, see figure 3.2c, the bands become very sharp and double transitions $Q_1(0) + S_0(0)$, show a complex structure. The Q_q and $S(1)$ completely disappear.
2. Broad bands Q_R , $S_R(0)$, $S_R(1)$ are interpreted as combinations of the molecular rotational-vibrational frequencies with vibrational frequencies of the crystal lattice (phonon spectra). The phonon spectra show a maximum at the Debye temperature of the solid, and, at higher resolution, a structure indicative of the various branches of the lattice frequencies. A long extension of phonon spectrum towards high frequencies is probably due to multiple phonon creation.
3. Weak double transitions of the type $2S(0) = S_1(0) + S_0(0)$ in which one molecule executes a rotational-vibrational transition and the second molecule a purely rotational transition in the ground vibrational state are more clear in the spectrum of pure $p\text{H}_2$.

From the infrared absorption spectrum of hydrogen matrices it is possible to determine the percentage of $o\text{H}_2$ with respect to $p\text{H}_2$. The dependence of the $Q_1(0)$ band integrated intensity on the $o\text{H}_2$ and $p\text{H}_2$ fractions (F_o and F_p , respectively; $0 \leq F \leq 1$) is given by⁸⁸:

$$\frac{1}{l} \int \log_{10} \left(\frac{I_0}{I} \right) d\nu = aF_o^2 + bF_oF_p = bF_o + (a - b)F_o^2 \quad (3.1)$$

where l is the thickness of the sample. Thus, in the limit of low $o\text{H}_2$ concentrations, the $Q_1(0)$ band intensity is directly proportional to the $o\text{H}_2$ concentration. Typical value for constant b is $\approx 30\text{cm}^{-2}$ (ν in cm^{-1} and l in cm).⁸⁸ In practice the $Q_1(0)$ band analysis can be complicated because of the new

bands that appear in the same region due to some impurities (such as nitrogen, water or CO₂) in the sample.⁹⁰ Then, it is necessary to use the $Q_1(0) + S_0(1)$ band to estimate the purity of pH₂. When the band $Q_1(0) + S_0(1)$ are in the noise level, the purity of pH₂ is better than 99.9%.⁹³

3.3 Matrix deposition.

The cryostat used for matrix-isolation studies is presented in a simplified scheme in figure 3.3. It is a liquid-He flow cryostat (SMC, Air Liquide) equipped with an internal diamond window in a copper block for sample deposition. This cryostat has a reservoir for liquid helium pre-cooled at liquid Nitrogen temperature from an external surrounding reservoir (see figure 3.3). The liquid helium passes through a capillary tube to a small cavity (heat exchanger) where the evaporation and expansion take place. The helium flow in the capillary tube is also regulated by a needle valve. When the needle valve is fully opened the diamond window can be cooled down to 6 K. In order to decrease temperature below 6 K a primary rotary pump (gas pumping speed 16 m³/h) is connected to the outlet of the expansion cavity operating at maximum capacity. The aim is to decrease the pressure of the cavity and make more favorable helium expansion. The pressure of the expansion cavity is measured by a pressure gauge (range 1-1000 Torr, MKS Baratron Instrument 255 SPF, France). The needle valve regulating the flow through the capillary tube is set to have the desired pressure (12-18 torr).

To maintain very low temperatures good vacuum is necessary. Turbo pump LEYBOLD Turbovac 1000 is connected to the bottom of the window chamber reaching pressures lower than 10⁻⁷ mbar. Under these conditions the diamond window can be cooled below 3.6 K. The temperature in the copper block with attached diamond window is measured by a Si diode and monitored by a cryogenic temperature regulator SMC-TBT RGP 3000 (stabilization accuracy 0.1 K).

In figure 3.4 a drawing of the experimental setup is shown. The matrix is deposited onto the diamond window using two parallel stainless-steel tubes with 4 mm of internal diameter. The distance between those tubes and the diamond window can be regulated from 2 mm to 3 cm to enter inside the thermal shield. Liquid Acetylacetone is kept in a small stainless steel reservoir (several ml). In order to maintain constant conditions during the experiment and between different experiments, the Acetylacetone reservoir is kept at 0°C in an ice and water mixture bath (*AcAc ice bath* in figure 3.4). The molecules of Acetylacetone are deposited from one of those parallel stainless-steel tubes, para-hydrogen molecules coming from the converter are deposited using the other tube. By using needle valves it is possible to regulate both flows in order to obtain the desired Acetylacetone to matrix rate. The parameters used for deposition of the pH₂ matrices are typically:

Temperature in converter: 19 K.

Pressure in the converter after condensation: (0.3 -0.4) bar.

3. EXPERIMENTAL SETUP.

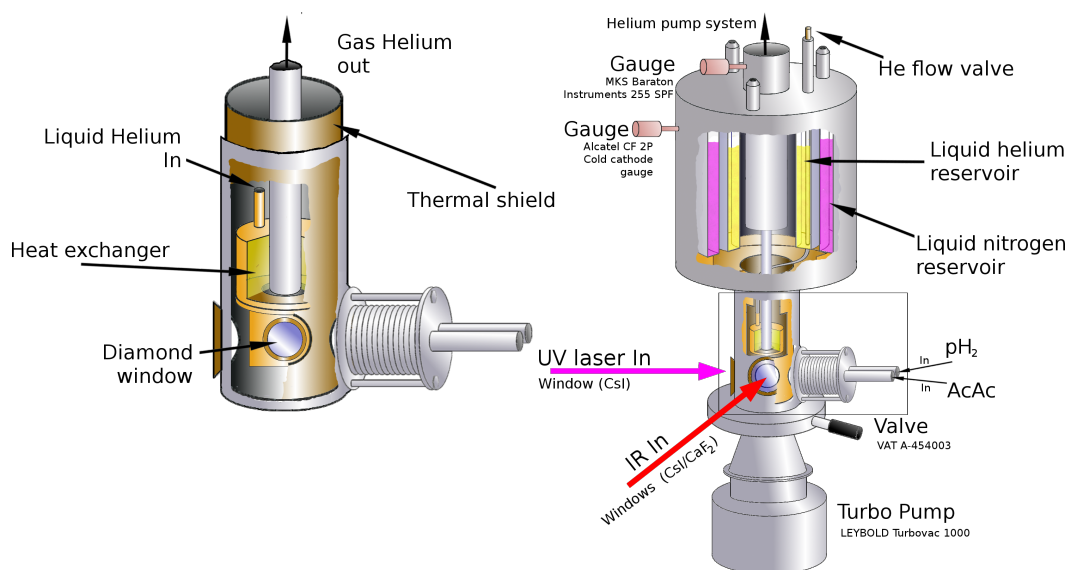


Figure 3.3: Simplify schema of the cryostat used for matrix deposition

Temperature of the diamond window: 4.1 K.

Distance between the inlet tubes and the diamond windows: 7 mm.

Pressure during deposition in the liquid-He SMC flow cryostat 10^{-6} mbar (control of the p_{H_2} flow).

Time of deposition 40-90 minutes.

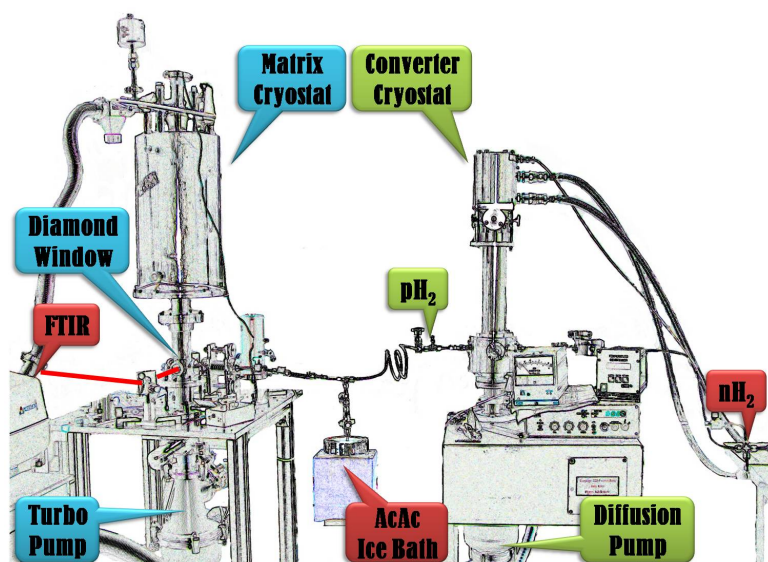


Figure 3.4: Drawing of the experimental setup

For Ne, nD_2 and nH_2 deposition, the same experimental setup configuration is used. For these

3.4 IR absorption spectroscopic technique.

hosts, no waiting time in the converter is necessary. In order to prevent Ne condensation in the converter the temperature of the converter is kept at ~ 40 K. In this way the converter cryostat is used to condense all the impurities that can be in the Ne gas. The needle valve for all experiments was set in such a way that matrix deposition conditions are kept similar as in pH_2 case.

The internal diamond window of the cryostat can rotate relatively to the outer shroud which is fixed to the optical table. The outer shroud has 3 external windows. Two external windows can be equipped with either CsI or CaF_2 windows to cover different spectral regions. And the 3rd one, used for UV irradiation, is a CaF_2 window. The main optical characteristics of the windows used for these experiments are summarized in table 3.1

	Diamond ⁹⁴	CsI ⁹⁵	CaF_2 ⁹⁵
Transmission	225nm to far IR, > 70% @ $10\mu\text{m}$	250nm to $55\mu\text{m}$	130nm to $9\mu\text{m}$
Refractive index	2.38 @ $10\mu\text{m}$, 2.41 @ 500nm	1.739 at $10.6\mu\text{m}$	1.40 @ $5\mu\text{m}$
Reflection Loss		13.6% @ $10.6\mu\text{m}$ (2 surfaces)	5.4% @ $5\mu\text{m}$ (2 surfaces)
Absorption coefficient	$\leq 0.10 \text{ cm}^{-1}$ @ $10\mu\text{m}$		
Bandgap	5.45 eV		
Dielectric constant	5.7		

Table 3.1: Main characteristics of the windows used in the experiments

3.4 IR absorption spectroscopic technique.

Infrared absorption spectra were measured using two Fourier Transform Infrared spectrometers “ATI Mattson Research Series FTIR” and “Nicolet Nexus 670/870”. Both spectrometers work in the mid infrared region ($500 - 5000 \text{ cm}^{-1}$). The highest resolution of Mattson spectrometer is 0.25 cm^{-1} and the highest resolution of Nicolet spectrometer 0.125 cm^{-1} . Both spectrometers have an infrared source Globar (SiC Silicon Carbide) heated to $\sim 1500 \text{ }^\circ\text{C}$

In most of the experiments, 0.5 cm^{-1} resolution was sufficient to completely resolve IR absorption bands. Several experiments were performed using 0.125 cm^{-1} resolution in order to check if the 0.5 cm^{-1} resolution is sufficient and record high resolution spectra when necessary. The spectrometers and the infrared beam pathway were purged with dry air in order to decrease the absorptions due to atmospheric water and CO_2 . Spectra were recorded using “Winfirst 3,61” software for Mattson spectrometer and “Omic 7.3” software for Nicolet spectrometer. In typical experiments 512 scans were recorded and averaged in order to get good signal to noise ratio in the spectrum. In all experiments a liquid nitrogen cooled MCT (HgCdTe Mercury Cadmium Telluride) detector was used which has an spectral range ($700\text{-}5000 \text{ cm}^{-1}$).

3. EXPERIMENTAL SETUP.

3.5 UV sources for irradiation of the sample

For UV irradiation five different sources were used. (1) YAG laser (266 nm) (Quantel) using two frequency doubling crystals. Excimer laser (Coherent Complex Pro 50 F) (2) using a gas mixture of ArF giving 193 nm and (3) using a gas mixture of KrF giving 248 nm, (4) Xe broad band lamp (Beckman Instrument GMBH) and (5) D₂ broad band lamp (200 - 400 nm) BAUSCH & LOMB DE 50A equipped with quartz glass. When it is necessary, metal grid are used to decrease the intensity of the lasers.

Chapter 4

Computational methods

This Chapter was written following essentially the formalism of three books, "*Handbook of Numerical Analysis*",⁹⁶ "*Computational Chemistry*"⁹⁷ and "*Essentials of Computational Chemistry. Theories and Models*".⁹⁸ The first section summarizes the necessity of theoretical simulation for better understanding of the experimental results. In this section the beginning of the theoretical calculation of molecular systems are also summarized. The Schrödinger equation and the need of Born–Oppenheimer approximations as a resolution method are also presented. The next two sections have extensive explanations of the Hartree-Fock (HF) and Density Functional Theory (DFT) methodologies for computational simulation of molecular systems. Then, the origin and meaning of some basis set are explained in the section **Basis sets**. Finally the anharmonic corrections are presented as a better but expensive method to improve the accuracy of computed vibrational frequencies for a molecular system.

4.1 General features

It is certainly not true that *all* macroscopic properties can be simply upscaled from the consideration of the short time behavior of a tiny sample of matter. Many of them proceed from ensemble or bulk effects, that are far from being easy to understand and to model. On the other hand, many macroscopic phenomena can be explained from elementary processes which take place at the atomic scale. For example the spectroscopical data of one system are the macroscopic observables of the spatial distribution of nuclei and electrons in the system. Interpretation of modern spectroscopical data is often impossible without high level theoretical calculations. One of the hardest parts of interpreting spectral data is the assignment of spectral bands to the corresponding vibrations of nucleus in the molecular system. This assignment for the large molecules can be quite difficult due to the large number of closely laying spectral bands. In order to aid this assignment computer simulations to

4. COMPUTATIONAL METHODS

calculate the vibrational frequencies of molecules must be employed. It is therefore founded to simulate the behavior of matter at the atomic scale in order to understand what is going on at the macroscopic one. Starting from the basic principles of quantum mechanics to model the matter at the subatomic scale, one finally uses statistical mechanics to reach the macroscopic scale. In the subatomic scale, the behavior of nuclei and electrons is governed by the Schrödinger equation, either in its time dependent form.^{96–98}

$$i\hbar\frac{\delta\Psi(t)}{\delta t} = \hat{H}\Psi(t) \quad (4.1)$$

or in its time independent form

$$\hat{H}\Psi = E\Psi \quad (4.2)$$

where H is a Hamiltonian operator, Ψ is the wavefunction and E energy as an eigenvalue of the system. The typical form of the Hamiltonian operator with which we will be concerned takes into account five contributions to the total energy of a system: the kinetic energies of the electrons and nuclei, the attraction of the electrons to the nuclei, and the interelectronic and internuclear repulsions.

$$H = -\sum_i \frac{\hbar^2}{2m_e} \nabla_i^2 - \sum_k \frac{\hbar^2}{2m_k} \nabla_k^2 - \sum_i \sum_k \frac{e^2 Z_k}{r_{ik}} + \sum_{i<j} \frac{e^2}{r_{ij}} + \sum_{k<l} \frac{e^2 Z_k Z_l}{r_{kl}} \quad (4.3)$$

where i and j run over electrons, k and l run over nuclei, \hbar is Planck's constant divided by 2π , m_e is the mass of the electron, m_k is the mass of nucleus k , ∇^2 is the Laplacian operator, e is the charge on the electron, Z is an atomic number, and r_{ab} is the distance between particles a and b .⁹⁸

In more complicated situations, e.g., in the presence of an external electric field, in the event of significant spin–orbit coupling in heavy elements, taking account of relativistic effects, etc., other terms are required in the Hamiltonian.⁹⁸

After Schrödinger wrote down his famous equation in 1926, quantitative aspects were investigated. But it rapidly appeared that an exact solution for the Schrödinger equation cannot be found when the system contains three particles or more. Consequently approximations had to be introduced. The first one historically speaking and on which rely almost all quantum chemical calculations is the so-called Born-Oppenheimer approximation (proposed by Born and Oppenheimer in 1927).⁹⁶

Under typical physical conditions, the nuclei of molecular systems are moving much more slowly than the electrons (recall that protons and neutrons are about 1800 times more massive than electrons and note the appearance of mass in the denominator of the kinetic energy terms of the Hamiltonian in equation 4.3). For practical purposes, electronic ‘relaxation’ with respect to nuclear motion is instantaneous. As such, it is convenient to decouple these two motions, and compute electronic energies for fixed nuclear positions. That is, the nuclear kinetic energy term is taken to be independent of the electrons, correlation in the attractive electron–nuclear potential energy term is eliminated, and

the repulsive nuclear–nuclear potential energy term becomes a simply evaluated constant for a given geometry. Thus, the *electronic* Schrödinger equation is taken to be⁹⁸:

$$(H_{\text{el}} + V_N)\Psi_{\text{el}}(\vec{q}_i; \vec{q}_k) = E_{\text{el}}\Psi_{\text{el}}(\vec{q}_i; \vec{q}_k) \quad (4.4)$$

where the subscript ‘el’ emphasizes the invocation of the Born–Oppenheimer approximation, H_{el} includes only the first, third, and fourth terms on the right hands (r.h.s.) of equation 4.3, V_N is the nuclear–nuclear repulsion energy, and the electronic coordinates \vec{q}_i are independent variables but the nuclear coordinates \vec{q}_k are parameters. The eigenvalue of the electronic Schrödinger equation is called the *electronic energy*.⁹⁸

In general, the Born–Oppenheimer assumption is an extremely mild one, and it is entirely justified in most cases. It is worth emphasizing that this approximation has very profound consequences from a conceptual standpoint – so profound that they are rarely thought about but simply accepted as dogma.

Quantum chemistry calculations performed in the Born–Oppenheimer approximation described above mainly consist⁹⁶:

- either in solving the geometry optimization problem, that is to compute the equilibrium molecular configuration that minimizes the energy of the system. Finding the most stable molecular configuration is an interesting result *per se* but is also a first stage in the computation of numerous properties like for instance infrared spectrum or elastic constants.
- or in performing an *ab initio* molecular dynamics simulation, that is to simulate the time evolution of the molecular structure according to the Newton law of classical mechanics

For a given nuclear configuration, it follows from the Born–Oppenheimer approximation that the energy of the system can be in turn obtained by solving a time independent Schrödinger equation of type 4.2 but of lower complexity than the original one since it concerns electrons only. Such a procedure permits to obtain an analytical calculation of the potential energy for the H_2^+ ion, which contains a unique electron; however, it is again not possible to solve (neither analytically nor computationally) for systems with more than one electron. One therefore resorts to further approximations of this problem. These approximations can typically be classified into two categories. The first category is that of the so-called *ab initio* methods. The term *ab initio* is Latin for ‘from the beginning’. These methods remain based only upon the first principles of quantum mechanics without any empirical parameter (except some fundamental constants of Physics). The typical example for such methods is the HF approximation and its improvements. Another wide class of instances of this category of methods consists of the ones issued from the DFT.⁹⁶

4.2 Hartree-Fock (HF) calculation

The most commonly used type of *ab initio* calculation is a Hartree-Fock (HF) calculation.⁹⁷ Because the Schrödinger equation does not have separate solutions due to the interelectronic interactions a first crude approximation was proposed by *Hartree* in 1928 who proposed an iterative self-consistent field (SCF) method. In the first step of the SCF process, one guesses the wave functions ψ for all of the occupied Molecular Orbital (MO) and uses these to construct the necessary one-electron operators. Solution of each differential equation provides a new set of ψ , presumably different from the initial guess. Then, new one-electron Hamiltonian are formed using these presumably more accurate ψ which are used as initial set. The process is repeated to obtain a still better set of ψ . At some point, the difference between a newly determined set and the immediately preceding set falls below some threshold criterion, and is referred the final set of ψ as the ‘converged’ SCF orbitals. The main problem of Hartree’s approximation is that it do not take into account the possibility of two electrons in the same MO.^{97,98}

The Hartree approximation was rapidly improved by Fock and Slater in 1930 as follows; first, due to the Pauli exclusion principle no more than two electrons can be in the same orbital state; secondly, electrons are physically indistinguishable from one to another and the wavefunction should be antisymmetric to the interchange of any two sets of coordinates. The fundamental assumption of HF theory, that each electron sees all of the others as an average field, allows for tremendous progress to be made in carrying out practical MO calculations. However, neglect of electron correlation can have profound chemical consequences when it comes to determine accurate wave functions and properties derived therefrom. Thus, HF theory, in spite of its fairly significant fundamental assumption, was adopted as useful in the *ab initio* philosophy because it provides a very well defined stepping stone on the way to more sophisticated theories (i.e., theories that come closer to accurate solution of the Schrödinger equation). To that extent, an enormous amount of effort has been expended on developing mathematical and computational techniques to reach the HF limit, which is to say to solve the HF equations with the equivalent of an infinite basis set, with no additional approximations.⁹⁸

Furthermore, from a practical standpoint, HF theory posed some very challenging technical problems to early computational chemists. One problem was the choice of a basis set. The linear combination of atomic orbitals (LCAO) approach using hydrogenic orbitals remains attractive in principle; however, this basis set requires numerical solution of the four-index integrals appearing in the Fock matrix elements, and that is a very tedious process. Moreover the number of four-index integrals is daunting. Since each index runs over the total number of basis functions, there are in principle N^4 total integrals to be evaluated, and this quadratic scaling behavior with respect to basis-set size proves to be the bottleneck in HF theory applied to essentially any molecule.⁹⁸

One of the limitations of HF calculations is that they do not include electron correlation. This means that HF takes into account the average effect of electron repulsion, but not the explicit electron-electron interaction. Within HF theory the probability of finding an electron at some location around an atom is determined by the distance from the nucleus but not the distance to the other electrons. This is not physically true, but it is the consequence of the central field approximation, which defines the HF method.⁹⁸

A number of types of calculations begin with a HF calculation and then performs correction for correlation. Møller-Plesset in 1934 based on Rayleigh-Schrödinger perturbation theory:

$$\mathbf{H} = \mathbf{H}^{(0)} + \lambda \mathbf{V} \quad (4.5)$$

proposed to use the sum of the one-electron Fock operators as the not perturbed operator and the electron correlation as a perturbation. The application of their prescription is now typically referred by the acronym MP n where n is the order at which the perturbation theory is truncated, e.g., MP2, MP3, etc.⁹⁸

The MP approach takes $\mathbf{H}^{(0)}$ to be the sum of the one-electron Fock operators f_i :

$$\mathbf{H}^{(0)} = \sum_{i=1}^n f_i \quad (4.6)$$

where n is the number of basis functions. In addition, $\Psi^{(0)}$ is taken to be the HF wave function, which is a Slater determinant formed from the occupied orbitals. It is straightforward to show that the eigenvalue of $\mathbf{H}^{(0)}$ when applied to the HF wave function is the sum of the occupied orbital energies:

$$\mathbf{H}^{(0)}\Psi^{(0)} = \sum_i^{occ.} \varepsilon_i \Psi^{(0)} \quad (4.7)$$

where the orbital energies are the usual eigenvalues of the specific one-electron Fock operators. In the equation 4.7 each orbital energy includes the repulsion of the occupying electron(s) with all of the other electrons. Thus, each electron–electron repulsion is counted twice (once in each orbital corresponding to each pair of electrons). So, the perturbation term \mathbf{V} must be the difference between counting electron repulsion once and counting it twice. Thus,

$$\mathbf{V} = \sum_i^{occ.} \sum_{j>i}^{occ.} \frac{e^2}{r_{ij}} - \sum_i^{occ.} \sum_j^{occ.} \left(J_{ij} - \frac{1}{2} K_{ij} \right) \quad (4.8)$$

where the first term on the r.h.s. is the proper way to compute electron repulsion (and is exactly as it appears in the Hamiltonian of Eq 4.3) and the second term is how it is computed from summing

4. COMPUTATIONAL METHODS

over the Fock operators for the occupied orbitals where J_{ij} and K_{ij} are the Coulomb and Exchange operators defined by:

$$J_{ij} = e^2 \iint |\psi_i(1)|^2 \frac{1}{r_{12}} |\psi_j(2)|^2 d\vec{r}_1 d\vec{r}_2 \quad (4.9)$$

$$K_{ij} = e^2 \iint \psi_i(1)\psi_j(1) \frac{1}{r_{12}} \psi_i(2)\psi_j(2) d\vec{r}_1 d\vec{r}_2 \quad (4.10)$$

By evaluation first-order in Møller-Plesset perturbation theory (e.g. MP1) we can easily note that the energy correct is in fact the Hartree-Fock energy. As MP1 does not advance us beyond the HF level in determining the energy, we must consider the second-order correction (e.g. MP2) to obtain an estimate of correlation energy. The scaling behavior of the MP2 method is roughly N^5 , where N is the number of basis functions. Analytic gradients and second derivatives are available for this level of theory, so it can conveniently be used to explore potential energy surfaces (PESs). MP2, and indeed all orders of MP_n theory, are size-consistent, which is a particularly desirable feature.⁹⁸

However, it should be noted that the Møller-Plesset formalism is potentially rather dangerous in design. Perturbation theory works best when the perturbation is small. But, in the case of MP theory, the perturbation is the full electron-electron repulsion energy, which is a rather large contributor to the total energy. So, there is no reason to expect that an MP2 calculation will give a value for the correlation energy that is particularly good. In addition, the MP_n methodology is not variational. Thus, it is possible that the MP2 estimate for the correlation energy will be too large instead of too small⁹⁸

In general, *ab initio* calculations give very good qualitative results and can yield increasingly accurate quantitative results as the molecules under study become smaller. The advantage of *ab initio* methods is that they eventually converge to the exact solution once all the approximations are made sufficiently small in magnitude. However, this convergence is not monotonic. Sometimes, the smallest calculation gives a very accurate result for a given property. There are four sources of error in *ab initio* calculations:

1. The Born-Oppenheimer approximation.
2. The use of an incomplete basis set
3. Incomplete correlation
4. The omission of relativistic effects

The disadvantage of *ab initio* methods is that they are expensive.⁹⁸ These methods often take enormous amounts of computer processor time, memory, and disk space. The HF method scales as N^4 , where N is the number of basis functions. This means that a calculation twice as big takes 16

times as long to complete. Correlated calculations (MP n for instance) often scale much worse than this. In practice, extremely accurate solutions are only obtainable when the molecule contains ten electrons or less.^{97,98}

4.3 Density functional theory (DFT)

”The wave function, depending on one spin and three spatial coordinates for every electron (assuming fixed nuclear positions), is not, in and of itself, particularly intuitive for systems of more than one electron. The wave function itself is essentially uninterpretable, it is an inscrutable oracle that returns valuably accurate answers when questioned by quantum mechanical operators, but it offers little by way of sparking intuition”.⁹⁸ Then, the idea of simplifying the problem of finding the energy and others properties of the molecules goes back, even earlier than HF formulation itself.

The Hamiltonian depends only on the positions and atomic numbers of the nuclei and the total number of electrons. The dependence on total number of electrons immediately suggests that a useful physical observable would be the electron density ρ , since, integrated over all space, it gives the total number of electrons N . As energy is separable into kinetic (T) and potential (V) components, if those components are evaluated in terms of the electronic density, i.e. $T=T(\rho(\vec{r}))$ and $V=V(\rho(\vec{r}))$, then the total energy of the system can be estimated. The Thomas–Fermi equations (1927), together with an assumed variational principle, represented the first effort to define a DFT; the energy is computed with no reference to a wave function. Thomas–Fermi DFT do not have application in modern chemistry because using this formulation, all molecules are unstable relative to dissociation into their constituent atoms. The larger error of this formulation is that it ignores the energetic effects associated with correlation and exchange. Later, the Thomas–Fermi–Dirac model takes into account the exchange energy:

$$E_x[\rho(\vec{r})] = -\frac{9\alpha}{8} \left(\frac{3}{\pi}\right)^{1/3} \int \rho^{4/3}(\vec{r}) d\vec{r} \quad (4.11)$$

Giving different values to α as a function of different derivations and computations employing equation 4.11 along these lines are termed (X_α) calculations. This particular DFT methodology has largely fallen out of favor in the face of more modern functionals, but still sees occasional use, particularly within the inorganic community.⁹⁸

It was not until Hohenberg and Kohn in 1964 proved two theorems critical to establishing DFT as a legitimate quantum chemical methodology. ”The first theorem of Hohenberg and Kohn is an existence theorem. It is the ground-state density that is employed, it is sufficient to show that this density determines the Hamiltonian operator. The proof that the ground-state density determines the

4. COMPUTATIONAL METHODS

external potential proceeds via *reductio ad absurdum*. The second theorem shown that, also just as with MO theory, the density obeys a variational principle”.⁹⁸

Kohn and Sham in 1965 simplified the problem considering a Hamiltonian operator for a *non-interacting* system of electrons. Such a Hamiltonian can be expressed as a sum of one-electron operators, has eigenfunctions that are Slater determinants of the individual one-electron eigenfunctions, and has eigenvalues that are simply the sum of the one-electron eigenvalues. In general this method is similar in structure to the HF-SCF method. The crucial bit of cleverness, then, is to take as a starting point a *fictitious* system of non-interacting electrons that have for their overall ground-state density the same density as some real system of interest where the electrons do interact, these quantities are necessarily identical in the non-interacting and in the real systems. The energy functional can be written by:

$$E[\rho(\vec{r})] = T_{ni}[\rho(\vec{r})] + V_{ne}[\rho(\vec{r})] + V_{ee}[\rho(\vec{r})] + E_{xc}[\rho(\vec{r})] \quad (4.12)$$

where T_{ni} is the kinetic energy of the non-interacting electrons, V_{ne} is the nuclear–electron interaction, V_{ee} the classical electron–electron repulsion and E_{xc} is the exchange–correlation energy. E_{xc} includes not only the effects of quantum mechanical exchange and correlation, but also the correction for the classical self-interaction energy and for the difference in kinetic energy between the fictitious non-interacting system and the real one.

Indeed, the similarities with HF theory extend well beyond the mathematical technology offered by a common variational principle. For instance, the kinetic energy and nuclear attraction components of matrix elements obtained by solving the secular equation are identical in both cases. Furthermore, if the density appearing in the classical interelectronic repulsion operator is expressed in the same basis functions used for the Kohn–Sham orbitals, then the same four-index electron–repulsion integrals appear. ”The key contrast between HF and DFT (in the limit of an infinite basis set) is that HF is a deliberately approximate theory, whose development was in part motivated by an ability to solve the relevant equations exactly, while DFT is an exact theory, but the relevant equations must be solved approximately because a key operator (i.e E_{xc}) has unknown form”.⁹⁸ The advantage of using electron density is that the integrals for Coulomb repulsion are done only over the electron density, which is a three-dimensional function, thus scaling as N^3 .⁹⁷ Furthermore, at least some electron correlation can be included in the calculation. The results are obtained faster for DFT calculations than HF calculations (which scale as N^4) and computations are a bit more accurate as well. The better DFT functionals give results with accuracy similar to that of an MP2 calculation.

There is a whole list of different functionals that may have advantages or disadvantages. Some of these functionals were developed from fundamental quantum mechanics and some were developed by parameterizing functions to reproduce better the experimental results. Thus, there are in essence *ab*

initio and semi-empirical versions of DFT. Density functionals can be broken down into several classes. The simplest is called the X_α method. This type of calculation includes electron exchange but not correlation. It was introduced by J.C. Slater in 1951, who in attempting to make an approximation to Hartree-Fock unwittingly discovered the simplest form of DFT.⁹⁷ Within Slater's derivation, the value for the constant α is 1, defines so-called 'Slater exchange'. Starting from the uniform electron gas, Bloch and Dirac in 1930 had derived a similar expression, except that in that case $\alpha = \frac{2}{3}$. Empirical analysis in a variety of different systems suggests that $\alpha = \frac{3}{4}$ provides more accurate results than the earlier.⁹⁸ The X_α method is similar in accuracy to HF and sometimes better.

The simplest approximation to the complete problem is one based only on the electronic density, called a local density approximation (LDA). For high-spin systems, this is called the local spin density approximation (LSDA). LDA calculations have been widely used for bond structure calculations. Their performance is less impressive for molecular calculations, where both qualitative and quantitative errors are encountered. For example, bonds tend to be too short and too strong. In recent years, LDA, LSDA, and VWN (the Vosko, Wilks, and Nusair functional) have become synonymous in the literature.⁹⁷ A more complex set of functionals utilizes the electronic density and its gradient. They are called gradient-corrected methods. There are also hybrid methods that combine functionals from other methods with pieces of a Hartree-Fock calculation, usually the exchange integrals. In general, gradient-corrected or hybrid calculations give the most accurate results. Some of the more widely used functionals are listed in Table 4.1

The accuracy of DFT calculation results can be from poor to fairly good, depending on the choice of basis set and density functional. "The choice of the density functional is more difficult because creation of new functionals is still an active area of research. Recently B3LYP hybrid functional is one of the most widely used for molecular calculations by a fairly large margin".⁹⁹ This is due to the accuracy of the B3LYP results obtained for a large range of compounds, particularly organic molecules. However, it would not be surprising if this functional's dominance will be changed within a few years. At the present time, DFT results have been very good for organic molecules, particularly those with closed shells. Results have not been so encouraging for heavy elements, highly charged systems, or systems known to be very sensitive to electron correlation. Also, the functionals listed in table 4.1 do not perform well for problems dominated by dispersion forces¹⁰⁰.

4.4 Basis sets

The basis set is the set of mathematical functions from which the wave function is constructed. Both in *ab initio* and in DFT calculation a set of functions used to describe the shape of the orbitals in an atom has to be chosen. Molecular orbitals and entire wavefunctions are created by taking linear

4. COMPUTATIONAL METHODS

Acronyms	Name	Type
X_α	X alpha	Exchange only
HFS	Hartree-Fock Slater	HF with LDA exchange
VWN	Vosko, Wilks, and Nusair	LDA
BLYP	Becke correlation functional with Lee, Yang, Parr Exchange	Gradient-corrected
B3LYP	Becke 3 term with Lee, Yang, Parr Exchange	Hybrid
PW91	Perdue and Wang 1991	Gradient-corrected
G96	Gill 1996	Exchange
P86	Perdew 1986	Gradient-corrected
B96	Becke 1996	Gradient-corrected
B3P86	Becke exchange, Perdew correlation	Hybrid
B3PW91	Becke exchange, Perdew and Wang correlation	Hybrid

Table 4.1: *Density Functionals*^{96–98, 98}

combinations of basis functions and angular functions. The type of calculation performed and basis set are the two biggest factors which determines the accuracy of results.⁹⁷

The functions used mostly are linear combinations of Slater-type orbitals (STO) or Gaussian-type orbitals (GTO).⁹⁷ STOs have a number of attractive features primarily associated with the degree to which they closely resemble hydrogenic atomic orbitals (AO). In *ab initio* HF theory, however, they suffer from a fairly significant limitation. There is no analytical solution for the integrals. They required to be solved by numerical methods which severely limits their utility in molecular systems of any significant size. Nevertheless, high quality STO basis sets have been developed for atomic and diatomic calculations, where such limitations do not arise.⁹⁸

Boys (1950) proposed an alternative to the use of STOs. All that is required for there to be an analytical solution of the general four-index integral formed from such functions is that the radial decay of the STOs be changed from e^{-r} to e^{-r^2} . That is, the AO-like functions are chosen to have the form of a Gaussian function. The general functional form of a normalized GTO in atom-centered Cartesian coordinates is⁹⁸:

$$\phi(x, y, z; \alpha, i, j, k) = \left(\frac{2\alpha}{\pi}\right)^{\frac{3}{4}} \left[\frac{(8\alpha)^{i+j+k} i! j! k!}{(2i)!(2j)!(2k)!}\right]^{\frac{1}{2}} x^i y^j z^k e^{-\alpha(x^2+y^2+z^2)} \quad (4.13)$$

where α is an exponent controlling the width of the GTO, and i , j , and k are non-negative integers that dictate the nature of the orbital in a Cartesian sense.

In particular, when all three of these indices are zero, the GTO has spherical symmetry, and is called an s-type GTO. When exactly one of the indices is one, the function has axial symmetry about a single Cartesian axis and is called a p-type GTO. There are three possible choices for which index is one, corresponding to the p_x , p_y , and p_z orbitals. When the sum of the indices is equal to two, the orbital is called a d-type GTO. Note that there are six possible combinations of index values (i , j , k) giving the sum equal to two. This leads to possible cartesian prefactors of x^2 , y^2 , z^2 , xy , xz , and yz . As one increases the indexing, the disparity between the number of Cartesian functions and the number of canonical functions increases. Thus, with f-type GTOs (indices summing to 3) there are 10 Cartesian functions and 7 canonical functions, with g-type 15 and 10, etc. GTOs can be taken arbitrarily high in angular momentum.⁹⁸

In order to combine the best feature of GTOs (computational efficiency) with that of STOs (proper radial shape), most of the first basis sets developed with GTOs used them as building blocks to approximate STOs. That is, the basis functions ψ used for SCF calculations were not individual GTOs, but instead a linear combination of GTOs fit to reproduce as accurately as possible a STO.⁹⁸

Hehre, Stewart, and Pople in 1969 were the first to systematically determine optimal contraction coefficients and exponents for mimicking STOs with contracted GTOs for a large number of atoms in the periodic table. They constructed a series of different basis sets called STO-MG, for ‘Slater-Type Orbital approximated by M Gaussians’. In particular, they considered $M = 2$ to 6.⁹⁸ It was discovered that the optimum combination of speed and accuracy was achieved for $M = 3$. STO-3G basis functions have been defined for most of the atoms in the periodic table.⁹⁸

The STO-3G basis set is what is known as a ‘single- ζ ’ basis set, or, more commonly, a ‘minimal’ basis set. This nomenclature implies that there is one and only one basis function defined for each type of orbital core through valence. From a chemical standpoint, then, there is more to be gained by having flexibility in the valence basis functions than in the core, and recognition of this phenomenon led to the development of so-called ‘split-valence’ or ‘valence-multiple- ζ ’ basis sets. In such basis sets, core orbitals continue to be represented by a single (contracted) basis function, while valence orbitals are split into arbitrarily many functions.⁹⁸

Amongst the most widely used split-valence basis sets are those commonly referred to as the Pople basis sets. These basis sets include 3-21G, 6-21G, 4-31G, 6-31G, and 6-311G. The nomenclature is a guide to the contraction scheme. The first number indicates the number of primitives used in the contracted core functions. The numbers after the hyphen indicate the numbers of primitives used in the valence functions – if there are two such numbers, it is a valence-double- ζ basis, if there are three, valence-triple- ζ .^{97,98} One feature of the Pople basis sets is that they use a so-called ‘segmented’

4. COMPUTATIONAL METHODS

contraction. This implies that the primitives used for one basis function are not used for another of the same angular momentum.⁹⁸

A variety of other molecular properties prove to be sensitive to the presence of polarization functions. Pople and co-workers introduced a simple nomenclature scheme to indicate the presence of these functions, the ‘*’ (pronounced ‘star’). Thus, 6-31G* implies a set of d functions added to polarize the p functions in 6-31G. A second star implies p functions on H and He, e.g., 6-311G**.^{98,101} Adding polarization functions usually decreases the variational total energy by about the same amount as adding another contraction. However, this energy change is almost completely systematic, so it changes the relative energies very little.⁹⁷ Moreover, one or two plus signs can also be added, such as 6-31+G* or 6-31++G*. A single plus sign indicates that diffuse functions have been added to atoms other than hydrogen. The second plus sign indicates that diffuse functions are being used for all atoms. These diffuse functions are primitives with small exponents, thus describing the shape of the wavefunction far from the nucleus. Diffuse functions are used for anions, which have larger electron density distributions. They are also used for describing interactions at long distances, such as van der Waals interactions. The effect of adding diffuse functions is usually to change the relative energies of the various geometries associated with these systems. Basis sets with diffuse functions are also called augmented basis sets.⁹⁷ Recognizing the tendency to use more than one set of polarization functions in modern calculations, the standard nomenclature for the Pople basis sets now typically includes an explicit enumeration of those functions instead of the star nomenclature. Thus, 6-31G(d) is to be preferred over 6-31G* because the former obviously generalizes to allow names like 6-31G(3d2fg,2pd), which implies heavy atoms polarized by three sets of d functions, two sets of f functions, and a set of g functions, and hydrogen atoms by two sets of p functions and one of d (note that since this latter basis set is only valence double- ζ , it is somewhat unbalanced by having so many polarization functions).⁹⁸

An alternative method to carrying out a segmented contraction is to use a so-called ‘general’ contraction.¹⁰² In a general contraction, there is a single set of primitives that are used in all contracted basis functions, but they appear with different coefficients in each. The general contraction scheme has some technical advantages over the segmented one. One advantage in terms of efficiency is that integrals involving the same primitives, i.e. need in principle be calculated only once, and the value can be stored for later reuse as needed. Examples of split-valence basis sets using general contractions are the cc-pVDZ, cc-pVTZ, etc. sets of Dunning and co-workers, where the acronym stands for ‘correlation-consistent polarized Valence (Double/Triple/etc.) Zeta’.^{98,103,104}

4.5 Harmonic/anharmonic vibrational frequencies

In practice the choice of the computational method and correct basis set is always a problem.^{100,105} One approach is to choose the basis set which was already tested on the similar systems and shown the best results. The choice of the calculation method also depends on the information one wants to obtain about molecular system. For the interpretation of spectroscopic data one has to calculate frequencies (wavenumbers) of normal vibrations, intensities of infrared absorption bands and sometimes intensities of Raman scattering bands. Both *ab initio* or DFT calculations can be used for this purpose. Unfortunately in most cases calculated wavenumbers are not in very good agreement with experimental values. In most cases deviation from experimentally measured values are related to the harmonic approximation used in the calculations. Basically it means assumption that nucleus is in the potential well which can be described by parabolic function. Real potential function of nucleus is anharmonic therefore some discrepancy between calculated and experimental results exists. Differences between calculated frequencies and experimental ones are similar for most of the systems when the same method and basis set is used.

As it was mentioned above, before vibrational frequencies can be computed, the geometry of the molecule has to be calculated because the normal vibrational modes are centered at the equilibrium geometry. Harmonic frequencies have no relevance to the vibrational modes of the molecule, unless computed at the exact same level of theory that was used to optimize the geometry. Orbital-based methods can be used to compute transition structures. When imaginary frequency is computed, it indicates that the geometry of the molecule corresponds to a maximum of potential energy with respect to the positions of the nuclei. The transition state of a reaction is characterized by having one imaginary frequency. Structures with two imaginary frequencies are called second-order saddle points. These structures have little relevance to chemistry since it is extremely unlikely that the molecule will be found with that structure.¹⁰⁵

For very high accuracy *ab initio* calculations, the harmonic oscillator approximation may be the largest source of error. The harmonic oscillator frequencies are obtained directly from the Hessian matrix, which contains the second derivative of energy with respect to the movement of the nuclei. One of the most direct ways to compute anharmonic corrections to the vibrational frequencies is to compute the higher-order derivatives (3rd, 4th, etc.). The frequency for a potential represented by a polynomial of this order can then be computed. This requires considerably more computer resources than harmonic oscillator calculations therefore it can be done only for very small molecular systems.

4. COMPUTATIONAL METHODS

Chapter 5

Acetylacetone Infrared spectra

The infrared spectra of Acetylacetone (AcAc) in different environments have been used to characterize this molecule and its geometrical structure. In this chapter infrared spectrum of AcAc in para-Hydrogen (pH₂) is compared with other matrices such as normal-Hydrogen (nH₂), normal-Deuterium (nD₂) and Neon (Ne). Next, a discussion about chelated enol form structure and symmetry (C_{2v} or C_s), based on theoretical calculation and spectral data is presented. In the following two sections the assignment of the bands of AcAc chelated enol form and its tautomer Keto form in all matrices based on theoretical calculation is detailed. Finally the keto/enol ratio (R_{ke}) is calculated for each matrix and a comparison between them is discussed.

5.1 Acetylacetone Infrared spectra

A typical IR spectrum of AcAc isolated in 4 K pH₂ matrix is shown in trace (a) of Figure 5.1. Traces (b), (c) and (d) display normalized spectra of AcAc in nH₂, nD₂ and Ne matrices for comparison. We focus here on the 850–1800 cm⁻¹ region which relates to the most characteristic bands of AcAc. In all matrices, the vibrational bands of CH₂ stretching modes (2900–3020 cm⁻¹) are indeed weak and that of OH stretch is not visible.

The spectra in hydrogen matrices (Figure 5.1) look quite similar to those in traditional cryogenic matrices.^{50,57} According to previous studies, the chelated enol isomer is responsible for the most intense bands. Weaker bands are also visible in the wings of enol bands, they match very well with the keto tautomer as reported by Nagashima *et al.*⁵⁸ In all pH₂ experiments a very sharp band at 1167 cm⁻¹ is observed of which intensity correlates with the thickness of the pH₂ matrix. This band is associated with the pure (J = 0 → J = 4) rotational transition of pH₂ molecule⁸⁵

5. ACETYLACETONE INFRARED SPECTRA

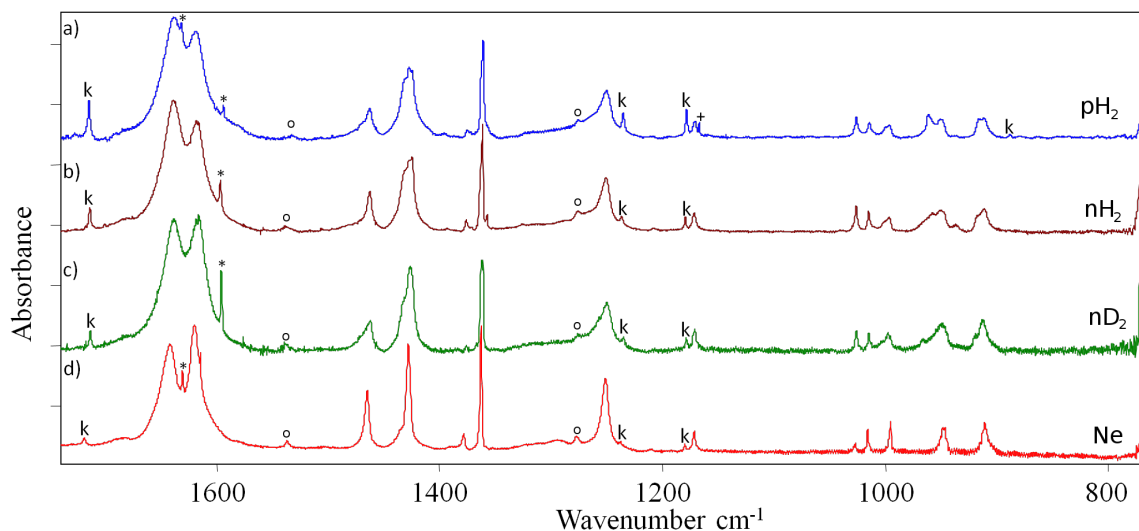


Figure 5.1: Normalized IR spectra of acetylacetonone isolated in different matrices: (a) $p\text{H}_2$, (b) $n\text{H}_2$, (c) $n\text{D}_2$, (d) Ne. The letter ‘k’ indicates bands assigned to the keto tautomer of AcAc, asterisks denotes water bands and the ‘+’ denotes pure rotational transition of $p\text{H}_2$. (o) denotes overtones.

5.2 Chelated enol form

The spectrum of the chelated enol tautomer exhibits broad bands and looks quite similar in the $p\text{H}_2$, $n\text{H}_2$, $n\text{D}_2$ and Ne matrices. Experimental frequencies of AcAc vary only little from one matrix to another (mainly within 3 cm^{-1} for the most intense bands, see table 5.1). These results compare well with IR spectra in classical Ar, Xe and N_2 matrices, which all show a similar signature for the chelated enol form.^{50,106} Bandwidths are found to be very different from one mode to another in all matrices, with a similar behavior in ‘quantum’ and ‘classical’ solids. Typical values in $p\text{H}_2$ range from 2 cm^{-1} (band at 1026 cm^{-1} for example) to 25 cm^{-1} (very intense doublet at $1638\text{--}1618\text{ cm}^{-1}$). All these remarks indicate that bandwidths are mainly characteristic of the guest molecule rather than due to the matrix (trapping site effects). Such a mode-dependence reflects the intrinsic properties of the molecule, in particular those correlated to the intramolecular hydrogen bond, which differently perturbs the vibrational dynamics depending on the mode.

Bands in the $900\text{--}1040\text{ cm}^{-1}$ and $1355\text{--}1370\text{ cm}^{-1}$ regions show the most pronounced dependence on the host matrix. In the Figure 5.2 these two specific regions of the IR spectra of acetylacetonone isolated in different matrices are shown. Most of those bands show a structure in $n\text{H}_2$ (a and b) and $n\text{D}_2$ matrix (c) while in Ne matrix there are only single bands.

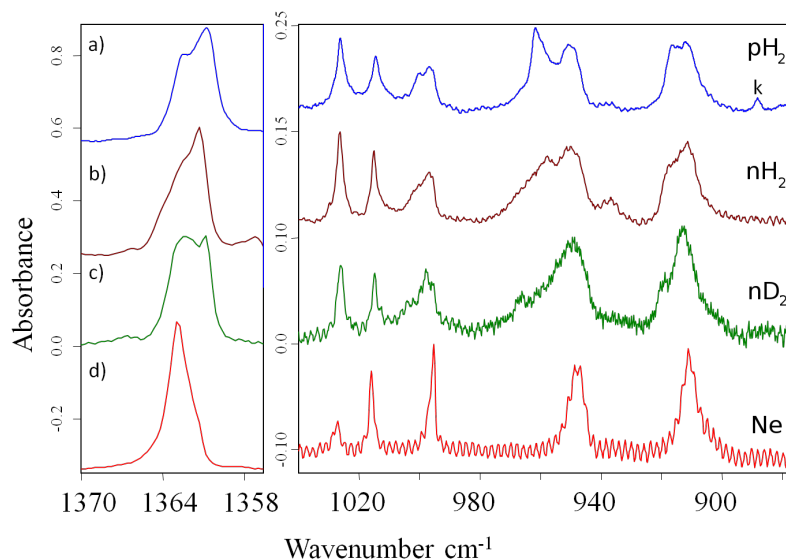


Figure 5.2: Selected regions of the infrared spectra of acetylacetonone isolated in different matrices: (a) pH_2 , (b) nH_2 , (c) nD_2 , (d) Ne .

5.2.1 Bands assignments: comparison with simulated infrared spectra

As have been pointed out in the chapter 1, many theoretical and experimental works focused on the chelated enol tautomer. Most were dedicated to the electronic structure of this enol form, of which conclusion led to the structure with C_s symmetry being more stable than the structure having C_{2v} symmetry.⁶³ The C_s symmetry structure has been confirmed by gas phase experimental studies.¹⁰ Vibrational frequencies have also been computed at various levels of theory but mostly within the harmonic approach.^{44,57,107} One can also mention few theoretical studies using the anharmonic approach for frequency calculations.^{108,109}

In figure 5.3 a comparison between experimental IR spectra of AcAc in pH_2 matrix and simulated IR spectra calculated at the B3LYP/6-311++G(3df, 3pd) level of theory for the AcAc in its C_s and C_{2v} chelated enol forms are shown. Neither the position or relative intensities of the IR bands suggest the presence of C_{2v} chelated enol form in pH_2 matrices. The calculation of this geometry predicts only one very intense band in the 1550-1700 cm^{-1} region. Another intense band, should be close to 1080 cm^{-1} . The rest of bands are medium or weak. Meanwhile the simulated spectrum of the C_s geometry predict two intense bands in the 1600-1700 cm^{-1} region, as well as a group of medium strength bands in the 1250-1500 cm^{-1} region and other weak in the 780-1075 cm^{-1} . This description of the spectra is in better agreement with that obtained experimentally. Absolute wavenumbers of calculated and experimentally observed bands does not agree perfectly. The disagreement between calculated and measured values is due to the anharmonic character in the potential function used

5. ACETYLACETONE INFRARED SPECTRA

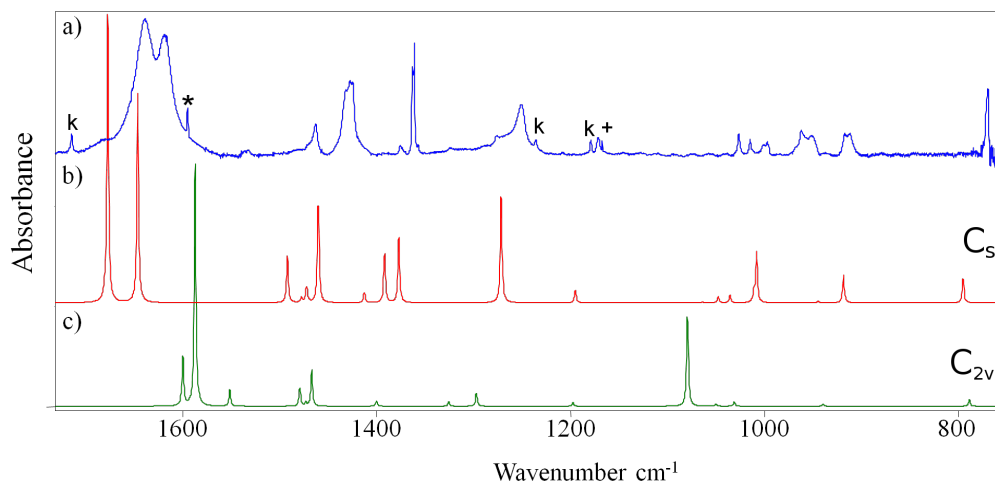


Figure 5.3: (a) Experimental IR spectra of AcAc in pH_2 matrix compared with simulated IR spectra of AcAc calculated at the B3LYP/6-311++G(3df, 3pd) level of theory. (b) Simulated IR spectra of C_s AcAc molecule. (c) Simulated IR spectra of C_{2v} AcAc molecule

to describe the atoms interaction. To improve the agreement between theoretical calculations and experimental results, calculations with the same basis set but with anharmonic corrections were done.

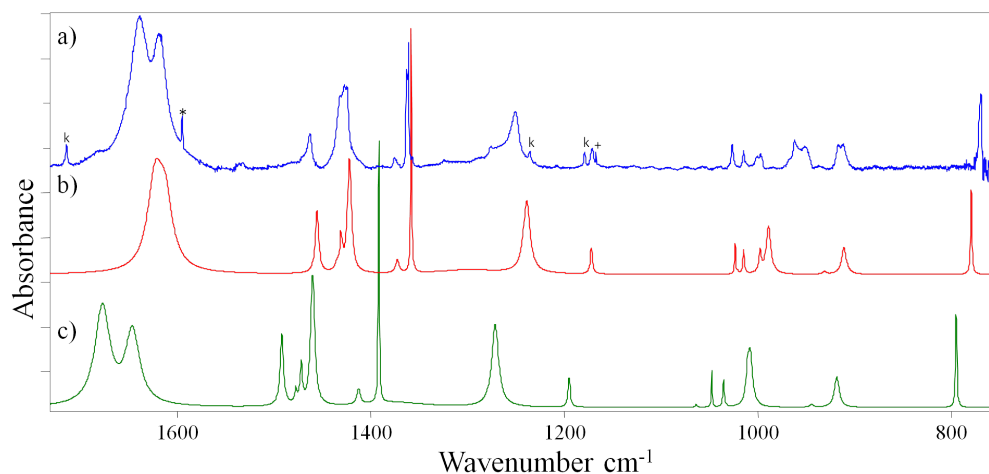


Figure 5.4: (a) Experimental IR spectra of AcAc in pH_2 matrix compared with simulated IR spectra of AcAc chelated enol form calculated at the B3LYP/6-311++G(3df, 3pd) level of theory. (b) Simulated IR spectra with anharmonic correction. (c) Simulated IR spectra with harmonic approximation. Experimental bandwidths, calculated harmonic intensities and Lorentzian function were used to build both simulated spectra.

The comparison of those calculation are shown in the Figure 5.4. In the first panel (a) the experimental spectrum of AcAc in pH_2 matrix is shown, followed by simulated spectra of the theoretical

calculation of IR frequencies (b) with anharmonic correction (c) with only harmonic approximation. Both simulated spectra were done using calculated harmonic intensities, experimental bandwidths and Lorentzian function to describe the band shape. Calculated harmonic and anharmonic frequencies are reported in Table 5.1 for the modes which are experimentally observed in the 800–3600 cm^{-1} range, together with their predicted intensity in the harmonic approximation. A rough description of the modes is also presented. Anharmonic calculations are consistent with those reported in Refs.,^{108,109} leading to the same vibrational assignment as in previous studies.^{57,108}

The comparison between experimental and anharmonic calculated frequencies of the chelated enol tautomer gives a very satisfactory agreement. It is interesting that the computed frequencies with the high cc-pVQZ basis set calculated by Giuseppe Buemi¹⁰⁹ do not give a better match with experiment than our calculations at the B3LYP/6-311++G(3df,3pd) level of theory. The calculated intensities of the unobserved modes are very low, except in the case of the OH stretch. This specific mode, predicted to be very intense, is found to be strongly down-shifted from harmonic to anharmonic approach (- 646 cm^{-1}). The very strong intramolecular hydrogen-bond encountered by the chelated enol tautomer is responsible for such an unusual red-shift, and leads to a very broad OH stretching band that would be barely visible in the spectrum. This band was reported in the gas phase at room temperature as an extremely broad absorption covering the 3500–2200 cm^{-1} region^{13,110} but it has never been detected in matrix experiments so far.^{57,106} The improvement between calculated and experimental frequencies is significant from harmonic to anharmonic approach even when using a scaling factor for the harmonic values. This emphasizes the large mode-dependence of the anharmonicity. A better discussion of harmonic and anharmonic calculation will be done in section 6.3.1. Interestingly, one can notice that the highest mismatch between experiment and theory is found for the bands at 1276 cm^{-1} (involving the in-plane OH bend) and around 960 cm^{-1} (out-of-plane OH bend). Anharmonic calculations show that these two modes are strongly coupled with the OH stretch and are therefore highly perturbed by the internal hydrogen bond.

5.2.2 Keto form

As it had been said in the previous paragraph, in as-deposited samples, a few weak and narrow bands observed in the wings of AcAc enol bands. They are assigned to the AcAc keto form. In figure 5.1 those bands are labeled with (k). Keto bands are more intense in pH_2 than in nH_2 , nD_2 and traditional matrices such as Ne. In pH_2 , we have been able to detect four keto absorption bands in the IR spectrum of the as-deposited sample, but only three of them are visible in the spectra of AcAc in nH_2 , nD_2 and Ne matrices. The nature of the matrix only slightly affects the position of keto bands, leading to small spectral shifts (2 cm^{-1}) depending on the vibrational mode. They are

5. ACETYLACETONE INFRARED SPECTRA

ρH_2	$n\text{H}_2$	$n\text{D}_2$	Ne	Anh.	Harm.	Int. ^a	Description ^b [sym.]
				3093.3	3211.8	3	νCH_{ol} . [a']
3020-3006	3014	3014	3024	3049.7	3137.9	9	$\nu_{as}\text{CH}$ methyl-OH side [a']
				3003.6	3143.0	12	$\nu_{as}\text{CH}$ methyl-C=O side [a']
2973.7	2974.2	2978	2985.6	2963.6	3088.0	7	$\nu_{as}\text{CH}$ methyl-C=O side [a'']
				2949.6	3090.1	5	$\nu_{as}\text{CH}$ methyl-OH side [a'']
2934.4	2935.0	2935.7	2951	2929.6	3038.3	18	$\nu_s\text{CH}$ methyl-OH side [a']
				2919.5	3034.3	4	$\nu_s\text{CH}$ methyl-C=O side [a']
				2360.9	3007.1	358	νOH [a']
1638	1639	1638	1641	1622.7	1677.1	372	$\nu\text{C}=\text{O} + \nu_{as}\text{C}=\text{C}-\text{O} + \delta\text{OH}$ [a']
1618	1618	1617	1620	1612.2	1646.1	270	$\nu_s\text{C}=\text{C}-\text{C}=\text{O} + \delta\text{OH}$ [a']
1533.4	1537.5	1538.9	1536.6	1552.9	1589.3		$2\gamma\text{CH}$ [a']
1462.6	1462.4	1461.9	1464.8	1455.3	1491.6	61	$\delta\text{CH}_{ol} + \delta_{as}\text{CH}(\text{methyl-OH})$ [a']
1431.7	1431.8	1432	1435	1434.5	1472.4	10	$\delta_{as}\text{CH}(\text{methyl-OH})$ [a'']
1427.3	1427.3			1430.8	1471.4	14	$\delta_{as}\text{CH}(\text{methylns ip}) + \delta\text{CH}_{ol} + \delta\text{OH}$ [a']
				1429.1	1477.2	7	$\delta_{as}\text{CH}(\text{methyl-C}=\text{O})$ [a'']
1424.2	1424.7	1425	1427.8	1421.8	1459.8	131	$\delta_{as}\text{CH}(\text{methylns op}) + \delta\text{CH}_{ol} + \delta\text{OH}$ [a']
1375.2	1376.2	1375.8	1378.4	1372.3	1412.3	13	$\delta_s\text{CH}(\text{methyl-OH})$ umbrella [a']
1360.8	1361.4	1360.8	1362.8	1357.8	1391.5	64	$\delta_s\text{CH}(\text{methyl-C}=\text{O})$ umbrella [a']
1289.0	1290.3	1292.6	1297.2	1297.8	1376.7	84	$\delta\text{OH} + \delta_{as}\text{C}=\text{C}-\text{C}-\text{O}$ [a']
1275.6	1275.5	1275.4	1276.9	1272.2	1296.5		$2\nu_s\text{C-methyl} + \delta_s\text{O}=\text{C}-\text{C}$
1250.5	1250.6	1250.3	1251.3	1238.6	1271.1	142	$\nu_s\text{C}-\text{C}-\text{C}=\text{C}-\text{C}$ ring breath [a']
1171.0	1171.5	1171.2	1171.5	1171.8	1194.7	16	δCH_{ol} [a']
				1020.6	1063.5	1	twist methyl-OH side [a'']
1025.8	1026.4	1026.4	1027.9	1023.1	1047.4	8	twist methyl-C=O side [a'']
1014.7	1015.0	1014.9	1015.5	1014.3	1035.1	10	ρCH_3 (OH side) [a']
998.4	998.6	997	995.2	997.4	1010.5	15	ρCH_3 (C=O side) + bb [a']
961.8	959.3	962.4					
950.4	949.2	949.4	947.9	988.7	1007.6	65	γOH [a'']
936.0	936.4	-	-	930.9	944.0	3	$\rho\text{CH}_3(\text{C}=\text{O} \text{ side}) + \text{bb}(\nu\text{C}-\text{C})$ [a']
916.9	917.3	919.7					
914.3	911.4	912.5	910.7	910.7	918.1	37	$\nu_{as}\text{C}-\text{CH}_3 + \rho\text{CH}_3(\text{CO} \text{ side}) + \nu\text{C}-\text{O}$ [a']
769.0	772.2	771.1	770.7	779.1	794.6	32	γCH [a'']

^a Calculated intensities in the harmonic approximation in km/mol.

^b Main vibrational motions: ν : stretch, δ : in-plane bending, ρ : rocking, γ : out-of-plane bending; s : symmetric, as : asymmetric, ol : olefinic, bb : backbone motions.

Table 5.1: Experimental frequencies (cm^{-1}) of the chelated enol form of AcAc in different matrices compared with theoretical anharmonic and harmonic frequencies (cm^{-1}) calculated at the B3LYP/6-311++G(3df, 3pd) level in the 750–4000 cm^{-1} region. Broad bands are written without decimals.

reported in table 5.2. Keto bands are sharper than those of the chelated enol form. A striking example is illustrated by the C=O stretch showing a bandwidth of 2 cm^{-1} for keto and up to 25 cm^{-1} for enol.

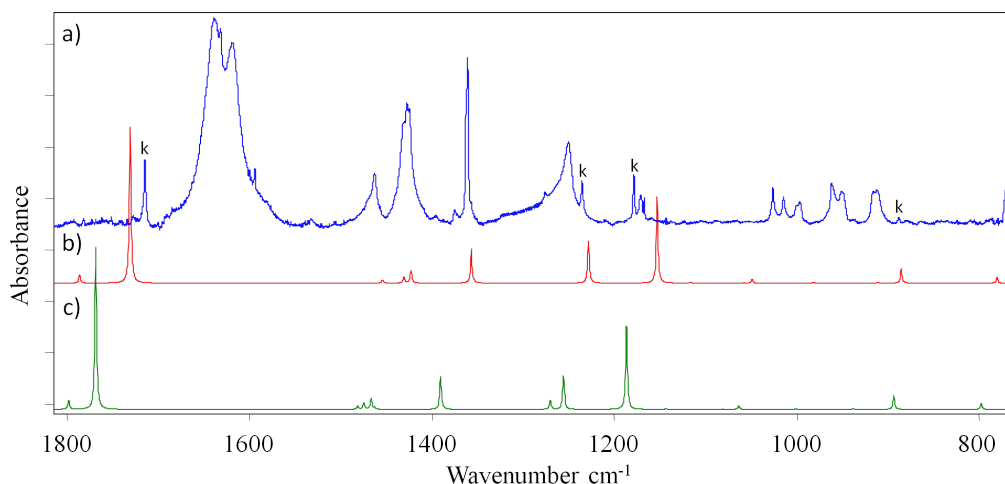


Figure 5.5: (a) Experimental IR spectra of AcAc in pH_2 matrix compared with simulated IR spectra of AcAc keto form calculated at the B3LYP/6-311++G(3df, 3pd) level of theory. (b) Simulated IR spectra with anharmonic corrections. (c) Simulated IR spectra without the anharmonic approach. The same bandwidths (2.0 cm^{-1}), harmonic intensities and Lorentzian function were used to build both simulated spectra.

The vibrational assignment is based on theoretical calculations, which are also reported in table 5.2. In figure 5.5 a comparison between the experimental spectrum of AcAc in pH_2 matrix (a) and simulated spectra with anharmonic approach (b) and with harmonic approach (c). The same bandwidths (2.0 cm^{-1}), harmonic intensities and Lorentzian function were used to build both simulated spectra. The anharmonic calculation seems to be in better agreement with the experiment. The biggest difference between anharmonic calculations and experimentally measured absorption bands is observed for two bands. Calculated band at 1768 cm^{-1} which is associated with antisymmetrical C=O stretch vibrations and 1153 cm^{-1} associated with C-C stretch and CH_3 rock vibrations.

To date, only one study has investigated theoretically the vibrational frequencies of the keto form.⁵⁸ Harmonic level calculations (B3LYP/6-311++G(3df,3pd) level of theory) predict few intense keto bands to absorb in the close vicinity of the chelated enol bands, so that they would be hidden by the broad and intense enol bands in the IR experimental spectrum. In order to get rid of these enol bands and make the keto bands more visible, the samples have been irradiated with an excimer laser. The results of the UV irradiation are described in a later chapter 8, where the discussion on the IR spectrum of keto is also presented and full band assignment presented in table 5.2 are explained.

5. ACETYLACETONE INFRARED SPECTRA

pH ₂	nH ₂	nD ₂	Ne	Ar ^a	Anh.	Harm.	Int. ^b	Description ^c
				1740	1786.8	1798.0	21	ν C=O (ip)
1714.9	1713.5	1713.7	1718.4	1714	1730.5	1768.1	384	ν C=O (opp)
					1422.7	1466.4	28	δ CH ₃ scissor (opp)
				1357	1356.4	1390.0	73	δ CH ₃ umbrella (opp)
1235.3	1236.8	1235.9	1237.7	1240	1228.2	1255.5	84	Rock CH ₂
				1256	1227.6	1270.1	22	Twist CH ₂
1178.2	1179.9	1179.1	1179.6	1176	1152.6	1186.5	201	$[\nu$ C(H ₃)-C(=O)+ ν C(H ₂)-C(=O)] _{as} +rock CH ₃ (opp)
888.2			890.9	891	885.2	893.4	33	ν C(H ₂)-C(=O)+rock CH ₃ (opp)
				792	780.4	797.5	14	$[\nu$ C(H ₃)-C(=O)+ ν C(H ₂)-C(=O)] _s (opp)

^a From Nagashima *et al.*⁵⁸

Calculated intensities in the harmonic approximation in km/mol.

^c Only main motions are described. ν : stretch, δ : bending, s : symmetric, as : asymmetric; the keto form contains two CH₃-C=O groups, the motions of each group can be in phase (ip) or in opposition of phase (opp).

Table 5.2: Experimental frequencies (cm^{-1}) of the keto form of AcAc in different matrices compared with theoretical frequencies in cm^{-1} (anharmonic and harmonic) calculated at the B3LYP/6-311++G(3df, 3pd) level.

Very few experimental data are available on the vibrational spectrum of the keto form. Mohaček-Grošev *et al.* have published the IR spectrum of keto in liquid phase and its Raman spectrum in argon matrix but the keto bands are not precisely identified since the vibrational spectra are assigned in the mixture of enol and keto.¹¹¹ In most of matrix-isolation experiments, keto bands are not easily observed in the spectra of as-deposited samples.^{57,58} Only one keto band (C=O stretch) was visible after deposition of AcAc in Ar matrices. Only after UV irradiation ($\lambda < 280$ nm) of the sample, the authors were able to identify more bands for the keto form.⁵⁸ The four bands assigned in pH₂ are among the eight bands reported by Nagashima *et al.* in the 700–3700 cm^{-1} range.

5.2.3 Keto/enol ratio

Keto/enol ratio (R_{ke}), estimated from the intensities of experimentally observed spectral bands, seems to be higher when AcAc is isolated in pH₂ matrices than in nH₂, nD₂ and rare gas matrices such as Ne (see figure 5.1). From the experimental spectra it was possible to estimate the R_{ke} of all samples. R_{ke} is calculated from the relative intensities of the keto and chelated enol bands in the IR spectra, weighted by their relative calculated IR intensities. To get reliable values from one sample to another, R_{ke} is estimated from the intensity of the most intense keto band at 1714.9 cm^{-1} and that of the strong enol doublet at 1638 and 1618 cm^{-1} . C=O stretching motions are strongly involved in these three modes of AcAc. As remarked previously, the highest R_{ke} is found in pH₂ matrices. It is found to be

slightly sample-dependent with a maximum value of 4.5%. The influence of experimental conditions for the sample preparation was checked by isolating AcAc in Ne matrices.

The R_{ke} measurements confirm that keto bands are more intense in pH_2 than in other solids. AcAc IR spectrum in solid Ne is similar to that of previous studies,^{50,106} leading to $R_{ke}(\text{Ne}) = 1\text{--}1.5\%$. The ratio in nH_2 and nD_2 is found to be intermediate between pH_2 and Ne hosts with $R_{ke} \sim 2\%$. The low abundance of keto observed in the present work is in very good agreement with gas-phase NMR studies at 298 K⁵¹ and with Irving and Wadsö results.⁵³ A 2.5% abundance of keto can be extracted from the thermodynamic results of Fokendt *et al.*⁵¹ while Irving and Wadsö⁵³ gives an abundance of 6.7%.

As said before, it was observed that the ratio was sometimes slightly different from one sample to another. This could be due to a temperature effect connected to the deposition process on the cold window of the cryostat: at high flow rates, the incoming gases warm up the window and thus the outer layers of the matrix may not be very rigid. With such a ‘soft surface’ molecules may convert from the keto to the enol form before being completely covered by the host gas and finally trapped in the matrix. Nevertheless, the nature of the matrix remains the main factor for the variation of R_{ke} . A 10% abundance for keto in Xe matrix was reported in a previous work⁷ but this has not been confirmed by other experiments.^{50,106} The R_{ke} value found in most matrix-isolation studies in rare gases is in good agreement with experimentally obtained value of 1% in Ne. The enhancement of the keto form in pH_2 matrices is not well understood. A very qualitative explanation could rely on the ‘quantum’ versus ‘classical’ nature of the host in terms of trapping temperatures. In hydrogen matrices (‘quantum’ solid), guest molecules are immediately trapped inside the solid which is very soft, whereas there is enough time for interaction at the surface in the case of more ‘classical’ hosts such as inert gases.¹¹² In these conditions, the gas-phase ratio at room temperature is kept in hydrogen matrices, while a ratio corresponding to a lower temperature could be found in the other solids. This effect should thus be more pronounced in pH_2 solids.

5. ACETYLACETONE INFRARED SPECTRA

Chapter 6

Coupling between spin states and torsional levels

Enolic Acetylacetone (AcAc) exhibits three coupled large amplitude motions involving hydrogen atoms with different barriers, the intramolecular H-atom (H_{int}) transfers between the two oxygen atoms and the two non equivalent methyl torsions. A complex energy level pattern is thus expected, as recently theoretically investigated by Chou.⁶⁵ This claims for investigating experimentally the hierarchy of couplings between the vibrational levels involved in the (H_{int}) transfer process. In this chapter is presented a thoughtful spectroscopic analysis for documenting the dynamics related to the three entangled large amplitude motions of AcAc in the ground electronic state. It is based on IR spectroscopy of AcAc trapped in a solid para-Hydrogen (pH_2) matrix.

In the section 6.1 the experimental evidence of the spin species of the chelated enol form of AcAc are described. Next in the section 6.2 start with a short discussion of the spin configuration expected in the AcAc molecule due to the CH_3 groups followed by theoretical treatment of this system supported by the DFT calculation performed with the aim to explain the spectra. Finally a comparison between different host and they influence in the infrared spectra are discussed in the last section.

6.1 Experimental evidence of NSC

Since pH_2 matrix is a very soft “quantum” solid in which interaction host-guest is very weak, narrow bands in the infrared spectrum are expected. The IR spectrum recorded immediately after AcAc was trapped in pH_2 contains broad bands belonging to the enolic form (average width of the order of 10 cm^{-1}) and a few narrow bands which were assigned to the keto form (see section 5.2.2). The most

6. COUPLING BETWEEN SPIN STATES AND TORSIONAL LEVELS

interesting spectral range are reproduced in Figure 6.1. Bands are quite broad and some of them have doublet structure. One can think about sites effect, but it is very unlikely due to the softness of the solid. Moreover, annealing at 6K does not modify the spectrum shape.

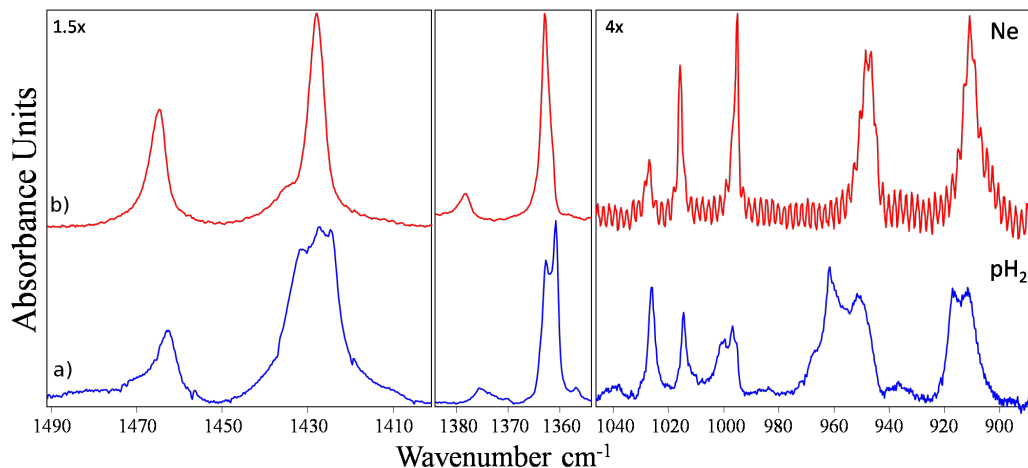


Figure 6.1: Selected regions of the spectrum of AcAc in (a) pH_2 , (b) Ne. Both spectra are recorded just after deposition

In order to clarify the effect of sites for AcAc and be able to compare with pH_2 matrices, AcAc in Ne matrices were built in exactly the same experimental conditions (See experimental-setup). The AcAc in Ne spectra recorded just after deposition is shown in figure 6.1b. All bands seem to be only singlets and most of them are narrow. When compared with pH_2 and Ne some bands are surprisingly broader in pH_2 and the doublet structure does not appear in Ne.

When AcAc in pH_2 matrix was kept on dark during 24 hours, recording infrared spectra each 90 min approximately, some bands have time evolution of their intensities. The effect is very clear on the bands with doublet structure. The time evolution of some of those bands are shown in figure 6.2. In the panel (a) the spectral region between $1350-1370\text{ cm}^{-1}$ is shown. At initial moment $t=0$ this band has a doublet structure with maximum at 1362.7 and 1360.8 cm^{-1} and the band at 1360.8 cm^{-1} is 12% higher than the 1362.7 cm^{-1} band. As time increases, the differences in intensities also increase and at time close to 24 hours the difference in intensities is around 54%. In the panel (b) the same analysis can be done for the bands that display a doublet structure, for instance the bands close to 998 , 955 and 914 cm^{-1} concluding that there are groups of bands with increasing and others with decreasing intensities. Because the tendency is completely opposite, the two components in these bands can be extracted by spectral subtraction.

The whole spectrum is then separated into two components related to two “species”, labelled as most stable (ms) and less stable (ls). The Figure 6.3 shows the AcAc isolated in pH_2 matrices (a)

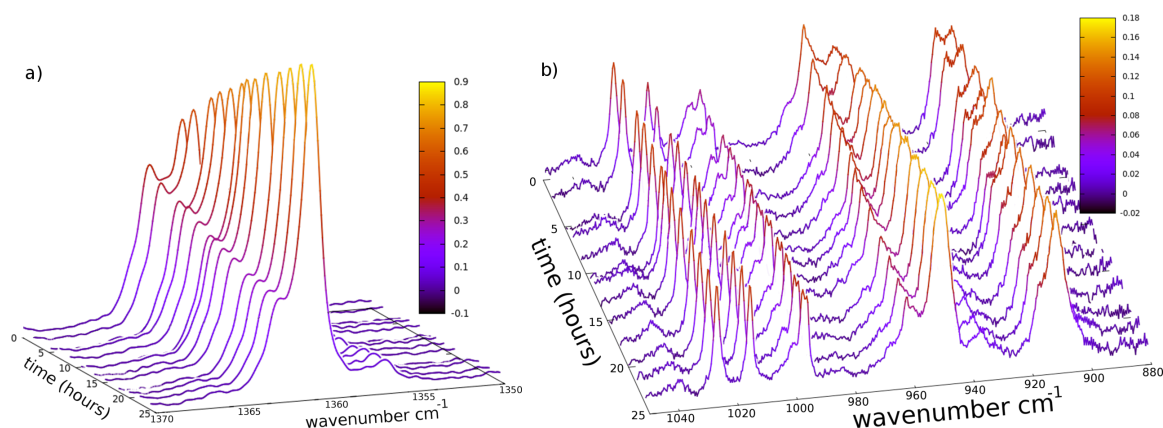


Figure 6.2: Time evolution of the spectra of AcAc in pH₂ when the sample is kept in dark. (a) 135-1370 cm⁻¹ region. (b) 880-1050 cm⁻¹ region.

as deposited sample, (b) the spectrum of the *ls* molecule (c) the spectrum of the *ms* molecule. For comparison AcAc isolated in Ne is shown in the panel (d). Both spectra (b) and (c) are very similar then, almost identical molecules or different states of the same molecule are trapped in pH₂ and one convert into the another one in time. The spectrum of the *ms* specie in pH₂ (see figure 6.3c) is very similar to Ne matrices, moreover no bands have doublet structure and most of them are very thin. It is clear that in Ne matrices only one of those states is stabilized or the conversion to the most stable is very fast.

For mathematical analysis of the changing dynamics, a fit of the band close to 1363 cm⁻¹ for each spectrum was done. The deconvolution of this band can be done by three Lorentzian, corresponding to each *ls* and *ms* species and keto tautomer (see chapter 8 for keto completely assignment). The calculated integral absorbance of both enol species bands were plotted as a function of time in the figure 6.4

The total amount of enol (*ms*+*ls*) is constant along the experiment and was easily checked by the sum of the integrated intensities of *ms* and *ls* in each time instant. The time evolution of the *ms* and *ls* “species” can be fitted by an exponential growth and decay, respectively, with a common rate constant of 0.042 h⁻¹. This value is of the same order of magnitude as the nuclear spin conversion (NSC) rates measured in solid pH₂ on other molecules carrying a methyl group such as CH₃OH³² and CH₃F.¹¹³

As was told in the experimental setup section, the purity of pH₂ in this experiment is 99.9%. Due to the softness of the hydrogen solids, ortho-Hydrogen (oH₂) molecules can diffuse through the matrix and because its has quadrupole momentum the interaction with AcAc molecule is stronger and will be next to the AcAc molecule. Then, one can think about the effect of oH₂ close to AcAc producing

6. COUPLING BETWEEN SPIN STATES AND TORSIONAL LEVELS

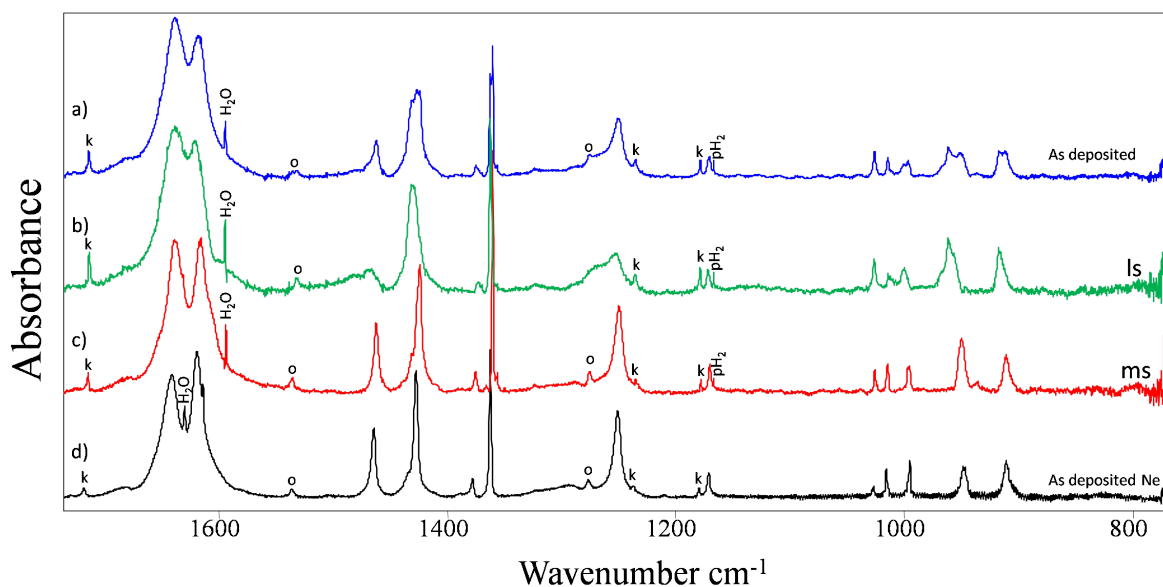


Figure 6.3: *AcAc* in pH_2 (a) as deposited sample. (b) less stable “*ls*” specie. (c) most stable “*ms*” specie. (d) *AcAc* in *Ne* matrix as deposited sample. *k*-keto assigned bands. H_2O -Water assigned bands. *o*-overtones assigned bands. pH_2 -matrix signature

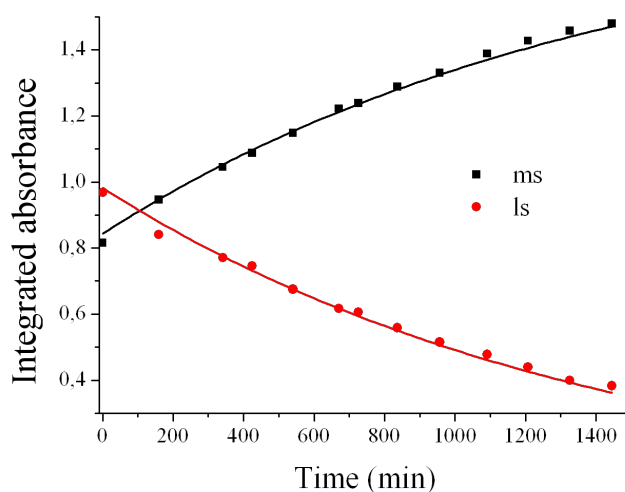


Figure 6.4: Time evolution of the integral absorbance of the bands at 1360.8 and 1361.3 cm^{-1} corresponding to the *ms* and *ls* species respectively. The experimental data points were fitted to an exponential growth and decay respectively, with a common rate constant of 0.042 h^{-1} .

splitting of bands and the $oH_2 \rightarrow pH_2$ NSC been the process that takes place in the experiment. To clarify this hypothesis, similar experiment was done in normal-Hydrogen (nH_2) matrices which have

75% of oH₂ (see chapter 2). In nH₂ matrices, all AcAc are surrounded by oH₂. If the presence of oH₂ next to the AcAc have any effect should be magnified in this kind of experiment.

In nH₂ similar behavior was observed. In time, a group of bands decreases and others increase. Spectra of both, *ms* and *ls*, species were obtained by spectral subtraction. In nH₂ the high concentration of oH₂ broaden the IR absorption bands of both *ms* and *ls* components. For instance, the bands under analysis (1350-1370 cm⁻¹ region), the *ms* band have a bandwidth of 1.12 cm⁻¹ in pH₂ and 1.27 cm⁻¹ in nH₂ while the *ls* band have a bandwidth of 1.46 cm⁻¹ in pH₂ and 3.20 cm⁻¹ in nH₂. In table 6.2 the bandwidths of *ms* specie in pH₂, nH₂ and Ne are reported. In general, bands corresponding to the *ms* specie are narrower in pH₂ than in nH₂.

Hence, the oH₂ → pH₂ NSC would correspond to reducing linewidths in the spectra of both *ms* and *ls* components, whereas the linewidths in the *ms* and *ls* spectra remain constant as a function of time in the experiments. The spectral evolution observed is thus assigned to NSC in AcAc and more precisely in methyl groups of AcAc.

6.2 Nuclear Spin Conversion (NSC)

The multidimensional nature of the intramolecular H-atom transfers (labelled hereafter as intramolecular hydrogen (H_{int}) transfer) process was well established, even in a simple molecule such as the enol form of malonaldehyde (MA), the prototypical dialdehyde.¹¹⁴ In the enol tautomer of 2-methylmalonaldehyde, the interplay between H_{int} transfer and methyl rotation was reported.¹¹⁵ These two latter processes involve large amplitude motions and their coupling can induce complex behaviors. For example, it was predicted theoretically¹¹⁶ and confirmed experimentally¹¹⁷ that the transfer of the H-bonded H-atom in 5-methyltropolone can drive the rotation of the remote methyl group through long range chemical interactions.

The weak effect of pH₂, as a matrix host, on the methyl torsion or rotation has already been proved in the study of small molecules carrying a single methyl group (methanol,³² methylfluorine¹¹³) in pH₂. The nuclear spin of a methyl group is fully coupled to its rotation by symmetry reason. The A-state is associated with the totally symmetric nuclear spin wavefunction (I=3/2) whereas the E-state corresponds to the non symmetric case (I=1/2). Consequently, the A-E transfer of population implies NSC, a slow process compared to thermalisation.¹¹⁸ Hence, immediately after trapping the molecules in pH₂, in the case of a large A-E splitting (i.e. slightly hindered rotation), A and E state populations differ from the Boltzmann distribution at the low matrix temperature (4K).

Indeed, a slow NSC process is observed in AcAc through the evolution in time of its infrared spectrum in solid pH₂. Its analysis can be used to compare the dynamics of the ground vibrational state with that of an excited state related to torsional motion in a methyl hindered rotation. The

6. COUPLING BETWEEN SPIN STATES AND TORSIONAL LEVELS

key point here is that the extra energy in the excited state is not sufficient to overcome the barrier of H_{int} transfer (see energetics in Figure 6.5). Nevertheless, it is deposited in a mode which is expected to trigger the reaction.¹¹⁹ This offers the possibility to probe the efficiency of such triggering when exciting other vibrational modes which turn on the H_{int} transfer by comparing the width of the IR bands for both the ground and torsionally excited states.

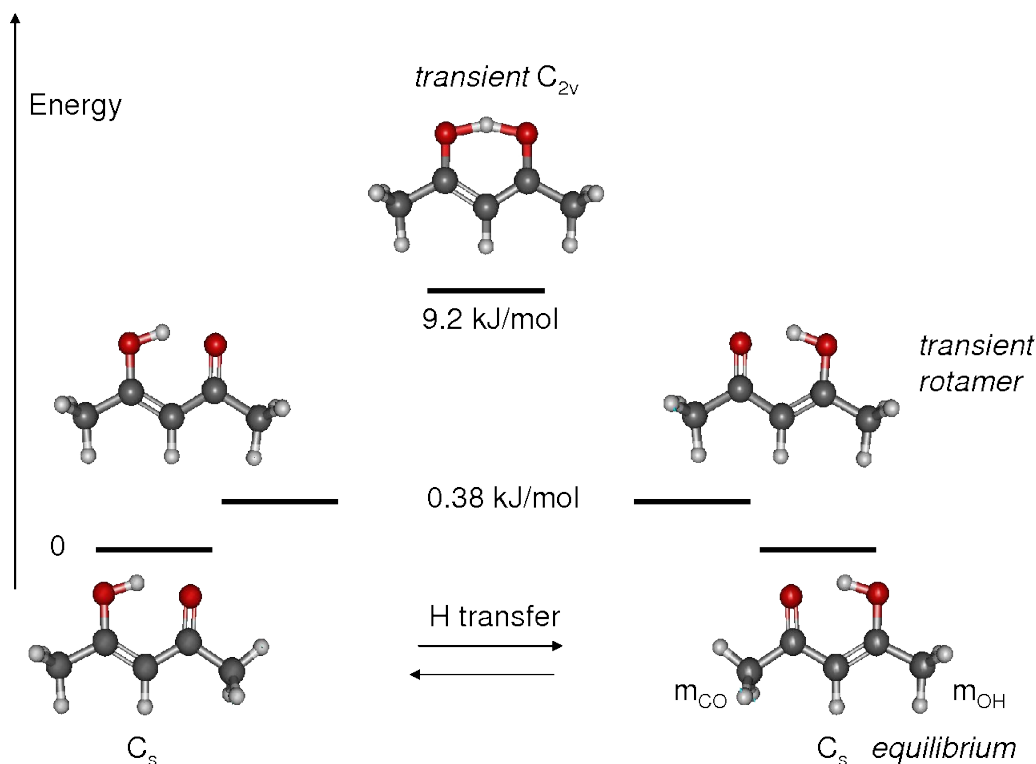


Figure 6.5: Calculated (B3LYP/6-311++G(3df,3pd)) structures and energies of AcAc conformers. C_s equilibrium structures and saddle-point structures: the transient rotamer, a saddle-point in the methyl m_{CO} rotation, and the transient C_{2v} , a saddle-point in the H_{int} transfer. The bottom right structure defines the labels m_{CO} and m_{OH} used throughout this thesis for the methyl groups

6.2.1 Theoretical calculation

DFT calculations of different geometries due to the relatively position of the methyl groups were performed using Gaussian program with B3LYP/6-311++G(3df,3pd) basic set (see chapter calculation). The predicted relevant structures and energetics are shown in Figure 6.5. Geometrical structures and energetics of the stable C_s tautomers and of several transients were also calculated at the MP2 level, using the same basis functions. DFT calculations predict torsional barriers of 32 and 411 cm^{-1} for the methyl on the C=O group side (m_{CO}) and for the methyl on the C-O-H side (m_{OH}) whereas they

are found at 77 and 466 cm^{-1} at the MP2 level, respectively. Such order of magnitude and differences between the two barriers are in qualitative agreement with previous theoretical estimations.¹¹⁹ A large tunnelling splitting (few wavenumbers) is thus expected in the torsional levels of m_{CO} in the isolated molecule. Others calculations^{63,120} suggest that the hindered rotations of the methyl groups couple with the H_{int} transfer as in 2-methylmalonaldehyde. The resulting change in the methyl positions due to the H_{int} transfer appears in the two C_s equilibrium structures at the bottom of Figure 6.5.

Since the CH_3 rotor has a threefold symmetry axis (C_3), the torsional energy levels would be triply degenerate if it were not for the tunneling effect; this, however, splits them into two sublevels, one of which is non-degenerate (symmetry species A of the C_3 -group) and the other doubly degenerate (species E), the A being the lowest.^{118,121} Calculations conclude that the two methyl groups are associated with very different torsional barriers in AcAc. The splitting associated with the m_{CO} torsion, the less hindered methyl rotor, is larger than the other splittings, and can be greatly enhanced due to the coupling with the H_{int} transfer.⁶⁵ The two tunneling splittings have been measured in solid acetylacetone as $40\mu\text{eV}$ (0.32 cm^{-1}) and $0,5\mu\text{eV}$ ($4.0 \cdot 10^{-3}\text{ cm}^{-1}$) for m_{CO} and m_{OH} respectively.¹²²

The potential energy surface of internal rotation of the two methyl groups of AcAc was calculated by Sliznev *et al.*¹²³ The form of the potential surface indicates that the two methyl groups rotate independently of each other: the potential curve describing the rotation of one of the groups is independent of the orientation of the other group.¹²³ In first approximation, the rotation of m_{CO} can be treated as the rotation of a methyl group relative to a reference framework. The potential energy surface of the m_{CO} rotor was calculated using DFT at the same basic functions as before. The molecule was optimized in each step keeping the torsional angle fixed. The values are plotted in figure 6.6.

For simplicity, in a model of a rigid symmetric top (i.e. a CH_3 group) attached to a rigid framework which may be completely asymmetrical, the potential energy hindering rotation may be expressed in a Fourier series as^{121,124,125}:

$$V(\alpha) = \frac{V_3}{2} (1 - \cos(3\alpha)) + \frac{V_6}{2} (1 - \cos(6\alpha)) + \dots \quad (6.1)$$

where V_3 is the height of the threefold potential barrier, V_6 of the sixfold one, and so on.

Herschbach^{124,125} developed a theoretical method to calculate the energy levels for the internal rotation problems and also he has tabulated matrix elements and perturbation sums associated with certain of the periodic solutions of Mathieu's equation. His main idea was to fit the potential energy surface of the rotation of CH_3 to a threefold barrier and use the sixfold part (V_6) as a perturbation to the problem.

In Figure 6.6 the fit a) is done taking into account only the first term of the equation 6.1. As can be seen, even when the height of the barrier was forced to fit the calculated data points, the width is

6. COUPLING BETWEEN SPIN STATES AND TORSIONAL LEVELS

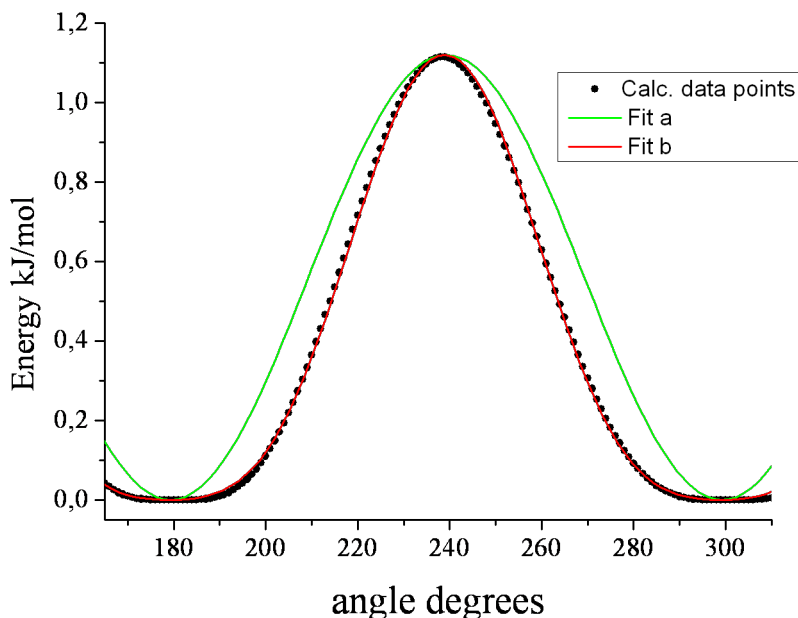


Figure 6.6: Section of the threefold PES of m_{CO} rotation. In dots the calculated data point using DFT(B3LYP/6-311++G(3df,3pd)) method and basis set. Fit a correspond to a fit using only the first term of the equation 6.1. Fit b correspond to a fit including also the second term in the equation 6.1. For the Fit a, the height of the barrier was a constraint

not reproduced at all. Then, a second term V_6 (sixfold) is necessary to fit the calculated data points (see figure 6.6 fit b). In the later fit, the values of $V_3=1.121$ kJ/mol and $V_6=-0,234$ kJ/mol.

The Herschbach method¹²⁵ was used by Fateley *et al.*¹²¹ to estimated the barrier of several small molecules with a single CH_3 rotor. One of the contraction of this method¹²⁵ and the tabulated values¹²⁴ is that (V_6/V_3) must be less than 0.05. In our case this rapport is 0.21 and maybe it can not be treated as a perturbation. Another supposition is that the barrier should be relatively high because for small barrier the error of calculation increases. Nevertheless there is a proposition to treat the very low barriers on the free rotor representation which results in the splitting between levels very sensitive to the barrier height. Theoretical analysis should be develop for this specific system taking into account the coupling between H_{int} transfer and rotation of m_{CO} and m_{OH} .

In Figure 6.6 the width of the barrier is thinner than a simple cosine shape, making higher the difference between the A and E levels than in the case of a simple V_3 threefold barrier. Accurate calculations of the tunneling splitting related to the m_{CO} rotor are lacking, but the “E” levels, higher in energy than the “A” one, should be closer to the top of the barrier. Then, E level should be close to the transient rotamer which is drawn in Figure 6.5. The frequencies of ms (ν_{ms}), ls (ν_{ls})

and the frequency shifts ($\nu_{ms}-\nu_{ls}$) between *ms* and *ls* provided by the experiment are compared in table 6.1 to the calculated frequencies of the stable C_s (ν_s) and transient C_r (ν_r) structures of AcAc and to the difference $\nu_s-\nu_r$ between frequencies of the later species and those of the transient rotamer (both calculated at the same level of theory: B3LYP, harmonic). The experimental values of the *ms* bandwidths and the ratio between (*ls/ms*) bandwidths are also tabulated.

The experimental shifts ($\nu_{ms}-\nu_{ls}$) are strongly mode dependent, and follow essentially the theoretical difference ($\nu_s-\nu_r$). In particular, the large shifts are observed for the OH out of plane bending mode (γ_{OH} , see chapter 5 for bands assignments) at 949.9 cm^{-1} for the *ms* species. This vibration is well explained by the simplified picture of the transient rotamer: the hydrogen bond is stronger in this structure than in the C_s stable one and an almost pure OH bending mode such as γ_{OH} has consequently a higher frequency. The other larger shifts are those of bands at 1269.6 and 1485.8 cm^{-1} which are tentatively assigned to the doublet bands at 1253.0 and 1468.6 cm^{-1} on the *ls* species and will be discussed later in this section.

As the tunneling splitting $\Delta(\text{A-E})$ in the AcAc ground state is the same for all vibrational transitions, the IR spectra reveal also those due to proton tunnelling or change in the methyl torsion in the various vibrational excited states. $|\nu_{ms}-\nu_{ls}|$ values can reach few wavenumbers (till 23 cm^{-1}). This suggests that the observed shifts reflect couplings which perturb the tunneling splittings of the m_{CO} torsions, highlighting the influence of the H_{int} transfer and coupling with the other methyl torsion. In fact, the influence of the H_{int} bond on the m_{CO} methyl rotor was already observed experimentally in solid AcAc where deuteration of the OH group decreases strongly the tunneling splitting of the weaker hindered methyl rotor, but not of the other.¹²²

A striking difference between the *ms* and *ls* spectra concerns the width of the bands, which are narrower in *ms* (see table 6.1). A first origin is that *ls* may include several levels. Nevertheless, the H_{int} transfer is likely involved also. The corresponding line broadening is expected to be mode dependent, hence probing the vibrational dynamics in torsionally excited levels. The barrier height to H_{int} transfer can be estimated as the energy difference between the stable C_s structure and the transient (saddle-point) C_{2v} structure (Figure 6.5). The value of 1359.2 cm^{-1} obtained for MA in CCSD(T)/aug-cc-pVTZ calculations¹²⁶ can be compared to 1276.7 cm^{-1} for AcAc in CCSD(T)/aug-cc-pVDZ calculations.⁶³ In spite of a lower barrier height, tunneling splitting due to hydrogen transfer in AcAc is expected to be smaller than in MA because of the presence of methyl groups which makes the reaction coordinate heavier.

Assuming as above that *ls* has similarities with transient rotamer, the hydrogen transfer in the “E” state should mimic that in MA and has a smaller energy barrier than in the “A” state, hence allowing promoted transfer with vibrational excitation on other modes than the previously described δOH mode at 1298.9 cm^{-1} . Actually, two bands at 1253.0 cm^{-1} and 1468.62 cm^{-1} have a doublet structure in

6. COUPLING BETWEEN SPIN STATES AND TORSIONAL LEVELS

ν_{ms}	ν_{ls}	ν_s	ν_r	Exp-dif	Theo-dif	Bandwidths	
IR-Exp	IR-Exp	IR-Harm	IR-Harm	$\nu_{ms}-\nu_{ls}$	$\nu_s-\nu_r$	ms-Exp	ratio (ls/ms)
771.1	769.3	794.6	799.5	1.8	-4.9	1.3	1.3
910.7	915.9	918.1	930.1	-5.2	-12.0	5.8	1.1
936.3	n.m.	944.0	949.7	-	-5.7	3.1	-
949.9	960.4	1007.7	1025.8	-10.5	-18.1	5.8	1.6
995.3	1000.4	1010.5	1021.8	-5.1	-11.3	3.2	1.7
1014.9	1012.8	1035.1	1034.4	2.1	0.7	1.8	3.2
1025.9	1026.6	1047.4	1045.7	-0.7	1.7	1.4	1.7
1170.5	1171.8	1194.7	1195.0	-1.3	-0.3	3.2	1.1
1250.4	*1253.0	1271.1	1268.5	-2.6	2.6	8.6	1.6
	*1269.6			-19.2			3.1
1298.9	n.m.	1376.7	1367.8	-	8.9	103	-
1360.8	1362.8	1391.5	1392.5	-2.0	-1.0	1.1	1.4
1375.8	1373.2	1412.3	1410.2	2.6	2.1	2.6	1.1
1425.2	1428.9	1459.8	1462.0	-3.7	-2.2	6.3	1.6
1427.1	1432.9	1471.4	1480.6	-5.8	-9.2	1.6	3.7
1432.4	n.m.	1472.4	1471.8	-	0.6	5.6	-
1462.8	*1468.6	1491.6	1498.0	-5.8	-6.4	4.7	1.9
	*1485.8			-23.0			6.6
1617.0	1619.7	1646.1	1642.2	-2.7	3.9	17.4	0.9
1638.9	1639.7	1677.1	1668.9	-0.8	8.2	17.9	1.5

* tentatively assignments to be doublets

Table 6.1: Characteristics of selected modes appearing in the enol infrared spectrum of AcAc isolated in solid pH_2 . ν_{ms} and ν_{ls} are measured frequencies of the ms and ls species respectively; ν_s and ν_r are harmonic calculated frequencies (DFT B3LYP/6-311++G(3df,3pd) of C_s equilibrium structure and of the transient rotamer respectively. Bandwidths extracted from the ms and the ratio of bandwidths ls/ms are also reported. All values in cm^{-1} .

the ls spectrum (see Table 6.1). The first one involves δOH bending and stretching deformation of the pseudo ring whereas the m_{OH} motion, which is the second rotor coupled with the H_{int} transfer, participates to the second band. Finally, the δOH mode at 1298.9 cm^{-1} does not show up in the ls spectrum, either it is too broad to be detected, or it is hidden by the very broad doublet band at 1253.0 cm^{-1} . All these broadening origins reflect the delocalization of the hydrogen atom on the vibrationally excited potential energy surface (PES), coupled with low frequency motions, inducing fast vibrational dephasing. The origins of those doublets are still under study.

No clear evidence of a tunneling splitting due to the internal hydrogen bond can be observed from the IR spectrum of the ms specie. Either (i) the tunneling splitting in the vibrational ground state is negligible as suggested by Chou⁶⁵ in order to explain microwave experiments,⁶⁴ and its possible

enhancement with vibrational excitation is hidden by the bandwidths, or (ii) it is large enough to get only the lower state of the doublet populated at the matrix temperature (4K) and all the vibrational bands originate from this level alone. Alternatively, the H_{int} tunneling process could be quenched by coupling with phonon in the matrix environment. Such process was observed for MA in inert gas matrices^{7,127} and Ar clusters¹²⁸ but it is unlikely in the present soft parahydrogen environment: as H_{int} transfer is coupled with methyl torsions, this quenching should also affect “A”-“E” tunneling splitting and it is obviously only a weak effect in solid pH_2 . AcAc spectra in solid neon (Figure 6.3 d) and solid xenon¹²⁹ are very similar to the *ms* spectrum (Figure 6.3 c). NSC is more efficient in these hosts containing magnetic isotopes, and the fact that only the “A” state is populated explains the spectroscopic similarities. Nevertheless, the “E” state can be thermally populated when the matrix temperature is increased but no temperature effect was observed in these classical hosts, revealing the important “heavy” matrix effect on large amplitude motions in a complex molecule such as AcAc. Note that such a thermal effect was observed in the case of methanol isolated in Neon.¹³⁰

6.3 Bandwidths matrices dependent

Once there is only one species in the sample, the comparison of the effect of the host over the guess makes sense. Table 6.2 shows the position and bandwidths of the *ms* species of AcAc in three matrices (pH_2 , nH_2 and Ne). The calculated frequencies, both anharmonic and harmonic, using Density Functional Theory (DFT) method with B3LYP/6-311++G(3df, 3pd) level/basis-set (see chapter 4) are also tabulated. Next column has the scaled harmonic frequencies using an estimated scaling factor (0.97492) and the last two columns show the ratio between experimental frequencies with anharmonic frequencies and with scaled harmonic frequencies. The scaling factor was estimated as the average value of the ratio experimentally frequencies and harmonic frequencies. Because the bands in the C-H region ($2900\text{-}3030\text{ cm}^{-1}$) are very weak, the estimation of their positions is very inaccurate; even if they are tabulated, they were not used for the calculation of the scaling factor and no discussion about them will be done.

In general, bands in pH_2 matrices are narrower than in the other two solids, i.e nH_2 and Ne. In nH_2 the bands are even broadest than in Ne, confirming that the presence of oH_2 molecules around the AcAc molecules broadening the bands. There is only one band which is really broader in pH_2 than the others: the band at 1298.9 cm^{-1} . This band, assigned to $(\delta_{OH} + \nu_{as}\text{ C}=\text{C}-\text{C}-\text{O})$ is expected to be very sensitive to the nature of the host. As softer is the host the movement δ_{OH} is more free, then larger band in the IR spectra. In Ne as in nH_2 the effect of the interaction between OH and the shell is more important, the available frequencies are restricted and narrower band is expected.

6. COUPLING BETWEEN SPIN STATES AND TORSIONAL LEVELS

pH ₂		nH ₂		Ne		Theory					
position	width	position	width	position	width	Anh	Harm	Int	harm*sf	exp/anh	exp/harm*sf
771.1	1.3	772.9	3.3	770.8	2.0	779.1	794.6	31.7	774.7	0.9897	0.9953
910.7	5.8	911.0	7.1	910.6	6.3	910.7	918.1	36.6	895.1	0.9999	1.0174
936.3	3.1	937.1	5.5	unm.	unm.	930.9	944.0	2.5	920.3	1.0059	1.0174
949.9	5.8	950.4	9.2	947.9	5.5	988.7	1007.7	64.8	982.4	0.9607	0.9669
*995.3	1.4	*995.4	1.6	*995.2	1.4	997.4	1010.5	14.5	985.2	0.9979	1.0103
1014.9	1.8	1015.0	2.1	1015.8	1.8	1014.3	1035.1	10.2	1009.1	1.0006	1.0057
1024.6	1.7	1024.8	2.8	unm.	unm.	1020.7	1063.5	1.1	1036.8	1.0039	0.9883
1025.9	1.4	1026.1	1.8	1027.2	2.6	1023.1	1047.4	7.8	1021.1	1.0027	1.0047
1170.5	3.2	1171.0	3.6	1171.5	3.3	1171.8	1194.7	16.1	1164.7	0.9989	1.0049
1250.4	8.6	1251.0	9.9	1251.4	7.3	1238.6	1271.1	141.7	1239.2	1.0095	1.0090
1298.9	103.0	1297.9	125.6	1297.2	77.5	1297.8	1376.7	83.9	1342.2	1.0008	0.9677
1360.8	1.1	1361.3	1.3	1362.9	1.5	1357.9	1391.5	64.3	1356.6	1.0022	1.0031
1375.8	2.6	1376.2	2.0	1378.6	2.6	1372.3	1412.3	12.7	1376.9	1.0025	0.9992
1425.2	6.3	1425.5	6.8	1428.1	4.3	1421.8	1459.8	130.7	1423.2	1.0024	1.0014
1427.1	1.6	unm.	unm.	unm.	unm.	1430.8	1471.4	14.4	1434.5	0.9974	0.9948
1432.4	5.6	1432.4	8.5	1435.8	6.6	1434.5	1472.4	9.8	1435.5	0.9985	0.9978
1462.8	4.7	1462.7	5.1	1465.1	4.6	1455.3	1491.6	60.6	1454.2	1.0051	1.0059
*1617.0	11.9	*1616.9	12.4	*1619.7	10.5	1612.2	1646.1	269.2	1604.8	1.0029	1.0076
*1638.9	16.3	*1638.5	17.6	*1642.0	15.5	1622.8	1677.1	371.9	1635.0	1.0099	1.0024
2932.5		2931.6		2923.7		2919.5	3034.3	5.4	2958.2	1.0044	0.9913
2935.0		2935.5		2947.5		2929.6	3038.3	17.7	2962.1	1.0018	0.9908
2973.1		2971.7		unm.		2949.7	3090.1	4.8	3012.6	1.0079	0.9869
2974.5		2974.5		2979.7		2963.6	3088.0	6.5	3010.5	1.0037	0.9880
3009.8		3008.0		3021.5		3049.7	3137.9	9.2	3059.2	0.9869	0.9839
3018.9		3016.1		3032.6		3003.7	3143.0	12.1	3064.2	1.0051	0.9852
						3093.3	3211.9	3.1	3131.3		
Overtones											
1275.7	3.3	1276.0	4.1	1276.8	3.3						
1536.9	8.1	1539.4	3.5	1536.7	4.0						
Keto bands											
1178.3	1.4	1179.0	1.8	1179.9	2.1						
1235.2	1.5	1236.0	0.9	1237.3	2.4						
1360.3	0.6	1360.8	0.6	1361.9	1.3						
1424.1	1.5	1423.9	2.0	1426.8	2.0						
1715.3	1.6	1714.5	1.6	1718.9	2.3						
H ₂ O bands											
1594.1	1.1	1595.5	1.4								
				1614.3	0.5						
				1630.6	0.8						

* Bands with shoulder
unm. Unmeasured Bands

Table 6.2: *Experimental frequencies and bandwidths (cm^{-1}) of the chelated enol form of AcAc in different matrices compared with theoretical anharmonic and harmonic frequencies (cm^{-1} calculated at the B3LYP/6-311++G(3df, 3pd) level in the 750–4000 cm^{-1} region.*

Another important remark of the infrared spectra of AcAc is that some bands have shoulder, those bands are labeled with an asterisk in table 6.2. In Ne and nH₂ matrices, regarding to this effect, one

can think about size effect but annealing of the sample does not show change. On the other hand, in pH_2 matrices the same shoulder band can be found (see table 6.2). Size effect is very unlikely in pH_2 matrices due to the softness of the solid then, the cleavage of these bands should have another origin. These modes have very strong coupling with OH movement and H_{int} transfer can be the responsible of those shoulders bands. Unfortunately no accurate theoretical calculations are done to explain the coupling between the H_{int} transfer and others modes in this molecule.

6.3.1 Anharmonic calculations

As was told before, table 6.2 reports a comparison between calculated frequencies for the stable C_s chelated enol form of AcAc in both, anharmonic and harmonic approximation. The anharmonic correction to the frequencies improve very much the quality of calculation, making easier the assignments of AcAc bands. A very common method for comparison between calculated frequencies and experimental ones is applying a scaling factor to the harmonic frequencies. This scaling factor is very dependent of the mode and the method and basis set used for making the theoretical calculation (see chapter 4).

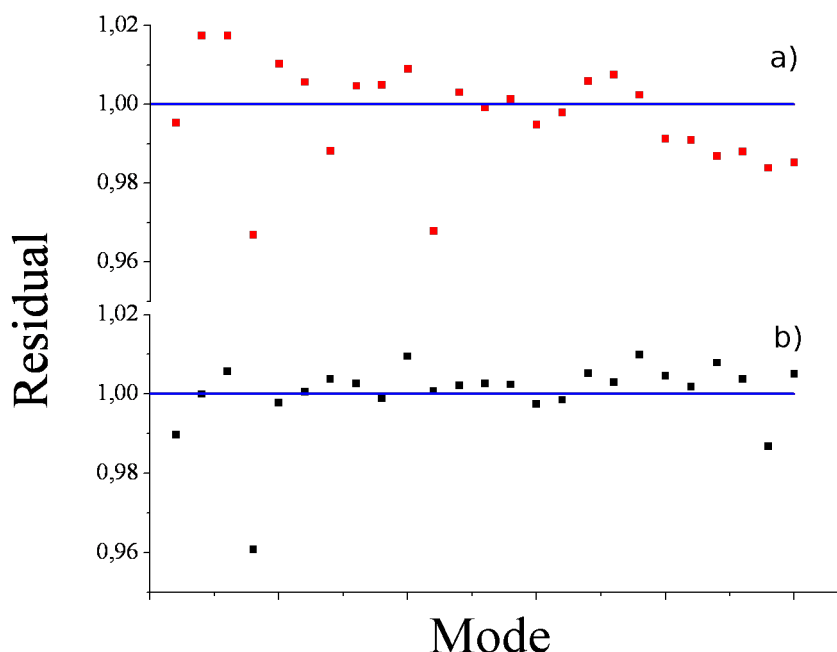


Figure 6.7: Dispersion around the value of 1 of (a) ratio between experimental and scaled harmonic frequencies, (b) experimental and anharmonic frequencies. The scaling factor used was 0.97492 (see text).

Figure 6.7 shows a dispersion around the value one of the ratios between (a) experimental and scaled

6. COUPLING BETWEEN SPIN STATES AND TORSIONAL LEVELS

harmonic frequencies and (b) experimental and anharmonic frequencies. The greatest disagreement between the scaled harmonic frequencies and experimental are the mode that include or are coupled to the γOH , δOH or methyl torsion. i.e large-amplitude motions. Due to the hydrogen atom both the C-H and the O-H bond can be described by a very anharmonic potential energy surface. That is why harmonic approximation can not described those modes in the proper way, then anharmonic correction is necessary.

In figure 6.7b anharmonic calculation have better agreement with experimental frequencies. Only one frequency has a big mismatch respect to the experimental values. This frequency, which is estimated at 988.7 cm^{-1} by anharmonic calculation, is assigned to the bending OH out of plane (γOH). This mode is very much coupled with the torsion of the m_{CO} . The performed DFT calculation can not resolve the torsional frequency of m_{CO} giving a negative value for this mode. Then, because of the coupling between them, no good value can be expected for the γOH mode. Nevertheless all others large-amplitude motion are very well described in the anharmonic approximation.

6.4 summary

In summary, isolation of acetylacetone in solid $p\text{H}_2$ has revealed new vibrational behavior directly related to the complex dynamics intramolecular H-atom (H_{int}) transfer. The isolation of AcAc in solid $p\text{H}_2$ which, on the contrary to classical hosts, preserves subtle intrinsic dynamical properties of the guest molecule such as the large amplitude motions which are at play in AcAc. In particular the experimental evidence of proton tunnelling within the less hindered methyl group of AcAc and related NSC is clearly observed. All the results are in full agreement with a C_s stable structure of the chelated enol form with a nearly free rotation of one methyl.

On the other hand, the observed band widths and positions, by informing on the intrinsic properties of the molecule, offer a quantitative benchmark for future calculations of the H_{int} transfer process. These will be certainly very challenging (but manageable) since they will need to consider the two methyl torsions and the pseudo cycle deformation modes which both host the H_{int} transfer coordinate and interplay with the simultaneous change of the electron configuration.

Chapter 7

UV laser irradiation at 266 nm

This chapter is related with the UV 266 nm YAG laser irradiation of the Acetylacetone (AcAc) isolated in para-Hydrogen ($p\text{H}_2$) matrices. It appears that as soon as irradiation begins, the spectral bands assigned to the CCC conformer have a decreasing intensity, while new bands emerge. Longer irradiation reveals a different behavior of the new bands. A general overview of the AcAc in $p\text{H}_2$ behavior under UV irradiation is presented in the first section. Based on the change of the bands' intensity as a function of irradiation time, the absorption bands of the photoproducts are separated in two groups. Bands of the first group increase in the first several minutes of irradiation, then decrease. The second group of bands continuously increases along the irradiation. The contribution of the first and second groups of bands are then separated by subtracting IR spectra recorded at different irradiation times and their assignment will be discussed in the sections 7.3.1 and 7.3.2 .

UV irradiation experiments at 266 nm have also been performed in normal-Hydrogen ($n\text{H}_2$), in normal-Deuterium ($n\text{D}_2$) and in Neon (Ne) matrices. As in the $p\text{H}_2$ experiments, the new bands appearing upon UV irradiation are divided in two groups. The differences between these and $p\text{H}_2$ matrices will be remarked in each section of this chapter.

An explanation of the kinetics of isomerization processes in $p\text{H}_2$ and compared with theoretical calculation on the excited state will be detailed in the section 7.4. Finally, few very weak bands assigned to fragmentation products are observed after prolonged UV irradiation at higher laser power. They are discussed in Section 7.5.

7.1 General overview

In Figure 7.1 a comparison of spectra recorded after different times of UV laser irradiation at 266nm is presented. (a) as deposited sample where mainly chelated enol form (CCC) is present. (b) mid-

7. UV LASER IRRADIATION AT 266 NM

irradiation point ~ 40 min of irradiation and (c) long irradiation time ~ 300 min. The irradiation time in order to reach similar conditions as those shown in figure 7.1 depends on the sample and laser power. The IR spectra recorded after UV irradiation at 266 nm exhibit many new narrow bands (bandwidths < 2 cm^{-1}). The spectra and the intensity distribution of the bands are not modified in the absence of UV irradiation indicating that no dark nor infrared induced processes are observed all along the experiments. The middle and top spectra in Fig 7.1 correspond to several minutes and several hours of irradiation respectively. The spectra at different irradiation times are very different. Narrow bands appear in spectra (b) and (c) compared to (a) but the bands differ between (b) and (c).

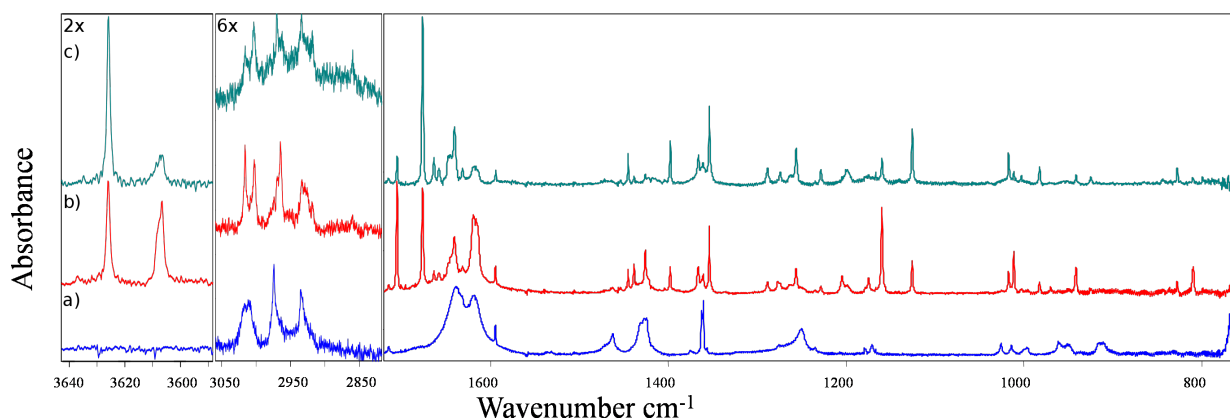


Figure 7.1: IR spectra of AcAc isolated in pH_2 matrix at different UV irradiation times with the 266 nm laser. (a) As-deposited sample (mainly CCC enol form). (b) Mid-irradiation point (~ 40 min of irradiation): the amount of CTC isomer is at maximum. (c) Long irradiation (~ 300 min of laser irradiation): mainly TCC and TTC isomers are present

Figure 7.2 shows irradiated AcAc spectra in different matrices (a) pH_2 , (b) nH_2 , (c) nD_2 and (d) Ne. In all spectra, the bands of the chelated enol form (CCC) were subtracted for better comparison. In Ne matrices the spectrum looks very similar as in pH_2 matrix suggesting the same products are formed in both matrices after UV 266 nm laser irradiation. On the other hand, in nH_2 and nD_2 experiments (See figure 7.2) a new group of bands labeled with '+' appear after UV irradiation. All the new bands can be assigned to open enol isomers (*see later*).

In all four matrices, two groups of isomers bands can be distinguished. The first group of bands increases with the irradiation time during the first several minutes and after decreases when irradiation continues. The second group of bands is always increasing with the irradiation reaching saturation condition when the CCC bands and first group of bands are almost depleted. Because of these behaviors, first and second groups of bands can be separated by subtraction of spectra recorded at different times of irradiation.

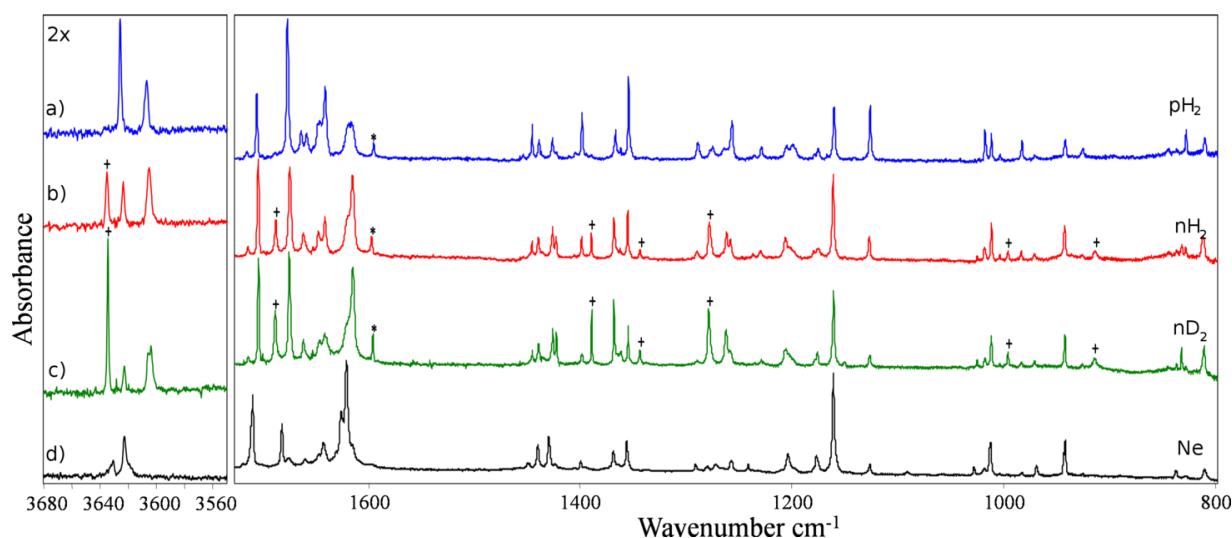


Figure 7.2: Irradiated AcAc in different matrices. (a) pH_2 , (b) nH_2 , (c) nD_2 and (d) Ne. The spectra were recorded after several min and the bands of the chelated enol form CCC were subtracted in all spectra. (+) new bands that appear only in nH_2 and nD_2 . (*) water bands

7.2 Theoretical calculations

Density Functional Theory (DFT) calculation of single molecule of all possible isomers of AcAc were performed using Gaussian package. The basis set used for these calculation was B3LYP/6-311++G(3df,3dp). First, the geometry optimization was done followed by the calculation of the IR frequencies in both harmonic and anharmonic approaches. The values of all IR frequencies obtained in the simulations are listed in the appendix B. Schemes of the molecule were reported in figure 1.5 in chapter 1 with calculated relatively energies. The results obtained are in good agreement with the values reported in the literature.⁶⁷

The isomerization processes concerning to the rotation around the C-O bond of the OH group of the enolic AcAc from a *cis* to *trans* configuration and vice versa ($XYC \rightleftharpoons XYT$) were also calculated. The geometry was optimized each 5 degrees of the rotational angle. For construction of the potential energy surface (PES) the energy for each geometry using the same method and basis set as before.

7.3 Spectroscopic analysis

7.3.1 Assignment of the First Group

The IR spectrum of the first group in pH_2 is presented in figure 7.3(a), together with DFT calculated spectra of CTC (b) and CTT (c). As expected, no site effect due to the pH_2 matrix is apparent.

7. UV LASER IRRADIATION AT 266 NM

Moreover, bands are very sharp except for the band at 1617 cm^{-1} (9 cm^{-1} bandwidth) which is discussed in section 7.3.3

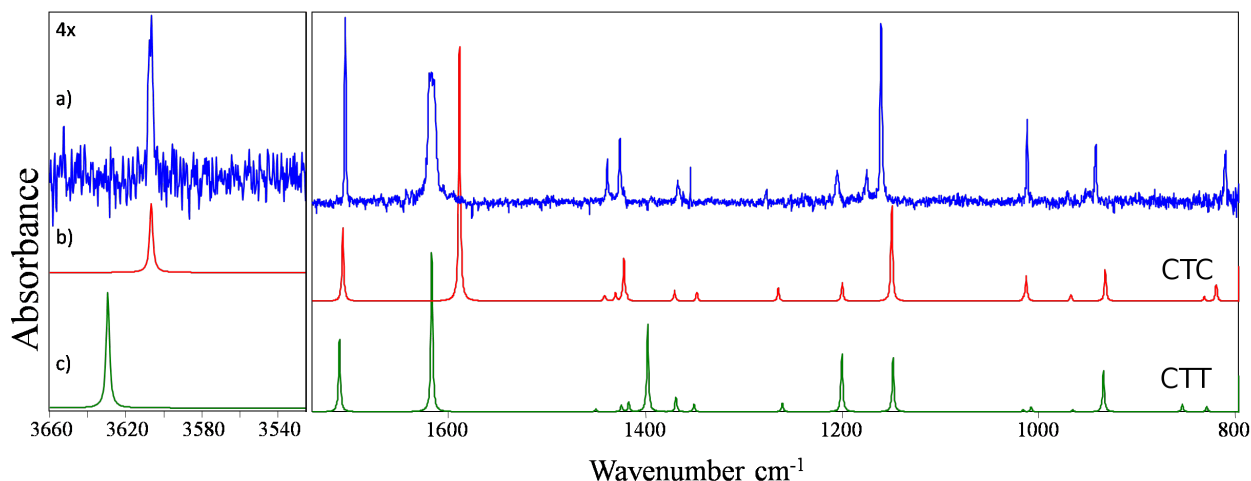


Figure 7.3: (a) Experimental spectrum of the first group of isomers in pH_2 and DFT anharmonic calculated spectra of CTC (b) and CTT (c). Theoretical bands are represented by Lorentzian profiles with bandwidths of 2 cm^{-1} where the intensities correspond to the harmonic calculation

In the OH stretching region, a single band is observed at 3606.7 cm^{-1} . This mode is quite intense and is very sensitive to the conformer. Hence, the first group likely consists of only one conformer. Effectively, comparison in the whole spectrum confirms the assignment to a single conformer. Predicted values of CTT and CTC are close to experimental frequencies (see Fig. 7.3) but the best agreement in terms of frequencies and intensity distribution is obtained for CTC, hence supporting assignment of the observed spectrum to the IR absorption of CTC.

Experimental frequencies and CTC anharmonic calculated frequencies are summarized in Table 7.1. The additional experimental band at 1175.2 cm^{-1} in pH_2 , which matches no fundamental mode of enol conformers, is assigned to a combination band.

In pH_2 the isomerization of the chelated enol form occurs and in the first several minutes leads mainly to CTC isomer. In previous studies, a first group of isomers was also extracted from UV irradiated samples of AcAc isolated in matrices and was assigned to the CTZ pair (with $Z = T$ or C), with the CTT/CTC ratio depending on the host. The CTT form was clearly observed in solid nitrogen⁵⁷ but in argon and neon matrices, CTT was either not identified⁵⁸ or was found unstable.⁵⁰ This conformer is predicted to lie 3 kJ mol^{-1} above CTC. The rotational barrier of the hydrogen atom around the C-O bond is roughly estimated to 21 kJ mol^{-1} by our DFT calculations.

Under such conditions, a proton tunnelling process through the barrier can explain the non-observation of CTT: even if CTT was formed under UV irradiation, $CTT \rightarrow CTC$ isomerization

Ne	nH ₂	nD ₂	pH ₂	CTC calculations
			625	623.0 (40.1)
810.7	812.8	811.1	810.3	819.3 (38.1)
837.4	837.0	837.2	836.9	831.5 (10.3)
942.2/943.6	942.5/943.5	942.2	942.0	932.0 (70.4)
969.3	971.2	971.1	970.9	967.0 (15.0)
1012.9	1011.7	1011.9	1011.7	1012.5 (60.5)
1161.0	1161.2	1160.6	1160.2	1149.3 (214.7)
1177.2 ^a	1174.8 ^a	1176.1	1175.2 ^a	
1204	1206.0	1206.6	1204.9	1199.6 (41.5)
1279/1281	1277.6	1277.2	1277.1	1264.7 (30.2)
1356.1	1355.0	1354.3	1354.1	1347.4 (20.4)
1368.4	1368.1	1367.4	1366.6	1370.1 (24.9)
1429	1425.9	1425.6	1425.9	1421.7 (95.2)
1440	1439.5	1439.2	1438.7	1430.2 (17.8)
1620.5	1614.7	1614.3	1615.1	1588.8 (579.9)
1625.6 ^a	1620.0 ^a	1619.9 ^a	1619.2 ^a	1634.2 ^b
1709/1710.5	1703.7	1703.6	1705.1	1707.4 (167.9)
2944	2929	2927.8	2927	2923.5 (16.1)
2973 (vb)	2966	2966.0	2964	2938.2 (10.3)
3003/3010	3003.5	3001.8	3002	3002.1 (12.1)
3019	3016.5	3017.2	3015	3019.6 (15.3)
3622.6	3605.0	3605.5	3606.7	3606.4 (43.8)

^a Combination bands.

^b Tentatively assigned to 2* γ_{CH} with γ_{CH} calculated at 819.3 cm⁻¹

Table 7.1: *Experimental vibrational frequencies (cm⁻¹) assigned to CTC (first group of isomers) in Ne, nH₂, nD₂ and pH₂ and calculated CTC anharmonic frequencies (cm⁻¹). Theoretical harmonic intensities (km mol⁻¹) given in parentheses. vb: very broad*

would occur faster than our observation time window by means of IR spectroscopy. Such proton tunnelling associated with a torsional rotation was explicitly observed in the case of formic acid isolated in argon¹³¹; the authors concluded that the main tunnelling pathway is phonon-assisted tunnelling between different vibrational levels of the two *cis* and *trans* species.

7.3.2 Assignment of the second group

The spectra of the second group, see figure 7.4, cannot be explained by the absorption of a single conformer. In pH₂, in the OH stretch spectral range, two bands were observed, a strong one at 3625.8 cm⁻¹ and a weaker one at 3607.4 cm⁻¹. The latter is very close to the previously assigned CTC band.

7. UV LASER IRRADIATION AT 266 NM

It was carefully checked that this weak band was not due to bad compensation with the first group. Therefore it was assigned to a conformer belonging to the second group.

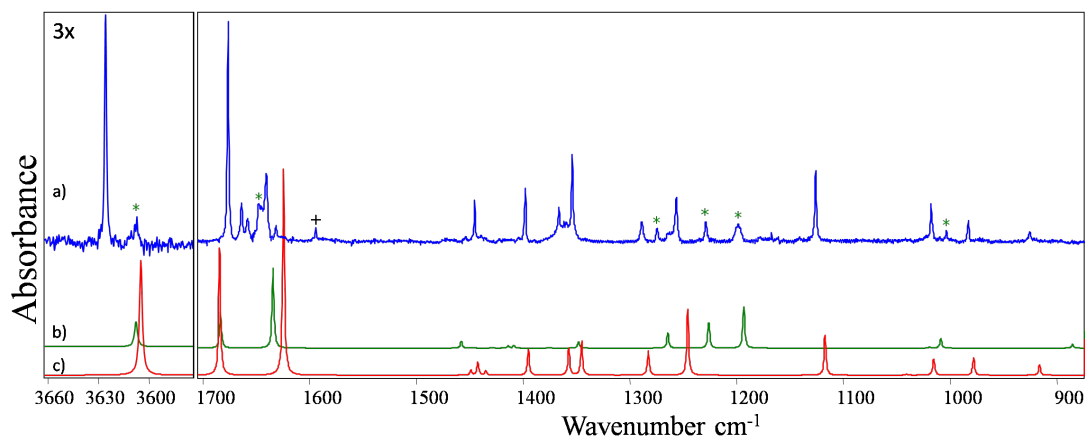


Figure 7.4: Experimental spectra of the second group of isomers in $p\text{H}_2$ (a) and DFT calculated anharmonic frequencies spectra of TTC (b), TCC (c). Theoretical bands are represented by Lorentzian profiles with bandwidths of 2 cm^{-1} and intensities from harmonic calculation. (+) labeled the water bands. In the experimental spectrum, TTC isomer is labeled with green (*)

The Figure 7.4 compares theoretical spectra of TCC and TTC conformers with the experimental spectra of second group isomers. TCC is identified based on the spectral bands observed in the $1800\text{--}800\text{ cm}^{-1}$ range which have an overall agreement with calculations. In particular the pattern in the $1100\text{--}900\text{ cm}^{-1}$ region satisfactorily reproduces the observed spectrum. The other conformer is assigned to TTC, in particular because the 1193.1 cm^{-1} and 1225.9 cm^{-1} calculated vibrational frequencies are very close to the experimental bands at 1198.8 cm^{-1} and 1228.9 cm^{-1} . Calculations fail in predicting the frequency shift between the OH stretching modes (νOH) of both conformers. Nevertheless we can confidently assign the 3625.8 cm^{-1} high-frequency band to TCC and that at 3607.4 cm^{-1} to TTC based on the overall vibrational intensity distribution of both species. Experimental frequencies and corresponding theoretical values are listed in Table 7.2.

The figure 7.5 compare the second group of bands in different matrices, (a) $p\text{H}_2$, (b) Ne, (c) $n\text{H}_2$ and (d) $n\text{D}_2$. The bad compensated bands denoted with label (1) in Ne, $n\text{H}_2$ and $n\text{D}_2$ are assigned to the first group. It is impossible to get the pure spectra of the second group of isomers in these matrices. In classical cryogenic matrices site effect is important, unlike in the $p\text{H}_2$. Some bands show doublets when only single transition is expected. During the sample irradiation with UV laser, the temperature of the matrices increases locally and when the laser is turned off the local temperature goes down again. Then matrices are submitted to annealing processes during all the experiment because of the laser radiation. It is well know that the relative intensities of doublets bands could

7.3 Spectroscopic analysis

Ne	pH ₂	nH ₂	nD ₂	Calc. TCC	Calc TTC	Calc TCT
828.5	827.8	828.3	828.1	836.3 (16.4)		
		832.0	832.2			843.2 (24.4)
845.5	844.7	844.7	844.9		846.2 (34.8)	
		913.7	914.2			910.9 (55.3)
926	925.6	926.4	926.9	916.0 (19.6)		
983	983.0	983.8	983.6	977.9 (32.4)		
		996.2	996.2			986.8 (41.9)
1004	1003.4	1003.9	1003.8		1008.5 (49.3)	
1018	1017.7	1018.0	1017.7	1015.3 (28.0)		
		1025.0	1025.0			1026.1 (7.1)
1126.5	1126.2	1127.1	1126.8	1116.9 (74.9)		
		1150.3	1150.3			1120.8 (10.6)
1197(?)	1198.8	1200.9	1200.4		1193.1 (220.9)	
1230	1228.9	1229.5	1228.8		1225.9 (138.2)	
1257.5	1256.8	1258.1	1258.4	1245.6 (123.6)		
		1261.9	1262.1			1239.0 (141.3)
1266/1273	1274.6	1276.8 ^{sh}	1275.9 ^{sh}		1264.3 (80.8)	
		1278.3	1278.6			1266.8 (172.0)
1291	1288.8	1289.7	1289.8	1282.6 (45.2)		
		1343.7	1343.5			1342.1 (65.3)
1355	1354.1	1355.2	1355.1	1345.0 (63.5)		
1368.5	1366.6	1367.7 ^{sh}	1367.2 ^{sh}	1357.1 (49.6)		
		1368.2	1368.1			1360.2 (49.7)
		1389.3	1389.0			1384.1 (28.0)
1399.5	1398.1	1398.5	1398.6	1394.9 (47.4)		
		1422.8	1422.6			1421.6 (24.1)
1449.5	1445.3	1445.5	1445.3	1442.3 (25.7)		
	1453.8	1453.9	1453.5		1457.7 (38.0)	
1642	1640.9	1641.0	1641.1	1624.3 (389.2)		
1647/1651	1647.1	1647.0	1646.8		1634.0 (426.8)	
1660 ^a	1658.1 ^a			1664.2 ^a		
		1661.1 ^{a,b}	1661.4 ^{a,b}	1664.2 ^a	1677.8 ^a	1678.9 ^a
1672 ^a	1663.9 ^a				1677.8 ^a	
		1673.2 ^{sh}	1674.0 ^{sh}			1671.7 (391.4)
1681.5	1676.2	1674.5	1675.0	1684.1 (237.0)	1683.3 (192.1)	
		1687.3	1687.8		1686.6 (111.9)	
2929	2919	2921.2	2921.6	2924.8 (7.3)		
2949	2933	2934.4	2934.4	2930.4 (11.2)	2938.0 (11.7)	
		2949.2	2949.5			2918.6 (23.3)/2918.4 (10.6)
2984	2970	2970.2	2976.8	2960.4 (8.9)	2974.3 (13.3)	
		2981.0	2983.5			2958.9 (7.2)
3008	3003	3004.8	3008.9	2987.2 (5.5)	2990.0 (9.9)	
		3009.8	3016.6			2998.3 (12.7)/3002.9 (5.2)
3024	3017	3017.5	3024.4	3000.4 (6.9)		
	3607.4	3605.0	3603.9		3607.8 (49.9)	
3631.4	3625.8	3623.8	3623.3	3604.9 (86.2)		
		3635.3	3634.6			3644.3 (89.1)

^a Tentatively assigned to 2* γ_{CH} . ^b Mean value corresponding to the maximum of the envelop of the three combination bands. ^{sh}:Shoulder

7. UV LASER IRRADIATION AT 266 NM

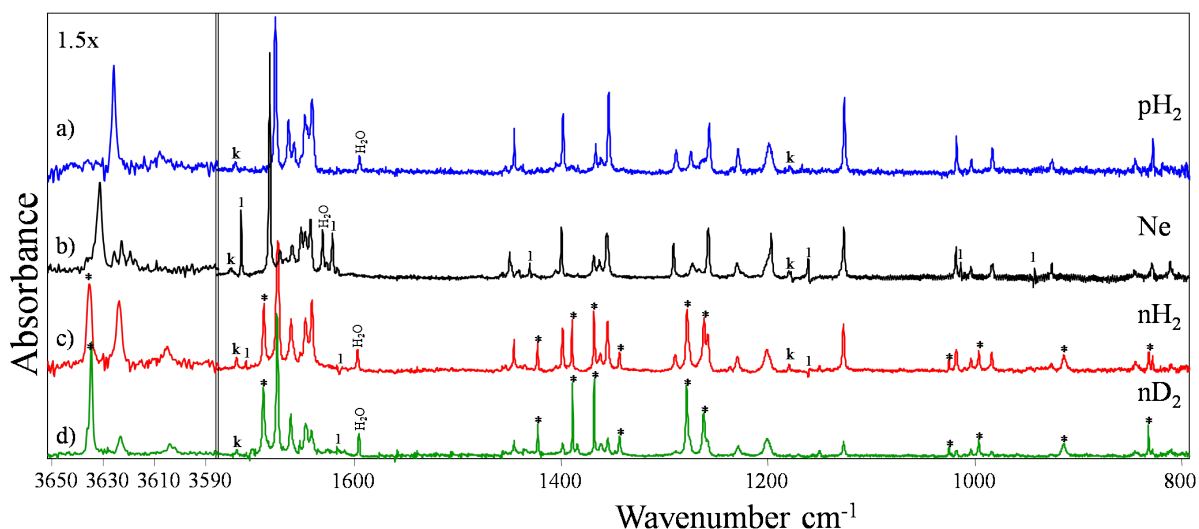


Figure 7.5: Second group bands in different matrices. (a) pH_2 , (b) Ne, (c) nH_2 and (d) nD_2 . Negative bands are assigned to the first group. Bands labeled with asterisk are the new isomer that appear in nH_2 and nD_2 . The label (k) denotes keto bands. H_2O label the water trapped in the matrices. The label (l) means the bands corresponding to the first group that cannot be compensated in the spectral subtraction.

change under annealing when site effect is present then the band structure of each isomer is not the same during the experiment. This makes impossible to obtain pure spectra of the second group of the isomers.

The spectrum of the second group in Ne is very similar to that in pH_2 , allowing the same assignment to TCC and TTC conformers. Experimental frequencies observed in Ne study are presented in Table 7.2. One can notice that the TTC/TCC ratio in Ne is not the same as in pH_2 confirming the presence of these two isomers in both experiments. This ratio is lower in Ne explaining why TTC was not identified in some previous studies in Ne.⁵⁰

Surprisingly, the spectrum of the second group in nH_2 and nD_2 has several additional bands. Bands labeled with asterisk in the Figure 7.5 highlights the differences between nH_2 and pH_2 hosts. In the νOH spectral range, a new band at 3635.3 cm^{-1} for nH_2 and 3634.6 cm^{-1} for nD_2 matrices is observed. The pattern of additional bands is in good agreement with the calculated frequencies of the TCT conformer. Experimental and theoretical values are reported in Table 7.2. The figure 7.6 shows a comparison between bands of second group isomers in nH_2 and the calculated IR spectra in the anharmonic approximation of the TCT isomer. The bands labeled with asterisk are the bands assigned to the TCT isomer. The non-observation of these bands in pH_2 and Ne confirms the absence of TCT in these media.

Vibrational frequencies reported in Ar⁵⁸ for the TCT conformer are in very good agreement with

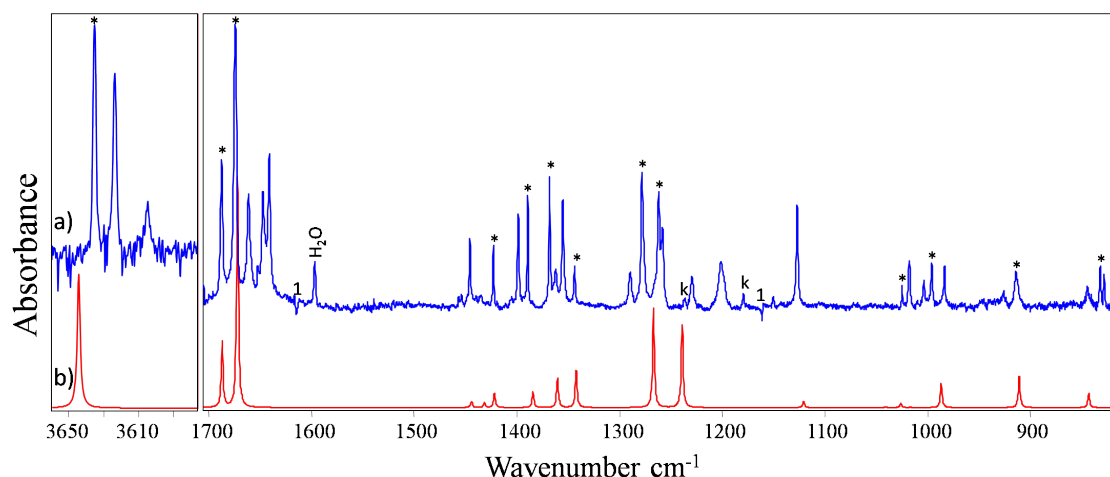


Figure 7.6: Comparison between the experimental spectrum of the second group of isomers in nH_2 matrix (a) and calculated infrared spectrum of the TCT isomer using B3LYP/6-311++G(3df,3dp) basis set in the anharmonic approximation (b). The experimental bands of TCT are labeled with an asterisk. Keto bands are labeled with (k) and water bands are labeled with H_2O . The label (1) denotes the bad compensated first group bands during spectral subtraction.

our IR measurements in nH_2 and in nD_2 . As TCC is lower in energy than TCT by 4.43 kJ mol^{-1} , we assume that TCT isomerizes to TCC in pH_2 and Ne by a proton tunnelling process, as previously discussed for CTC and CTT. The weak electrostatic guest–host interaction in $nH_2(nD_2)$ is strong enough to quench this process. This highlights the matrix effect on the TCT to TCC conversion process.

In previous works on AcAc isolated in inert gas matrices, TCT and TCC were identified after prolonged UV irradiation.^{50,57,58} In contrast, none of the bands assigned to TTC in the present work were observed by Coussan and co-workers.^{50,57} This suggests that the TTC conformer was either not formed or destroyed under their experimental conditions. The experimental band at 3631.7 cm^{-1} assigned to the TCT/TCC pair in Ne by the authors thus supports our assignment for the high-frequency band at 3625.8 cm^{-1} in pH_2 to the ν_{OH} mode of TCC. One can note from Tables 7.1 and 7.2 that among the observed open isomers, the lowest ν_{OH} frequency (LF) belongs to CTC and the highest one (HF) to TCT.

7.3.3 Combinations bands

Previous works drew a peculiar attention to the $1800\text{--}1500 \text{ cm}^{-1}$ spectral range which was used as the IR signature of the conformers.^{2,23,50,57} For each enol conformer, only two strong IR modes are predicted in this range, involving mainly a combination of C=C and C=O stretches (ν_{CC} and ν_{CO})

7. UV LASER IRRADIATION AT 266 NM

more or less coupled depending on the isomer. The lowest energy mode is the most intense and involves ν_{CC} and ν_{CO} in-phase vibration. In the high-energy component they are in phase opposition. These two bands are observed experimentally but additional bands are also visible in this region. As reported in Tables 7.1 and 7.2, these bands are tentatively assigned to an overtone of the out of plane CH bending mode (γ_{CH}). Likely, an interaction exists (Fermi resonance) between this non-fundamental mode and the low-frequency component of the ν_{CC} - ν_{CO} doublet. This might account for the non-negligible intensity of the additional band and the reduced intensity of the in-phase ν_{CC} - ν_{CO} band, compared to calculated intensities. Moreover, the frequency measured experimentally for this band is more shifted from the theoretical value than the other bands. The interaction regarding this fundamental mode is probably more pronounced in the case of CTC conformer. Indeed the strong low-frequency band of the doublet around 1617 cm^{-1} appears much broader than any other band, and this broadening hides a double band with two components of similar intensities at 1615.1 and 1619.2 cm^{-1} . A structure is observed in the corresponding band in Ne, which may be due to site effects.

7.4 Relaxation process

7.4.1 Kinetic study

The isomerization process induced by irradiating AcAc/pH₂ samples at 266 nm has been monitored by recording the time evolution of all conformers. IR spectra have been measured at different times during the irradiation. Low energy pulses are used for these irradiations and the kinetics is observed to be linear on the average laser energy. The pulse energy is kept constant all along the kinetic measurements. As the spectra of the four isomers (CCC, CTC, TCC and TTC) strongly overlap, the choice of a characteristic spectral range to measure the time evolution of each isomer turns out to be delicate. In particular, the CCC isomer presents broad bands, hiding a complex structure. Its time evolution has thus been deduced by measuring the intensity of CCC in the whole spectrum at all time intervals. Bands of open isomers are narrower and direct measurement of their time evolution is performed on different bands of each isomer. This analysis can be used to clarify the assignment of bands to a specific isomer, in particular to distinguish the bands of TCC and TTC isomers. Specific main bands for each isomer are thus chosen to study the overall kinetics. The clearest results are obtained using bands at 1705 , 1126 and 1229 cm^{-1} to represent CTC, TCC and TTC isomers respectively.

The time evolution upon UV irradiation is shown in Figure 7.7a. CCC decreases during irradiation, reaching a very low level at the end of the experiment. CTC increases in the beginning of irradiation and decreases after about 40 minutes under the experimental conditions shown in Figure 7.7. TCC

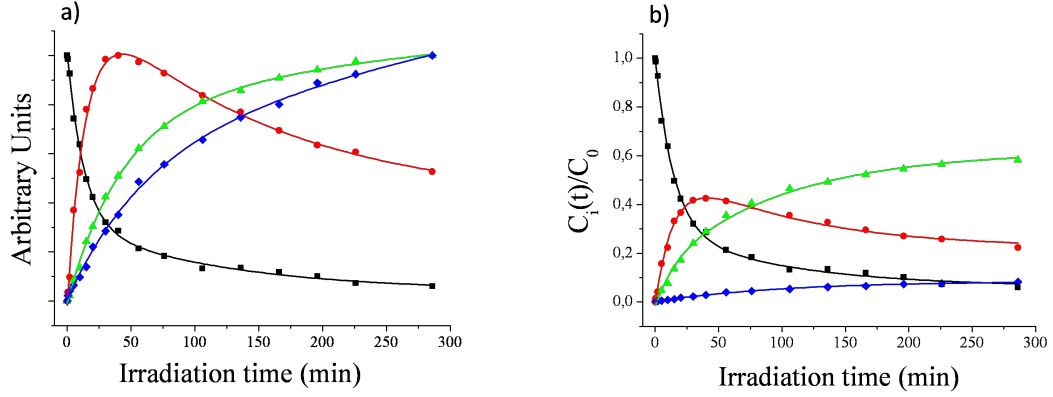


Figure 7.7: Time evolution of the normalized intensities (a) and concentrations (b) of the four enol isomers of AcAc observed in parahydrogen: CCC (black squares), CTC (red circles), TCC (green triangles upward) and TTC (blue diamonds). Intensities of the open isomers are measured on specific bands at 1705 cm^{-1} (CTC), 1126 cm^{-1} (TCC), 1229 cm^{-1} (TTC), and from the whole spectrum for CCC.

and TTC continuously increase without reaching a stationary value. The integrated absorption of each band were first normalized to distinguish between TCC and TTC isomers. As it is shown in the figure 7.7a, the time evolutions of TCC and TTC are different enough to clarify their assignments, but too similar for extracting the spectrum of each conformer in the so-called second group of isomers.

Rate constants are extracted from the experimental data using a simple model of elementary reactions where fragmentation is neglected and where TCC and TTC isomers are not distinguished (labelled as TYC). The processes considered are as follows (detailed explanation is in appendix A):



with

$$C_{t=0} = C_0(t) + C_1(t) + C_2(t) \quad (7.4)$$

Where

$C_0(t)$ is the concentration of the CCC isomer of AcAc

$C_1(t)$ is the concentration of the CTC isomer of AcAc

$C_2(t)$ is the sum of concentration of the TCC and TTC isomers of AcAc

7. UV LASER IRRADIATION AT 266 NM

and

$C_{t=0}$ is the initial concentration of CCC isomer, i.e $C_{t=0} = C_0(t = 0)$.

Kinetic analysis gives an equation for the time evolution of each of the three species, involving the kinetic rate constants and the three concentrations. Because of relation (7.4) only two of them are linearly independent, a linear system of two first order differential equations needs to be solved. Solving the kinetic equations leads to equation (7.5) which expresses the concentration C_i of each species as a sum of two exponential functions involving the same characteristic times τ_1 and τ_2 for the three species, in addition to a constant value:

$$C_i(t) = A_i e^{-\alpha_1 t} + B_i e^{-\alpha_2 t} + D_i \quad (7.5)$$

with

$$\alpha_{12} = \frac{1}{\tau_{12}} = \frac{-(D_1 + D_2) \pm \sqrt{(D_1 - D_2)^2 + 4D_3 D_4}}{2} \quad (7.6)$$

and

$$D_1 = k_{01} + k_{02} + k_{20}$$

$$D_2 = k_{12} + k_{10} + k_{21}$$

$$D_3 = k_{10} - k_{20}$$

$$D_4 = k_{01} - k_{21}$$

The values measured are integrated absorbance ($A_{bi}(t)$), proportional to concentrations $A_{bi}(t) = \varepsilon_i C_i(t)$, and their time evolutions obey similar equations involving the same two exponential decays. Such expressions reproduce very well the time evolutions of all species (Fig. 7.7). From the experimental data (See Appendix A), values of $\tau_1 = 105 \pm 12$ min and $\tau_2 = 15.9 \pm 0.8$ min are obtained. These characteristic times are functions of all six k_{ij} kinetic constants, which necessarily depend on experimental conditions such as the laser fluency and the irradiation wavelength. In order to have the k_{ij} values, one needs the relative concentrations $C_i(t)$ from the measured $A_{bi}(t)$ values and thus the coefficients ε_i linking $C_i(t)$ and $A_{bi}(t)$. From equation (7.4), one can obtain the ratio between absorbance factors $\left(\frac{\varepsilon_0}{\varepsilon_1}\right)$ and $\left(\frac{\varepsilon_0}{\varepsilon_2}\right)$ (see Appendix A) and then determine the relative concentrations $C_{i=0,1}$, referring to CCC and CTC respectively .

In order to have a quantitative view of the kinetic processes in terms of concentrations, in figure 7.7b the time evolutions of C_i for the four species is reported: $C_0 = [\text{CCC}]$ is normalized to 1 at $t = 0$, $C_1 = [\text{CTC}]$ is obtained from A_{b1} and parameter $\left(\frac{\varepsilon_0}{\varepsilon_1}\right)$, $C_2 = [\text{TCC}]$ and $C_3 = [\text{TTC}]$ are obtained from A_{b2} and A_{b3} weighted by the theoretical harmonic intensities of the characteristic extracted bands of these two species (at 1126 and 1229 cm^{-1}). From figure 7.7b one clearly sees that CTC is the main

k_{01}	k_{02}	k_{12}	k_{10}
0.034(0.005)	0.014(0.004)	0.006(0.005)	0.019(0.003)

Table 7.3: Calculated values of the rate constants (k_{ij}) in min^{-1} . In parentheses are tabulated the estimated error.

product after excitation of CCC and that TTC remains a minor product all along the irradiation. This shows that the kinetic constants related to TYC mainly reflect the evolution of TCC.

From the parameters obtained by fitting equation (7.5) to the experimental data, the k_{ij} rate constants can be obtained. The calculated values are listed in table 7.3, k_{20} and k_{21} are found negligible (see Appendix A). A simplified diagram of the isomerization kinetic is presented in the figure 7.8. It could have been thought that the second group of isomers (TCC + TTC) is populated at the expense of the first group (CTC), but the present quantitative exploration of the kinetics indicates that it is not the case ($k_{02} \neq 0$). Nevertheless, the rate constant for forming CTC from CCC is by factor 2.4 larger than that for forming TCC + TTC, implying that upon irradiation at 266 nm, CCC mainly undergoes isomerization to CTC. In turn CTC isomerizes essentially to CCC ($k_{01}/k_{12} = 3.2$) but this reverse process is less efficient than the $\text{CCC} \rightarrow \text{CTC}$ isomerization. These rate constants reflect the probabilities to form isomers after UV excitation and are the product of the branching ratio to the observed isomer times the excitation efficiency.

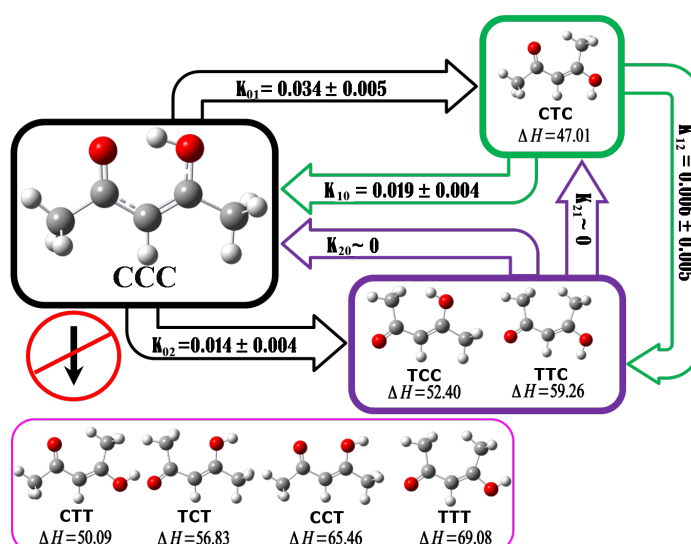


Figure 7.8: Simplified kinetics' diagram of isomerization processes. $\Delta H(\text{kJ/mol})$ are the differences in theoretically calculated energy between each isomer and the CCC form, using B3LYP/6-311++G(3df,3dp) basis set. $k_{\pm i}$ in min^{-1} are the estimated values of rate constants.

7. UV LASER IRRADIATION AT 266 NM

At 266 nm, CCC is efficiently excited to the S_2 state but from previous experimental and theoretical studies,^{2,22,50,57} electronic excitation of the other isomers at 266 nm is expected to be less efficient. One can notice that UV spectra of different enol conformers measured in nitrogen and rare gas matrices^{2,50,57} shown that absorption bands of open conformers are blue shifted from the CCC band, in agreement with theoretical investigations of the $S_2 \leftarrow S_0$ transition for all the enol conformers.²² The first allowed $\pi\pi^*$ transition of CTC is blue shifted from that of CCC by ~ 0.4 eV (20 nm) and this transition is even more blue shifted in the case of TYC isomers. Hence, CTC is only weakly excited at 266 nm and TYC even less. This result is consistent with non-measurable rate constants k_{20} and k_{21} for the back isomerization processes of TYC.

7.4.2 Mechanism

As was explained in the chapter 1, recent time-resolved experiments revealed the first steps of the relaxation pathway from the S_2 state of the CCC isomer of AcAc excited at 266 nm in the gas phase. A very fast $S_2(\pi\pi^*)-S_1(n\pi^*)$ transfer occurs in less than 2 ps,⁶⁷ followed by a slower intersystem crossing process to the lowest triplet state $T_1(\pi\pi^*)$ (~ 250 ps).⁶⁶ It seems that OH elimination, which is the only channel reported in the gas phase at long time delay after excitation at 266 nm, occurs in this triplet state in a short time compared to 250 ps.^{20,48} In contrast, isomerization processes to various non-chelated isomers are observed in inert gas matrix experiments under the same electronic excitation of the CCC isomer of AcAc. The energy transfer from AcAc to the lattice via phonons occurs at the picosecond timescale and leads to a 'thermalisation' in the lowest triplet state.⁵⁰ The geometry of AcAc in this triplet state is non-planar and corresponds to a weakening of the C=C bond of the ground state because of the $\pi\pi^*$ excitation and the intramolecular H-bond is broken.²¹ Relaxation to the ground state is then likely to produce non-chelated conformers of AcAc.

Upon UV 266 nm laser irradiation of AcAc in pH_2 matrices, isomerization is the almost exclusive relaxation pathway. At first glance, the quenching of the OH-loss in pH_2 is very surprising because a cleavage/recombination sequence - a source of 'thermalization' - is very unlikely in this very soft "quantum" matrix. The energies reported by Trivella *et al.*⁵⁰ shows that the OH-loss is 4.5 eV endothermic with respect to ground state AcAc (CCC isomer). This puts the dissociation limit between the bottom of the S_1 and S_2 potential wells. The rate of the transfer to triplet states is slow compared to the vibrational energy relaxation to the pH_2 matrix. Indeed the excess energy for the OH-loss, which is provided by the laser, is 0.16 eV only and the equilibrium geometries of the states involved along the sequence $S_2 \rightarrow S_1 \rightarrow T_{1,2}$ are very different²¹: S_2 is excited with the planar geometry of the ground state S_0 whereas its equilibrium geometry is significantly tilted about the C=C bond; S_1 is essentially planar and T_1 , because of its very large $\pi\pi^*$ character, is extremely tilted

about the C=C bond. This suggests that, for example, the torsion about the C=C bond is excited several times along the $S_0 \rightarrow S_2 \rightarrow S_1 \rightarrow T_{1,2}$ sequence: the excess energy deposited in this mode is expected to relax extremely rapidly towards the soft pH₂ matrix. This is likely to quench the OH-loss efficiently.

Actually, experiments where classical matrices are doped with O₂ suggest that isomerization of CCC to non-chelated isomers do not proceed from a fragmentation/recombination sequence⁵⁰ and the relaxation mechanism sketched above by path indeed such fragmentation/recombination picture. In pH₂ matrices experiments goes to the same conclusion much more directly. The most probable pathway consists of a cooling of the excited species in the triplet state which prevents them from fragmentation because of the existence of an energy barrier in the excited T₁ state (theoretically predicted at 46.8 kcal mol⁻¹ (195.94 kJ mol⁻¹)).²¹

Following the relaxation scheme described above upon 266 nm irradiation, the relative probabilities to form one conformer or another by an S₀-S₂ excitation of CCC should map the projection of the equilibrium geometry of AcAc in the T₁(ππ*) into ground state geometries. From the kinetic studies shown in Fig. 6 and their fit by the rate eqn (1)–(3), these probabilities are in decreasing order: CTC > TCC > TTC. The present data do not inform quantitatively on the branching between isomerization and the return to CCC.

As was said above, only XYZ conformers are observed in pH₂ because of a XYT → XYZ tunnelling process, so the order sequence is better written: CTZ > TCZ > TTZ. The optimized structure of the T₁(ππ*) state provided in by Chen *et al.*²¹ seems to support the expectation that the relaxation from the bottom well of T₁(ππ*) to the singlet ground state is not accompanied by a drastic geometrical rearrangement. In particular, the weakening of the C=C double bond in the triplet state explains the occurrence of the *cis-trans* isomerization around this bond in the relaxation leading to the important formation of CTZ isomers.

Interestingly, the k₀₁/k₀₂ ratio in the present pH₂ experiments and k_{1C}/k_{1T} ratio of Coussan and co-workers⁵⁰ both describe the branching ratio of the CCC isomerization to CTC and TCC + TTC (TTC is not observed by Coussan⁵⁰). This ratio varies enormously according to the nature of the matrix. It is measured to 2.4 in the present pH₂ experiment whereas it varies between 0.36 (Ne matrix)⁵⁰ and 7.5 (Ar matrix).⁵⁰ The consistency mentioned in the paragraph above between those results on branching ratios and the geometry calculation done by Chen²¹ seems to support the idea that tracking the geometry of a reaction intermediate in pH₂ matrices by its effect on subsequent dynamics should be fairly related to the properties of the isolated molecule because of a less intrusive confinement of the guest molecule in the 'quantum' host.

7.5 Fragmentation

7.5.1 In pure solid parahydrogen

After long irradiation times of AcAc/pH₂ with the laser at high energy (6 mJ pulse⁻¹ at 266 nm), low intensity absorption bands appear in the 2110-2170 cm⁻¹ region (see figure 7.9 (a)). Bands assigned to CO are visible in the middle panel of the figure with a 6-times magnification. Given the strong IR activity of CO, this suggests that the fragmentation of AcAc as CO + products is a very minor channel. This is not surprising given the strong bond rearrangement it implies.

Surprisingly, no band which can be assigned to a product formed by a single bond cleavage is observed. In particular the OH stretch around 3570 cm⁻¹, which would have revealed a fragmentation to OH + products, has not been observed although OH is the main photoproduct when AcAc is irradiated at 266 nm in the gas phase.⁶⁶ The OH vibrational frequency is slightly matrix dependent, but no band appears in the whole 3600–3400 cm⁻¹ spectral range. OH radical could react with H₂ producing H₂O but no increase of water bands appears during irradiation at 266 nm of AcAc/pH₂ samples. Although they are more favorable energetically than the OH-loss, other dissociation channels involving a single bond cleavage (Norrish fragmentation about the C=O group wiving CH₃ then CH₃+H₂ →CH₄) are not detected.

The observed elimination of CO necessitates indeed that two bonds are broken and for an energetic reason (the photon energy is only 4.66 eV) a new bond must be formed in a concerted process with the CO elimination. An alcohol would be formed in this process, which is not observed, presumably because its IR activity is much lower than that of CO. Its band intensity is too low to allow the study of its formation under the experimental conditions of the present work. As it comes from a minor process, it could also be formed through a weak direct $n - \pi^*$ excitation of AcAc in S₁ or S₃ states, as suggested by Trivella *et al.*⁵⁰

In pure Ne matrices a similar fragmentation as in pH₂ matrices is observed after very long time of irradiation (more than 5 hours, see figure 7.9a and 7.9c). The irradiation time in Ne matrices, in order to reach similar IR spectra of isomers as pH₂ is three times longer suggesting that the isomerization processes are more effective in pH₂ matrices than in Ne matrices. In both cases, CO appears after long irradiation times, when the CCC is depleted and the first group of isomers is already decreasing. CO probably comes from excitation of non-chelated enol conformers, but a real analysis is not possible because of the weakness of the process.

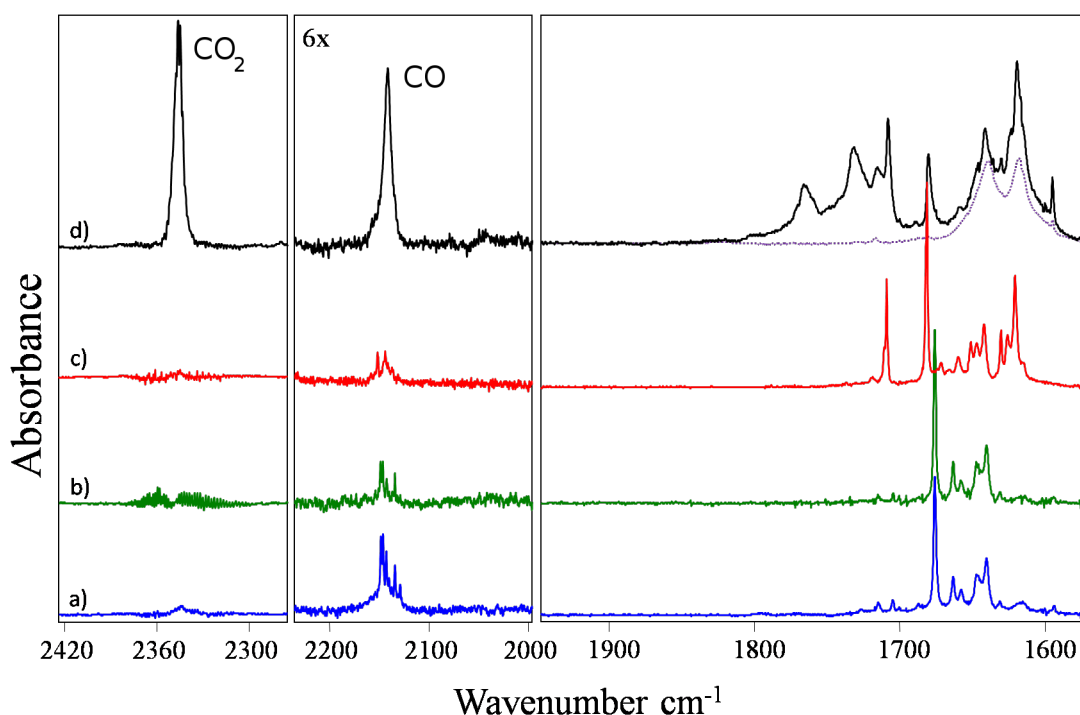


Figure 7.9: IR spectra in selected regions after strong and prolonged irradiation at 266 nm, showing the formation of CO and CO₂ due to fragmentation of AcAc. Left panel: CO₂; middle panel: CO; right panel: AcAc. (a) AcAc/pH₂, 1h30 irradiation; (b) AcAc/O₂/pH₂, 1h30 irradiation; (c) AcAc/Ne, 5h30 irradiation; (d) AcAc/O₂/Ne, 3h00 irradiation. The spectra in dots lines represents the deposited sample AcAc/O₂/Ne.

7.5.2 O₂ doping

In rare gas matrices mixed with oxygen molecules, the additional O₂ molecules enhance fragmentation but have almost no effect on the isomerization rates to non-chelated isomers.⁵⁰ In their work, Coussan and co-workers⁵⁰ suggested that the additional O₂ molecules should reveal fragmentation by preventing efficient recombination of photofragments caged by the matrix. It has been concluded that isomerization proceeds from the T₁ state directly and does not involve an intermediate fragmentation-recombination process.

Following this idea some irradiation experiments at 266 nm in mixed AcAc/O₂/pH₂ and AcAc/O₂/Ne matrices were performed. O₂ molecule was introduced with the AcAc vapor in the same deposition tube. The experiments in Ne reveal an influence of O₂ (Figure 7.9c and 7.9d) which is in agreement with the results reported by Trivella *et al.*⁵⁰ A small amount of CO₂ is detected in this case, in addition to CO (Figure 7.9d) that indicate a direct reaction of CO and O₂. In the experiments using Ne matrix, presence of fragments is observed before CCC isomer is completely depleted. This is not the case in the hydrogen matrices, where the fragments always appear after depletion of CCC and almost

7. UV LASER IRRADIATION AT 266 NM

complete depletion of first group isomers. In the similar experiment done in pH_2 at different amounts of O_2 as an impurity, the results reveal that the elimination of CO does not rely on the presence of O_2 molecules (Figure 7.9b).

A series of experiments with neon gas premixed with O_2 (O_2 : Ne ranging from 1 : 5000 to 1 : 500), were also performed, and no significant influence of O_2 is observed on the fragmentation of AcAc. The effect of O_2 on the fragmentation is observed only when O_2 is directly mixed with AcAc and then co-deposited with Ne. This suggests that the formation of an AcAc- O_2 complex is required to observe an effect of O_2 and that this complex exists prior to deposition into the matrix. It is very unlikely that this complex is not produced in the pH_2 experiment. The fact that the amount of CO does not rely on the presence of O_2 molecules in pH_2 experiment is thus an indication that this process is an intrinsic behaviour of AcAc under intense prolonged irradiation, which does not need to be stimulated by the presence of O_2 . This conclusion is in agreement with the absence of cage effect in pH_2 : the presence of O_2 in the neon cage around AcAc in order to avoid radical recombination by cage effect is not necessary in the pH_2 cage. We may wonder why the efficiency of this reaction is higher in O_2/Ne matrix than in solid pH_2 . This may be in relation with subtle differences on the excitation efficiency of precursors depending on the environment, especially because these are very weakly allowed processes.

Chapter 8

UV laser irradiation at 248 nm

UV irradiation at 266 nm wavelength using YAG laser of Acetylacetone (AcAc) in para-Hydrogen (pH_2) matrices results mainly in isomerization of the chelated enol form. Products of this photoreaction are at least four conformers. Previous studies (Nagashima *et al.*)⁵⁸ revealed that irradiation of AcAc using shorter UV wavelength radiation could also result in tautomerization of the enol form, e.g. the spectral bands assigned to the keto form is increasing after irradiation. Fragmentation of the molecule can also occur.

In order to study this phenomena in a more detailed manner, a series of experiments in which the AcAc was isolated in pH_2 , normal-Hydrogen (nH_2), normal-Deuterium (nD_2) and Neon (Ne) matrices and using a shorter laser wavelength (248 nm) as an irradiation source were performed.

This chapter is presented in two sections. The first section is dedicated to the analysis of the spectra of AcAc after UV 248 nm laser irradiation allowing the complete assignment of keto form bands. The assignment was performed with the help of theoretical Density Functional Theory (DFT) calculation. The second section devoted to the discussion about the dynamics of appearing of keto tautomer as one of the products of irradiation of open enol isomers. The fragmentation of the AcAc is also discussed.

8.1 Keto IR spectrum

After deposition, matrix isolated AcAc sample is illuminated with a Excimer UV laser at 248 nm (energy/pulse of 10 mJ at 10 Hz). Irradiation was stopped during the measurement of the infrared spectra. Figure 8.1 compares the AcAc spectrum in pH_2 before (a) and after (b & c) UV 248 nm laser irradiation. Dots lines labels the bands assigned to the keto form of AcAc. In the first steps of irradiation (figure 8.1b), many new bands appear due to the formation of the non-chelated enol

8. UV LASER IRRADIATION AT 248 NM

conformers. The increase of the keto bands is detected after prolonged irradiation, concomitantly with the decrease of the non-chelated enol forms.

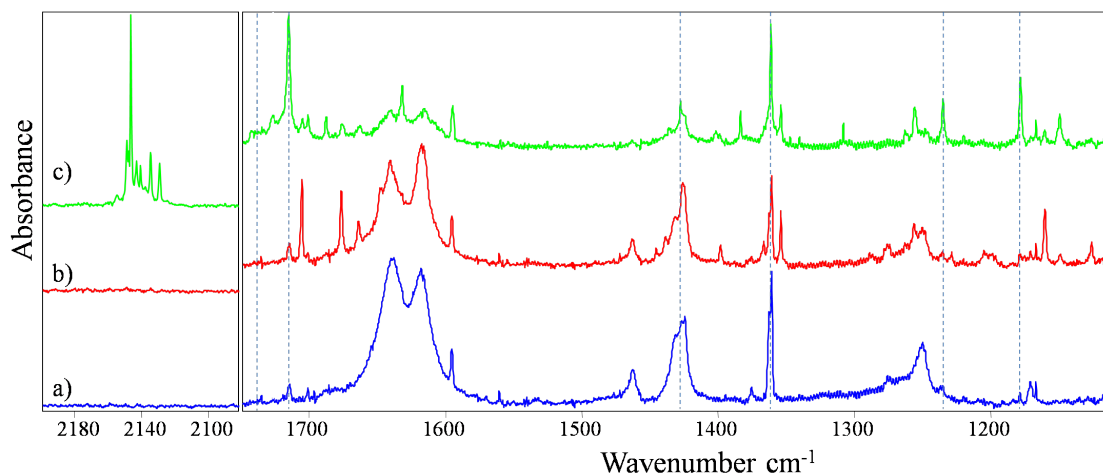


Figure 8.1: Comparison of IR spectra of AcAc in pH_2 before and after various UV irradiation times at 248 nm (energy/pulse of 10 mJ at 10 Hz): (a) as deposited; (b) after 10 min irradiation and (c) after 370 min irradiation. Traces are vertically translated for view purpose. The position of the keto bands is followed by vertical dot lines through the three traces.

Figure 8.2 displays the spectra of AcAc in pH_2 (a) after 30 minutes of UV 266 nm laser irradiation, (b) after 10 min UV 248 nm laser irradiation and (c) after several hours (~ 6 hours) UV 248 nm laser irradiation. For easier comparison the contribution of the chelated enol form of AcAc (CCC) was subtracted in all spectra. The spectra of irradiated AcAc in pH_2 with a wavelength at 266 nm has only the bands corresponding to open enol forms. Bands previously assignment (see chapter 7) to CTC isomer are labeled with (+) and TCC and TTC are labeled with (*). By direct comparison between panel (a) and (b) is obvious that the same non-chelated enol forms of AcAc are formed after irradiation with both lasers. After prolonged irradiation at 248 nm (unlikely as at 266 nm) the open enol isomers of AcAc start to disappear and new bands start to grow. Some of the new growing bands are the assigned to the keto tautomer of AcAc.

In Ar matrix Nagashima *et al.*⁵⁸ identified eight bands for the keto form (reported in Table 8.1), of which seven were observed upon broadband UV irradiation but bands are rather weak, except three of them (at 1714, 1357 and 1176 cm^{-1}). Some assignments regarding the weakest bands are not completely confirmed in pH_2 experiments. A band was reported at 1740 cm^{-1} in Ar and at 1736 cm^{-1} in Xe,⁷ but it is not clearly observed in pH_2 , it could be inside the broad band in the region 1720 to 1745 cm^{-1} . Tentatively weak bands at 1733.7 cm^{-1} in pH_2 and 1730.6 cm^{-1} in nD_2 could be identified, but the assignment is very doubtful due to the weakness of the signal and the presence of

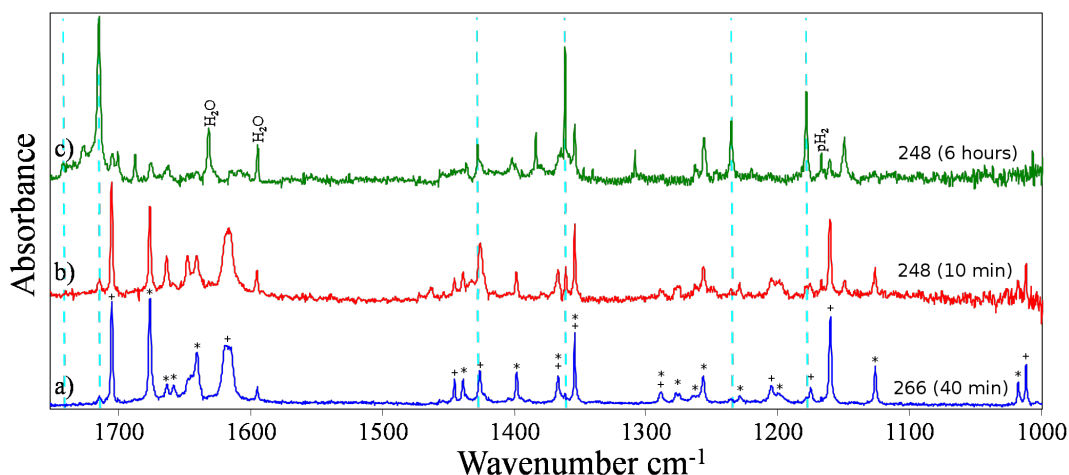


Figure 8.2: Comparison of IR spectra of irradiated AcAc in $p\text{H}_2$ (a) after several minutes (~ 40 min) using UV 266 nm; (b) after few minutes (~ 10 min) using UV 248 nm and (c) after few hours (~ 6 hours) using UV 248 nm. The contribution of the CCC form were subtracted in all spectra for easier comparison. The position of the keto bands is followed by vertical dot lines through the three traces. (+) refers the first group of isomers and (*) refers the second group of isomers.

other bands corresponding to the fragments as will be discussed in the chapter 9.

The assignment of keto bands is performed with the help of DFT calculations at B3LYP/6-311++G(3df,3pd) level in both harmonic and anharmonic approximation. Figure 8.3 displays the spectra after some hours of irradiation of AcAc in (a) $n\text{D}_2$ matrices and (b) $p\text{H}_2$ matrices. For direct comparison, the theoretical infrared spectra in the (c) anharmonic and (d) harmonic approximation are also shown. The simulated spectra were obtained by Lorentzian (function) bands contour fitting the calculated harmonic infrared intensities with 1.0 cm^{-1} width. Values of experimental and theoretical frequencies are listed in table 8.1. The theoretical calculations are in good agreement with previous studies.⁵⁸ However, compared to scaled (0.978) harmonic frequencies, the anharmonic approach does not improve that much the agreement between computations and experiments. Nevertheless, only few bands are observed for keto then, applying scaling factor gives more accurate results than with chelated enol where the match is much better with the anharmonic frequencies.

According to calculations only four vibrational modes of keto have significant IR intensity, i.e. higher than 50 km/mol , three of which are readily detected in the as-deposited $p\text{H}_2$ sample (at 1714.9 , 1235.3 and 1178.2 cm^{-1}), see chapter 7. The first effect of the UV irradiation results in a fast decrease of the chelated enol form (CCC). The complete disappearance of this enol form effectively reveals the hidden keto band at 1361.3 cm^{-1} (value in $p\text{H}_2$ matrices). This band is also detected after UV irradiation in $n\text{H}_2$, $n\text{D}_2$ and Ne matrices at 1362.1 , 1361.4 and 1363.2 cm^{-1} respectively. A more extensive study has been performed in $p\text{H}_2$, revealing a new very weak band at 1427.7 cm^{-1}

8. UV LASER IRRADIATION AT 248 NM

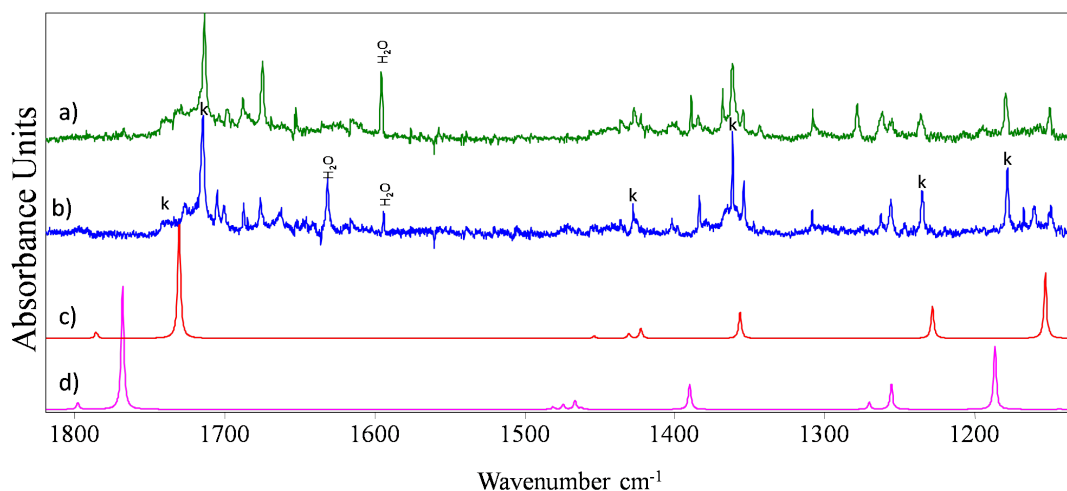


Figure 8.3: Spectra of several hours irradiated AcAc in (a) nD_2 matrix and (b) pH_2 matrix using UV laser at 248nm. Simulated spectra using DFT calculated frequencies (c) with anharmonic corrections and (d) in harmonic approximation. For the simulated spectra 1.0 cm^{-1} bandwidth Lorentzian function was used.

in agreement with the predicted theoretical value of a medium band at 1423 cm^{-1} (Table 8.1). In particular neither calculation method correctly reproduces the band at 1178.5 cm^{-1} , involving the motion of all atoms and mainly that of the C–C stretches.

The most notorious difference between vibrational harmonic and anharmonic calculation are the bands associated to the CH₂ Rock and CH₂ Twist predicted at 1255.5 and 1270.1 cm^{-1} respectively in the harmonic approximation and shifted to 1228.2 and 1227.6 cm^{-1} with the anharmonic correction. Since both modes include hydrogen atoms, the potentials are expected to have an important anharmonic component which explains the big shift when anharmonic corrections are applied. In Ar matrices two bands corresponding to Keto tautomer seems to appear under UV $\lambda < 280\text{ nm}$, one strong band at 1240 cm^{-1} and another weak band at 1256 cm^{-1} .⁵⁸ In pH₂ matrices, similar assignment can not be done. Band at 1235.3 cm^{-1} (in pH₂) can be assigned to the CH₂ rock mode. A very weak band can be observed at 1246.9 cm^{-1} in pH₂ after very long irradiation time is observed. This band could be a good candidate to the assignment of the CH₂ twist as in Ar matrices. Unfortunately the same band was not found in similar experiments in nD₂ matrices and as will be discussed in the chapter 9 this band also appear after UV 193 nm laser irradiation even when almost no keto signature is left in the sample. The absence of this mode in pH₂ matrices is well explained by the anharmonic calculation. Since this frequency shift to 1227.6 cm^{-1} very close to the 1228.2 cm^{-1} then in the experimental spectrum the band at 1235.3 cm^{-1} could possibly be composed of two vibrational modes.

pH ₂	nH ₂	nD ₂	Ne	Ar ^a	Anh.	Harm.	Int. ^b	Description ^c
1733.7 [?]		1730.6 [?]		1740	1786.8	1798.0	21	ν C=O (ip)
1714.9	1713.5	1713.7	1718.4	1714	1730.5	1768.1	384	ν C=O (opp)
1427.7		1427.0			1422.7	1466.4	28	δ CH ₃ scissor (opp)
1361.3	1362.1	1361.4	1363.2	1357	1356.4	1390.0	73	δ CH ₃ umbrella (opp)
1235.3	1236.8	1235.9	1237.7	1240	1228.2	1255.5	84	ρ CH ₂
					1256	1227.6	22	τ CH ₂
1178.2	1179.9	1179.1	1179.6	1176	1152.8	1186.5	201	$[\nu$ C(H ₃)-C(=O)+ ν C(H ₂)-C(=O)] _{as} +rock CH ₃ (opp)
888.2		886.6	890.9	891	885.2	893.4	33	ν C(H ₂)-C(=O)+ ρ CH ₃ (opp)
				792	780.4	797.5	14	$[\nu$ C(H ₃)-C(=O)+ ν C(H ₂)-C(=O)] _s (opp)

^a From Nagashima *et al.*⁵⁸

Calculated intensities in the harmonic approximation in km/mol.

[?] Values which were obtained from a deconvolution in Lorentzian of a very broad band

^c Only main motions are described. ν : stretch, δ : bending, ρ : Rock, τ : Twist s : symmetric, as : asymmetric; the keto form contains two CH₃-C=O groups, the motions of each group can be in phase (ip) or in opposition of phase (opp).

Table 8.1: Experimental frequencies (cm^{-1}) of the keto form of AcAc in different matrices compared with theoretical frequencies in cm^{-1} (anharmonic and harmonic) calculated at the B3LYP/6-311++G(3df, 3pd) level. Bold values indicate bands already present in *as*-deposited spectra.

8.2 Fragments

Other bands observed after long irradiation times (Figure 8.3) cannot be assigned to the keto form based on the analysis of the kinetics of the different bands. Some bands are assigned to water impurities or to a non-chelated enol form of AcAc. Other bands are assigned to photoproducts such as CO and methane which are detected at small amounts. The photofragmentation is also observed in Ar matrices,⁵⁸ but not assignment of photoproducts was done. The band observed at 1256 cm^{-1} in Ar matrices can be due to photoproducts rather than a keto band.

The main fragments observed during these experiments where: CO with the intense structured band in the 2125 to 2150 cm^{-1} region,¹³² CH₃ identified by the doublet at 3170.6 and 3171.4 cm^{-1} assigned to the ν_3 band and the ν_4 band (doublet at 1401.7 and 1402.9 cm^{-1}),^{27,34} CH₄ identified by the ν_4 band observed at 1308.3 and ν_3 band at 3025.3 cm^{-1} ,^{11,27} H₂O from the ν_2 band at 1631.7 cm^{-1} .³³

8.3 Kinetics

The decrease of the chelated enol form and the increase of the keto form have been followed during the long irradiation at 248 nm of pH₂ isolated samples and changes of integrated absorbance have been monitored by FTIR spectroscopy. UV irradiation has been stopped while recording IR spectra. Figure 8.4 shows the variation in time of keto (black squares) chelated enol (red circles), first group of isomers (green triangles) and the second group of isomers (blue triangles) in two different experiments. Normalized values of integrated absorption were plotted for easier comparison. In the 400 min irradiation experiment (figure 8.4a), IR spectra have been recorded approximately every hour, except at the very beginning. In order to check more precisely what happens in the beginning of the irradiation, IR spectra have been recorded on a more concentrated sample at shorter irradiation periods ranging from few minutes to 30 min and at a lower laser power. The result is shown in panel (b) of Figure 8.4. Note that the graph for chelated enol is represented along a decreasing vertical axis in order to easily compare with the increase of keto.

A very fast decrease of the chelated enol is detected in the first minutes of irradiation, followed by a slower decrease all along the irradiation. On the contrary, the increase of keto seems to be smoother and is more regular when looking at the evolution at larger time intervals (Figure 8.4). Both groups of isomers seem to have a very similar kinetics, reaching a maximum value at the same time. A focus on the first stages of the evolution of keto (figure 8.4b) reveals that this increase of keto form is not immediate. In contrast, enol isomers increased with the very fast decreasing of CCC form in the first minutes. When the open enols reach the maximum value and start to decrease then, the keto form starts to increase. In the experiment plotted in the panel (b) in figure 8.4 the maximum point is around 25 minutes. In panel (a) the first 10 minute isomers reach the maximum value. The appearance of keto definitively does not correlate with the depletion of the chelated enol form, suggesting that the formation of keto does not directly proceed from this enol form. Keto more likely originates from open isomers. Keeping the sample in dark do not make change in the intensity of keto bands suggesting that the formation of keto is due to the direct UV 248 nm irradiation of open enol isomers.

From the figure 8.4 is visible that both group of open enol isomers (see chapter 7) have not a very different time evolution. Moreover, the kinetics of the two isomers of the second group (TCC and TTC no represented in the figure) can not be separated. Then the irradiation at 248 nm do helps to distinguish the three observed open enol forms.

No mechanism has been proposed regarding the formation of keto in the work of Nagashima *et al.*⁵⁸ Nevertheless, from the UV absorption spectra of the chelated and non-chelated enol forms published in different matrices,⁵⁰ it is known that the excimer laser (248 nm) can efficiently excite all enol forms. The enol-keto tautomerization process is triggered by the appearance of non-chelated isomers, which are

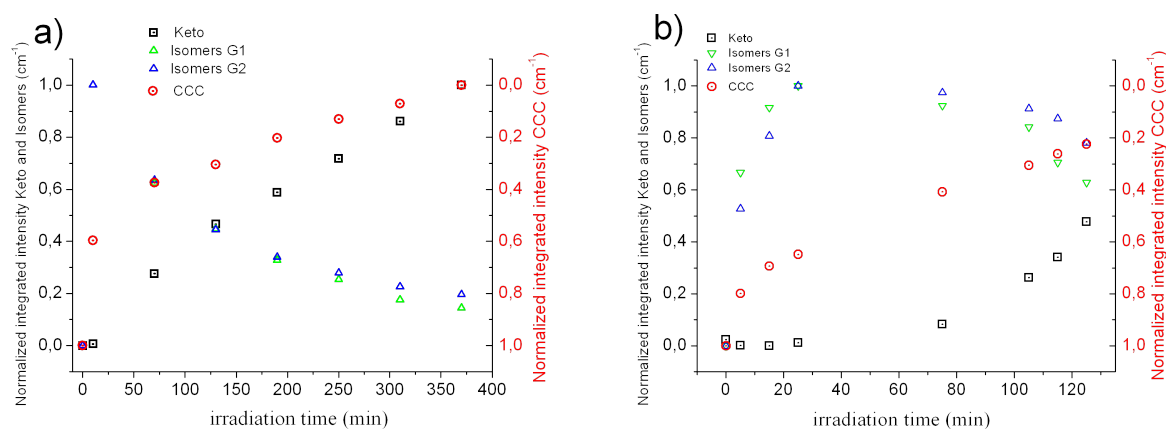


Figure 8.4: UV irradiation kinetics at 248 nm in pH_2 matrix for the chelated enol (red circle); the keto (black square) forms of AcAc; first group of isomers (green triangles) and second group of isomers (blue triangles). (a) 10 mJ/pulse laser power, (b) more concentrated sample and 4 mJ/pulse laser power. Normalized integrated absorbances are reported against irradiation time, with vertical axis up (numbers in black, left-hand side) for keto and isomers, and down (numbers in red, right-hand side) for enol, for an easier comparison. Dots are obtained from experimental integrated absorbances at 1714.9 cm^{-1} for keto; 1705.3 cm^{-1} for the first group of isomers; 1636.3 cm^{-1} for the second group of isomers and at 1462.6 cm^{-1} for chelated enol.

formed in the first minutes of UV irradiation. This structure does not have intramolecular hydrogen-bond stabilizing the labile hydrogen atom responsible for the tautomerization toward the keto form. Trivella *et al.* have shown that the first triplet state, in which the molecule has a non-planar geometry, is likely the key step to isomerization from one conformer to another.⁵⁰

Figure 8.5 display the time evolution of keto form (black squares) and two of the observed fragments CO (red diamond) and CH_4 (blue triangles). Normalized values of integrated absorbance were used for easier comparison. The appearance of keto tautomer as well as fragments seems to follow the same kinetics. As have been said, the UV excitation of the chelated enol form leads to fragmentation instead of isomerization in gas phase.^{21,67} In fact, the formation of keto through recombination of fragments due to a cage effect in the matrix cannot be excluded since fragments are also observed in the 248 nm irradiation experiments. Because the kinetics of fragments is found to be very similar to that of the keto form. This supports the hypothesis of fragment recombination as the origin of the increase of keto.

The kinetics model should be as follows: under 248 nm irradiation of AcAc isolated in pH_2 in the first minutes of irradiation, mainly isomerization to the open enol forms take place. By irradiation of isomers two channels can be open, the tautomerization by the transfer of the H in the OH bond to the central carbon and the fragmentation of the molecule giving smaller molecules such as CO and

8. UV LASER IRRADIATION AT 248 NM

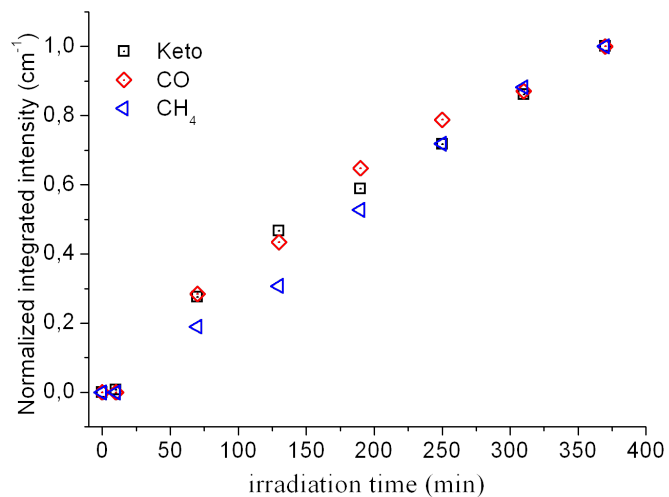


Figure 8.5: Time evolution under UV 248 nm laser irradiation of AcAc in pH₂ matrix of keto (black squares); CO (red diamond) and CH₄ (blue triangles). Dots are obtained from experimental integrated absorbances at 1714.9 cm⁻¹ for keto; region 2125-2150 cm⁻¹ for CO and at 1308.3 cm⁻¹ for CH₄.

CH₄ and radicals such as CH₃. Prolonged irradiation eliminate all enol forms of AcAc leaving only the keto tautomer, fragments and smaller molecules.

Chapter 9

UV laser irradiation at 193 nm

Chapters 7 and 8 discuss the photochemistry of Acetylacetone (AcAc) in para-Hydrogen (pH_2) when an excitation up to the S_2 electronic level is done using two different UV (266 and 248 nm) laser wavelengths. The relaxation path is quite dependent on the wavelength. In both cases the main result due to the irradiation of the chelated enol form seems to be the isomerization to the non-chelated enol (open conformers) species. Open conformers can be excited by UV 248 nm laser and new molecules and radicals appeared in the IR spectra after prolonged irradiation at 248 nm.

In this chapter the excitation of the AcAc up to a S_3 state is analyzed. UV excimer laser at 193 nm is used to perform the excitation of the molecule and FT-IR is used to analyze the photoproducts. The structure of this chapter is as follow: In the first section the infrared spectra obtained after irradiation of AcAc in pH_2 matrix with 193 nm are briefly described. The second section is split in four subsections. (1) The “first” products obtained in the fragmentation processes of AcAc (2) The necessity of a second photon to produce other molecules.(3) The reaction mechanisms for formation of C_2H_2 , C_2H_4 , C_2H_6 and C_3 from irradiated photo-fragments (4) Formation of HCO radical and formaldehyde from the reaction of CO and photo produced H-atom in a sequential mechanism. Unassigned bands that appear in the spectra are discussed in a third part. At the end, is a small summary of this chapter. Some experiments were performed in solid deuterium for comparison and are described along the chapter.

9.1 IR Spectra

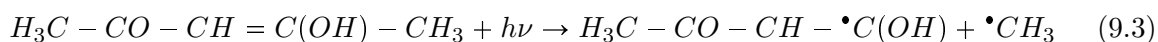
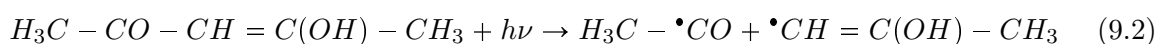
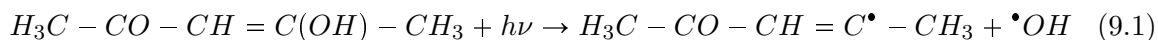
Similarly to previous experiments, the matrix isolated AcAc in pH_2 is irradiated with a UV laser, this case being an excimer laser at 193 nm (energy/pulse of 10 mJ at 10 Hz). IR spectra were recorded after each UV irradiation period. During the registration of IR spectra, the laser was turned off. Figure 9.1 displays four characteristic spectra of AcAc in pH_2 before (a) and after (b-d) UV 193 nm laser

9. UV LASER IRRADIATION AT 193 NM

irradiation. Panels (I) and (II) shows different spectral regions but recorded after the same irradiation times; (b) \sim 20 min, (c) \sim 120 min and (d) \sim 220 min (for more detailed spectra see appendix C). The first effect of the irradiation is the depletion of CCC form which transforms into other molecules such as open enol isomers, keto, radicals and smaller molecules due to the photofragmentation. In trace (b), bands corresponding to isomers CTC and TCC (labeled with (I)) can be assigned. Keto molecules are also formed at this time and can be verified by the increasing of the corresponding bands (labeled with (K)). The photofragmentation of AcAc is also observed from the very beginning, trace of CO and CH₄ can be seen with only 20 min of irradiation.

When the irradiation continues (see figure 9.1 (c) and (d)), bands corresponding to open enol isomers and keto also decrease with decreasing of the CCC form. Only photofragments of AcAc remains.

The photodissociation dynamics of AcAc was studied using pulsed laser photolysis laser, induced fluorescence (LIF) and “pump-probe” technique at room temperature by Upadhyaya *et al.*²⁰ They also performed *Ab initio* Molecular Orbital (MO) calculations to investigate the potential energy surface (PES) of the ground and excited electronic states of AcAc. Three fragmentation mechanisms were proposed for AcAc from the lowest triple state T₁ when the molecule is irradiated at 266 nm and 248 nm.



They concluded that at 193 nm laser photo-excitation of AcAc, fragmentation takes place from either the ground state or an excited repulsive σ^* state but not from the lowest triple T₁ state. Nevertheless reactions 9.1 and 9.2 are confirmed using this wavelength for excitation.²⁰ The detection of OH in the case of reaction 9.2 is explained from the unimolecular dissociation of the primary radical HC=C(OH)-CH₃. This radical dissociates to give OH and propyne (HC≡C-CH₃).

The present observations in pH₂ solid show obviously much more photoinduced reactions than those deduced from equations (9.1, 9.2, 9.3). Beside AcAc isomer bands, a lot of bands belonging to different fragments appear in the IR spectra. Some IR bands belonging to fragments appear in the beginning of the UV irradiation whereas others are observed only after a long laser irradiation time. The fragments can react with their surrounding or photoreact under further 193 nm irradiation. The next section describes the products assigned from their IR spectra and discusses the possible mechanisms of their formation.

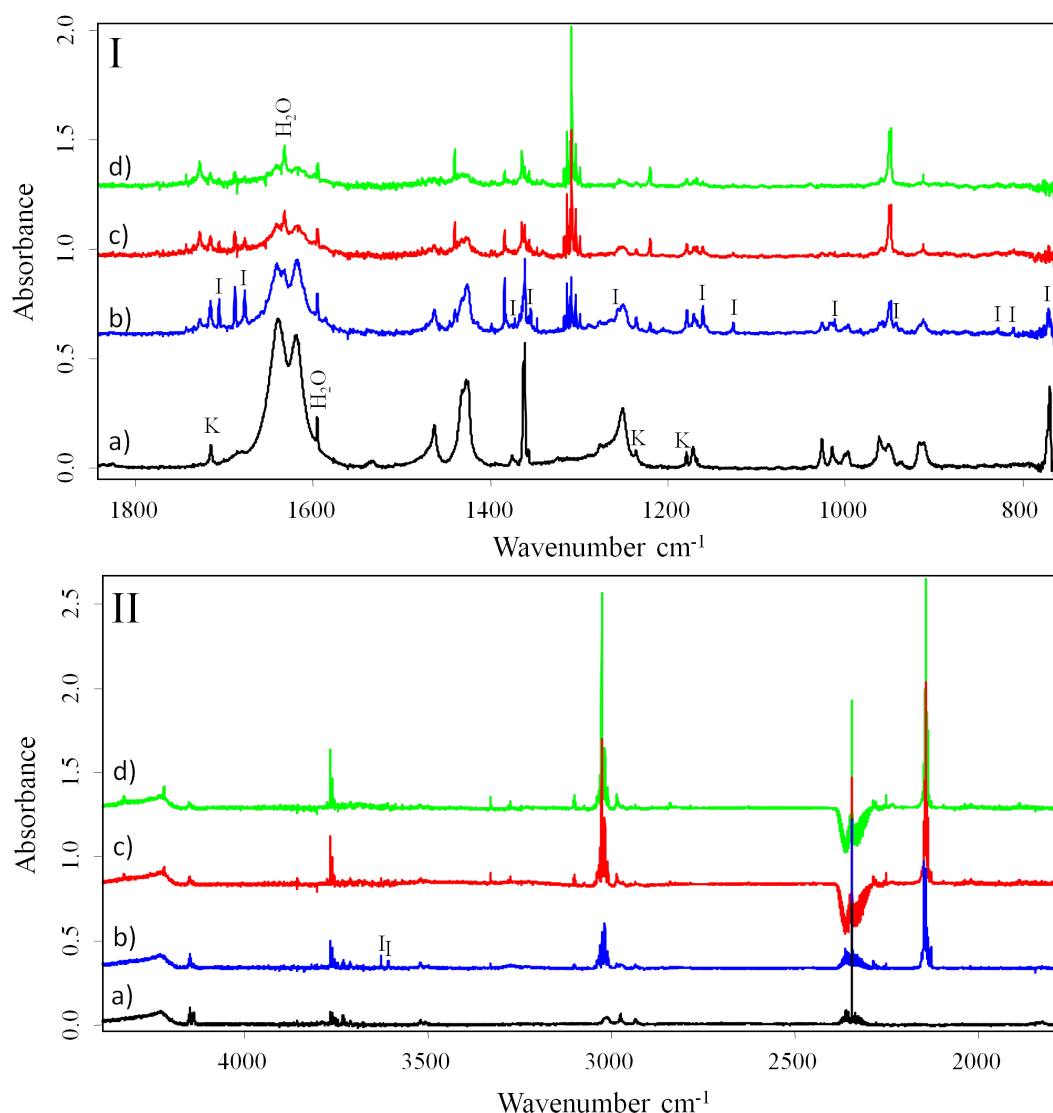


Figure 9.1: Infrared spectra of AcAc in $p\text{H}_2$ matrix. (a) As deposited sample. After ArF (193 nm) excimer laser irradiation (energy/pulse 10 mJ at 10 Hz) (b) 20 min, (c) 120 min and (d) 220 min. Open enol forms are labeled (I), keto form with (K), water bands as (H_2O)

9.2 Assigned products

Some of the observed fragments can obviously correspond to the above reactions 9.1, 9.2 and/or 9.3. They will be called “first” products. The formation of CH_4 and H_2O is produced by a secondary process, involving hydrogens, and will be discussed as “secondary” products. The production of small hydrocarbons is presented in a third part, with mechanisms deduced from the photolysis of acetylene. Finally, observed oxygenated radicals are identified and they are presented in the fourth part.

9. UV LASER IRRADIATION AT 193 NM

9.2.1 “First” products

The propyne molecule ($\text{CH}_3\text{-C}\equiv\text{CH}$) is one of the fragments which results from the 193 nm laser irradiation of AcAc isolated in pH_2 . The mechanisms to obtain propyne can be the same as described by Upadhyaya *et al.*²⁰

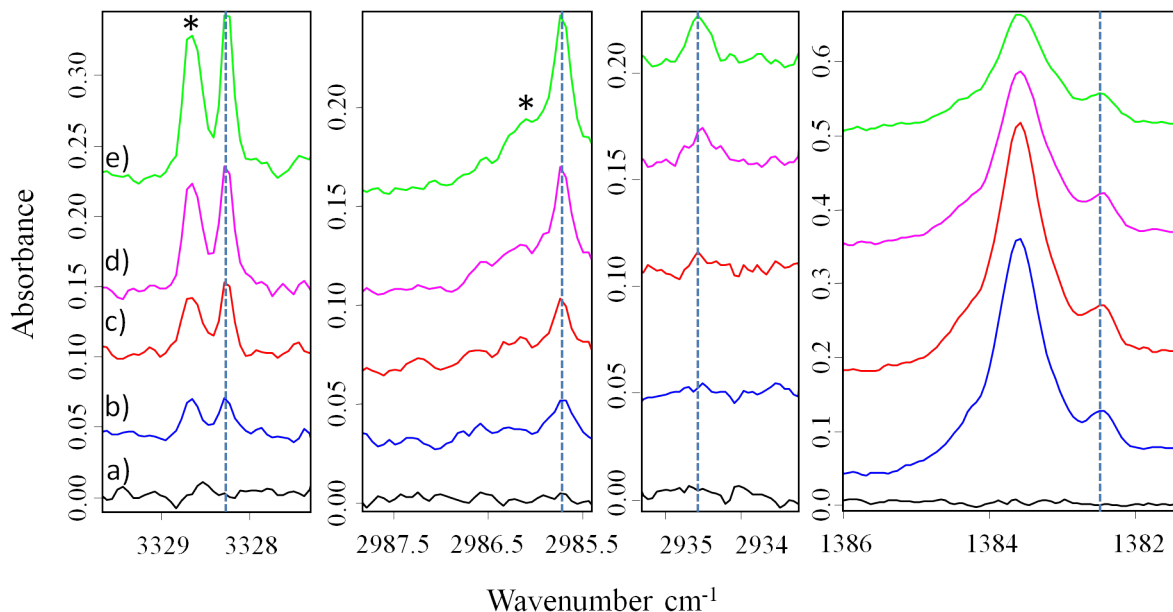


Figure 9.2: Part of IR spectra recorded after different time of 193 nm laser irradiation of AcAc in pH_2 . As deposited (a), 15 min (b), 30 min (c), 75 min (d) and 135 min (e). Resolution 0.125 cm^{-1} . Dots lines refer bands assigned to propyne. Bands labeled with (*) are assigned to complexes with surrounding molecules.

Following reaction (9.2), AcAc splits into CH_3CO and $\text{HC}=\text{C}(\text{OH})\text{-CH}_3$ radicals. The last one dissociates to give OH and propyne $\text{HC}\equiv\text{C-CH}_3$.²⁰ In table 9.1 the infrared frequencies of propyne are listed, compared with gas phase and argon matrices. All frequencies are in cm^{-1} . Figure 9.2 displays fragments of the infrared spectra of AcAc in pH_2 at different times of irradiation. As deposited (a), 15 min (b), 30 min (c), 75 min (d) and 135 min (e). Doted lines refer to the bands assigned to propyne. In all spectra the bands corresponding to the chelated enol form of AcAc were subtracted. The bands of the doublets at 3328.5 and 2985.8 cm^{-1} may be due to complexes of propyne with surrounding molecules such as CH_4 and/or CO. Similar behavior was found by Momose and co workers³⁰ in their study of photolysis of ethyl iodide in solid parahydrogen and will be discussed later in this chapter. Some experiments were done using D_2 as a host matrix for comparison and the frequency values of propyne in this matrix are listed in table 9.1. The frequency values in normal-Deuterium (nD_2) are very close to those in pH_2 ($\sim 1 \text{ cm}^{-1}$).

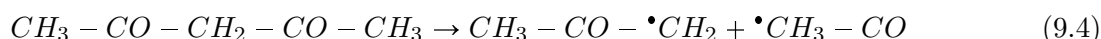
Propyne CH ₃ -CCH				
This Work		Literature		
pH ₂	nD ₂	gas ¹³³	Ar ¹³⁴	assignment
3328.3	3327.6	3334	3323	(CH stretch)
3328.6	3327.2			
2985.7	2987.3	3008	2978	(CH ₃ asym stretch)
2985.9				
2934.6	2935.0	2941	2935	(CH ₃ sym stretch)
2142.1	-	2142	2137	(CC stretch)
1447.6	-	1452	1444	(CH ₂ bend)
1382.5	-	1382	1383	(CH ₃ umbrella)
1031.2	-	1053	1032	(CH ₃ rock)

All frequencies are in cm⁻¹

Table 9.1: IR frequencies in cm⁻¹ assigned to Propyne molecule in pH₂ and nD₂ compared with the values reported in the literature

If reaction 9.2 is assumed to occur, the CH₃CO should be also produced. Another source of this radical could be the keto form. As it was said in chapter 1, Nakanishi *et al.*¹⁴ measured the near and vacuum UV absorption spectra of acetylacetone in the vapor phase and in several organic solvents at various temperatures. They assign the Rydberg excitation bands observed at 193 nm to the keto form. To date, no study about photolysis of keto has been done.

The keto form has two C-C single bonds which are equivalent. Once the molecule absorbs and one C-C bond brakes then the following reaction may occur:



As in the case of formation of propyne the excited radical $CH_3 - CO - \bullet CH_2$ may dissociates as follow.



Both reactions 9.2, 9.4 and 9.5 predict formation of CH₃CO radicals, but no trace of this radical is found in the infrared spectra after irradiation of the sample. Woodbridge *et al.*¹³⁵ studied the photodissociation of acetone at 193 nm irradiation. They concluded that photofragmentation of acetone is a two-step mechanism. The first is the dissociation into CH₃ and CH₃CO. The energy which remains in the CH₃CO radical is enough to overpass the expected 72 kJ mol⁻¹ energy barrier and brake into CH₃ radical and CO¹³⁵ by reaction 9.6.



9. UV LASER IRRADIATION AT 193 NM

CO and CH₃ can be identified in the infrared spectra of AcAc after UV (193 nm) laser irradiation suggesting that CH₃CO dissociates to form CH₃ and CO by reaction 9.6. Table 9.2 lists the frequencies in cm⁻¹ of the infrared spectra of carbon monoxide (CO) in pH₂. The values obtained in this work are compared with the those of Fajardo *et al.*¹³² who assign the rotational structure of the infrared spectra of CO in pH₂. The assignment were done using the Fajardo's notations.¹³² It is known that pH₂ matrices can be in a fcc or hcp unit cell structure or mixture of both (see chapter 2). The hcp/fcc refers to the site of pH₂ matrices, i.e. if the molecule is in a hcp o fcc unit cell. The ⊥ on || nomenclature are related with the polarized IR absorption spectroscopy (PIRAS). The crystal field interaction partially lifts the (2J+1)-fold M-degeneracy of the gas-phase rotational states associated with the isotropic nature of free space, giving rise to perpendicular transitions with ΔM = ±1 (⊥-polarization) and parallel transitions with ΔM = 0 (||-polarization).

Carbon Monoxide CO in pH ₂					
This Work			Literature ^a		
pH ₂	pH ₂	Assignment	pH ₂	pH ₂	Assignment
			2141.78		
2147.13	2147.12	R(2) hcp ⊥	2141.43		(CO) _n
2146.40	2146.14	R(1) hcp	2141.13		
2145.98	2145.93	R(1) hcp ⊥	2140.69		oH ₂ -CO
2145.35	2145.28	R(1) hcp ⊥	2140.29	2140.27	Q(1) hcp ⊥
2143.80	2143.82	R(0) hcp	2137.63	2137.61	P(1) hcp ⊥
2143.36	2143.33	R(0) fcc	2137.28	2137.26	P(1) fcc
2142.99	2142.95	R(0) hcp ⊥	2136.81	2136.74	P(1) hcp
			2135.14	2135.20	P(2) hcp ⊥
			2134.49	2134.55	P(2) hcp ⊥

^aAssignment and nomenclature from reference,¹³² see text.

All frequencies are in cm⁻¹

Table 9.2: IR frequencies in cm⁻¹ assigned to Carbon Monoxide molecule after UV irradiation of AcAc in pH₂ compared with the values reported in the literature

The presence of CH₃ radical in the spectrum is almost imperceptible. The infrared values obtained in this work are listed in Table 9.3 and those values are compared with the values reported by Momose and co-workers.^{27,34}

The total amount of CO is clearly much larger than CH₃, nevertheless if they are formed due to the dissociation of CH₃-CO radical then we should expect similar amount. On the other hand, huge amount of methane (CH₄) is detected in the infrared spectra, which could come from CH₃, as will be discussed in the next section.

Radicals						
This Work	gas	pH ₂	Ar	Xe	Ne	Assignment
2020.99	2022.64		2019.5		2023.7	Ethynyloxy radical HCCO (CCO a-stretch) ^{136,137}
3170.89	3174.29	3170.60	3150.0		3162.0	Methyl radical CH ₃ (ν_3) ^{27,34}
1401.70		1401.60	1397.5		1396.0	Methyl radical CH ₃ (ν_4) ^{27,34}
2449.23	2434.48		2483	2442.3		Formyl radical COH (CH stretch) ¹³⁶⁻¹³⁸
1864.77			1862.5	1856.6		Formyl radical COH (CO stretch) ¹³⁶⁻¹³⁸
1081.44			1083.3	1076.5		Formyl radical COH (bend) ¹³⁶⁻¹³⁸
2250.26	2257.22		2243	2237.2		Tricarbon Monoxide CCCO ^{137,139}

All frequencies are in cm⁻¹

Table 9.3: IR frequencies in cm⁻¹ assigned to radicals after UV irradiation of AcAc in pH₂ compared with the values reported in the literature

9.2.2 “Second” products

T. Momose *et al.* studied the photolysis of methyl iodide (CH₃I) in solid pH₂ irradiating sample with low-pressure mercury lamp producing methyl radicals (CH₃), methane (CH₄) and ethane (C₂H₆).³⁴ They observed that once they have CH₃ by keeping the sample in dark no reaction takes place to form CH₄. The reaction occurs only when the sample is illuminated by the mercury lamp. The wavelength at 193 nm has enough energy to excite the methyl radical to the S₃ Rydberg but not to ionize it.¹⁴⁰ Once the methyl radical is in the excited state the following reaction takes place¹⁴⁰:



Followed by the reaction¹⁴⁰:



Table 9.4 lists the frequencies values of CH₄ in both ν_3 and ν_4 regions of the infrared spectrum. The values obtained in this work are compared with the values reported in the literature. As in the case of CO, CH₄ surrounded by fcc unit cells of pH₂ molecules can be assigned.

In order to confirm the mechanisms described by reactions (9.7) and (9.8) when the AcAc isolated in pH₂ is irradiated with 193 nm laser, similar experiments were done using nD₂ as a host matrix. After 193 nm laser irradiation of AcAc in nD₂, CH₄, CDH₃, CD₂H₂, CD₃H and CD₄ can be identified in the infrared spectra. The possibility to observe all these molecules means that reaction mechanisms to describe their formation are more complicated than the mechanisms described previously, and/or that methane is formed from another precursor. Values of infrared frequencies of these methane molecules

9. UV LASER IRRADIATION AT 193 NM

Methane CH ₄					
ν_3 region ¹⁴¹			ν_4 region ^{11,141}		
This Work		Literature ^a	This Work		Literature ^a
pH ₂	pH ₂	Assignment	pH ₂	pH ₂	Assignment
3044.1	3044.1	R(1)	1316.5	1316.5	R(1) hcp \perp
3043.4	3043.4	R(1)	1313.6	1313.6	R(1) hcp \perp
3038.0	3038.0	R(1) \perp	1313.1	1313.1	R(1) fcc
3033.5	3034.4	R(1) \perp	1313.0	1313.0	R(1) hcp \parallel
3031.1	3031.0	R(1) \parallel	1312.3	1312.3	R(1) hcp \perp
3030.4	3030.3	R(1) \perp	1309.2	1309.2	R(0) hcp \perp
3026.1	3025.9	R(0) \parallel	1308.4	1308.4	R(0) hcp \parallel
			1308.4	1308.4	R(0) fcc ?
3025.3	3025.2	R(0) \perp	1308.3	1308.3	R(0) hcp \perp
3017.6	3017.5	Q(1) \perp	1303.9	1303.9	Q(1) hcp \perp
3017.1	3017.0	Q(1) \parallel	1303.6	1303.6	Q(1) hcp \parallel
3016.4	3016.3	Q(1) \perp	1303.4	1303.3	Q(1) fcc
3008.8	3008.7	P(1) \perp	1303.0	1302.9	Q(1) hcp \perp
3008.2	3008.1	P(1) \parallel	1300.1	1300.1	?
			1298.9	1298.9	P(1) hcp \perp
			1298.3	1298.3	P(1) fcc

^aAssignment and nomenclature from reference¹⁴¹ and reference,¹¹ explanations are the same as Table 9.2.

All frequencies are in cm⁻¹

Table 9.4: *Methane*

in nD₂ matrix are listed in table 9.5. The amount of molecules is much smaller than in pH₂ matrices because now CH₄, CH₃D, CH₂D₂, CHD₃ and CD₄ come from the same amount of AcAc and the intensity seen before is spread over five different molecules. Thus, only the most intense bands can be seen after irradiation of AcAc in nD₂ matrices.

The formation of propyne due to the dissociation of HC=C(OH)-CH₃, when reaction (9.2) takes place, should be accompanied by another fragment, the OH radical. This fragment was also clearly observed in the gas phase following reaction 9.1²⁰ after 193 nm irradiation. In the present experiments no spectral bands which could be associated with OH radical was observed. On the other hand an increase of the absorption bands associated with H₂O is observed. It is known that free H-atoms can diffuse through the pH₂ matrix.¹⁴⁶ The formation of H₂O can be explained from the OH radical which recombine with the free H-atom, coming from the reaction (9.7)³⁴ for example. In similar experiments performed in nD₂ matrices no trace of H₂O nor any heavy water (HDO or D₂O) was found in the spectra. This case is similarly to the formation of all isotopes of methane. The bands may be so

Methane isotopes in nD ₂					
This Work	pH ₂	Assignment	This Work	pH ₂	Assignment
3027.2	3025.94 ^c	CH ₄	2262.1	2261.32 ^d	CD ₄
3025.7	3025.16 ^c	CH ₄	2261.0	2260.61 ^d	CD ₄
3023.3	^a	CDH ₃	1160.7	^a	CDH ₃
3022.0	^a	CDH ₃	1160.0	^a	CDH ₃
3018.3	^a	CD ₂ H ₂	1308.1	1309.16 ^c	CH ₄
3016.8	^a	CD ₂ H ₂	1307.8	1308.25 ^c	CH ₄
2995.6	2995 ^b	CD ₃ H	1036.2	^a	CD ₂ H ₂
2991.9	^a	CD ₃ H	1034.9	^a	CD ₂ H ₂
2980.3	^a	CD ₂ H ₂	996.9	997.16 ^d	CD ₄
2978.8	^a	CD ₂ H ₂	996.4	996.56 ^d	CD ₄

^a Assignment was done based Reference¹⁴² and Reference,¹⁴³ but not specific frequencies were written.

^b Reference¹⁴⁴

^c Reference³⁰

^d Reference^{31,145}

All frequencies are in cm⁻¹

Table 9.5: *Methane isotopes*

weak that their intensities are in the noise level and they are not detectable in the spectra. The non observation of water bands (H₂O) means that the H/D atom with react with the OH radical to form H₂O come from the matrix and not form the reaction 9.7

H ₂ O in pH ₂			
This Work	Gas Phase	pH ₂ ³³	Assignment
4217.93		4217.50	Q ₁ (0) H ₂ + [2 ₀₂ ← 0 ₀₀] pH ₂ O
4149.83		4149.81	Q ₁ (0) H ₂ {oH ₂ O}
4139.71		4139.65	oH ₂ - pH ₂ O
3773.42		3773.42	oH ₂ - pH ₂ O
3765.52	3779.49	3765.47	ν ₃ [1 ₀₁ ← 0 ₀₀]
3758.47		3758.44	oH ₂ -pH ₂ O [1,1 ← 1,0]
1631.64	1634.97	1631.50	ν ₂ [1 ₁₁ ← 1 ₀₀]
1608.89		1608.48	oH ₂ - pH ₂ O
1594.78			
1594.30		1593.7 mult.	oH ₂ -H ₂ O
1593.74			

All frequencies are in cm⁻¹

Table 9.6: *Water*

9. UV LASER IRRADIATION AT 193 NM

Table 9.6 lists the frequency values of H₂O bands and pH₂ bands induced by neighboring H₂O molecule in pH₂ matrices compared with the values reported in the literature. The nomenclature has been used from Fajardo *et al.*³³ Briefly, ortho-Hydrogen (oH₂)-pH₂O means complexes formed between oH₂-H₂ and *para*-H₂O molecules. In the rotational level $J_{K_a K_c}$, $K_a = |K|$ in the prolate rotor limit ($I_B=I_C$); and $K_c = |K|$ in the oblate rotor limit ($I_A=I_B$). J is the total rotational angular momentum, and K is the constant component of J about the axis defined by both planes of symmetry of the molecule. Q₁(0)H₂{oH₂O} means a Q₁(0)H₂ transition induced by oH₂O. Finally Q₁(0)H₂+ $[J''_{K_a K_c} \leftarrow J'_{K_a K_c}]Y$ is a cooperative absorptions in which the neighboring dopant species Y undergoes a pure rotational transition.

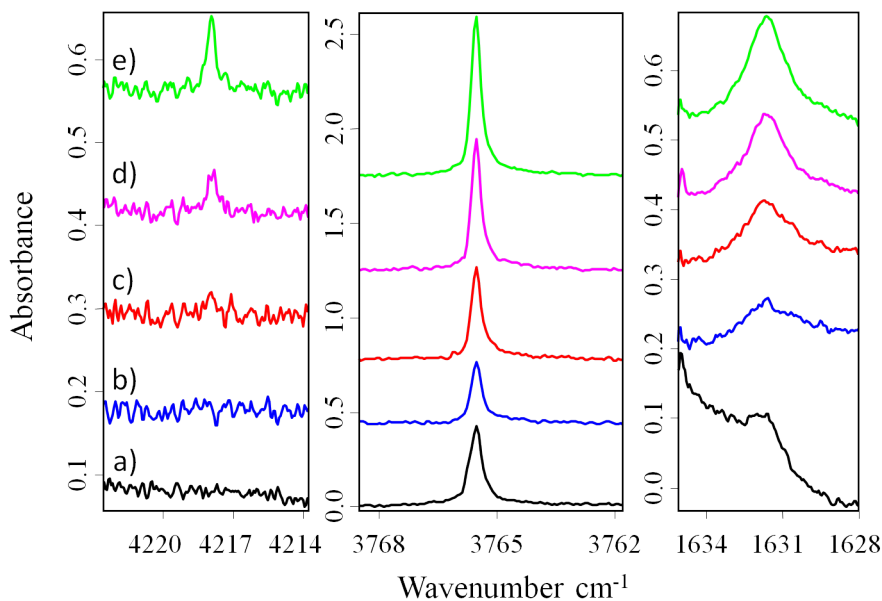
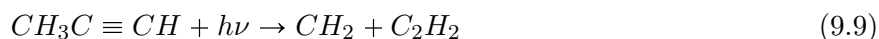


Figure 9.3: Growing water bands and pH₂ absorption induced by close water molecule due to the photolysis of AcAc in pH₂. (a) As deposited sample. After UV (193nm) laser irradiation (b) 15 min, (c) 30 min, (d) 75 min and (e) 135 min. Spectrum resolution 0.125 cm⁻¹

Figure 9.3 displays a fragment of the infrared spectra in the pH₂ and H₂O absorption regions during the irradiation of AcAc. (a) As deposited sample, (b) after 15 min of irradiation, (c) after 30 min of irradiation, (d) after 75 min of irradiation and (e) after 135 min of irradiation. Right panel the $\nu_2[1_{11} \leftarrow 1_{00}]$ band is shown, central panel the $\nu_3[1_{01} \leftarrow 0_{00}]$ and left panel correspond to the cooperative absorption Q₁(0) H₂ + $[2_{02} \leftarrow 0_{00}]$ pH₂O.

9.2.3 Formation of C₂H₂, C₂H₄, C₂H₆ and C₃

Seki and Okabe studied the photodissociation of Methylacetylene (Propyne) at 193 nm in gas phase founding Acetylene (C₂H₂) as a main product.¹⁴⁷ The photodissociation process is described by:



The Acetylene molecule and some Acetylene clusters are also detected in the infrared spectra after UV (193 nm) irradiation of AcAc in pH₂. Table 9.7 lists the frequencies values in cm⁻¹ of C₂H₂ compared with the values reported in the literature.

Acetylene C ₂ H ₂			
This Work	pH ₂	Ar ¹³⁴	
3279.53	3279.20 ^a	3288	ν_3
3277.23			ν_3 Clusters ^b
3274.80			ν_3 Clusters ^b
3273.50			ν_3 Clusters ^b
3265.48	3265.80 ^a	3268	Dimer T-shaped
1340.40	1340.10 ^a	1335	$\nu_4 + \nu_5$

^a Reference¹⁴⁸

^b Assignment was done based Reference,¹⁴⁹ but not specific frequencies were written.

All frequencies are in cm⁻¹

Table 9.7: *Acetylene*

Seki and H. Okabe¹⁵⁰ also studied the photochemistry of acetylene at 193.3 nm. Once the acetylene is irradiated with 193 nm ArF excimer, laser mainly two processes compete¹⁵⁰:



While the reaction 9.11 is more favorable than 9.10 the H₂CC does not react chemically with H₂ molecule¹⁵⁰ and maybe it relaxes to acetylene by phonon dissipation. On the other hand C₂H due to reaction 9.10 can react with the H₂ molecules as¹⁵⁰:

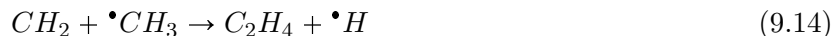


This reaction mechanism described by 9.10 followed by 9.12 is a cyclic way to produce free hydrogen atoms. The C₂H₂ reacts with a free H-atom to form C₂H₃.¹⁵⁰ The C₂H₃ radical is not observed in the spectrum, it can react with the pH₂ matrix.¹⁵¹



9. UV LASER IRRADIATION AT 193 NM

From the photolysis of keto form of AcAc (see reaction 9.5) as well as photolysis of propyne (see reaction 9.9) another possible fragment is the CH_2 radical. It can react with the matrix to form CH_4 (see reaction 9.8) but it can also react with CH_3 as follow¹⁵²:



The presence of C_2H_4 is confirmed in this work by the infrared spectra recorded after UV irradiation of the sample. Frequencies in cm^{-1} of C_2H_4 are listed in table 9.8. The presence of C_2H_4 in nD_2 matrices confirm that the reaction 9.14 can occur.

Ethylene C_2H_4				
This Work		Literature ^{30,35}		
pH_2	nD_2	gas	pH_2	Assignment
3101.5				
3100.3		3105.5	3101.00	ν_9 (CH_2 a-str)
3098.7	3098.1			
3073.0			3073.00	$\nu_2 + \nu_{12}$
2984.5	2948.2			
2984.2	2983.8	2989	2984.40	ν_{11} (CH_2 s-str)
2983.9	2983.5			
1887.1			1887.40	$\nu_7 + \nu_8$
1440.1	1440.6	1443.5	1440.00	ν_{12} (CH_2 scis)
957.3	952.8			
950.2	950.8	949	957.30	ν_7 (CH_2 wag)
949.3	949.1			
948.5				

All frequencies are in cm^{-1}

Table 9.8: *Ethylene*

The split in most of the bands are explained by Momose and co-workers when they studied the photolysis of Ethyl Iodide in pH_2 matrices.³⁰ They observed High Frequence Ethylene (E_H) and Low Frequence Ethylene (E_L).³⁰ The E_L is the Ethylene which have a Iodine atom in the nearby.³⁰ In this work, structured bands of C_2H_4 may be due to complexes with surrounding molecules formed during UV irradiation such as CH_4 or CO for example.

It is known that C_2H_2 clusters absorb at 193 nm.¹⁴⁹ Photolysis of C_2H_2 clusters in pH_2 matrix were studied by H. Hoshina *et al.* using the ArF excimer laser at 193 nm.¹⁴⁹ As a result carbon clusters (C_{2n+1}), CH_4 , C_2H_4 , C_2H_5 , C_2H_6 , and C_4H_2 are formed. In this experiment C_2H_2 clusters can be found (see table 9.7) as a result of photolysis of AcAc in pH_2 matrix. Assuming that there are only one AcAc molecule per matrix trapping site, i.e. no clusters of AcAc, only dimers of acetylene should

be expected. Mechanisms of formation of these C_2H_2 cluster have yet to be clarified. Nevertheless only C_3 clusters (See figure 9.4) are found in the infrared spectra after UV irradiation which seems to confirm the presence of only $(C_2H_2)_2$ clusters. The frequencies values in cm^{-1} are listed in table 9.9.

Carbon Cluster (C_3)						
This Work			Literature ^{149,153}			
pH ₂	nD ₂	gas	pH ₂	Ar	Ne	Assignment
3244.4			3244.3 3244.5	3245.2		$\nu_1 + \nu_3$
2036.0	2036.6	2040.02	2035.9	2038.9	2036.4	ν_3
2034.5	2034.4		2034.5			

All frequencies are in cm^{-1}

Table 9.9: Carbon Clusters

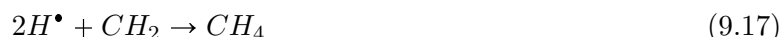
The mechanism of formation of C_3 cluster from photolysis of C_2H_2 dimers may be as follow: If the photon at 193 nm excites one of the C_2H_2 molecule by reaction 9.11 the metastable acetylene can be formed.



Instead of relaxing through phonon, H_2CC^* can react with the other acetylene molecule:



followed for example by:



Both H-atoms may also react to form H_2 molecule and CH_2 reacts with the matrix as reaction 9.8.

As it was said before, C_2H_5 can be formed from photolysis of acetylene clusters.¹⁴⁹ The C_2H_5 radical was also reported by Momose and co-workers after UV irradiation of ethyl iodide in pH₂ matrices¹⁴⁰ and Yu-Jong Wu *et al.* after UV (193 nm) irradiation of C_2H_3Cl in pH₂ matrices¹⁵¹ but not trace of this radical was founded in the present work. The absence of C_2H_5 radical means that, if it is formed by photolysis of C_2H_2 clusters then it is an intermediate step in the formation of other products. In the sample, hydrogen atoms are produced all the time due to the reaction 9.7 followed by reaction 9.8, for example. Because free H-atoms are able to migrate through the pH₂ matrix¹⁴⁶ reaction of C_2H_5 with one H-atom can then be possible to form C_2H_6 .³⁰



9. UV LASER IRRADIATION AT 193 NM

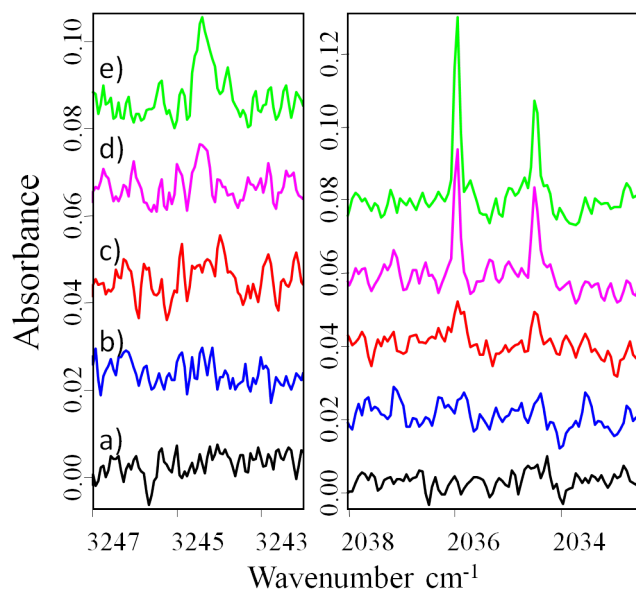
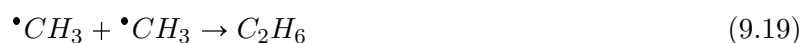


Figure 9.4: Growing bands of C_3 clusters due to the photolysis of AcAc in pH_2 . (a) As deposited sample. After UV (193nm) laser irradiation (b) 15 min, (c) 30 min, (d) 75 min and (e) 135 min. Spectrum resolution 0.125 cm^{-1}

Experiments of photolysis of methyl iodide as a guest molecule in pH_2 matrices reveal the formation of Ethane (C_2H_6) after UV irradiation of the sample. The reaction mechanism of formation of C_2H_6 is proposed from the formation of dimers of CH_3I which dissociates, after irradiation, in $2(CH_3) + I_2$ or $C_2H_6 + I_2$.³⁴ In the reaction 9.4 and 9.5 followed by the dissociation of CH_3-CO (reaction 9.6), two methyl radicals are available and they may recombine to form the Ethane.



This reaction mechanisms is quite unlikely in the present study because both CH_3 radicals need to be close enough to recombine before reacting with something else or absorb a photon and start the reaction mechanism 9.10 and 9.11 to form CH_4 . Table 9.10 list the frequencies values in cm^{-1} of C_2H_6 observed in the infrared spectra after irradiation of AcAc in pH_2 matrix.

Ethane C_2H_6			
This Work	gas ¹³⁷	pH_2 ^{34,35}	Assignment
2980.67	2985.4	2979.30	(CH_3 a-str)
2890.05	2895.8		(CH_3 s-str)
1467.25	1469	1467.1	(CH_3 d-deform Fermi reso $\nu_4 + \nu_{12}$)

All frequencies are in cm^{-1}

Table 9.10: Ethane

The amount of C_2H_4 is considerably large compared with other molecules, C_2H_6 for example, formed under UV irradiation of AcAc. No evidence of photolysis of these two molecules are reported after irradiation at 193 nm. The mechanisms for formation of C_2H_4 seems to be much more efficient than to form C_2H_6 . In the experiments performed in nD_2 matrices no evidence of C_2H_6 or any deuterated isotopes of C_2H_4 or C_2H_6 were found. If they are formed for any reaction mechanism similar to the proposed for pH_2 matrices, the intensities are so weak that they are not measurable.

9.2.4 HCO radical and Formaldehyde

Bands assigned to Formyl radical (HCO) are in agreement with values reported in the literature^{137–139} (See table 9.3). Milligan and Jacox¹³⁸ produce HCO radicals in Ar matrices from a photolysis of a H-atom source in a co-deposition with CO. Once the hydrogen atom is formed, it can reach the CO to react and form the HCO radical (see equation 9.20)

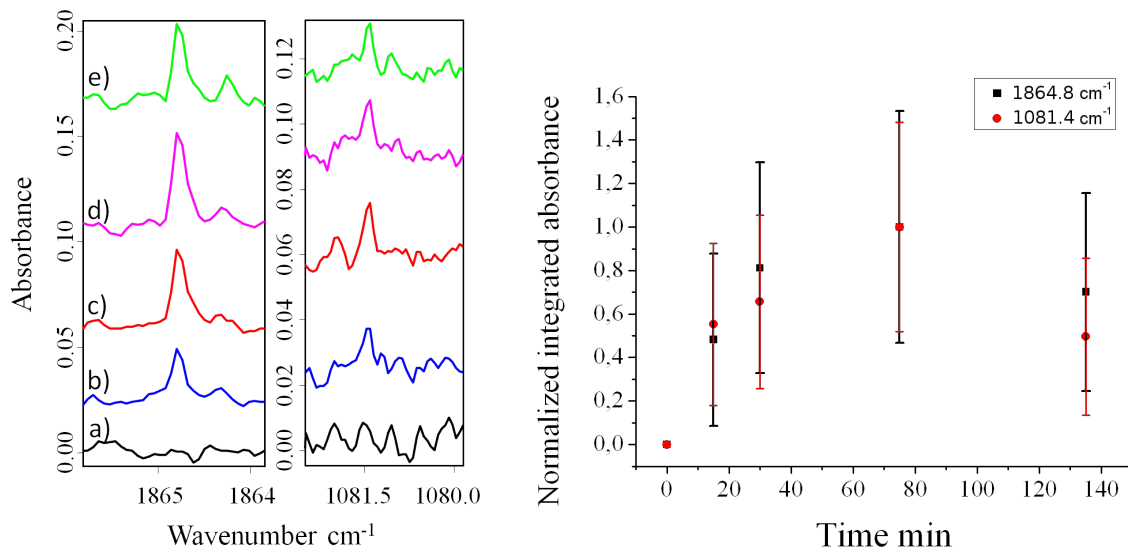


Figure 9.5: Left panel: Fragment of the infrared spectra of AcAc in pH_2 . (a) As deposited sample and after UV (193nm) laser irradiation (b) 15 min, (c) 30 min, (d) 75 min and (e) 135 min. Resolution 0.125 cm^{-1} . Growing bands are assigned to HCO radical. Right panel: Time evolution of 1864.8 and 1081.4 cm^{-1} bands assigned to HCO radical after irradiation of AcAc in pH_2 matrices with UV (193nm) laser.

Figure 9.5 shows, in the left panel, two fragments of the infrared spectra of AcAc in pH_2 with a resolution of 0.125 cm^{-1} . (a) As deposited sample and after UV (193nm) laser irradiation (b) 15 min,

9. UV LASER IRRADIATION AT 193 NM

(c) 30 min, (d) 75 min and (e) 135 min. In the right panel, the time evolution of these two bands are plotted as a function of time. Plot (1) helps to confirm the assignment of HCO radical in pH₂ matrix since no data in such matrix are available in the literature, (2) shows that the HCO radicals not remain after long irradiation times suggesting a reaction to form other more stable molecule. Due to the possibility of migration of hydrogen atom through the matrix¹⁴⁶ the HCO radical can react with another H-atom to produce Formaldehyde (H₂CO).



A spectrum of formaldehyde in pH₂ was recorded for comparison as there are no published data on infrared spectra of formaldehyde isolated in pH₂ matrices. Confirming the reaction 9.21, bands corresponding to formaldehyde were found in the infrared spectra after irradiation of AcAc in pH₂. The frequencies values are summarized in table 9.11

Formaldehyde H ₂ CO		
This Work	gas ¹³⁷	Assignment
2782.63	2782.5	(CH ₂ s-str)
1742.62	1746.1	(CO str)
1497.76		(CH ₂ bend)

All frequencies are in cm⁻¹

Table 9.11: *Formaldehyde*

Other radicals are found in the infrared spectra after irradiation. The assignment is supported by the data available in the literature. The radicals are: Ethynoxy radical (HCCO)^{136,137} and Tricarbon Monoxide (CCCO).^{137,139} For these radicals no mechanisms of formation can be described with the experimental data recorded during this experiment. Table 9.3 list the values of the infrared frequencies of these radicals in pH₂ matrix compared with those reported in the literature.

Figure 9.6 left panel displays the region of the infrared spectrum where HCCO radical is observed in pH₂ matrix; a) As deposited matrix, UV (193 nm) laser irradiation (b) 15 min, (c) 30 min, (d) 75 min, (e) 135 min. In the right panel of figure 9.6 a time evolution of integrated absorbance of the band represented in the left panel is shown. In this experiment, HCCO radical reach the maximum value around 30 min of irradiation and then starts to decrease.

Photolysis of Ketene (CH₂CO) at 193 nm at 297 K were performed by G. P. Glass *et al.*¹⁵⁴ The HCCO radical is one photo-product after irradiation of ketene and no UV (193 nm) absorption is reported for this radical.¹⁵⁴ Moreover they also found that the reaction 9.22 seems to be important after photolysis of ketene.



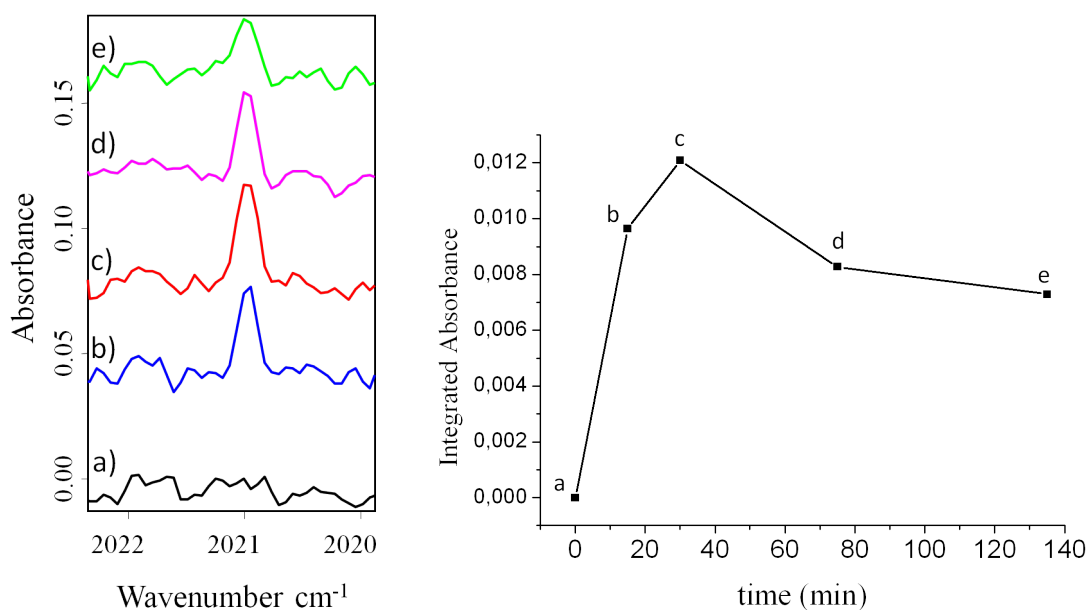
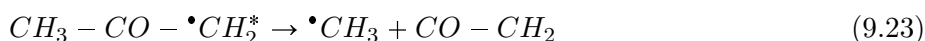


Figure 9.6: Left panel: Fragment of infrared spectra of AcAc in pH_2 matrices. (a) As deposited sample. After UV (193 nm) laser irradiation (b) 15 min, (c) 30 min (d) 75 min and (e) 135 min. The resolution is 0.125 cm^{-1} . Growing band is assigned to the CCO asymmetric-stretch of HCCO radical.

Ketene may be a product of photolysis of keto form of AcAc. From reaction 9.4 followed by 9.23 instead of 9.5:



In our experiments, ketene molecule was not observed. This means that there are two possibilities (1) if it is formed by any mechanism 9.4 and 9.23 then it is quickly photo-fragmented to form HCCO radical or (2) it is not formed at all and the HCCO fragment is formed from another mechanisms. The observation of HCCO in pH_2 matrices and the relatively slow decreasing of HCCO suggest that ketene is not formed at all. Ketene photolysis in facts generate a H-atom that may react again with the HCCO radical as 9.22. The velocity of this reaction should be as quick as the depletion of ketene then neither ketene or HCCO can be seen. The behavior of HCCO radical in the sample (see figure 9.6) suggests a reaction similar to 9.22 but with a H-atom formed not in the neighborhood.

9.3 Unassigned bands

Finally, many others bands remain unassigned in the present work. In general the behavior is not the same for all of them. Kinetic study of all unassigned bands is very difficult because most of them are

9. UV LASER IRRADIATION AT 193 NM

too close or weak or shoulder. Nevertheless three groups of bands can be separated based on their time evolution during the irradiation.

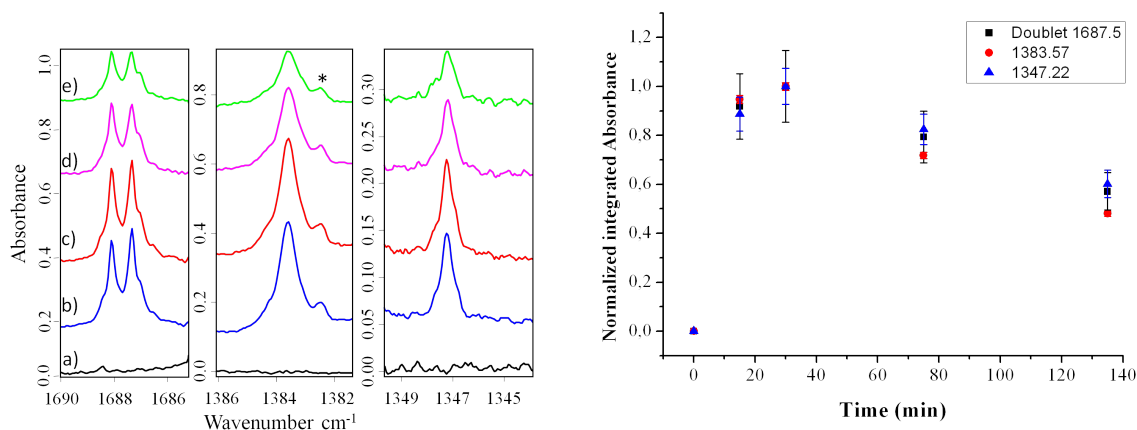


Figure 9.7: Left panel: Fragments of the infrared spectra of AcAc in pH₂ matrix. (a) As deposited sample. After UV laser irradiation at 193 nm, (b) 15 min, (c) 30 min, (d) 75 min and (e) 135 min. (*) represent a band assigned to propyne (see figure 9.2) Right panel: Time evolution of three unassigned bands which appear in the infrared spectra of AcAc in pH₂ after UV (193nm) laser irradiation. Corresponding bands are labeled in the graphic.

The first group are the bands that have a time evolution similar to isomers of acetylacetone, i.e. with the irradiation they grow up and at some instant of time start to decrease. Figure 9.7 show in the left panel fragments of the infrared spectra of AcAc in pH₂ matrices. (a) As deposited sample. After UV laser irradiation at 193 nm, (b) 15 min, (c) 30 min, (d) 75 min and (e) 135 min. Bands at 1347.22 cm⁻¹, 1383.57 cm⁻¹ and the doublet with center at 1687.5 cm⁻¹ show the same evolution with the irradiation. The right panel of figure 9.7 display the normalized integrated absorbance of these bands as a function of time. From the graphic, it is visible that, in this experiment, these bands reach the maximum value around 30 min of irradiation at 193 nm, and after this point, they start to decrease. The decreasing of those bands may be due to various factors, (1) this molecule may absorb at 193 nm wavelength and fragments into smaller molecules, (2) this molecule is a radical which reacts with a surrounding molecule or radical to form others molecules in reaction mechanisms similar to those described in the previous subsections. In both cases these bands may be assigned to a one molecule which is an intermediated step in the fragmentation of AcAc to smaller molecules.

The second group consists in bands that grow up all the time. This group in fact split in two subgroups because the kinetics are a bit different. The fragments of the infrared spectra which shows these bands are displayed in Figure 9.8 left panel. (a) As deposited sample, (b) after 15 min irradiation, (c) after 30 min irradiation, (d) after 75 min irradiation and (e) after 135 min irradiation. The spectra

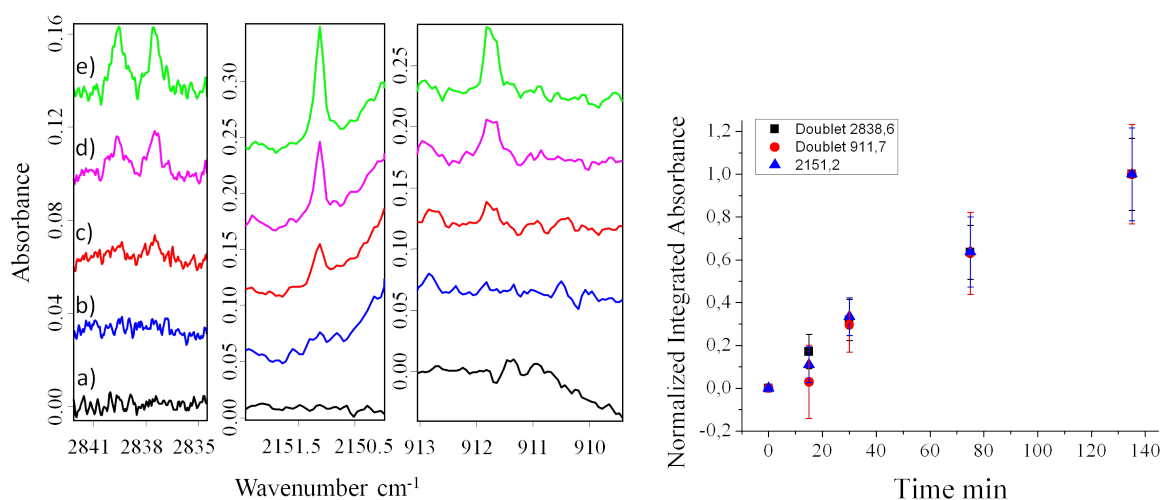


Figure 9.8: Left panel: Fragments of the infrared spectra of AcAc isolated in pH₂ at different UV irradiation times. (a) As deposited sample, (b) after 15 min irradiation, (c) after 30 min irradiation, (d) after 75 min irradiation and (e) after 135 min irradiation. Right panel: Time evolution of three unassigned bands which appear in the infrared spectra of AcAc in pH₂ after UV (193nm) laser irradiation. Corresponding bands are labeled in the graphic.

were recorded with a resolution of 0.125 cm⁻¹. In all spectra the contribution of the chelated enol form was subtracted. Bands at 2837.5, 2839.6, 2151.2 and 911.7 cm⁻¹ have similar behavior during time (see figure 9.8 right panel) then they should belong to the same unknown molecule.

The other subgroup of growing bands is represented in figure 9.9. Left panel displays the fragments of the infrared spectra corresponding with bands at 1727.1, 1364.2, 1356.4 and doublet at 1219.5 and 1220.3 cm⁻¹. (a) As deposited sample, (b) after 15 min irradiation, (c) after 30 min irradiation, (d) after 75 min irradiation and (e) after 135 min irradiation. The contribution on the chelated enol form was subtracted in the spectra after UV irradiation.

Right panel of figure 9.9 displays the temporal evolution of the bands represented in the left panel. Normalized integrated absorbance are plotted as a function of time. Even when bands of both subgroups grow up all the time, looking at the graphics, the curvature for the second subgroup (figure 9.9 right panel) is bigger than that of the first subgroup (Figure 9.8 right panel). That means that bands correspond to different molecules. Unfortunately the second subgroup of growing bands can not be assigned with the present experimental data.

On the other hand several other bands also appear in the infrared spectra and are not assigned. The kinetic treatment was not performed because most of these bands are weak or shoulder. The frequencies values in cm⁻¹ are listed in table 9.12

9. UV LASER IRRADIATION AT 193 NM

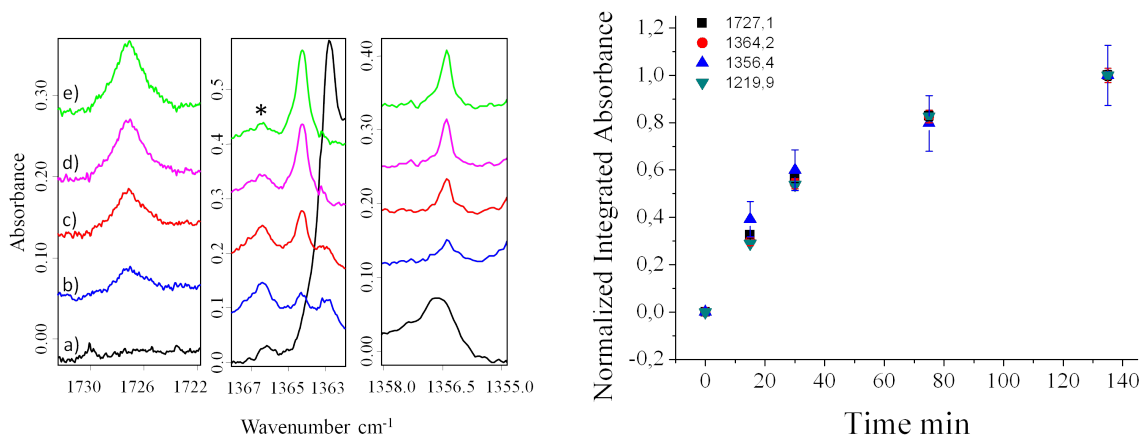


Figure 9.9: Left panel: Fragments of the infrared spectra of AcAc isolated in pH_2 at different UV irradiation times. (a) As deposited sample, (b) after 15 min irradiation, (c) after 30 min irradiation, (d) after 75 min irradiation and (e) after 135 min irradiation. Asterisk represent a band assigned to a open enol isomer of AcAc. Right panel: Time evolution of three unassigned bands which appear in the infrared spectra of AcAc in pH_2 after UV (193nm) laser irradiation. Corresponding bands are labeled in the graphic.

Unknown observed bands				
	Weak	Medium/Weak	Medium	
	4332.4	1585.5	2286.2	2129.3
	4327.1	1350.7	2285.6	2154.6
	4324.0	1306.8	2257.3	1308.0
	3244.4	1306.1	2095.8	
	3048.0	1301.2	1888.4	
	2626.7	1300.3	1774.3	
	2624.0	1216.1	1597.9	
	2278.3	1170.0	1347.2	
	1734.7			

All frequencies are in cm^{-1}

Table 9.12

9.4 Summary

In this chapter the photolysis of acetylacetone in pH_2 matrix was examined. Many photo-products appeared as a result of illumination of the sample with UV (193 nm) laser. The highest possible resolution for this experimental setup (0.125 cm^{-1}) was necessary to resolve very narrow bands corresponding to fragments. The main molecules produced after irradiation were CH_4 , CO , C_2H_4

and H₂O. Nevertheless other molecules in smaller amount such as C₂H₂, C₂H₆, CH₃CCH, CH₂O were also found in the infrared spectra. Radicals as CH₃, HCO, HCCO, CCCO are also observed as intermediated steps of the formation of chemically stable molecules as well as the formation of C₃ clusters. Unlikely for the other two wavelengths used for these experiments, a wavelength at 193 nm results to be very efficient for fragmentation of the AcAc. Reaction mechanisms were proposed in which manifest many processes in competition such as: (1) the fragmentation in which a photon is necessary for excite the molecule, (2) the recombination of photo fragments without photons involved, (3) chemical reactivity with/without necessity of photons and (4) the heating of the diamond windows which absorbs wavelength of 193 nm what allows allow the mobility of fragments through the matrix. The reactivity of H₂ molecules of the matrix were proved by substitution with D₂ matrix which also react with excited photofragments.

As was shown in kinetic graphics, the irradiation of the sample never arrived to the stationary state. The necessity of experiments which reach this stationary point are mandatory for better identification of finals products. On the other hand some reaction mechanisms seem to be second photon dependent. Then, experiments using less intense laser may be useful for better understanding of the reaction mechanisms of this system.

9. UV LASER IRRADIATION AT 193 NM

Conclusions

The structure, photochemistry, dynamic and photodynamic upon irradiation at 266, 248 and 193 nm of Acetylacetone (AcAc) isolated in hydrogen matrices were studied by the means of infrared absorption spectroscopy. Two coexisting tautomers of AcAc molecule (*enol* and *keto*) were observed in the low temperature hydrogen and deuterium matrices. The keto/enol ratio (R_{ke}) is found to be significantly higher in para-Hydrogen (pH₂) (~4.5%) than in other cryogenic solids. This appears to be specific to this “*quantum*” solid.

The infrared spectra of AcAc in pH₂ just after deposition shows that many absorption bands of the chelated enol form are broad, similarly to the case of AcAc isolated in rare gas or nitrogen matrices. This is mainly due to the internal strong intramolecular hydrogen (H_{int}) bond.

The theoretical calculations of chelated enol form of AcAc with both, C_s and C_{2v} symmetries were compared with the infrared spectrum of AcAc in pH₂ matrices. The vibrational analysis is supported by anharmonic theoretical calculations of the frequencies which have a very good agreement with the experimental ones. The C_s symmetry was confirmed. Anharmonic theoretical calculations also shows the influence of this H_{int} bond on specific modes.

The photochemistry of the chelated enol isomer (CCC) of AcAc was investigated. The excitation of AcAc up to the S₂ was done using two wavelength, 266 nm and 248 nm. The excitation at 266 nm results mainly in the isomerization of AcAc. The photoproducts were identified as non-chelated enol conformers by recording their infrared (IR) absorption spectra, combined with theoretical calculation using the harmonic and anharmonic approximations. In contrast with the case of the chelated form, the spectra of open isomers (isomers without H_{int} bond) display narrower absorption bands.

The character almost non-perturbative of the pH₂ solid has allowed the assignment of a new isomer (TTC) after UV laser irradiation of AcAc trapped therein. In other matrices such as normal-Hydrogen (nH₂) and normal-Deuterium (nD₂), CTC, TCC and TTC were formed as in pH₂ but another additional conformer TCT was observed. This suggests that the TCT→TCC tunnelling process is at play in pH₂ but is quenched in the more interacting nH₂ matrix. Quenching of such tunnelling processes in nH₂ in contrast with pH₂ might be a general effect.

CONCLUSIONS

Fragmentation is a very minor process at 266 nm. Neither the OH radical nor other products corresponding to a single bond cleavage are detected as photofragments. In contrast, CO which necessitates a drastic bond rearrangement is observed. This observation allows to conclude that the isomerization from chelated AcAc to non-chelated conformers does not proceed from a dissociation/recombination process. Meanwhile, the excitation with 248 nm leads to the formation of same open enol forms as after irradiation with 266 nm. Prolonged irradiation also depleted those isomers resulting in an increase of spectral bands assigned to keto form. CO, observed as a fragment, grows with a rate similar to that of keto, suggesting that keto could be formed in a dissociation/recombination process, even in pH₂.

A wavelength of 193 nm excites the AcAc up to a S₃ Rydberg state. All open enol isomers as well as keto form are produced at 193 nm as intermediated state of further reactions. In contrast with the gas phase experiment no OH radical was found in the sample, but the increase of H₂O bands is detected. The experiments show evidence of reactions of some radicals with the hydrogen molecule (H₂) of the matrix to form other radicals or chemically stable species. Similar experiments performed in nD₂ matrices confirm the reactions of radicals with the matrix when deuterated molecules were found.

The experimental setup used for making those experiments does not allow to keep the sample for very long time. Other experiments have to be performed with the aim of reaching the stationary conditions for better assignments of final photo-products after UV irradiation. On the other hand, some reactions seem to be dependent of the arrival of a second photon. The reaction mechanisms with a CH₃ radical is an example. Other experiment with a less intense laser may provide experimental data for better understanding of some reaction mechanisms on this system.

The reduced cage effect of pH₂ has permitted the isolation of radicals such as CH₃, HCO, HCCO after *in situ* UV laser irradiation of AcAc at 248 nm and 193 nm. Other stable molecules were also isolated as a result of the irradiation providing evidence of the reactivity of some radicals with the pH₂ molecule of the matrix. The rotational structure of absorption bands of CH₄ molecule proves its presence in the matrix as a result of the photo-reaction of CH₃ with pH₂.

The pH₂ host is found to preserve subtle intrinsic dynamical properties of the guest molecule, such as the large-amplitude motions that are at play in the chelated enol form of AcAc. Two of them are due to torsional motions of the methyl groups. Classical hosts such as Ne, quench those motions in AcAc. But solid pH₂ partly preserves these torsions and reveals new vibrational behavior directly related to the complex dynamics between the H_{int} transfer and the two methyl rotors. Due to the H-atoms in the methyl groups, nuclear spin conformers of the chelated enol form of AcAc exist and experimental evidence of them isolated in pH₂ matrix were presented.

Experimental evidence of proton tunnelling within the less-hindered methyl group of AcAc was provided and its relation with the clearly observed nuclear spin conversion (NSC) has been shown. Analysis of the experimental data has revealed that the H_{int} transfer is mediated by the torsion of the less-hindered methyl group. This was revealed using NSC in this methyl group as a tool to disentangle two IR absorption spectra corresponding to the ground vibrational state (most stable (*ms*) species) and a torsional excited state of enolic AcAc (less stable (*ls*) species).

The pH_2 matrices can be used to study the solvation effects in weakly bond complexes as well as molecular systems with coupled large-amplitude movements. The present work thus appears as a case study showing that NSC in solid pH_2 is a dedicated tool for investigating the spectroscopy of molecular species carrying energy in internal methyl torsion. For AcAc isolated in pH_2 is shown, with almost no host effect, which vibrational modes are coupled to promote the H_{int} transfer in a concerted fashion. The observed band widths and positions, by providing information on the intrinsic properties of the molecule, offer a quantitative benchmark for future calculations of the H_{int} transfer process. These will be certainly very challenging (but manageable) as they will need to consider the two methyl torsions and the pseudo cycle deformation modes that host the H_{int} transfer coordinate and interplay with the simultaneous change of the electron configuration. Beside all the spectroscopic advantages of pH_2 solids highlighted in this work, the photochemistry of molecules trapped in pH_2 matrices has also interest for astrophysics. Chemical reactions of molecules or radicals with H_2 that may be played in the interstellar space can be controlled and studied in this cryogenic systems.

Other theoretical calculations of this system have to be performed for better understanding of the processes that take place therein. Calculation of AcAc surrounded by pH_2 molecules may explain the sites occupied by this molecule in the matrix and the deformation of the matrix due to its presence. The theoretical simulation dynamics can provide more information about the intermediate steps for isomerization, tautomerization and fragmentation once the molecule is excited to the S_2 state as well as to the S_3 Rydberg state. These dynamical calculation may be conclusive regarding if the formation of open enol forms proceed from a dissociation/recombination process or from rotations around molecular bonds and why the XYT isomers are not stabilized in pH_2 but in more interacting nH_2 matrices. The influence of the matrix in the infrared spectra may be also explained.

CONCLUSIONS

References

- [1] E. WHITTLE, D. A. DOWS, AND G. C. PIMENTEL. **Matrix isolation method for the experimental study of unstable species.** *The Journal of Chemical Physics*, **22**:1943, 1954.
- [2] S. COUSSAN, C. MANCA, Y. FERRO, AND P. ROUBIN. **UV and IR photoisomerizations of an intramolecularly H-bonded molecule: acetylacetone trapped in nitrogen matrix.** *Chemical Physics Letters*, **370**:118, 2003.
- [3] KINYA IJIMA, ATSUSHI OHNOGI, AND SHUZO SHIBATA. **The molecular structure of acetylacetone as studied by gas-phase electron diffraction.** *Journal of Molecular Structure*, **156**:111, 1987.
- [4] K. N. WALZL, I. M. XAVIER, AND A. KUPPERMANN. **Electron-impact spectroscopy of various diketone compounds.** *Journal of Chemical Physics*, **86**:6701, 1987.
- [5] GASTONE GILLI, FABRIZIO BELLUCCI, VALERIA FERRETTI, AND VALERIO BERTOLASI. **Evidence for Resonance-Assisted Hydrogen Bonding from Crystal-Structure Correlations on the Enol Form of the β -Diketone Fragment.** *Journal of the American Chemical Society*, **111**:1023, 1989.
- [6] MIGUEL A. RIOS AND JESÚS RODRÍGUEZ. **An ab initio study of the conformation and intramolecular proton transfer in the enol form of acetylacetone.** *Journal of Molecular Structure: THEOCHEM*, **204**:137, 1990.
- [7] P. ROUBIN, T. CHIAVASSA, P. VERLAQUE, L. PIZZALA, AND H. BODOT. **FT-IR study of UV-induced isomerization of intramolecularly hydrogen-bonded carbonyl compounds isolated in xenon matrices.** *Chemical Physics Letters*, **175**:655, 1990.
- [8] A. H. LOWREY, C. GEORGE, P. D'ANTONIO, AND J. KARLE. **Structure of Acetylacetone by Electron Diffraction.** *Journal of the American Chemical Society*, **93**:6399, 1971.
- [9] A.L. ANDREASSEN AND S.H. BAUER. **The structures of acetylacetone, trifluoroacetyl-acetone and trifluoroacetone.** *Journal of Molecular Structure*, **12**:381, 1972.
- [10] RAMESH SRINIVASAN, JONATHAN S. FEENSTRA, SANG TAE PARK, SHOUJUN XU, AND AHMED H. ZEWAAL. **Direct Determination of Hydrogen-Bonded Structures in Resonant and Tautomeric Reactions Using Ultrafast Electron Diffraction.** *Journal of the American Chemical Society*, **126**:2266, 2004.
- [11] SIMON TAM, MARIO E. FAJARDO, HIROYUKI KATSUKI, HIROMICHI HOSHINA, TOMONARI WAKABAYASHI, AND TAKAMASA MOMOSE. **High resolution infrared absorption spectra of methane molecules isolated in solid parahydrogen matrices.** *The Journal of Chemical Physics*, **111**:4191, 1999.
- [12] G. A. JEFFREY AND W SAENGER. *Hydrogen Bonding in Biological Structures.* Springer, 1991.
- [13] JANEZ MAVRI AND GRDADOLNIK JOŽE. **Proton Transfer Dynamics in Acetylacetone: A Mixed Quantum-Classical Simulation of Vibrational Spectra.** *The Journal of Physical Chemistry A*, **105**:2045, 2001.
- [14] HIROSHI NAKANISHI, HIRODHI MORITA, AND SABURO NAGAKURA. **Electronic Structure and Spectra of the Keto and Enol Forms of Acetylacetone.** *Bulletin of the Chemical Society of Japan*, **50**:2255, 1977.
- [15] NATALYA V. BELOVA, VALERIY V. SLIZNEV, HEINZ OBERHAMMER, AND GEORGIY V. GIRICHEV. **Tautomeric and conformational properties of β -diketones.** *Journal of Molecular Structure*, **978**:282, 2010.
- [16] MANUEL TEMPRADO, MARIA VICTORIA ROUX, PATAMAPORN UMNAHANANT, HUI ZHAO, AND JAMES S. CHICKOS. **The Thermochemistry of 2,4-Pentanedione Revisited: Observance of a Nonzero Enthalpy of Mixing between Tautomers and Its Effects on Enthalpies of Formation.** *The Journal of Physical Chemistry B*, **109**:12590, 2005.
- [17] J. N. SPENCER, ERICS S. HOLMBOE, MINDY R. KIRSHENBAUM, DANIEL W. FIRTH, AND PATRICIA PINTO. **Solvent effects on the tautomeric equilibrium of 2,4-pentanedione.** *Canadian Journal of Chemistry*, **60**:1178, 1982.
- [18] JANE L. BURDETT AND MAX T. ROGERS. **Keto-Enol Tautomerism in β -Dicarbonyls Studied by Nuclear Magnetic Resonance Spectroscopy. 1. Proton Chemical Shifts and Equilibrium Constants of Pure Compounds.** *Journal of the American Chemical Society*, **86**:2105, 1964.
- [19] ARTHUR CAMERMAN, DONALD MASTROPAOLO, AND NORMAN CAMERMAN. **Molecular Structure of Acetylacetone. A Crystallographic Determination.** *Journal of the American Chemical Society*, **105**:1584, 1983.
- [20] HARI P. UPADHYAYA, AWADHESH KUMAR, AND PRAKASH D. NAIK. **Photodissociation dynamics of enolic-acetylacetone at 266, 248, and 193 nm: Mechanism and nascent state product distribution of OH.** *Journal of Chemical Physics*, **118**:2590, 2003.
- [21] XUE-BO CHEN, WEI-HAI FANG, AND DAVID LEE PHILLIPS. **Theoretical Studies of the Photochemical Dynamics of Acetylacetone: Isomerization, Dissociation, and Dehydration Reactions.** *The Journal of Physical Chemistry A*, **110**:4434, 2006.
- [22] S. COUSSAN, Y. FERRO, A. TRIVELLA, M. RAJZMANN, P. ROUBIN, R. WIECZOREK, C. MANCA, P. PIECUCH, K. KOWALSKI, M. WŁOCH, S. A. KUCHARSKI, AND M. MUSIAL. **Experimental and Theoretical UV Characterizations of Acetylacetone and Its Isomers.** *The Journal of Physical Chemistry A*, **110**:3920, 2006.

REFERENCES

- [23] A. TRIVELLA, S. COUSSAN, T. CHIAVASSA, P. THEULÉ, C. MANCA, AND P. ROUBIN. **Comparative study of structure and photo-induced reactivity of malonaldehyde and acetylacetone isolated in nitrogen matrices.** *Fizika Nizkikh Temperatur*, **32**:1372, 2006.
- [24] MICHAEL HAWKINS AND LESTER ANDREWS. **Reactions of Atomic Oxygen with Ethene in Solid Argon. The Infrared Spectrum of Vinyl Alcohol.** *Journal of the American Chemical Society*, **105**, 1983.
- [25] THÈRHÉ MERLE-MEJEAN, COLETTE COSSE-MERTENS, SAÏD D BOUCHARÉB, FLORENCE CALAN, JOËLLE MASCETTI, AND MICHEL TRANQUILLE. **Raman, Infrared, and UV-Visible Studies of Matrix-Isolated NiO-Complexes with Ethylene, Propylene, and Butadiene.** *The Journal of Physical Chemistry*, **96**:9148, 1992.
- [26] MATTHEW G. K. THOMPSON AND J. MARK PARNIS. **Photoinduced Ethane Formation from Reaction of Ethene with Matrix-Isolated Ti, V, or Nb Atoms.** *Journal of Physical Chemistry A*, **109**:9465, 2005.
- [27] TAKAMASA MOMOSE AND TADAMASA SHIDA. **Matrix-Isolation Spectroscopy Using Solid Parahydrogen as the Matrix: Application to High-Resolution Spectroscopy, Photochemistry, and Cryochemistry.** *Bulletin of the Chemical Society of Japan*, **71**:1, 1998.
- [28] ISAAC F. SILVERA. **The solid molecular hydrogens in the condensed phase: Fundamentals and static properties.** *Reviews of Modern Physics*, **52**:393, 1980.
- [29] P.C. SOUERS. *Hydrogen Properties for Fusion Energy*. University of California Press, 1986.
- [30] NORIHITO SOGOSHI, TOMONARI WAKABAYASHI, TAKAMASA MOMOSE, AND TADAMASA SHIDA. **Infrared Spectroscopic Studies on Photolysis of Ethyl Iodide in Solid Parahydrogen.** *Journal of Physical Chemistry A*, **101**:522, 1997.
- [31] HIROMICHI HOSHINA, TOMONARI WAKABAYASHI, TAKAMASA MOMOSE, AND TADAMASA SHIDA. **Infrared spectroscopic study of rovibrational states of perdeuterated methane (CD₄) trapped in parahydrogen crystal.** *Journal of Chemical Physics*, **110**:5728, 1999.
- [32] YUAN-PERN LEE, YU-JONG WU, R. M. LEES, LI-HONG XU, AND JON T. HOUGEN. **Internal Rotation and Spin Conversion of CH₃OH in Solid para-Hydrogen.** *Science*, **311**:365, 2006.
- [33] MARIO E. FAJARDO, SIMON TAM, AND MICHELLE E. DEROSE. **Matrix isolation spectroscopy of H₂O, D₂O, and HDO in solid parahydrogen.** *Journal of Molecular Structure*, **695-696**:111, 2004.
- [34] TAKAMASA MOMOSE, MIKIO UCHIDA, NORIHITO SOGOSHI, MASAOKI MIKI, SHINYA MASUDA, AND TADAMASA SHIDA. **Infrared Spectroscopic Studies of photoinduced reaction of methyl radical in solid parahydrogen.** *Chemical Physics Letters*, **246**:583, 1995.
- [35] JAY C. AMICANGELO, BARBARA GOLEC, MOHAMMED BAHOU, AND YUAN-PERN LEE. **Infrared spectrum of the 2-chloroethyl radical in solid para-hydrogen.** *Physical Chemistry Chemical Physics*, **14**:1014, 2012.
- [36] Y. POKER AND G. T. SPYRIDIS. **Modulation of Tautomeric Equilibria by Ionic Clusters. Acetylacetone in Solutions of Lithium Perchlorate-Diethyl Ether.** *Journal of the American Chemical Society*, **124**:10373, 2002.
- [37] CATALOGUE. *Aldrich Chemie*, **102**. 2005-2006.
- [38] A. D. MCNAUGHT AND A. WILKINSON, editors. *IUPAC. Compendium of Chemical Terminology, (the "Gold Book")*. Blackwell Scientific Publications, 1997.
- [39] R. H. HOLM AND F. A. COTTON. **Spectral Investigations of Metal Complexes of β -Diketones. I. Nuclear Magnetic Resonance and Ultraviolet Spectra of Acetylacetonates.** *Journal of the American Chemical Society*, **80**:5658, 1958.
- [40] GEORGE S. HAMMOND, WILFRED G. BORDUIN, AND GERALD A. GUTER. **Chelates of β -Diketones. I. Enolization, Ionization and Spectra.** *Journal of the American Chemical Society*, **81**:4682, 1959.
- [41] BODO BOCK, KARSTEN FLATAU, HELMUT JUNGE, MANFRED KUHR, AND HANS MUSSO. **% bf Bond Character of β -Diketone Metal Chelates.** *Angewandte Chemie International Edition*, **10**:225, 1971.
- [42] MARK S. GORDON AND ROBERT D. KOOB. **An INDO Investigation of the Structure and Bonding of Acetylacetone and Trifluoroacetylacetone.** *Journal of the American Chemical Society*, **95**:5863, 1973.
- [43] DELANO P. CHONG AND CHING-HAN HU. **Density-functional calculation of the inner-shell spectra for two stable enol tautomers: acetylacetone and malonaldehyde.** *Journal of Electron Spectroscopy and Related Phenomena*, **94**:181, 1998.
- [44] J. J. DANNENBERG AND RAPHAEL RIOS. **Theoretical Study of the Enolic Forms of Acetylacetone. How Strong Is the H-Bond?** *The Journal of Physical Chemistry*, **98**:6714, 1994.
- [45] TATEKI ISHIDA, FUMIO HIRATA, AND SHIGEKI KATO. **Thermodynamic analysis of the solvent effect on tautomerization of acetylacetone: An ab initio approach.** *The Journal of Chemical Physics*, **110**:3938, 1999.
- [46] S. L. WALLEN, C. R. YONKER, C. L. PHELPS, AND C. M. WAI. **Effect of Fluorine substitution, pressure and temperature on the tautomeric equilibria of acetylacetonate β -diketones.** *Journal of the Chemical Society, Faraday Transactions*, **93**:2391, 1997.
- [47] J. POWLING AND H. J. BERNSTEIN. **The Effect of Solvents on Tautomeric Equilibria.** *Journal of the American Chemical Society*, **73**:4353, 1951.
- [48] MIN-CHUL YOON, YOUNG S. CHO, AND SANG KYU KIM. **Photodissociation dynamics of acetylacetone: The OH product state distribution.** *Journal of Chemical Physics*, **110**:11850, 1999.
- [49] MIN-CHUL YOON, YOUNG S. CHOI, AND SANG KYU KIM. **The OH production from the π - π^* transition of acetylacetone.** *Chemical Physics Letters*, **300**:207, 1999.

- [50] A. TRIVELLA, T. N. WASSERMANN, J. M. MESTDAGH, C. MANCA TANNER, F. MARINELLI, P. ROUBIN, AND S. COUSSAN. **New insights into the photodynamics of acetylacetone: isomerization and fragmentation in low-temperature matrices.** *Physical Chemistry Chemical Physics*, **12**:8300, 2010.
- [51] MICHAEL M. FOKENDT, BORIS E. WEISS-LOPEZ, J. PAUL CBAUVEL, JR., AND NANCY S. TRUE. **Gas-Phase ^1H NMR Studies of Keto-Enol Tautomerism of Acetylacetone, Methyl Acetoacetate, and Ethyl Acetoacetate.** *The Journal of Physical Chemistry*, **89**:3347, 1985.
- [52] MINORU TANAKA, TOSHIYUKI SHONO, AND KOICHIRO SHINRA. **Tautomerism in 3-Substituted-2,4-pentanediones and Their Copper Chelates.** *Bulletin of the Chemical Society of Japan*, **42**:3190, 1969.
- [53] R. J. IRVING AND I. WADSSÖ. **Enthalpy of Vaporization of Organic Compounds at 25°C . V. Acetylacetone.** *Acta Chemica Scandinavica*, **24**:589, 1970.
- [54] ARMIN SCHWEIG, HANS VERMEER, AND ULRICH WEIDNER. **A photoelectron spectroscopic study of keto-enol tautomerism in acetylacetones - a new application of photoelectron spectroscopy.** *Chemical Physics Letters*, **26**:229, 1974.
- [55] S. H. BAUER AND C. F. WILCOX. **On malonaldehyde and acetylacetone: are theory and experiment compatible?** *Chemical Physics Letters*, **279**:122, 1997.
- [56] V. V. SLIZNEV, S. B. LAPSHINA, AND G. V. GIRICHEV. **AB Initio study of the structure of enolic and ketonic forms of β -Diketones with the general formula $\text{R}''\text{COCH}_2\text{COR}'$ (R' AND $\text{R}'' = \text{H, CH}_3, \text{CF}_3$).** *Journal of Structural Chemistry*, **47**:220, 2006.
- [57] A. TRIVELLA, P. ROUBIN, P. THEULE, M. RAJZMANN, AND S. COUSSAN. **UV and IR Photoisomerization of Acetylacetone Trapped in a Nitrogen Matrix.** *The Journal of Physical Chemistry A*, **111**:3074, 2007.
- [58] NAKO NAGASHIMA, SATOSHI KUDOH, MASAO TAKAYANAGI, AND MUNETAKA NAKATA. **UV-Induced Photoisomerization of Acetylacetone and Identification of Less-Stable Isomers by Low-Temperature Matrix-Isolation Infrared Spectroscopy and Density Functional Theory Calculation.** *The Journal of Physical Chemistry A*, **105**:10832, 2001.
- [59] THOMAS STEINER. **The Hydrogen Bond in the Solid State.** *Angewandte Chemie International Edition*, **41**:48, 2002.
- [60] CHARLES L. PERRIN AND JENNIFER B. NIELSON. **"Strong" Hydrogen bonds in Chemistry and Biology.** *Annual Review of Physical Chemistry*, **48**:511, 1997.
- [61] PAOLA GILLI, VALERIO BERTOLASI, VALERIA FERRETTI, AND GASTONE GILLI. **Covalent Nature of the Strong Homonuclear Hydrogen Bond. Study of the O-H—O System by Crystal Structure Correlation Methods.** *Journal of the American Chemical Society*, **116**:909, 1994.
- [62] STEVE SCHEINER. **Theoretical Studies of Proton Transfers.** *Accounts of Chemical Research*, **18**:174, 1985.
- [63] STACY A. BROADBENT, LORI A. BURNS, CHANDRIMA CHATTERJEE, AND PATRICK H. VACCARO. **Investigation of electronic structure and proton transfer in ground state acetylacetone.** *Chemical Physics Letters*, **434**:31, 2007.
- [64] WALTHER CAMINATI AND JENS-UWE GRABOW. **The C_{2v} Structure of Enolic Acetylacetone.** *Journal of the American Chemical Society*, **128**:511, 2006.
- [65] YUNG-CHING CHOU. **Group-theoretical investigation of the tunneling splitting patterns of enolic acetylacetone.** *Journal of Molecular Spectroscopy*, **263**:34, 2010.
- [66] SHOUJUN XU, SANG TAE PARK, JONATHAN S. FEENSTRA, RAMESH SRINIVASAN, AND AHMED H. ZEWAIL. **Ultrafast Electron Diffraction: Structural Dynamics of the Elimination Reaction of Acetylacetone.** *The Journal of Physical Chemistry A*, **108**:6650, 2004.
- [67] LIONEL POISSON, PASCALE ROUBIN, STEPHANE COUSSAN, BENOÎT SOEP, AND JEAN-MICHEL MESTDAGH. **Ultrafast Dynamics of Acetylacetone (2,4-Pentanedione) in the S_2 State.** *Journal of the American Chemical Society*, **130**:2974, 2008.
- [68] J. M. CHALMERS AND P. R. GRIFFITHS, editors. *Handbook of Vibrational Spectroscopy*, **1**. Jhon Wiley & Sons Ltd, 2002.
- [69] JOHN F. W. HERSHEL. **On the Chemical Action of the Rays of the Solar Spectrum on Preparations of Silver and Other Substances, Both Metallic and Non-Metallic, and on Some Photographic Processes.** *Philosophical Transactions of the Royal Society of London*, **130**:1, 1840.
- [70] W. ABNEY AND E. R. FESTING. **On the Influence of the Atomic Grouping in the Molecules of Organic Bodies on Their Absorption in the Infra-Red Region of the Spectrum.** *Philosophical Transactions of the Royal Society of London*, **172**:887, 1881.
- [71] J. MICHAEL HOLLAS. *Modern Spectroscopy*. Jhon Wile & Sons, Lts, fourth edition edition, 2004.
- [72] PETER ATKINS AND JULIO DE PAULA. *Atkins' Physical Chemistry*. W. H. Freeman and Company, Oxford New York, eighth edition edition, 2006.
- [73] GERHARD HERZBERG. *Molecular Spectra and Molecular Structure*. D. Van Nostrand Company, Inc, New Jersey, seventh printing edition, 1956.
- [74] PETER FELLGETT. **I. - les principes généraux des méthodes nouvelles en spectroscopie interférentielle - A propos de la théorie du spectromètre interférentiel multiplex.** *Journal de Physique et Le Radium*, **19**:187, 1958.
- [75] W. W. COBLENTZ. **Infra-red absorption spectra: I. Gases.** *The Physical Review*, **20**:273, 1905.
- [76] P. JACQUINOT. **Caractères communs aux nouvelles méthodes de spectroscopie interférentielle ; Facteur de mérite.** *Journal de Physique et Le Radium*, **19**:223, 1958.
- [77] J. KAUPPINEN AND J. PARTANEN. *Fourier Transforms in Spectroscopy*. Wiley-VCH Verlag GmbH, 2001.

REFERENCES

- [78] JUSTINAS ČEPONKUS AND BENGT NELANDER. **Water Dimer in Solid Neon. Far-Infrared Spectrum.** *The Journal of Physical Chemistry A*, **108**:6499, 2004.
- [79] **Encyclopedia of spectroscopy and spectrometry.** 2000.
- [80] BEAT MEYER. *Low Temperature Spectroscopy.* American Elsevier Publishing Company, Inc, New York, 1971.
- [81] Y. HAAS AND U. SAMUNI. **Reactions in Rare Gas Matrices – Matrix and site Effects.** *Progress in Reaction Kinetics*, **23**:211, 1998.
- [82] BERNHARD SCHRADER, editor. *Infrared and Raman Spectroscopy.* VCH Verlagsgesellschaft mbH, 1995.
- [83] D. HALLAMASEK, E. BABKA, AND E. KNÖZINGER. **How inert is an argon matrix?** *Journal of Molecular Structure*, **408/409**:125, 1997.
- [84] DENNIS P. STROMMEN, DIETER M. GRUEN, AND ROBERT L. MCBETH. **Vibrational spectra of water isolated in deuterium matrices.** *The Journal of Chemical Physics*, **59**:4028, 1973.
- [85] MITCHIO OKUMURA, MAN-CHOR CHAN, AND TAKESHI OKA. **High-Resolution Infrared Spectroscopy of Solid Hydrogen: The Tetrahexacontapole-Induced $\Delta J=6$ Transitions.** *Physical Review Letters*, **62**:32, 1989.
- [86] TAKESHI OKA. **High-resolution spectroscopy of solid hydrogen.** *Annual Review of Physical Chemistry*, **44**:299, 1993.
- [87] L. H. NOSANOW. **Theory of Quantum Crystals.** *Physical Review*, **146**:120, 1966.
- [88] TAM SIMON AND MARIO E. FAJARDO. **Ortho/para hydrogen converter for rapid deposition matrix isolation spectroscopy.** *Review of Scientific Instruments*, **70**:1926, 1999.
- [89] SIMON TAM AND MARIO E. FAJARDO. **Single and Double Infrared Transitions in Rapid-Vapor-Deposited Parahydrogen Solids: Application to Sample Thickness Determination and Quantitative Infrared Absorption Spectroscopy.** *Applied Spectroscopy*, **55**(12), 2001.
- [90] ROBERT J. HINDE, DAVID T. ANDERSON, SIMON TAM, AND MARIO E. FAJARDO. **Probing quantum solvation with infrared spectroscopy: infrared activity induced in solid parahydrogen by N₂ and Ar dopants.** *Chemical Physics Letters*, **356**:355, 2002.
- [91] H. P. GUSH, V. F. J. HARE, E. J. ALLIN, AND H. L. WELSH. **The infrared fundamental band of liquid nad solid Hydrogen.** *Canadian Journal of Physics*, **38**:176, 1960.
- [92] J. VAN KRANENDONK. **Induced infra-red absorption in gases: Calculation of the binary absorption coefficients of symmetrical diatomic molecules.** *Physica*, **24**, 1958.
- [93] LESTER ANDREWS AND XUEFENG WANG. **Simple ortho-para hydrogen and para-ortho deuterium converter for matrix isolation spectroscopy.** *Review of Scientific Instruments*, **75**:3039, 2004.
- [94] **The CVD diamond booklet.**
- [95] <http://www.internationalcrystal.net>.
- [96] P. G. CIARLET AND C. LE BRIS, editors. *Handbook of Numerical Analysis*, **X**. ELSEVIER SCIENCE B.V., P.O. Box 211. 1000 AE Amsterdam. The Netherlands, special volume computational chemistry edition, 2003.
- [97] DAVID C. YOUNG. *Computational Chemistry.* Wiley-Interscience, 2001.
- [98] CHRISTOPHER J. CRAMER. *Essentials of Computational Chemistry. Theories and Models.* John Wiley & Sons Ltd, The Atrium, Southern Gate, Chichester, West Sussex PO19 8SQ, England, second edition edition, 2004.
- [99] AXEL D. BECKE. **Densityfunctional thermochemistry. III. The role of exact exchange.** *The Journal of Chemical Physics*, **98**:5648, 1993.
- [100] BRANKO S. JURSIĆ. **Can hybrid DFT methods correctly compute the potential energy surface formic acid dimerization and proton transfer in the formic acid dimer? A comparison of hybrid DFT computed values with experimental and C1, G2, and G2MP2 generated data.** *Journal of Molecular Structure: THEOCHEM*, **417**:89, 1997.
- [101] R. KRISHNAN, M. J. FRISCH, AND J. A. POPLE. **Contribution of triple substitutions to the electron correlation energy in fourth order perturbation theory.** *The Journal of Chemical Physics*, **72**:4244, 1980.
- [102] RICHARD C. RAFFENETTI. **General contraction of Gaussian atomic orbitals: Core, valence, polarization, and diffuse basis sets; Molecular integral evaluation .** *The Journal of Chemical Physics*, **58**:4452, 1973.
- [103] THOM H. DUNNING. **Gaussian basis sets for use in correlated molecular calculations. I. The atoms boron through neon and hydrogen .** *The Journal of Chemical Physics*, **90**:1007, 1989.
- [104] DAVID E. WOON AND THOM H. DUNNING. **Gaussian basis sets for use in correlated molecular calculations. III. The atoms aluminum through argon.** *The Journal of Chemical Physics*, **98**:1358, 1993.
- [105] ANTHONY P. SCOTT AND LEO RADOM. **Harmonic Vibrational Frequencies: An Evaluation of Hartree-Fock, Møller-Plesset, Quadratic Configuration Interaction, Density Functional Theory, and Semiempirical Scale Factors .** *The Journal of Physical Chemistry*, **100**:16502, 1996.
- [106] AURELIEN TRIVELLA. PhD thesis, Université de Provence, Marseille, France, 2007.
- [107] VASSIL B. DELCHEV, HANS MIROSCHE, AND GEORGI ST. NIKOLOV. **The Keto-Enol Equilibrium of Pentane - 2,4-dione Studied by ab initio Methods.** *Monatshefte für Chemie*, **132**:339, 2001.
- [108] I. MATANOVIĆ AND N. DOŠLIĆ. **Anharmonic Vibrational Spectra of Acetylacetone.** *International Journal of Quantum Chemistry*, **106**:1367, 2006.

- [109] GIUSEPPE BUEMI. **Computational note on acetylacetone IR spectrum.** *Journal of Molecular Structure: THEOCHEM*, **808**:167, 2007.
- [110] S.F. TAYYARI AND F. MILANI-NEJAD. **Vibrational assignment of acetylacetone.** *Spectrochimica Acta Part A*, **56**:2679, 2000.
- [111] VLASTA MOHAČEK-GROŠEV, KREŠIMIR FURIĆ, AND HRVOJE IVANKOVIĆ. **Luminescence and Raman Spectra of Acetylacetone at Low Temperatures.** *The Journal of Physical Chemistry A*, **111**:5820, 2007.
- [112] JUSTINAS ČEPONKUS, P. UVDAL, AND B. NELANDER. **Complex Formation of Small Molecules during Isolation in Low Temperature Matrices: Water Dimers in pH₂ and Ne Matrices.** *The Journal of Physical Chemistry A*, **114**:6829, 2010.
- [113] YUAN-PERN LEE, YU-JONG WU, AND JON T. HOUGEN. **Direct spectral evidence of single-axis rotation and ortho-hydrogen-assisted nuclear spin conversion of CH₃F in solid parahydrogen.** *Journal of Chemical Physics*, **129**:104502, 2008.
- [114] ALEXANDRA VIEL, MAURÍCIO D. COUTINHO-NETO, AND UWE MANTHE. **The ground state tunneling splitting and the zero point energy of malonaldehyde: A quantum Monte Carlo determination.** *The Journal of Chemical Physics*, **126**:024308, 2007.
- [115] YUNG-CHING CHOU AND JON T. HOUGEN. **Two-dimensional tunneling Hamiltonian treatment of the microwave spectrum of 2-methylmalonaldehyde.** *The Journal of Chemical Physics*, **124**:074319, 2006.
- [116] HIROSHI USHIYAMA AND KAZUO TAKATSUKA. **Methyl Group Rotation Driven by Proton Transfer through a Long-Range Chemical Interaction**.** *Angewandte Chemie International Edition*, **44**:1273, 2005.
- [117] VADIM V. ILYUSHIN, EMILY A. CLOESSNER, YUNG-CHING CHOU, AND LAURA B. PICRAUX. **A microwave study of hydrogen-transfer-triggered methyl-group rotation in 5-methyltropolone.** *The Journal of Chemical Physics*, **133**:184307, 2010.
- [118] A.J. HORSEWILL. **Quantum tunnelling aspects of methyl group rotation studied by NMR.** *Progress in Nuclear Magnetic Resonance Spectroscopy*, **35**:359, 1999.
- [119] IVANA MATANOVIĆ, NADJA DOŠLIĆ, AND ZLATKO MIHALIĆ. **Exploring the potential energy surface for proton transfer in acetylacetone.** *Chemical Physics*, **306**:201, 2004.
- [120] I. MATANOVIĆ AND N. DOŠLIĆ. **Infrared Spectroscopy of the Intramolecular Hydrogen Bond in Acetylacetone: A Computational Approach.** *Journal of Physical Chemistry A*, **109**:4185, 2005.
- [121] W. G. FATELEY AND FOIL A. MILLER. **Torsional frequencies in the far infrared-1. Molecules with a single methyl rotor.** *Spectrochimica Acta*, **172**:857, 1961.
- [122] M. R. JOHNSON, N. H. JONES, A. GEIS, A. J. HORSEWILL, AND H. P. TROMMSDORFF. **Structure and dynamics of the keto and enol forms of acetylacetone in the solid state.** *Journal of Chemical Physics*, **116**:5694, 2002.
- [123] V. V. SLIZNEV, S. B. LAPSHINA, AND G. V. GIRICHEV. **Ab initio Structure investigation of the enol forms of β -Diketones RCOCH₂COR (R = H, CH₃, CF₃).** *Journal of Structural Chemistry*, **43**:47, 2002.
- [124] DUDLEY R. HERSCHBACH. **Tables of Mathieu Integrals for the Internal Rotation Problem.** *The Journal of Chemical Physics*, **27**:975, 1957.
- [125] DUDLEY R. HERSCHBACH. **Calculation of Energy Levels for Internal Torsion and Over-All Rotation. III*.** *The Journal of Chemical Physics*, **31**:91, 1959.
- [126] YIMIN WANG, BASTIAAN J. BRAAMS, JOEL M. BOWMAN, STUART CARTER, AND DAVID P. TEW. **Full-dimensional quantum calculations of ground-state tunneling splitting of malonaldehyde using an accurate ab initio potential energy surface.** *The Journal of Chemical Physics*, **128**:224314, 2008.
- [127] A. TRIVELLA, S. COUSSAN, T. CHIAVASSA, P. THEULÉ, P. ROUBIN, AND C. MANCA. **Comparative study of structure and photo-induced reactivity of malonaldehyde and acetylacetone isolated in nitrogen matrices.** *Low Temperature Physics*, **32**:1042, 2006.
- [128] T. N. WASSERMANN, D. LUCKHAUS, S. COUSSAN, AND M. A. SUHM. **Proton tunneling estimates for malonaldehyde vibrations from supersonic jet and matrix quenching experiments.** *Physical Chemistry Chemical Physics*, **80**:2344, 2006.
- [129] T. CHIAVASSA, P. VERLAQUE, L. PIZZALA, AND P. ROUBIN. **Vibrational studies of methyl derivatives of malonaldehyde: Determination of a reliable force field for β -dicarbonyl compounds.** *Spectrochimica Acta Part A*, **50**:343, 1994.
- [130] J.P. PERCHARD. **The torsion-vibration spectrum of methanol trapped in neon matrix.** *Chemical Physics*, **332**:86, 2007.
- [131] M. PETTERSSON, E. M. S. MAÇOAS, L. KHRIACHTCHEV, J. LUNDELL, R. FAUSTO, AND M. RÄSÄNEN. **Cis \rightarrow trans conversion of formic acid by dissipative tunneling in solid rare gases: Influence of environment on the tunneling rate.** *Journal of Chemical Physics*, **117**:9095, 2002.
- [132] MARIO E. FAJARDO, C. MICHAEL LINDSAY, AND TAKAMASA MOMOSE. **Crystal field theory analysis of rovibrational spectra of carbon monoxide monomers isolated in solid parahydrogen.** *The Journal of Chemical Physics*, **130**:244508, 2009.
- [133] GALINA M. CHABAN AND R. BENNY GERBER. **Anharmonic vibrational spectroscopy calculations with electronic structure potentials: comparison of MP2 and DFT for organic molecules.** *Theoretical Chemistry Account*, **120**:273, 2008.
- [134] JAMES A. HARRISON AND HEINZ FREI. **Visible Light-Induced Oxygen Transfer from Nitrogen Dioxide to Ethyne and Propyne in a Cryogenic Matrix. 1. Identification of Products.** *Journal of Physical Chemistry*, **98**:12142, 1994.

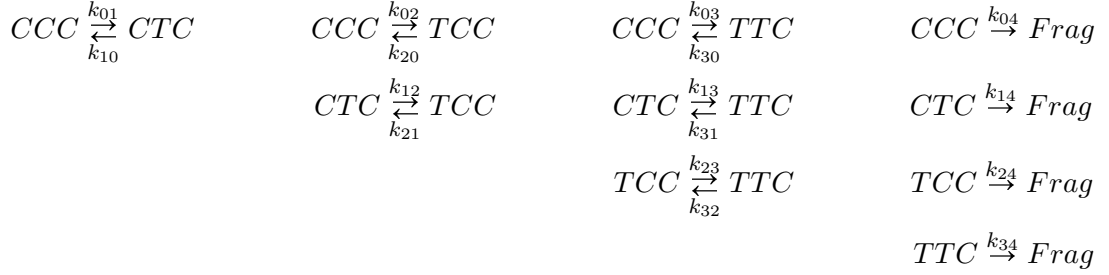
REFERENCES

- [135] ERIC L. WOODBRIDGE, T. RICK FLETCHER, AND STEPHEN R. LEONE. **Photofragmentation of Acetone at 193 nm: Rotational- and Vibrational-State Distributions of the CO Fragment by Time-Resolved FTIR Emission Spectroscopy**. *Journal of Physical Chemistry*, **92**:5387, 1988.
- [136] MATTHEW G. K. THOMPSON, MATTHEW R. WHITE, BRYAN D. LINFORD, KAITLYNN A. KING, MARK M. ROBINSON, AND J. MARK PARNIS. **Fourier transform infrared matrix-isolation analysis of acetaldehyde fragmentation products after charge exchange with Ar⁺ under varied ionization density conditions**. *Journal of Mass Spectrometry*, **46**:1071, 2011.
- [137] <http://webbook.nist.gov>.
- [138] DOLPHUS E. MILLIGAN AND MARILYN E. JACOX. **Matrix-Isolation Study of the Infrared and Ultraviolet Spectra of the Free Radical HCO. The Hydrocarbon Flame Bands**. *Journal of Chemical Physics*, **51**:277, 1969.
- [139] J. MARK PARNIS, KAITLYNN A. KING, AND MATTHEW G. K. THOMPSON. **The chemistry of ionized Acetone/Ar mixtures under varying gas flow and mole ratio conditions: A matrix-isolation study**. *Journal of Mass Spectrometry*, **44**:652, 2009.
- [140] MIZUHO FUSHITANI, TAKAMASA MOMOSE, AND TADAMASA SHIDA. **The $^2P_{1/2} \leftarrow ^2P_{3/2}$ transition of the iodine atom photoproduced from alkyl iodides in solid parahydrogen: detection of new absorptions**. *Chemical Physics Letters*, **356**:375, 2002.
- [141] TAKAMASA MOMOSE, MASAOKI MIKI, TOMONARI WAKABAYASHI, AND TADAMASA SHIDA. **Infrared spectroscopic study of rovibrational states of methane trapped in parahydrogen crystal**. *Journal of Chemical Physics*, **107**:7707, 1997.
- [142] HIROMICHI HOSHINA, MIZUHO FUSHITANI, AND TAKAMASA MOMOSE. **Tunneling chemical reactions in solid parahydrogen: Direct measurement of the rate constants of $R+H_2 \rightarrow RH+H$ ($R=CD_3, CD_2H, CDH_2, CH_3$) at 5 K**. *Journal of Chemical Physics*, **120**:3706, 2004.
- [143] TAKAMASA MOMOSE, HIROMICHI HOSHINA, MIZUHO FUSHITANI, AND HIROYUKI KATSUKI. **High-resolution spectroscopy and the analysis of ro-vibrational transitions of molecules in solid parahydrogen**. *Vibrational Spectroscopy*, **34**:95, 2004.
- [144] TAKAMASA MOMOSE, HIROMICHI HOSHINA, NORIHITO SOGOSHI, HIROYUKI KATSUKI, AND TOMONARI WAKABAYASHI. **Tunneling chemical reactions in solid parahydrogen: A case of $CD_3+H_2 \rightarrow CD_3H+H$ at 5 K**. *Journal of Chemical Physics*, **108**:7334, 1998.
- [145] HIROYUKI KATSUKI AND TAKAMASA MOMOSE. **Observation of Rovibrational Dephasing of Molecules in Parahydrogen Crystals by Frequency Domain Spectroscopy**. *Physical Review Letters*, **84**:3286, 2000.
- [146] TAKAYUKI KUMADA, MASAHIRO SAKAKIBARA, TOSHIMITSU NAGASAKA, HIROYUKI FUKUTA, JUN KUMAGAI, AND TETSUO MIYAZAKI. **Absence of recombination of neighboring H atoms in highly purified solid parahydrogen: Electron spin resonance, electron-nuclear double resonance, and electron spin echo studies**. *Journal of Chemical Physics*, **116**:1109, 2002.
- [147] KANEKAZU SEKI AND HIDEO OKABE. **Photodissociation of Methylacetylene at 193 nm**. *The Journal of Physical Chemistry*, **96**:3345, 1992.
- [148] YING-CHI LEE, V. VENKATESAN, YUAN-PERN LEE, P. MACKO, K. DIDIRICHE, AND M. HERMAN. **Infrared spectra of C₂H₂ under jet-cooled and para-H₂ matrix conditions**. *Chemical Physics Letters*, **435**:247, 2007.
- [149] HIROMICHI HOSHINA, YOSHIYASU KATO, YUSUKE MORISAWA, TOMONARI WAKABAYASHI, AND TAKAMASA MOMOSE. **UV and IR absorption spectra of C₃ embedded in solid para-hydrogen**. *Chemical Physics*, **300**:69, 2004.
- [150] KANEKAZU SEKI AND HIDEO OKABE. **Photochemistry of Acetylene at 193.3 nm**. *Journal of Physical Chemistry*, **97**:5284, 1993.
- [151] YU-JONG WU, XUEMING YANG, AND YUAN-PERN LEE. **Infrared matrix-isolation spectroscopy using pulsed deposition of p-H₂**. *Journal of Chemical Physics*, **120**:1168, 2004.
- [152] P. D. LIGHTFOOT, S. P. KIRWAN, AND M. J. PILLING. **Photolysis of Acetone at 193.3 nm**. *Journal of Physical Chemistry*, **92**:4938, 1988.
- [153] MASAOKI MIKI, TOMONARI WAKABAYASHI, TAKAMASA MOMOSE, AND TADAMASA SHIDA. **Infrared Spectroscopic Studies of Carbon Clusters Trapped in Solid Parahydrogen**. *Journal of Physical Chemistry*, **100**:12135, 1996.
- [154] G. P. GLASS, S. S. KUMARAN, AND J. V. MICHAEL. **Photolysis of Ketene at 193 nm and the Rate Constant for H + HCCO at 297 K**. *Journal of Physical Chemistry A*, **104**:8360, 2000.

Appendix A

Isomerization Kinetics

From the infrared spectra, four isomers of Acetylacetone (AcAc) and fragments are detected. The isomers are the CCC, CTC, TCC and TTC. Considering all possible combinations the reaction schema will be as follow:



The analytic equations for the kinetics as a result of the previews diagram can be written as:

$$\begin{aligned}
 \frac{dC_0}{dt} &= -(k_{01} + k_{02} + k_{03})C_0 + k_{10}C_1 + k_{20}C_2 + k_{30}C_3 \\
 \frac{dC_1}{dt} &= k_{01}C_0 - (k_{10} + k_{12} + k_{13} + k_{14})C_1 + k_{21}C_2 + k_{31}C_3 \\
 \frac{dC_2}{dt} &= k_{02}C_0 + k_{12}C_1 - (k_{20} + k_{21} + k_{23} + k_{24})C_2 + k_{32}C_3 \\
 \frac{dC_3}{dt} &= k_{03}C_0 + k_{13}C_1 + k_{23}C_2 - (k_{30} + k_{31} + k_{32} + k_{34})C_3 \\
 \frac{dC_4}{dt} &= k_{04}C_0 + k_{14}C_1 + k_{24}C_2 + k_{34}C_3 \\
 C_{t=0} &= C_0 + C_1 + C_2 + C_3 + C_4
 \end{aligned} \tag{A.1}$$

Where

$C_0(t)$ is the concentration of the CCC isomer of AcAc

$C_1(t)$ is the concentration of the CTC isomer of AcAc

A. ISOMERIZATION KINETICS

$C_2(t)$ is the concentration of the TCC isomer of AcAc

$C_3(t)$ is the concentration of the TTC isomer of AcAc

$C_4(t)$ is the concentration of fragments

and

$C_{t=0}$ is the initial concentration of CCC isomer, i.e $C_{t=0} = C_0(t = 0)$.

The system of equations can be written in a matrix notation as:

$$\frac{d}{dt} \begin{pmatrix} C_0 \\ C_1 \\ C_2 \\ C_3 \\ C_4 \end{pmatrix} = \begin{pmatrix} -(k_{01} + k_{02} + k_{03}) & k_{10} & k_{20} & k_{30} & \\ k_{01} & -(k_{10} + k_{12} + k_{13} + k_{14}) & k_{21} & k_{31} & \\ k_{02} & k_{12} & -(k_{20} + k_{21} + k_{23} + k_{24}) & k_{32} & \\ k_{03} & k_{13} & k_{23} & -(k_{30} + k_{31} + k_{32} + k_{34}) & \\ k_{04} & k_{14} & k_{24} & k_{34} & \end{pmatrix} \begin{pmatrix} C_0 \\ C_1 \\ C_2 \\ C_3 \\ C_4 \end{pmatrix}$$

The solution of this differential equation system is not too easy. Only a system with two linearly independent equations has analytic solution. Then, approximation have to be done.

A.1 Approximations

Figure A.1 display a temporal behavior of the normalized integrated absorbance of characteristic bands of each isomer. CCC is represented with black squares, CTC with red circles, TCC with green triangles upward and TTC with blue diamonds. Intensities of the open isomers are measured on specific bands at 1705 cm^{-1} (CTC), 1126 cm^{-1} (TCC), 1229 cm^{-1} (TTC), and from the whole spectrum for CCC.

From the graphic is visible that the kinetics of the TTC isomer is very close to the TCC compared with CCC and CTC isomers. Thus, the first approximation is consider the relation between $C_2(t)$ and $C_3(t)$ as follow:

$$C_2(t) = \beta C_3(t) \quad (\text{A.2})$$

where β is an arbitrary constant. This assumption eliminates one equation from the system A.1. Another important approximation is the fact that the fragmentation when the sample is irradiated with UV (266 nm) is negligible. If fragmentation is avoided $C_4(t) = 0$ and all coefficients $k_{i4} \sim 0$. The final system of equations is thus:

$$\begin{aligned} \frac{dC_0}{dt} &= -(k_{01} + k_{02})C_0 + k_{10}C_1 + k_{20}C_2 \\ \frac{dC_1}{dt} &= k_{01}C_0 + (k_{10} + k_{12})C_1 + k_{21}C_2 \end{aligned} \quad (\text{A.3})$$

$$\begin{aligned} \frac{dC_2}{dt} &= k_{02}C_0 + k_{12}C_1 - (k_{20} + k_{21})C_2 \\ C_{t=0} &= C_0(t) + C_1(t) + C_2(t) \end{aligned} \quad (\text{A.4})$$

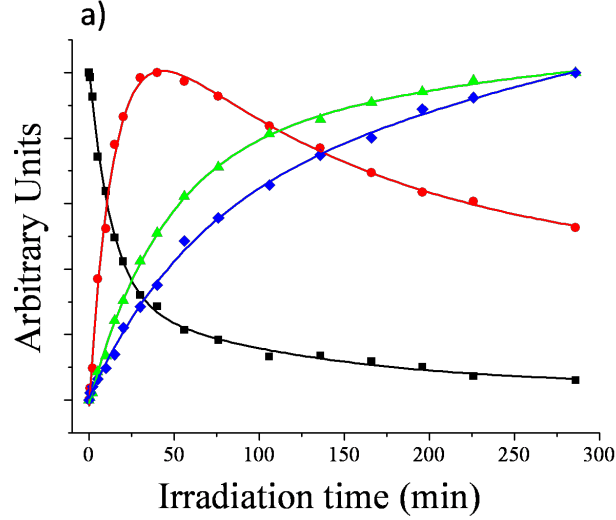


Figure A.1: Time evolution of the normalized intensities of the four enol isomers of AcAc observed in parahydrogen: CCC (black squares), CTC (red circles), TCC (green triangles upward) and TTC (blue diamonds). Intensities of the open isomers are measured on specific bands at 1705 cm^{-1} (CTC), 1126 cm^{-1} (TCC), 1229 cm^{-1} (TTC), and from the whole spectrum for CCC.

The only way that equation A.4 is valid is if C_2 is now the sum of the concentration of TCC and TTC isomers of AcAc.

The system A.3 and A.4 is a problem with three unknown variables and fourth equations. So, one of them is not independent. By using linking equation A.4, C_2 can be eliminated. The linearly independent equation system is:

$$\frac{d}{dt} \begin{pmatrix} C_0 \\ C_1 \end{pmatrix} = \begin{pmatrix} -(k_{01} + k_{02} + k_{20}) & (k_{10} - k_{20}) \\ (k_{01} - k_{21}) & -(k_{12} + k_{10} + k_{21}) \end{pmatrix} \begin{pmatrix} C_0 \\ C_1 \end{pmatrix} + \begin{pmatrix} k_{20} \\ k_{21} \end{pmatrix} C_{t=0} \quad (\text{A.5})$$

The system of differential equations A.5 is inhomogeneous and the solutions are the general solutions of the homogeneous problem plus a particular solution of the inhomogeneous problem.

A.2 Homogeneous problem:

$$\frac{d}{dt} \begin{pmatrix} C_0 \\ C_1 \end{pmatrix} - \begin{pmatrix} -(k_{01} + k_{02} + k_{20}) & (k_{10} - k_{20}) \\ (k_{01} - k_{21}) & -(k_{12} + k_{10} + k_{21}) \end{pmatrix} \begin{pmatrix} C_0 \\ C_1 \end{pmatrix} = 0 \quad (\text{A.6})$$

Which has the solution:

$$C_0(t) = A'_1 e^{-\alpha_1 t} + A'_2 e^{-\alpha_2 t} \quad (\text{A.7})$$

$$C_1(t) = B'_1 e^{-\alpha_1 t} + B'_2 e^{-\alpha_2 t} \quad (\text{A.8})$$

A. ISOMERIZATION KINETICS

With

$$\alpha_{12} = \frac{-(D_1 + D_2) \pm \sqrt{(D_1 - D_2)^2 + 4D_3D_4}}{2} \quad (\text{A.9})$$

and

$$D_1 = k_{01} + k_{02} + k_{20}$$

$$D_2 = k_{12} + k_{10} + k_{21}$$

$$D_3 = k_{10} - k_{20}$$

$$D_4 = k_{01} - k_{21}$$

A.3 Solution of inhomogeneous equation

It is proposed as particular solution of the inhomogeneous problem:

$$C_0 = A'_3$$

$$C_1 = B'_3$$

The values of A'_3 and B'_3 can be obtained by substitution in the system of differential equations A.5.

$$\frac{d}{dt} \begin{pmatrix} A'_3 \\ B'_3 \end{pmatrix} = \begin{pmatrix} -(k_{01} + k_{02} + k_{20}) & (k_{10} - k_{20}) \\ (k_{01} - k_{21}) & -(k_{12} + k_{10} + k_{21}) \end{pmatrix} \begin{pmatrix} A'_3 \\ B'_3 \end{pmatrix} + \begin{pmatrix} k_{20} \\ k_{21} \end{pmatrix} C_{t=0} \quad (\text{A.10})$$

Then the final system to solves is:

$$\begin{pmatrix} -D_1 & D_3 \\ D_4 & -D_2 \end{pmatrix} \begin{pmatrix} A'_3 \\ B'_3 \end{pmatrix} + \begin{pmatrix} k_{20} \\ k_{21} \end{pmatrix} C_{(t=0)} = 0$$

Which has the solution:

$$A'_3 = \frac{C_{t=0}(D_2k_{20} + D_3k_{21})}{D_3D_4 - D_1D_2}$$

$$B'_3 = \frac{C_{t=0}(D_4k_{20} + D_1k_{21})}{D_3D_4 - D_1D_2}$$

Then the solution of the differentials equations system A.5 is:

$$C_0(t) = A'_1 e^{-\alpha_1 t} + A'_2 e^{-\alpha_2 t} + A'_3 \quad (\text{A.11})$$

$$C_1(t) = B'_1 e^{-\alpha_1 t} + B'_2 e^{-\alpha_2 t} + B'_3 \quad (\text{A.12})$$

From the system of equations A.3 and A.4, eliminating the C_1 instead C_2 and following the same ideas $C_2(t)$ can be calculated. The resulting solution for the concentration of C_i is:

$$\begin{aligned}
 C_0(t) &= A'_1 e^{-\alpha_1 t} + A'_2 e^{-\alpha_2 t} + \frac{C_{t=0}(D_2 k_{20} + D_3 k_{21})}{D_3 D_4 - D_1 D_2} \\
 C_1(t) &= B'_1 e^{-\alpha_1 t} + B'_2 e^{-\alpha_2 t} + \frac{C_{t=0}(D_4 k_{20} + D_1 k_{21})}{D_3 D_4 - D_1 D_2} \\
 C_2(t) &= E'_1 e^{-\alpha_1 t} + E'_2 e^{-\alpha_2 t} + \frac{C_{t=0}(k_{02} k_{10} + (k_{01} + k_{02}) k_{12})}{D_3 D_4 - D_1 D_2}
 \end{aligned} \tag{A.13}$$

It is possible to obtain the values of k_{ij} by using equation A.13 and th experimental data related to the evolution of each isomer's concentration. From the infrared spectra the integrated absorbance can be calculated. Thus, using the Beer-Lambert's law is possible to write the equations A.13 in terms of absolute absorbance. Beer-Lambert's law said:

$$A_b(t) = \varepsilon l C(t) \tag{A.14}$$

Where ε is the absorbance factor and l is the length of the sample. Equations A.13 can be written as:

$$\begin{aligned}
 A_{b0}(t) &= A_1 e^{-\alpha_1 t} + A_2 e^{-\alpha_2 t} + A_3 = A_1 e^{-\alpha_1 t} + A_2 e^{-\alpha_2 t} + \frac{A_{b(t=0)}(D_2 k_{20} + D_3 k_{21})}{D_3 D_4 - D_1 D_2} \\
 A_{b1}(t) &= B_1 e^{-\alpha_1 t} + B_2 e^{-\alpha_2 t} + B_3 = B_1 e^{-\alpha_1 t} + B_2 e^{-\alpha_2 t} + \frac{A_{b(t=0)}(D_4 k_{20} + D_1 k_{21})}{D_3 D_4 - D_1 D_2} \\
 A_{b2}(t) &= E_1 e^{-\alpha_1 t} + E_2 e^{-\alpha_2 t} + E_3 = E_1 e^{-\alpha_1 t} + E_2 e^{-\alpha_2 t} + \frac{A_{b(t=0)}(k_{02} k_{10} + (k_{01} + k_{02}) k_{12})}{D_3 D_4 - D_1 D_2}
 \end{aligned} \tag{A.15}$$

Where

$$\begin{aligned}
 A_i &= \varepsilon l A'_i \\
 B_i &= \varepsilon l B'_i \\
 E_i &= \varepsilon l E'_i \\
 A_{b(t=0)} &= \varepsilon l C_{t=0}
 \end{aligned}$$

Experimental integrated absorbance are listed in table A.1 for each isomer. Values for integrated absorbance of the open isomers are measured on specific bands at 1705 cm^{-1} CTC, 1126 cm^{-1} TCC, 1229 cm^{-1} TTC, and from the whole spectrum for CCC. The values for CCC are normalized to one.

The values of the corresponding A_{bi} are plotted in the graphic A.2. There is represented A_{b0} with black squares, A_{b1} with red circles and A_{b2} with blue triangles. Solid lines represent the fitting of equations A.15 to the experimental values. From the fitting all parameter of equations A.15 can be estimated. Fitting parameters are summarized in table A.2. The fitting was done using Levenberg–Marquardt algorithm which is implemented in OriginPro 8 SR0 professional software. For

A. ISOMERIZATION KINETICS

Time (min)	CCC A_{b0}	CTC A_{b1}	TCC	TTC	TCC+TTC A_{b2}
0	1,000	0,000	0,000	0,000	0,000
0.5	0,986	0,057	0,006	0,005	0,011
2	0,927	0,155	0,018	0,009	0,028
5	0,742	0,589	0,073	0,014	0,087
10	0,638	0,833	0,115	0,022	0,136
15	0,496	1,245	0,208	0,031	0,239
20	0,423	1,379	0,260	0,049	0,309
30	0,320	1,568	0,363	0,064	0,427
40	0,286	1,594	0,437	0,079	0,515
56	0,213	1,552	0,532	0,109	0,641
76	0,183	1,480	0,608	0,124	0,733
106	0,132	1,334	0,697	0,147	0,843
136	0,135	1,226	0,733	0,167	0,901
166	0,119	1,107	0,778	0,179	0,957
196	0,101	1,013	0,807	0,199	1,005
226	0,073	0,967	0,835	0,207	1,042
286	0,060	0,839	0,856	0,224	1,079

Table A.1: *Integrated absorbance of each isomer detected in the infrared spectra of AcAc in pH_2 matrices during the UV (266 nm) laser irradiation*

making the fitting some constrain were used in order to reproduce the reality of the processes. Those constrains are the result of evaluating the equations A.15 in $t = 0$ and they are:

$$A_1 + A_2 + A_3 = 1$$

$$B_1 + B_2 + B_3 = 0$$

$$E_1 + E_2 + E_3 = 0$$

A.4 First and second derivate

Applying temporal derivative to equation A.5:

$$\frac{d^2 C_0}{dt^2} = \ddot{C}_0 = -(k_{01} + k_{02} + k_{20})\dot{C}_0 + (k_{10} - k_{20})\dot{C}_1$$

then, if it is divided by \dot{C}_0 results:

$$\frac{\ddot{C}_0}{\dot{C}_0} = -(k_{01} + k_{02} + k_{20}) + (k_{10} - k_{20})\frac{\dot{C}_1}{\dot{C}_0}$$

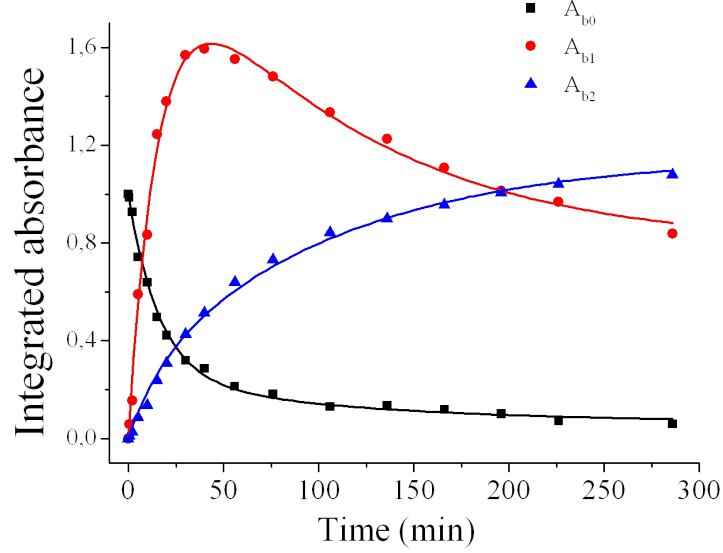


Figure A.2: Time evolution of the integrated absorbance A_{bi} of isomers. Values are listed in table A.1. The A_{b0} is represented with black squares, A_{b1} with red circles and A_{b2} with blue triangles. Solid lines represent the fit of equations A.15 to the experimental values

Equation	$y = A_1 e^{-\frac{x}{\tau_1}} + A_2 e^{-\frac{x}{\tau_2}} + A_3$		
R-Square	0,99583		
	Parameters	Value	Std Error
Common	$\tau_1 = 1/\alpha_1$	105,5442	12,0579
Common	$\tau_2 = 1/\alpha_2$	15,92533	0,79246
A_{b0}	A_1	0,19388	0,04742
	A_2	0,73981	0,03974
	A_3	0,0663	0,02112
A_{b1}	B_1	1,47938	0,08015
	B_2	-2,2625	0,09517
	B_3	0,78312	0,04637
A_{b2}	E_1	-0,92962	0,0425
	E_2	-0,22904	0,04999
	E_3	1,15866	0,0367

Table A.2: Values of the parameters of equations A.15 obtained from the fitting to the experimental values

By doing similar treatment for the second equation of A.5 the results is:

$$\frac{\ddot{C}_1}{\dot{C}_1} = -(k_{12} + k_{10} + k_{21}) + (k_{01} - k_{21}) \frac{\dot{C}_0}{\dot{C}_1}$$

A. ISOMERIZATION KINETICS

Applying the Beer-Lambert's law to the two previous equations is possible to write them in terms of absorbance.

$$\frac{\ddot{A}_{b0}}{\dot{A}_{b0}} = -(k_{01} + k_{02} + k_{03}) + (k_{10} - k_{20}) \frac{\varepsilon_0}{\varepsilon_1} \frac{\dot{A}_{b1}}{\dot{A}_{b0}}$$

$$\frac{\ddot{A}_{b1}}{\dot{A}_{b1}} = -(k_{12} + k_{10} + k_{21}) + (k_{01} - k_{21}) \frac{\varepsilon_1}{\varepsilon_0} \frac{\dot{A}_{b0}}{\dot{A}_{b1}}$$

or

$$\frac{\ddot{A}_{b0}}{\dot{A}_{b0}} = n_0 + m_0 \frac{\dot{A}_{b1}}{\dot{A}_{b0}} \quad (\text{A.16})$$

$$\frac{\ddot{A}_{b1}}{\dot{A}_{b1}} = n_1 + m_1 \frac{\dot{A}_{b0}}{\dot{A}_{b1}} \quad (\text{A.17})$$

Where:

$$n_0 = -(k_{01} + k_{02} + k_{20}) \quad m_0 = (k_{10} - k_{20}) \frac{\varepsilon_0}{\varepsilon_1} \quad (\text{A.18})$$

$$n_1 = -(k_{12} + k_{10} + k_{21}) \quad m_1 = (k_{01} - k_{21}) \frac{\varepsilon_1}{\varepsilon_0} \quad (\text{A.19})$$

and ε_0 and ε_1 are the absorbance coefficients of the CCC and CTC isomers of AcAc respectively.

Equations A.16 and A.17 are strike lines in which m_i and n_i are the slope and the interception respectively. Thus, by plotting $\left(\frac{\ddot{A}_{b0}}{\dot{A}_{b0}} \text{ vs } \frac{\dot{A}_{b1}}{\dot{A}_{b0}}\right)$ and $\left(\frac{\ddot{A}_{b1}}{\dot{A}_{b1}} \text{ vs } \frac{\dot{A}_{b0}}{\dot{A}_{b1}}\right)$, m_i and n_i can be calculated.

In equations A.15 all parameters are known from the fitting and are listed in table A.2. Thus, is possible to calculate the first $\left(\frac{dA_{bi}}{dt} = \dot{A}_{bi}\right)$ and the second $\left(\frac{d^2A_{bi}}{dt^2} = \ddot{A}_{bi}\right)$ order derivate. These equations can be evaluated for different times. The same experimental values of time were used. Figure A.3 display in the left panel the plot of $\left(\frac{\ddot{A}_{b0}}{\dot{A}_{b0}} \text{ vs } \frac{\dot{A}_{b1}}{\dot{A}_{b0}}\right)$ and in the right panel the plot of $\left(\frac{\ddot{A}_{b1}}{\dot{A}_{b1}} \text{ vs } \frac{\dot{A}_{b0}}{\dot{A}_{b1}}\right)$. In both cases, red line represents the fitting to a strike line. Values obtained from the fitting are summarized in table A.3

Equation	$y = a + bx$	
R-Square	0,99999	
Parameter	Value	Std Error
n_0	-0,048	0,004
m_0	0,0050	0,0007
n_1	-0,025	0,002
m_1	0,12	0,01

Table A.3: Values of the parameters of equations A.16 and A.17 obtained from the fitting of the experimental values

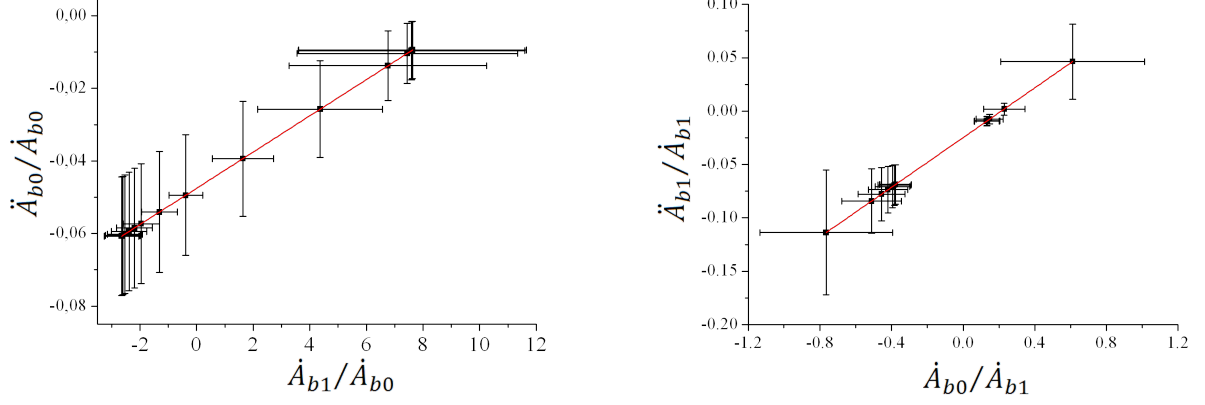


Figure A.3: Left panel plots $\left(\frac{\ddot{A}_{b0}}{\dot{A}_{b0}} \text{ vs } \frac{\dot{A}_{b1}}{\dot{A}_{b0}}\right)$. right panel plots $\left(\frac{\ddot{A}_{b1}}{\dot{A}_{b1}} \text{ vs } \frac{\dot{A}_{b0}}{\dot{A}_{b1}}\right)$. In both cases, red line represent the fitting to a strike line

A.5 Evaluation in (t=0)

From equations A.3, by evaluating the initial instant ($t = 0$), is obtained:

$$\begin{aligned}
\left.\frac{dC_0(t)}{dt}\right|_{t=0} &= -(k_{01} + k_{02})C_{t=0} & \rightarrow & \left.\frac{dA_{b0}(t)}{dt}\right|_{t=0} = -(k_{01} + k_{02})A_{b(t=0)} \\
\left.\frac{dC_1(t)}{dt}\right|_{t=0} &= k_{01}C_{t=0} & \rightarrow & \left.\frac{dA_{b1}(t)}{dt}\right|_{t=0} = k_{01}\frac{\varepsilon_1}{\varepsilon_0}A_{b(t=0)} \\
\left.\frac{dC_2(t)}{dt}\right|_{t=0} &= k_{02}C_{t=0} & \rightarrow & \left.\frac{dA_{b2}(t)}{dt}\right|_{t=0} = k_{02}\frac{\varepsilon_2}{\varepsilon_0}A_{b(t=0)}
\end{aligned} \tag{A.20}$$

From the experimental data and the parameters obtained in the fitting:

$$\begin{aligned}
A_{b(t=0)} &= 1 \\
\left.\frac{dA_{b0}}{dt}\right|_{t=0} &= -A_1\alpha_1 - A_2\alpha_2 \\
\left.\frac{dA_{b1}}{dt}\right|_{t=0} &= -B_1\alpha_1 - B_2\alpha_2 \\
\left.\frac{dA_{b2}}{dt}\right|_{t=0} &= -E_1\alpha_1 - E_2\alpha_2
\end{aligned} \tag{A.21}$$

A.6 Values of the constants rates

From equations A.20 and A.21 values of k_{01} and k_{02} can be obtained:

$$k_{01} = \frac{\varepsilon_0}{\varepsilon_1}(-B_1\alpha_1 - B_2\alpha_2) \tag{A.22}$$

$$k_{02} = \frac{\varepsilon_0}{\varepsilon_2}(-E_1\alpha_1 - E_2\alpha_2) \tag{A.23}$$

A. ISOMERIZATION KINETICS

In order to calculate the values of k_{01} and k_{02} there are needed the values of the relatively absorbance $\left(\frac{\varepsilon_0}{\varepsilon_1}\right)$ and $\left(\frac{\varepsilon_0}{\varepsilon_2}\right)$.

A.6.1 Calculation of relatively absorbance factors

For the calculation of the relatively absorbance factors $\left(\frac{\varepsilon_0}{\varepsilon_1}\right)$ and $\left(\frac{\varepsilon_0}{\varepsilon_2}\right)$ the equation A.4 has to be used. The equation A.4 is written in terms of absorbance with helps of the Beer-Lambert's law as:

$$\frac{A_{b0}(t)}{\varepsilon_0} + \frac{A_{b1}(t)}{\varepsilon_1} + \frac{A_{b2}(t)}{\varepsilon_2} = \frac{A_{b(t=0)}}{\varepsilon_0}$$

or

$$\frac{A_{b1}(t)}{A_{b2}(t)} \frac{\varepsilon_0}{\varepsilon_1} + \frac{\varepsilon_0}{\varepsilon_2} = \frac{(A_{b(t=0)} - A_{b0}(t))}{A_{b2}(t)} \quad (\text{A.24})$$

The equation A.24 is a strike line in which $\left(\frac{\varepsilon_0}{\varepsilon_1}\right)$ is the slope and $\left(\frac{\varepsilon_0}{\varepsilon_2}\right)$ is the interception. Figure A.4 display the plot of $(A_{b(t=0)} - A_{b0}(t))/A_{b2}(t)$ vs $A_{b1}(t)/A_{b2}(t)$. Red lines is constructed by the values obtained from the fitting. Those values are listed in table A.4

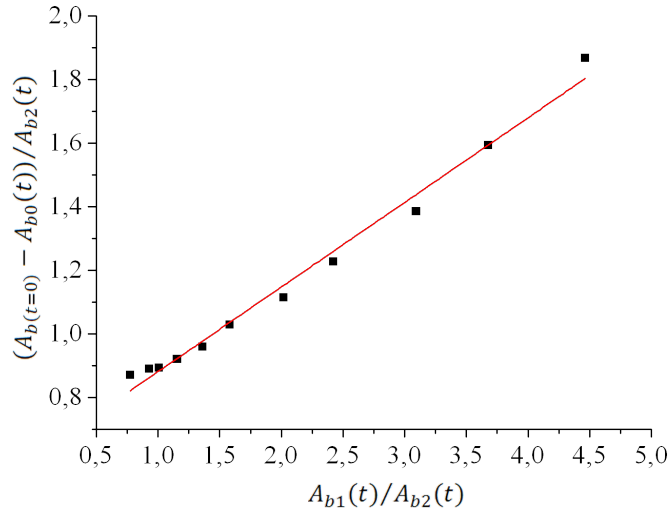


Figure A.4: Plots of $\frac{A_{b(t=0)} - A_{b0}(t)}{A_{b2}(t)}$ vs $\frac{A_{b1}(t)}{A_{b2}(t)}$. Red line represent the linear fitting of the values

With the obtained values of the relatively absorbance coefficients, the values of k_{01} and k_{02} are:

$$k_{01} = 0.034 \pm 0.005$$

$$k_{02} = 0.014 \pm 0.004$$

Equation	$y = a + bx$	
R-Square	0,98666	
Parameter	Value	Std Error
$\varepsilon_0/\varepsilon_2$	0,62	0.02
$\varepsilon_0/\varepsilon_1$	0,27	0.01

Table A.4: Values of the parameter of equations A.24 obtained from the fitting.

From equation A.18 the k_{20} and k_{10} can be expresses as.

$$k_{20} = -n_0 - k_{01} - k_{02}$$

$$k_{10} = \frac{\varepsilon_1}{\varepsilon_0} m_0 + k_{20}$$

Then

$$k_{20} = 0.00 \pm 0.01$$

$$k_{10} = 0.019 \pm 0.003$$

Finally, from equation A.19 the k_{21} and k_{12} rates have the form.

$$k_{21} = -\frac{\varepsilon_0}{\varepsilon_1} m_1 + k_{01} \tag{A.25}$$

$$k_{12} = -n_1 - k_{10} - k_{21} \tag{A.26}$$

Then

$$k_{21} = 0.00 \pm 0.01$$

$$k_{12} = 0.006 \pm 0.005$$

All error estimation for the values of k_{ij} were calculated from the method of linearly propagation of error.

From equations A.9 is easily to prove that:

$$\alpha_1 + \alpha_2 = k_{01} + k_{02} + k_{10} + k_{20} + k_{12} + k_{21}$$

Values of α_i are know from the fitting of the experimental data and all k_{ij} are just calculated. The previews equation can be used to check the calculations of k_{ij} .

$$\alpha_1 + \alpha_2 = 0.072$$

$$k_{01} + k_{02} + k_{10} + k_{20} + k_{12} + k_{21} = 0.073$$

A. ISOMERIZATION KINETICS

Appendix B

Tables of Theoretical frequencies of AcAc isomers

B. TABLES OF THEORETICAL FREQUENCIES OF ACAC ISOMERS

B.1 CCC

B3LYP/6-311++G(3df,3pd)			E=-345.93706437 a.u / $\Delta E=00.00$ kJ/mol		
Frequencies		Harmonic	Frequencies		Harmonic
Anharmonic	Harmonic	IR-Intensities	Anharmonic	Harmonic	IR-Intensities
-185,7870	30,3931	0,0538	1239,9480	1271,1720	141,5690
115,8080	119,4343	1,1710	1298,3010	1376,7281	83,9300
143,9910	149,5212	0,0052	1357,3350	1391,4697	64,3086
175,2290	182,3948	0,0391	1372,0500	1412,3149	12,6980
230,1360	232,4577	3,2901	1421,8560	1459,8300	130,7862
365,8510	373,5889	7,1070	1431,1720	1471,4445	14,2513
403,6060	397,9979	2,5492	1434,5040	1472,4080	9,8111
512,0920	513,3363	11,1711	1429,0590	1477,1836	6,5315
560,7290	559,9480	0,4478	1455,9600	1491,5970	60,7482
635,0850	648,3034	12,6830	1608,6650	1646,1379	268,8783
642,8710	652,4054	0,2844	1624,0400	1677,0457	372,0838
773,8070	794,8151	31,6685	2361,5730	3006,6128	358,3531
910,6080	918,1475	36,6001	2917,9570	3034,2751	5,2959
930,7420	943,9933	2,5451	2928,9470	3038,3369	17,4237
992,1390	1008,5784	64,8943	2965,0630	3087,9692	6,4884
996,4270	1010,5173	14,5123	2947,6680	3090,1677	4,7664
1014,0300	1035,0570	10,2261	3035,3369	3137,9551	9,2169
1022,7750	1047,3709	7,7667	3003,1670	3143,0002	12,1306
1178,2190	1063,4659	1,1090	3094,2681	3211,8044	3,1079
1171,2939	1194,6443	16,1025			

All frequencies are in cm^{-1}

Table B.1: *Chelated enol form of AcAc (CCC)*

B.2 Keto

B3LYP/6-311++G(3df,3pd)			E=-345,92728891 a.u / $\Delta E=25,67$ kJ/mol		
Frequencies		Harmonic	Frequencies		Harmonic
Anharmonic	Harmonic	IR-Intensities	Anharmonic	Harmonic	IR-Intensities
60,2700	47,3461	12,0615	1228,1670	1255,4567	81,9479
62,9880	56,7943	8,5006	1227,6620	1270,1061	21,8040
147,7520	143,3857	1,0309	1356,4440	1390,0172	77,4160
155,8940	161,7937	0,0636	1356,6290	1390,8092	3,9109
157,3690	162,7034	0,0283	1421,9120	1462,4312	4,9376
334,5610	322,7513	0,8439	1422,7240	1466,4388	27,9124
418,9940	411,1195	2,5925	1428,7980	1474,0752	1,1213
485,9730	489,2984	6,2270	1430,6080	1474,2532	14,7089
501,1410	501,9294	1,3502	1453,7490	1481,0276	7,8857
548,0970	552,7948	26,3815	1730,4630	1768,1360	387,2496
619,6310	628,0588	1,5071	1785,7581	1798,0305	20,8327
764,8770	784,6240	0,1465	2923,0659	3030,4192	2,1238
780,3690	797,5135	13,9650	2923,6211	3030,5283	0,6297
885,2460	893,3957	33,3450	2972,9500	3072,7234	2,4159
910,7930	937,9936	1,7998	2948,9399	3086,4902	0,2396
981,7970	1001,0487	1,4517	2948,9951	3086,8296	4,9558
1048,8540	1063,5225	9,1692	2992,3679	3138,9697	5,9206
1057,4320	1080,9716	0,6722	3000,1069	3145,4419	6,3039
1115,9520	1143,0903	1,7670	3000,2690	3145,5532	7,9055
1152,8459	1186,4888	205,1426			

All frequencies are in cm^{-1}

Table B.2: Keto form of AcAc

B. TABLES OF THEORETICAL FREQUENCIES OF ACAC ISOMERS

B.3 CCT

B3LYP/6-311++G(3df,3pd)			E=-345,9125591 a.u / $\Delta E=64,35$ kJ/mol		
Frequencies		Harmonic	Frequencies		Harmonic
Anharmonic	Harmonic	IR-Intensities	Anharmonic	Harmonic	IR-Intensities
54,8300	60,8919	3,5542	1164,0330	1197,2867	83,8016
91,6260	103,8828	0,3091	1265,6370	1304,0601	293,3618
138,1720	141,1909	2,0994	1348,9950	1380,9572	49,5560
175,2500	173,9609	3,6319	1381,3680	1411,4579	0,0846
184,7200	193,2310	1,7104	1392,8110	1426,3279	35,3397
344,3970	341,3431	0,2210	1436,0400	1467,9323	12,9766
374,1470	375,1478	5,0129	1452,1580	1477,5212	9,6403
387,1770	416,3000	80,3639	1450,0730	1481,7794	5,3601
485,3440	485,1507	15,4328	1465,2889	1487,1316	9,9602
536,1050	538,6145	4,8291	1628,2410	1673,0480	420,0835
622,0480	632,8404	12,3373	1723,3220	1759,6108	173,5312
637,3500	647,5701	0,6770	2909,1951	3015,1533	22,6192
805,9810	820,8823	24,6032	2947,1221	3025,7656	5,2169
872,0570	884,6539	76,4848	2921,3660	3061,5581	9,8173
895,8510	914,1853	2,6738	2940,4319	3079,1624	11,0459
973,0000	991,5737	22,7414	2993,9880	3135,4849	6,8486
1018,1770	1036,4556	1,1528	2997,6521	3141,1575	11,7507
1016,3740	1038,7335	5,7475	3058,3059	3188,6582	6,4693
1041,5420	1065,6732	1,5941	3629,6560	3817,5701	78,9629
1159,8010	1189,6936	5,0172			

All frequencies are in cm^{-1}

Table B.3: CCT form of AcAc

B.4 CTC

B3LYP/6-311++G(3df,3pd)			E=-345,91954437 a.u / $\Delta E=46,00$ kJ/mol		
Frequencies		Harmonic	Frequencies		Harmonic
Anharmonic	Harmonic	IR-Intensities	Anharmonic	Harmonic	IR-Intensities
56,5380	58,4995	1,3890	1199,6040	1225,0072	41,5432
83,6740	98,6777	0,1083	1264,7209	1300,4810	30,2538
94,9900	105,2031	1,2604	1347,4740	1383,3910	20,4290
170,0130	171,7149	0,4250	1370,1010	1398,9386	24,8943
226,1360	213,5676	3,2351	1418,6050	1455,4548	6,5902
347,6230	341,5816	1,6816	1421,7500	1461,0062	95,1582
395,8850	396,7696	1,5351	1430,2321	1471,6888	17,8129
486,1340	485,2372	12,4770	1441,9280	1477,9253	8,2796
469,1770	496,3002	79,0214	1440,7870	1492,6666	7,8697
535,2380	545,8206	9,9496	1588,8571	1639,9595	579,9703
593,4830	599,3581	0,2354	1707,4430	1743,3594	167,8945
623,0430	632,2508	40,1318	2920,5359	3027,5332	4,1541
819,3210	838,5285	38,1618	2923,5229	3034,5259	16,1387
831,5010	844,5910	10,3860	2939,6189	3081,1394	5,9926
932,0960	950,1339	70,4646	2938,2471	3081,9214	10,2832
967,0760	987,0562	15,0099	3019,6101	3129,9553	15,2755
1012,5780	1029,5564	60,5183	3002,1140	3143,4866	12,1253
1015,4340	1039,8688	3,8517	3028,6550	3176,6873	6,1081
1043,6470	1071,4312	0,4626	3606,4600	3790,9727	43,7913
1149,3409	1180,7876	214,7170			

All frequencies are in cm^{-1}

Table B.4: CTC form of AcAc

B. TABLES OF THEORETICAL FREQUENCIES OF ACAC ISOMERS

B.5 CTT

B3LYP/6-311++G(3df,3pd)			E=-345,91842524 a.u / $\Delta E=48,94$ kJ/mol		
Frequencies		Harmonic	Frequencies		Harmonic
Anharmonic	Harmonic	IR-Intensities	Anharmonic	Harmonic	IR-Intensities
62,0640	63,0688	8,9584	1199,9570	1228,6885	
80,6500	102,5030	0,0595	1260,5790	1297,7629	147,2867
126,4430	131,2863	0,0908	1350,4170	1383,2052	22,1270
172,1710	174,6216	0,2146	1368,6851	1399,0648	19,5613
218,7980	215,1845	10,7182	1397,5540	1433,3203	36,3608
351,4600	343,9859	2,2635	1416,7540	1461,2455	223,2995
396,9120	397,2985	0,9537	1424,0500	1468,1326	23,4541
382,8140	404,4145	91,1747	1424,4700	1476,9479	9,2608
483,8120	480,6915	5,5176	1450,3250	1501,4672	7,9667
530,0340	531,4257	8,0244	1617,0761	1662,7559	7,0122
594,4080	601,5820	1,2924	1710,8990	1745,4976	403,4922
622,7900	633,5051	38,5520	2913,9390	3011,9241	188,6482
828,9480	840,5267	13,4021	2919,9199	3028,4666	30,9634
853,7050	873,6974	19,7669	2918,0029	3058,5598	3,5284
933,9630	949,4236	104,5527	2939,9231	3082,1145	10,4818
965,1070	982,9104	5,3649	2999,1079	3142,9424	9,0510
1007,5110	1026,3997	11,3359	3019,4851	3159,9380	11,0899
1015,6920	1040,3619	5,0626	3042,4121	3175,2385	10,2594
1044,0990	1071,6987	0,4657	3629,3120	3818,6079	4,7035
1148,0970	1176,7902	138,1901			83,6696

All frequencies are in cm^{-1}

Table B.5: CTT form of AcAc

B.6 TCC

B3LYP/6-311++G(3df,3pd)			E=-345,91687211 a.u / $\Delta E=53,01$ kJ/mol		
Frequencies		Harmonic	Frequencies		Harmonic
Anharmonic	Harmonic	IR-Intensities	Anharmonic	Harmonic	IR-Intensities
63,3270	72,5553	3,4519	1245,5660	1278,9404	123,6128
133,5940	137,8796	0,0758	1282,5940	1319,5291	45,1533
168,5890	181,9178	2,4414	1345,0090	1378,5551	63,5258
207,1690	214,8710	2,9038	1357,0970	1394,8599	49,6154
214,2760	245,8874	1,3712	1394,9180	1427,0061	47,4422
338,5600	344,7877	1,8642	1434,8170	1473,7043	8,2810
386,8720	389,2695	3,6425	1442,2520	1482,8367	25,7181
452,8670	493,6877	67,2540	2095,2771	1488,2715	6,6268
531,0230	534,6439	18,3061	1448,7560	1496,1802	8,8161
537,6780	547,1570	2,0145	1624,2900	1669,1582	389,2644
615,5730	604,3839	2,8633	1684,1150	1718,6899	236,9986
614,4380	630,7970	5,2138	2960,3760	3004,4807	8,9005
782,0860	799,3285	4,9558	2930,4080	3036,0383	11,1513
836,3300	857,4587	16,3777	2924,8330	3063,4783	7,3367
916,0440	937,9924	19,5538	2943,0591	3084,8750	6,3407
977,7880	994,3385	32,4230	2987,2400	3134,5515	5,5323
1015,2970	1036,4304	27,9892	3000,3711	3144,9539	6,9339
1014,0350	1039,9579	5,6413	3063,2859	3196,7786	2,1518
1040,7570	1067,9344	1,7775	3604,8799	3803,7676	86,2020
1116,9010	1145,1309	74,9400			

All frequencies are in cm^{-1}

Table B.6: TCC form of AcAc

B. TABLES OF THEORETICAL FREQUENCIES OF ACAC ISOMERS

B.7 TCT

B3LYP/6-311++G(3df,3pd)			E=-345,91552367 a.u / $\Delta E=56,56$ kJ/mol		
Frequencies		Harmonic	Frequencies		Harmonic
Anharmonic	Harmonic	IR-Intensities	Anharmonic	Harmonic	IR-Intensities
63,3410	67,7082	3,9500	1239,0110	1277,7545	141,3424
142,8570	144,6093	1,6272	1266,7960	1300,8409	172,0013
151,4390	177,8752	0,0144	1342,0601	1380,2817	65,2948
191,3950	198,9084	1,8821	1360,2040	1394,5986	49,6552
196,0140	200,7801	3,8442	1384,1331	1418,5793	27,9940
332,0180	342,6016	0,5240	1421,6050	1462,3381	24,0548
333,5210	365,6584	82,1340	1431,4600	1475,8501	8,3521
379,8620	383,4239	2,5307	1443,7230	1482,0804	8,7803
534,6990	533,5369	8,4934	1444,8440	1483,8416	2,2391
533,3960	536,9488	4,1574	1671,7111	1708,8224	391,3931
589,4790	595,5432	9,7584	1686,6290	1719,6583	111,9231
618,9910	626,5842	0,9562	2918,6421	3013,3430	23,2555
795,3520	809,7593	11,4188	2933,3989	3042,2529	2,8086
843,1500	861,8079	24,3844	2918,3911	3058,7205	10,5684
910,8600	926,4384	55,2731	2958,8650	3100,2185	7,1997
986,7950	1008,3119	41,8656	3002,9089	3138,7930	5,2475
1016,6020	1035,5010	0,5350	2998,3311	3142,4021	12,6751
1026,0620	1047,5944	7,0711	3063,9050	3197,6387	3,0990
1041,0720	1067,3098	1,1340	3644,3210	3832,0676	89,0659
1120,8240	1163,0220	10,6065			

All frequencies are in cm^{-1}

Table B.7: *TCT form of AcAc*

B.8 TTC

B3LYP/6-311++G(3df,3pd)			E=-345,91434552 a.u / $\Delta E=59,65$ kJ/mol		
Frequencies		Harmonic	Frequencies		Harmonic
Anharmonic	Harmonic	IR-Intensities	Anharmonic	Harmonic	IR-Intensities
97,1360	49,9849	3,6625	1225,9000	1253,0153	138,1509
236,5130	76,5689	0,3035	1264,2950	1295,7386	80,8150
179,1540	180,9916	0,8206	1347,9351	1390,0872	34,0124
237,4000	228,2754	6,4240	1375,4860	1401,8932	3,7390
213,7050	228,7874	0,6915	1408,5480	1444,2246	13,3805
323,0030	324,0653	6,1196	1428,8680	1469,2949	3,1329
410,6970	409,5330	10,2628	1413,7729	1473,9679	14,1806
479,4020	497,5201	87,8030	1457,7430	1487,0590	37,9853
528,4110	535,0256	3,1561	1446,2130	1494,5946	1,5637
546,9040	550,0796	1,3228	1634,0380	1673,9281	426,8391
586,2420	586,1603	21,7824	1683,2720	1709,1031	192,0978
575,7930	591,7936	2,0667	2927,9561	3037,2903	5,7073
775,7420	790,1670	1,2759	2938,0229	3043,0034	11,6559
846,2110	881,7214	34,8249	2947,6870	3086,5996	5,3097
885,1600	909,5056	20,4727	2957,6331	3098,0586	7,6110
1008,5190	1018,5452	49,3071	2974,3169	3127,9629	13,2807
1010,3380	1025,2012	1,4664	2990,0359	3140,3306	9,8668
1018,8520	1046,4861	4,9268	3073,0081	3204,2290	2,5837
1040,1810	1065,2487	0,1866	3607,7759	3795,5991	49,9105
1193,1140	1214,0013	220,8652			

All frequencies are in cm^{-1}

Table B.8: *TTC form of AcAc*

B. TABLES OF THEORETICAL FREQUENCIES OF ACAC ISOMERS

B.9 TTT

B3LYP/6-311++G(3df,3pd)			E=-345,91079468 a.u / $\Delta E=68,97$ kJ/mol		
Frequencies		Harmonic	Frequencies		Harmonic
Anharmonic	Harmonic	IR-Intensities	Anharmonic	Harmonic	IR-Intensities
61,5610	48,3901	0,1303	1215,2600	1245,2264	90,2983
139,4570	110,9204	0,3570	1261,6639	1297,3839	70,8465
187,0780	187,3057	0,3252	1354,0240	1387,1570	39,3753
225,8530	230,6444	0,5766	1358,2310	1394,0242	124,9677
237,7970	237,6457	0,0074	1387,4750	1423,7122	59,2167
328,2640	323,1875	6,7435	1429,6479	1470,3082	4,0568
369,8380	350,4089	90,8617	1435,9449	1479,5250	14,6251
409,7580	412,2989	1,6287	1462,0500	1489,9233	14,8163
528,7290	526,9803	4,8495	1460,9960	1500,6356	0,2058
545,8610	546,2071	9,0721	1652,5820	1699,7250	426,7544
585,4760	585,8325	30,5051	1684,2600	1710,6487	94,2188
581,3510	588,3059	4,4793	2945,8469	3017,8005	23,4492
771,0230	784,4895	1,1138	2936,3721	3034,2146	7,4952
884,9260	899,9364	53,8963	2921,6860	3060,0935	8,6629
890,5400	911,9023	19,5086	2960,1340	3094,9343	8,9527
999,9980	1016,9703	4,0336	2997,5291	3138,5813	10,4549
1007,0530	1024,6584	2,3872	3060,2041	3174,7644	1,9437
1023,7950	1045,2855	6,2879	3053,3889	3198,2075	2,0527
1039,3390	1064,7219	0,0474	3648,5090	3830,0129	88,4503
1180,1520	1209,9550	219,5731			

All frequencies are in cm^{-1}

Table B.9: *TTT form of AcAc*

Appendix C

IR spectra of AcAc in pH₂ matrix under UV 193nm irradiation

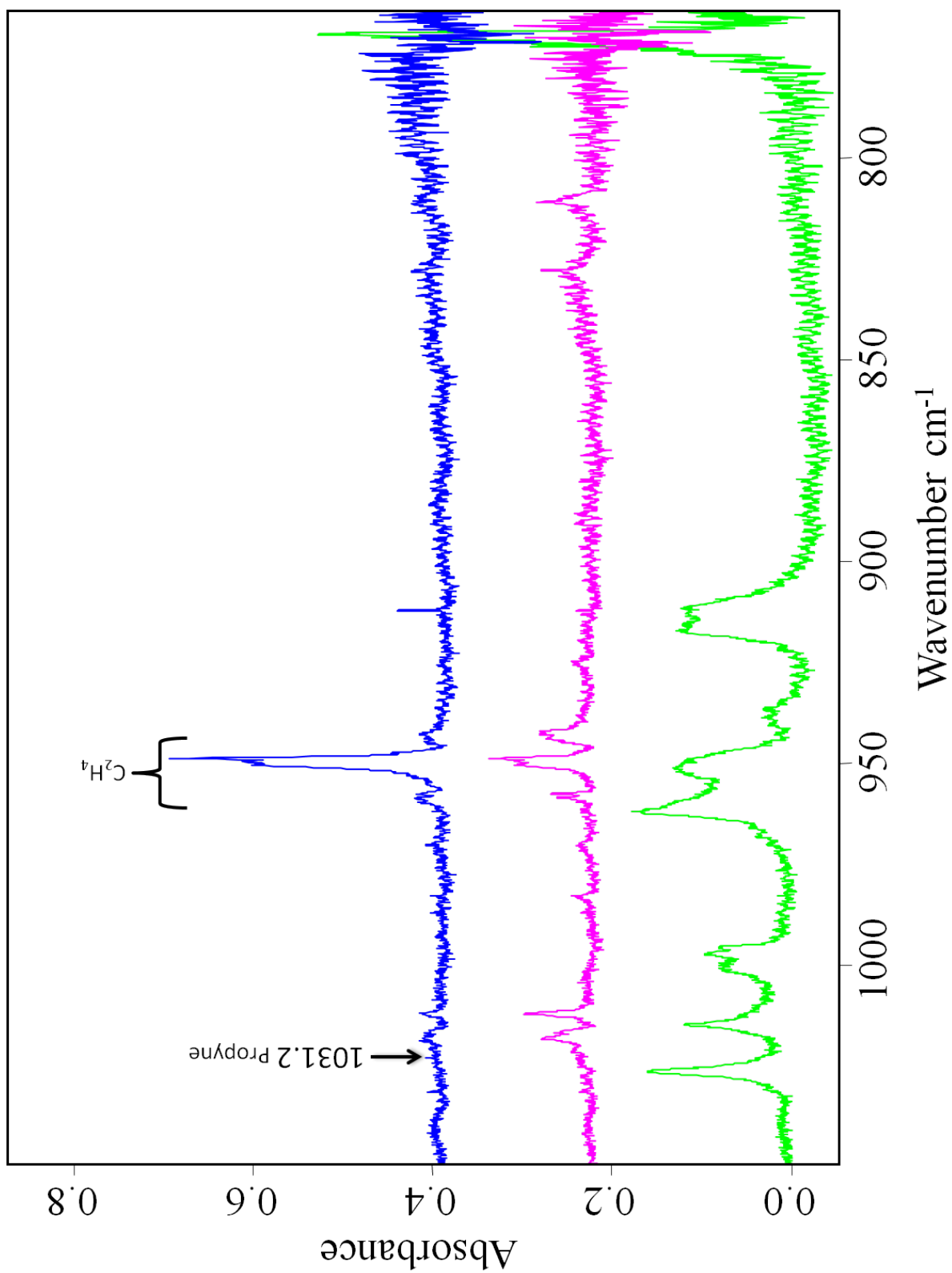
Legend

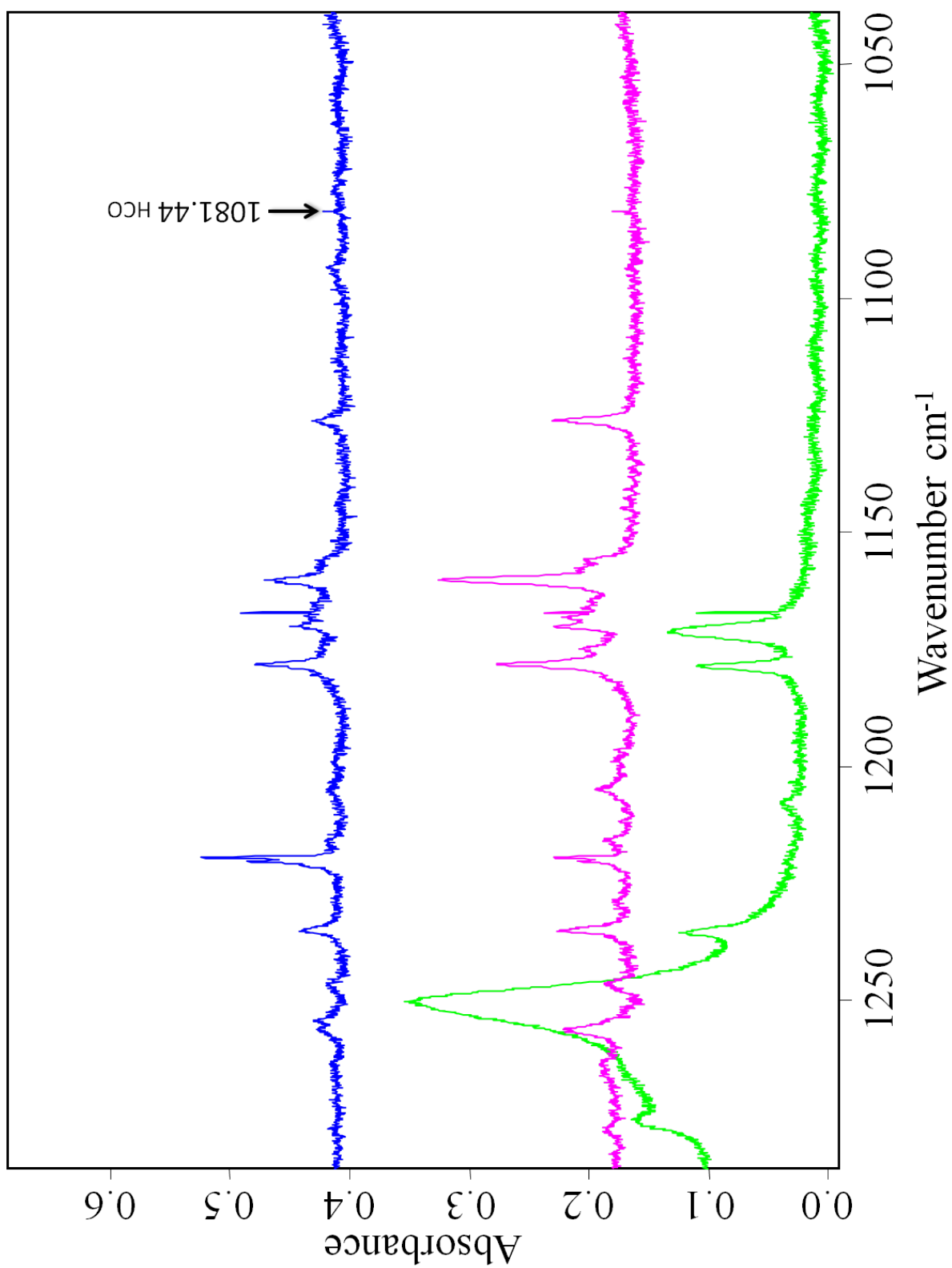
 After 135 min of UV laser irradiation

 After 30 min of UV laser irradiation

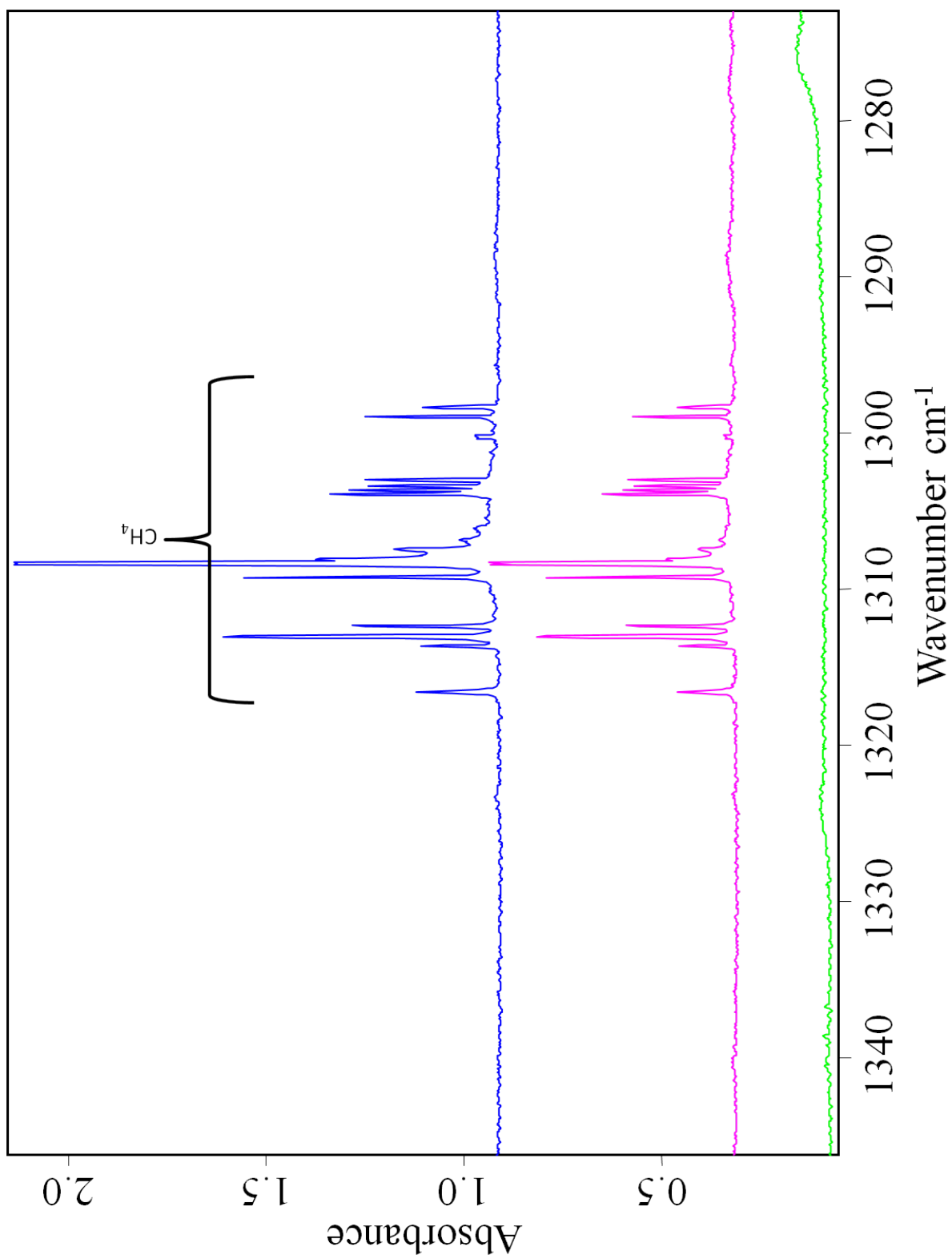
 As deposited Sample

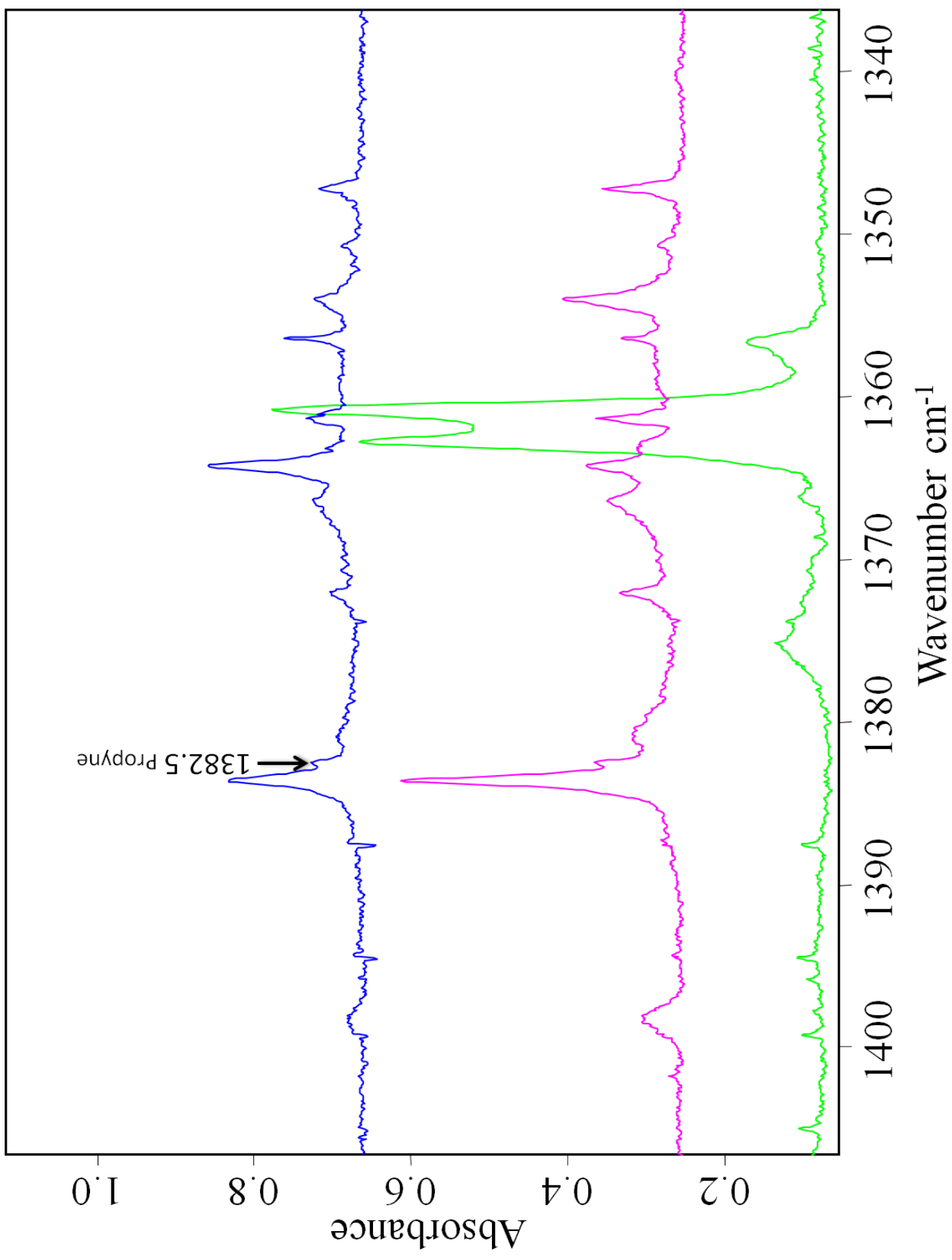
C. IR SPECTRA OF ACAC IN PH₂ MATRIX UNDER UV 193NM IRRADIATION



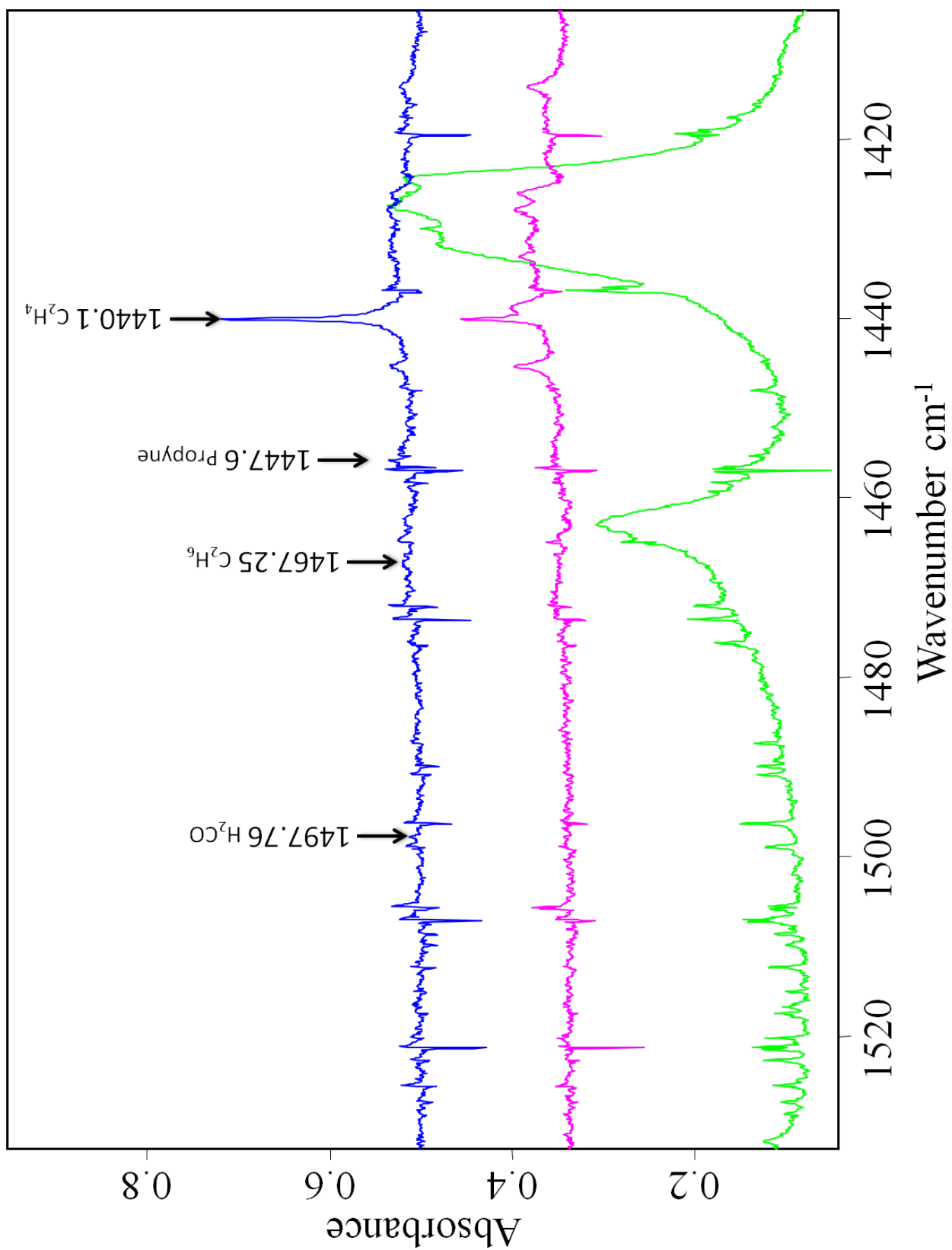


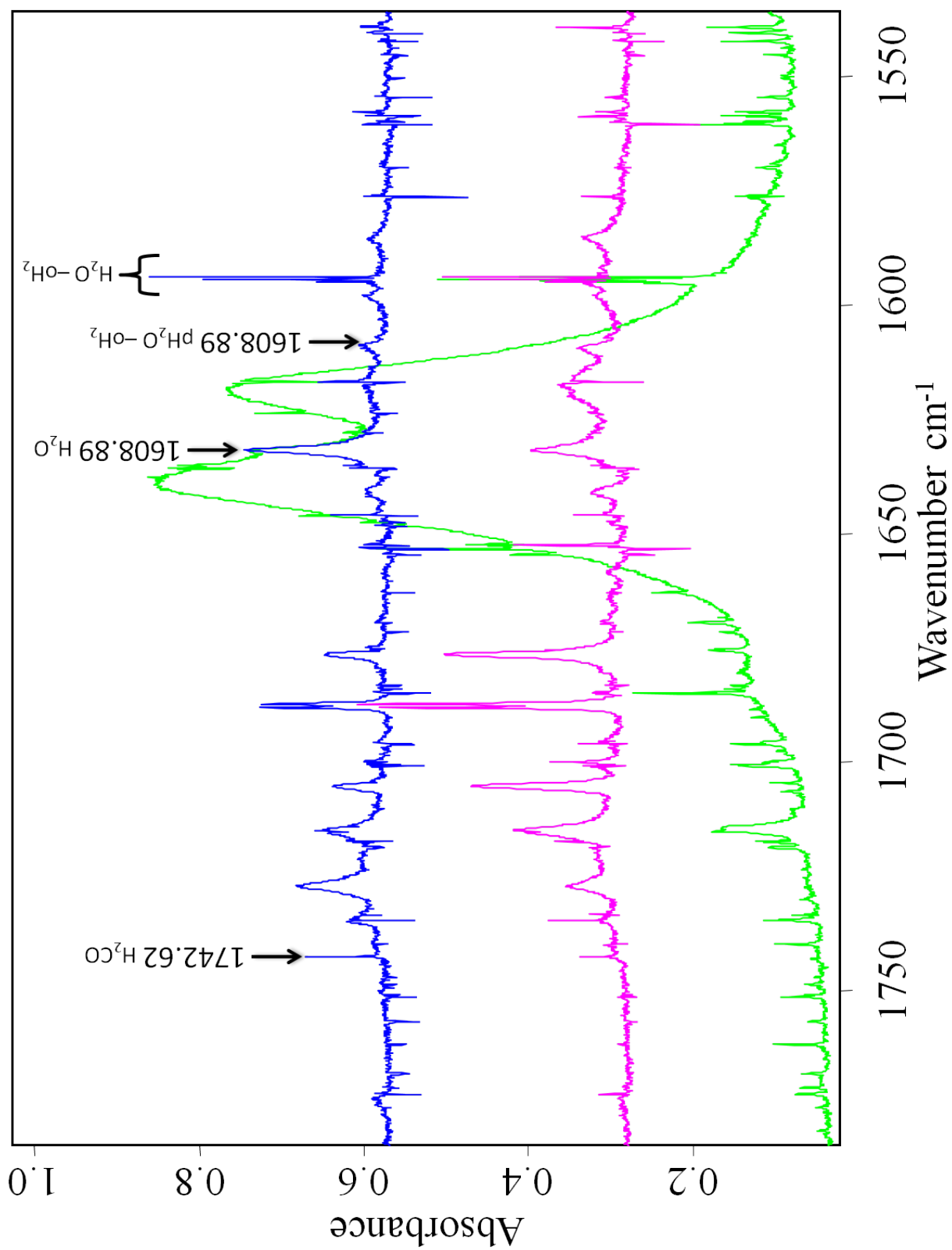
C. IR SPECTRA OF ACAC IN PH₂ MATRIX UNDER UV 193NM IRRADIATION



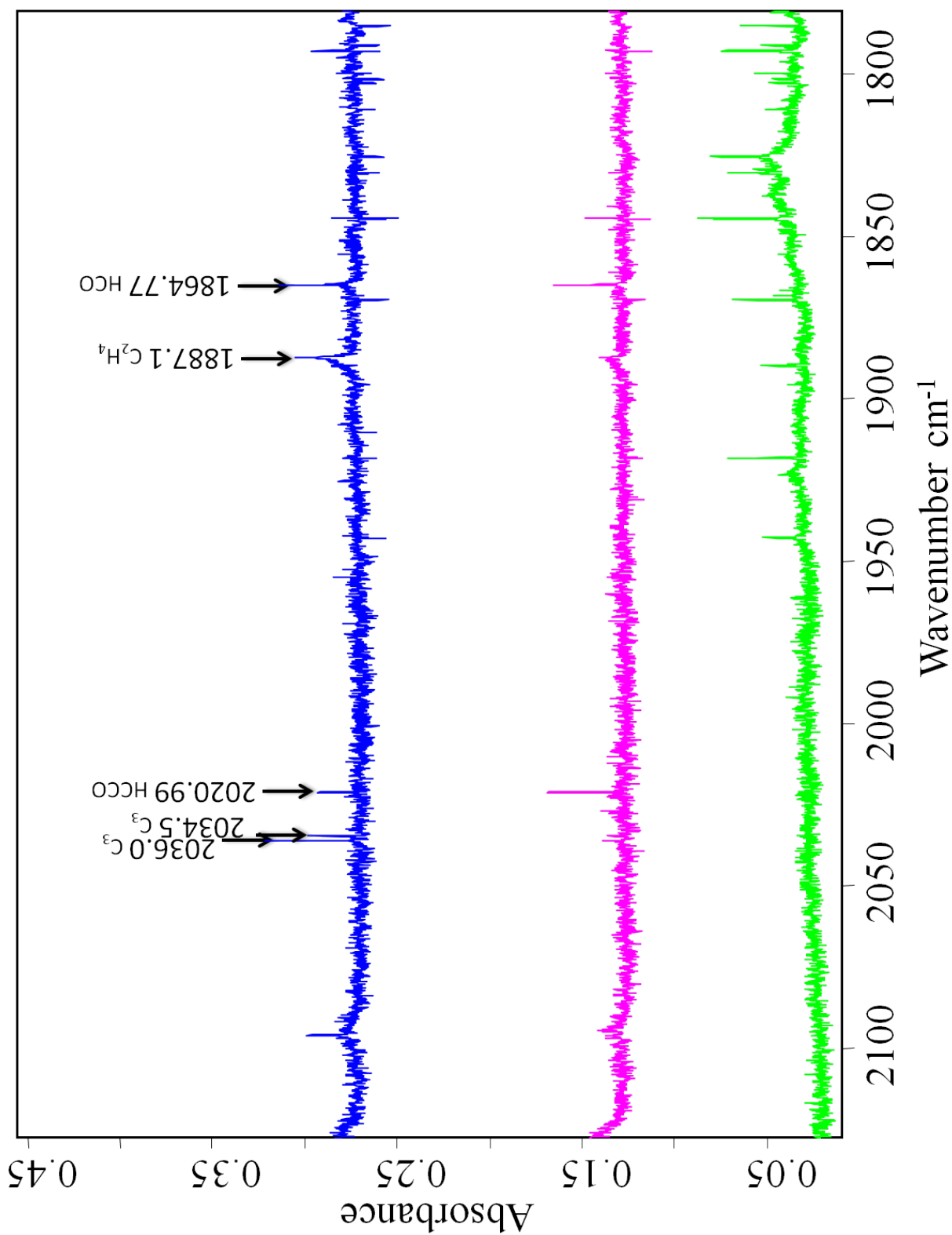


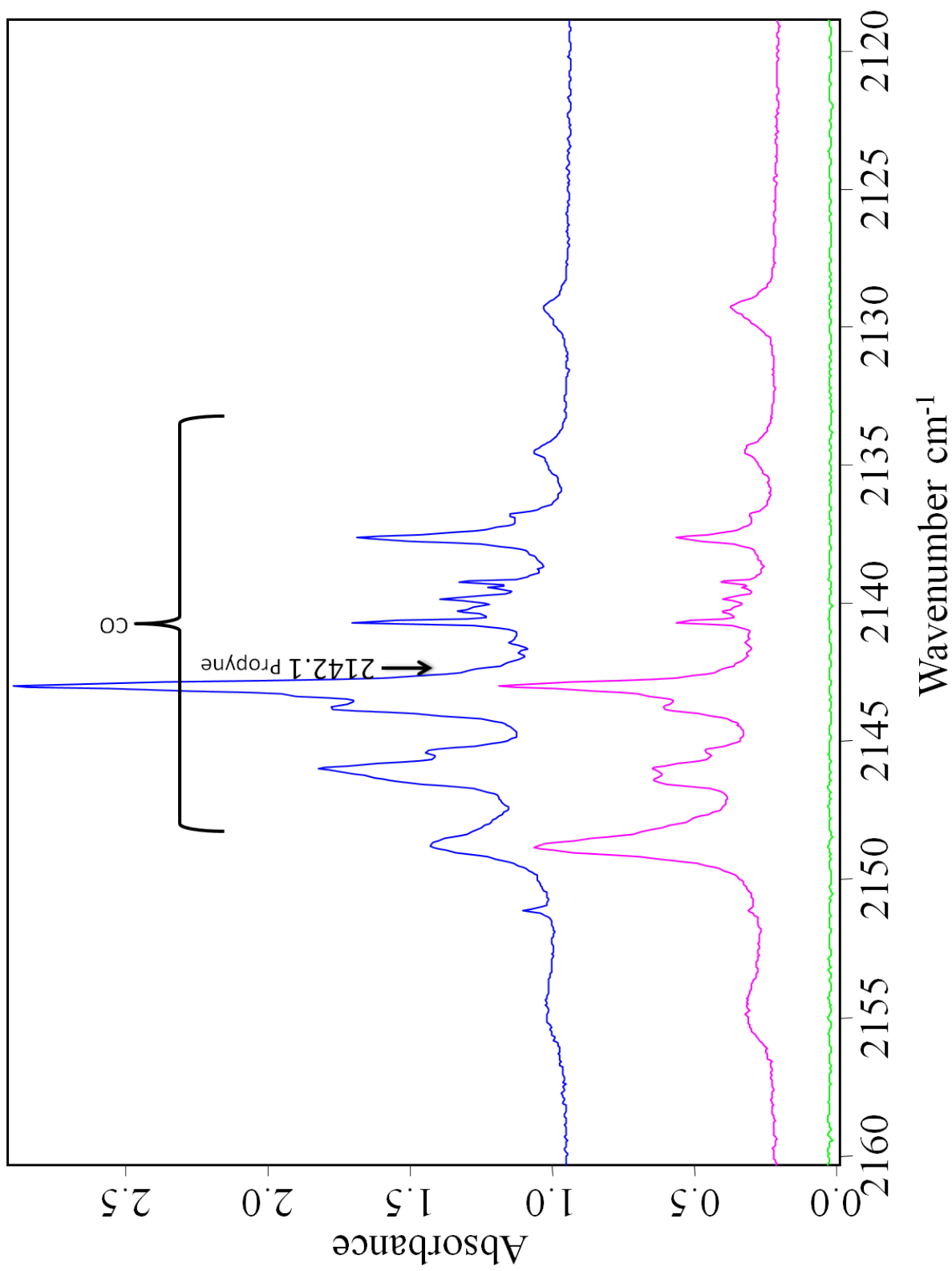
C. IR SPECTRA OF ACAC IN PH₂ MATRIX UNDER UV 193NM IRRADIATION



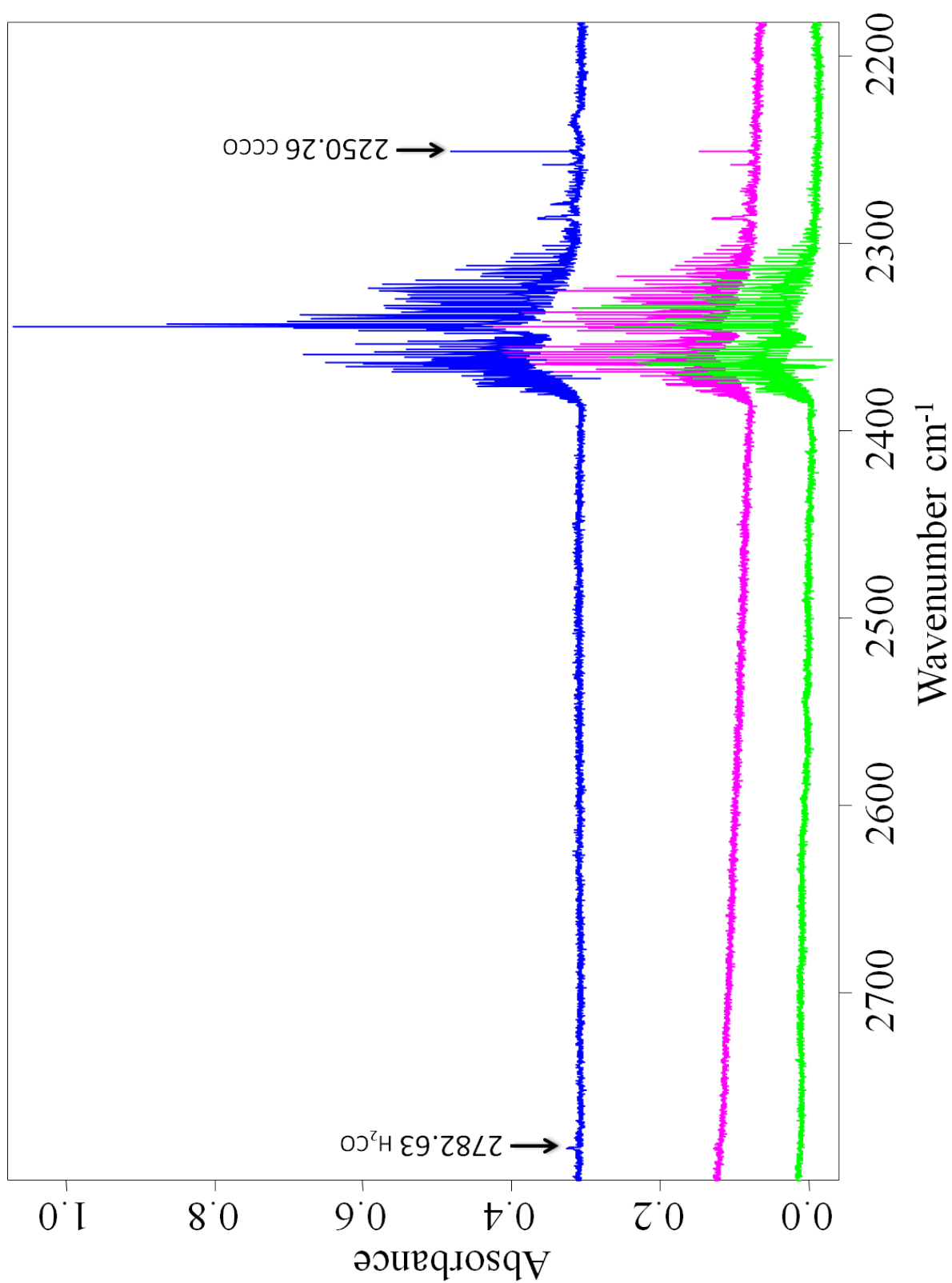


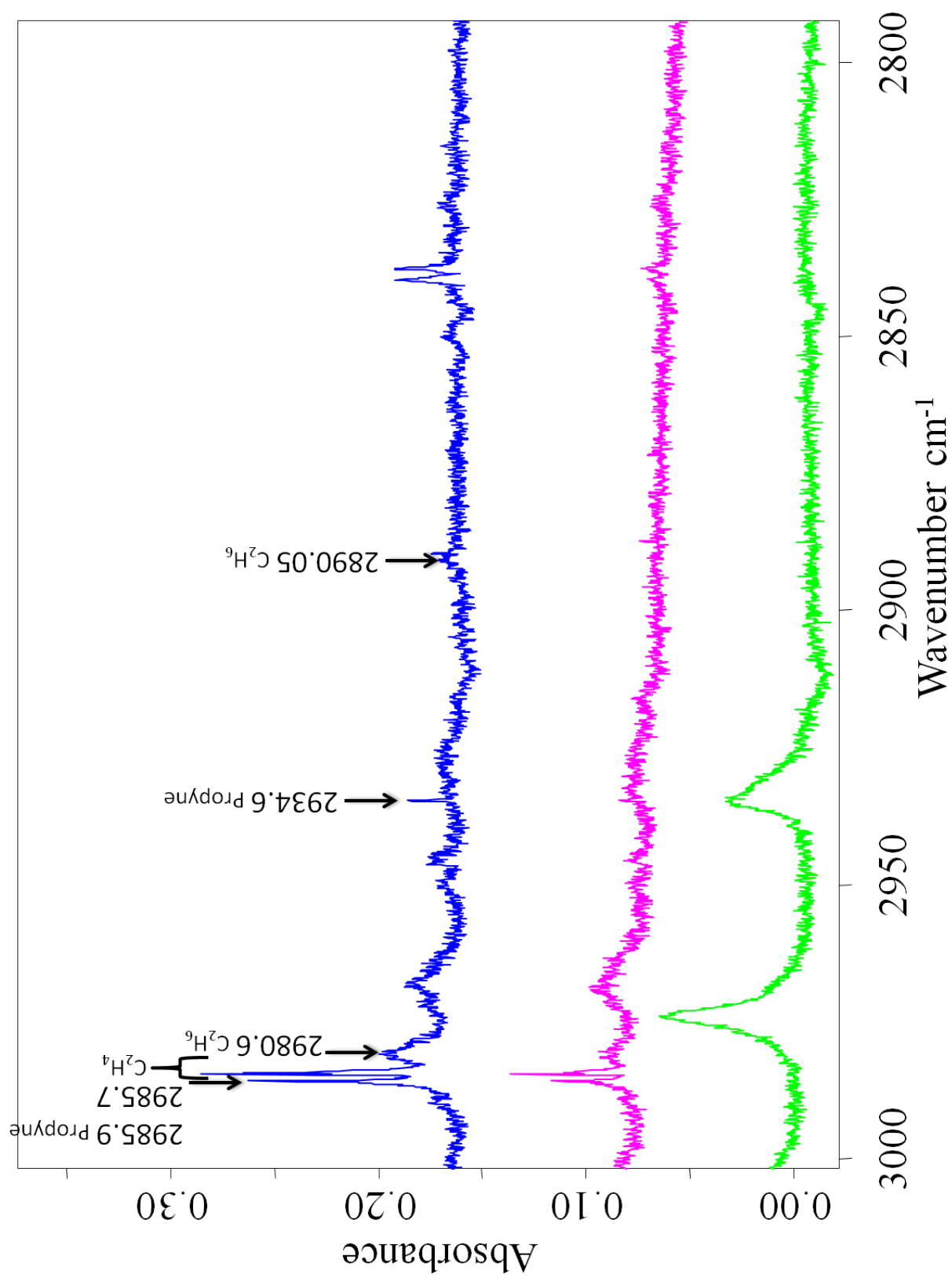
C. IR SPECTRA OF ACAC IN PH₂ MATRIX UNDER UV 193NM IRRADIATION



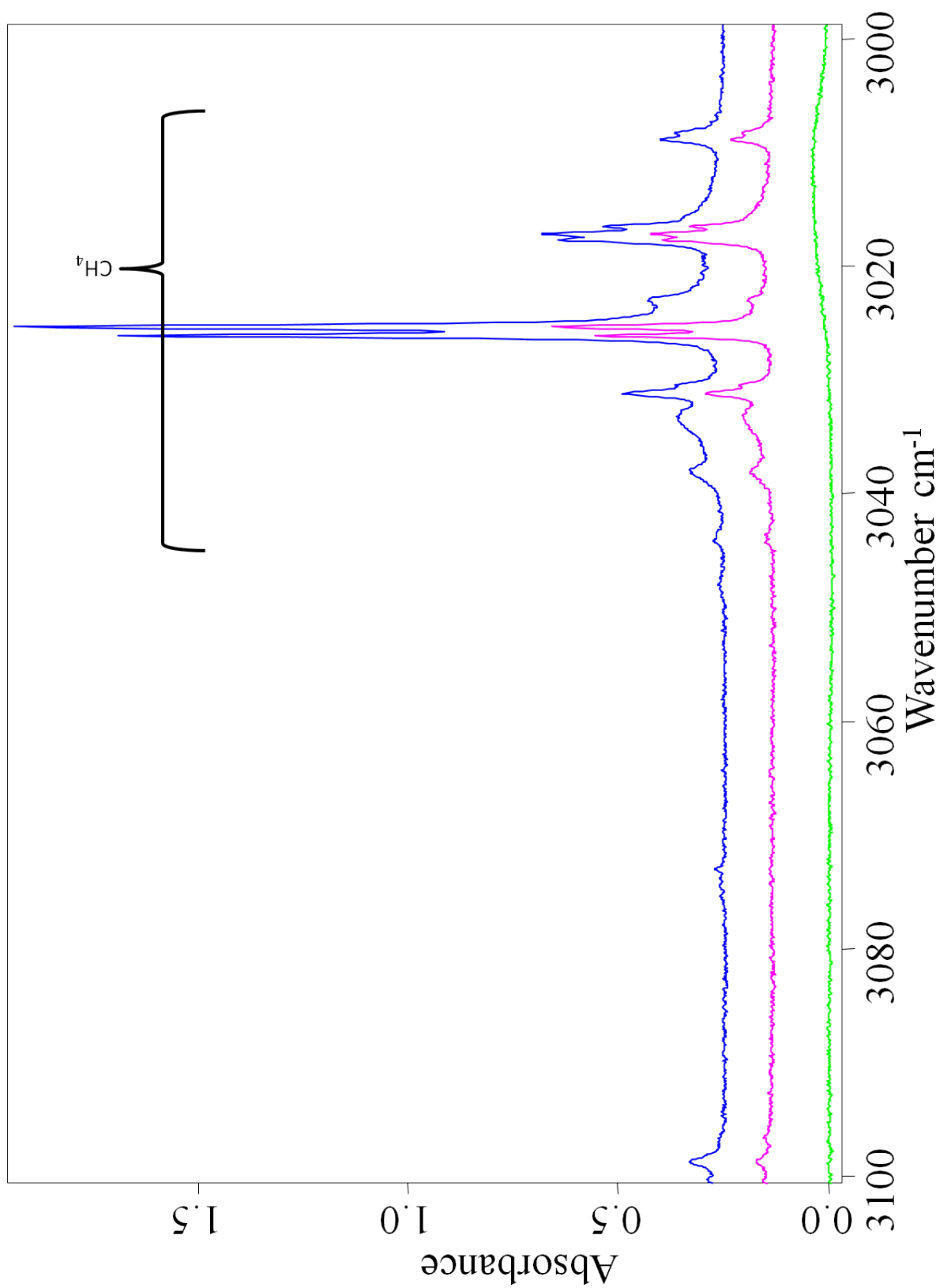


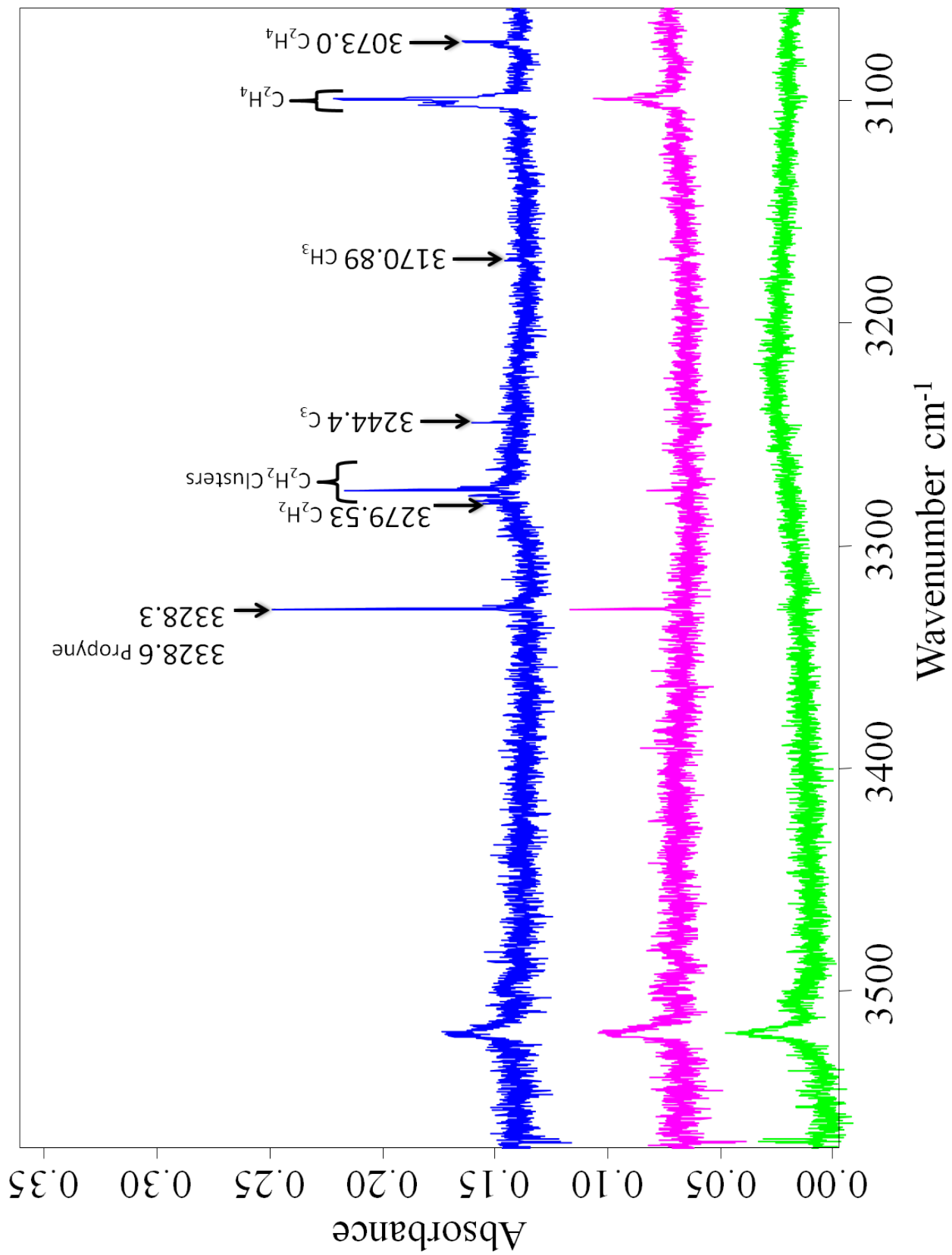
C. IR SPECTRA OF ACAC IN PH₂ MATRIX UNDER UV 193NM IRRADIATION



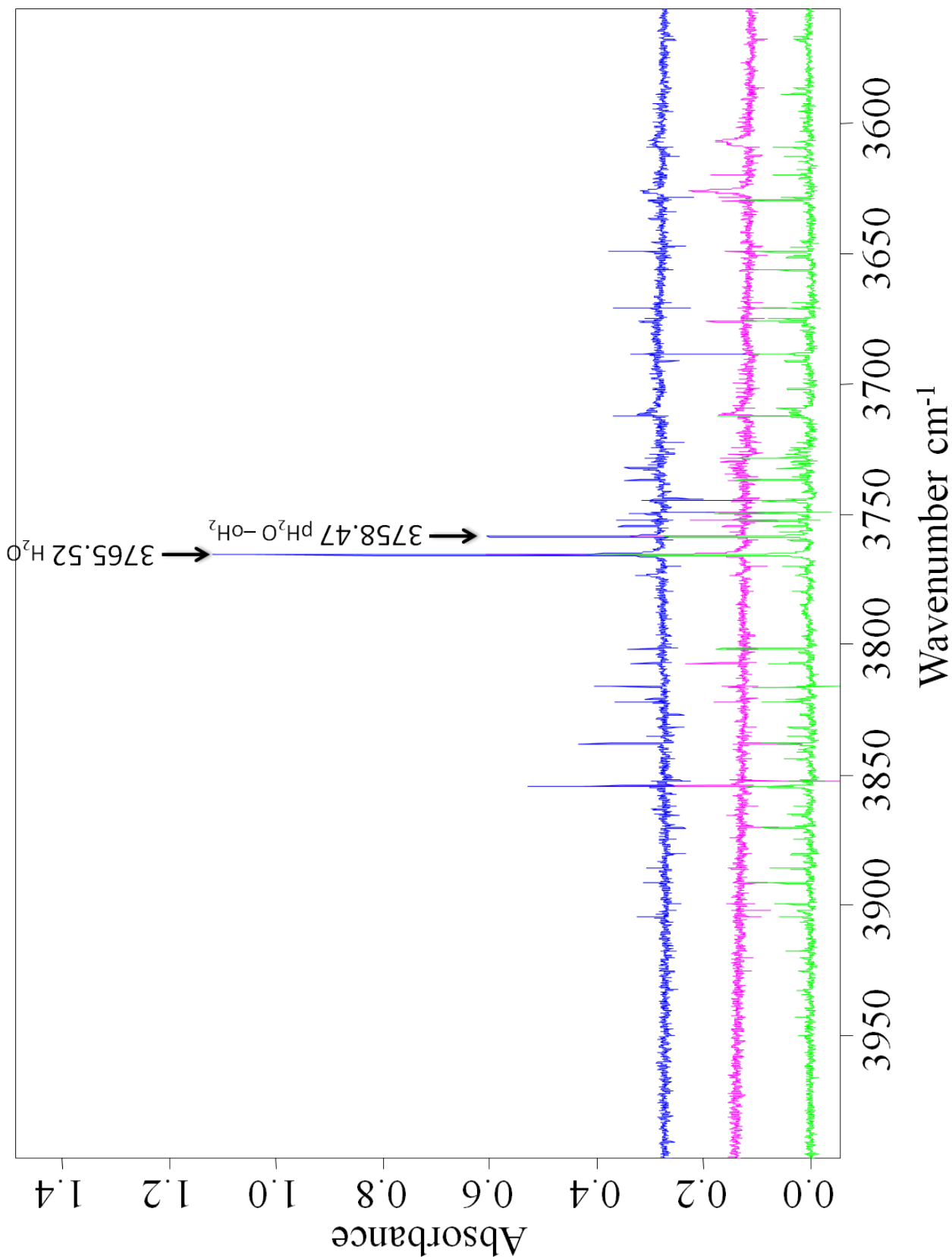


C. IR SPECTRA OF ACAC IN PH₂ MATRIX UNDER UV 193NM IRRADIATION





C. IR SPECTRA OF ACAC IN PH₂ MATRIX UNDER UV 193NM IRRADIATION



I

Resumen en Español

Introducción

Las investigaciones realizadas a través de la dinámica molecular y fotodinámica de procesos moleculares dan acceso a información sobre fenómenos elementales tales como la transferencia de energía o la reactividad química. La fotoquímica, como un caso particular de la fotodinámica, consiste en el estudio de reacciones químicas que sólo tienen lugar cuando una molécula alcanza, luego de absorber fotones, la “energía de activación” necesaria para que ocurra la reacción. La absorción de fotones por una molécula puede, además, cambiar la simetría de la configuración electrónica dando lugar a nuevos canales de reacción que no existen en el estado fundamental.

Si se utiliza un láser como fuente de fotones, es posible excitar una molécula hasta un nivel electrónico o vibracional deseado. Igualmente, la emisión desde un nivel excitado específico puede ser registrada y con ello estimar la población de ese estado. Si el sistema químico está en fase gaseosa a bajas presiones es posible observar la distribución de energía de los productos antes de que el sistema alcance el equilibrio debido a las colisiones entre las moléculas. Por otro lado, en este sistema, los productos de la reacción se dispersan y no se quedan en la zona de interacción. Como consecuencia, la recombinación no es posible y las reacciones secundarias son muy poco probables. Más aún, los reaccionantes y productos en la zona de observación están en una cantidad muy limitada lo cual proporciona señales de muy baja intensidad en el caso de procesos poco eficientes. Con el objetivo de tener grandes concentraciones de la molécula de interés resulta útil el uso de matrices criogénicas como medio en el que se producen estas reacciones, brindando la posibilidad de investigar varios procesos durante períodos largos de tiempo.

La técnica de espectroscopía por aislamiento matricial (MIS por sus siglas en inglés) es muy utilizada para investigar propiedades moleculares tales como la geometría y reactividad de las especies

atrapadas, especialmente en el caso de especies inestables o especies intermedias de una reacción. La técnica MIS ha sido usada desde 1954 para atrapar moléculas en un medio inerte.¹ Muchas moléculas tales como CO, CO₂, N₂, H₂, O₂, Cl₂, CCl₄, además de los gases nobles, se han empleado como este medio inerte para aislar moléculas pequeñas a las que se le harán estudios espectroscópicos. El uso de la molécula de hidrógeno (H₂) y en particular el para-hidrógeno (pH₂) brinda nuevas ventajas a la técnica MIS debido a las propiedades cuánticas del sólido. Las interacciones entre la matriz y la impureza son muy pequeñas lo cual permite que la especie bajo estudio mantenga sus características cercanas a las que presenta en fase gaseosa. Con el objetivo de beneficiarse de estas propiedades se han realizado estudios fotoquímicos de moléculas y complejos moleculares que presentan enlaces por puentes de hidrógeno en sólidos de pH₂.

Los enlaces por puente de hidrógeno son interacciones moleculares relativamente débiles, pero juegan un papel importante en la reactividad química de muchos sistemas. Se espera que estos enlaces sean débilmente afectados por las matrices de pH₂. Los estudios dinámicos y en especial los fotodinámicos de especies con enlaces por puente de hidrógeno en sólidos de pH₂ darán información pertinente, a escalas moleculares, para la solución de muchos problemas tales como la relación entre el solvente (matriz) y el elemento reactivo (impureza).

Este trabajo está dedicado al estudio de una molécula orgánica pequeña la cual presenta un enlace por puente de hidrógeno interno: Acetilacetona (AcAc). La AcAc es una β -Dicetona que pertenece a un grupo bien conocido de compuestos tautoméricos que han sido muy usados tanto en la química orgánica como la inorgánica. Durante años, las estructuras de sus formas cetónica y enólica (ver figura I.1) han sido tema de importantes estudios así como la naturaleza del fuerte enlace por puente de hidrógeno intramolecular O–H \cdots O de la forma quelato enólica de la AcAc. Los mismos se han realizado usando una variedad de métodos diferentes que incluyen técnicas IR, Raman, microondas y otras.²⁻¹⁰

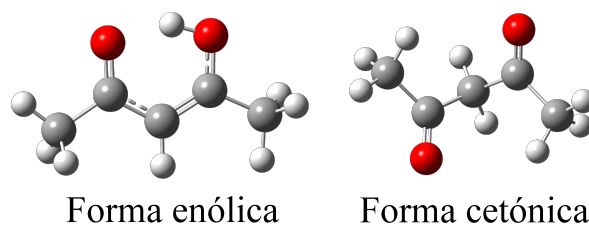


Figura I.1: Formas enólica y cetónica de la AcAc

El interés creciente sobre los compuestos con un corto (fuerte) enlace por puente hidrógeno que incluye formas quelato enólicas de β -dicetonas está relacionado con el estudio de la transferencia de un protón desde un átomo de oxígeno hacia otro a lo largo del enlace por puente de hidrógeno.

Este fenómeno es una de las reacciones más generales e importantes de la química. La transferencia de un protón juega un papel crucial en muchos procesos tales como la neutralización de reacciones ácido-base, la adición electrofílica y muchos otros procesos.¹¹ Ella tiene gran importancia para varios procesos bioquímicos, desde reacciones enzimáticas hasta interconversión por tautomerización de bases del ADN.¹² La AcAc es una de las β -Dicetonas más simples que presenta una transferencia de protón intramolecular entre dos átomos de oxígeno,² lo cual la convierte en una molécula modelo para el estudio de este fenómeno.¹³

Se ha prestado especial atención a las características estructurales de los tautómeros de la AcAc y los procesos de tautomerización en sí mismos. El equilibrio entre las formas cetónica y enólica (R_{ke}) de la AcAc en diferentes medios ha sido estudiado durante muchos años. Como resultado de estos estudios se ha encontrado que R_{ke} depende fuertemente de las condiciones y las características del medio que lo rodea.¹⁴⁻¹⁷ Se acepta de forma general que, a temperaturas cercanas a los 300 K, predomina la forma enólica tanto en su fase gaseosa como en la fase líquida.¹⁷⁻¹⁹

Los procesos que tienen lugar en la molécula de AcAc debido a la irradiación con luz ultravioleta (UV) tales como la isomerización, tautomerización y la fragmentación, también han estado bajo estudio tanto experimentales como teóricos.^{2,20,21} La irradiación de esta molécula cuando está en fase gaseosa conduce a su fragmentación liberando en primer lugar el radical OH.²⁰ Cuando la AcAc es embebida en una matriz criogénica de sólidos inertes como Ne, Ar, Kr y N₂, la irradiación con luz UV solo conduce a la isomerización.^{2,22,23}

La espectroscopía infrarroja (IR) es muy conveniente cuando se usan las técnicas de MIS. Debido a las bajas temperaturas ($< 70\text{K}$), en la mayoría de los casos, solo se pueblan los niveles vibracionales y rotacionales más bajos. En un medio matricial, las reacciones químicas pueden ser seguidas y controladas.²⁴⁻²⁶

Las matrices de hidrógeno y en especial el pH₂ son un medio muy interesante para la aplicación de las técnicas MIS.²⁷ Debido a las condiciones de simetría que tiene que cumplir la función de onda total de la molécula de hidrógeno (H₂) existen dos posibilidades de encontrarla en la naturaleza.²⁸ La molécula de H₂ que tiene espín nuclear ($I=0$) se llama para-hidrógeno (pH₂) y tiene un número cuántico rotacional J par, mientras que la que tiene $I=1$ se llama orto-hidrógeno (oH₂) y tiene un J impar. A temperatura ambiente, la población de equilibrio entre oH₂ y pH₂ es 3:1. La interconversión entre estos dos estados de espín ($I=0$, $I=1$) para una molécula idealmente aislada está prohibida por las reglas de selección de la mecánica cuántica. Los niveles rotacionales de la molécula de H₂ están bien distantes uno del otro (354.38 cm^{-1} para $J=0 \rightarrow J=2$ y 587.06 cm^{-1} para $J=1 \rightarrow J=3$). Para bajas temperaturas ($\leq 20\text{K}$) sólo los niveles $J=0$ y $J=1$ están poblados según la distribución de Boltzmann. Una molécula en el estado $J=1$ se mantendrá en estado meta-estable en ese nivel ya que la conversión al nivel $J=0$ es muy lenta en ausencia de un campo magnético externo.^{28,29}

La función de onda rotacional del H_2 en el estado $J=0$ tiene una simetría completamente esférica. La molécula de pH_2 no tiene momento eléctrico permanente de ningún orden. Por tanto, el cristal de pH_2 ($T = 6K$) provee un medio completamente homogéneo para una molécula atrapada en su interior. Este sólido posee una estructura de celda unitaria fcc, además de un movimiento de punto cero del orden del 20% de la distancia al vecino más próximo, lo cual lo hace de él un cristal muy suave. La suavidad de este cristal y el gran movimiento de punto cero minimizan las imperfecciones que pueda tener la matriz alrededor de la molécula bajo estudio.

En virtud de las características especiales que ostenta el sólido de pH_2 , el espectro IR de moléculas pequeñas atrapadas en su seno muestra bandas sorprendentemente finas asociadas a los estados cuánticos ro-vibracionales de la molécula huésped.^{11,31-33} Además, la matriz de pH_2 es muy útil para el estudio de reacciones químicas a temperaturas criogénicas. Como el efecto caja de este sólido está minimizado se espera que los productos primarios de una reacción química sean más parecidos a los que se obtienen en la fase gaseosa que a los que se obtienen en otras matrices inertes. Esto es una ventaja para estudiar reacciones fotoquímicas en fase condensada.^{30,34,35} En matrices de gases nobles, la fotólisis *in situ* está fuertemente influenciada por las paredes de la matriz. En la mayoría de los casos las especies resultantes del proceso de fotólisis no pueden escapar de la celda por el efecto caja. Por el contrario, los foto-fragmentos producidos en un sólido de pH_2 pueden separarse más fácil utilizando la energía en exceso de la foto-disociación porque el efecto caja es mucho menor. La recombinación *in situ* de los foto-fragmentos es menos probable, lo que permite reacciones secundarias de los mismos, que pueden tener lugar durante o después de la fotólisis. En cualquier caso, la medición de un espectro después de la fotólisis durante un período de tiempo largo, permite la observación de reacciones más lentas, así como la detección de foto-productos que se producen en pequeñas cantidades.³⁰

En el presente trabajo se estudia la fotodinámica de la molécula de AcAc aislada en matrices de pH_2 . La molécula es caracterizada con ayuda de espectros IR medidos en la región $700-5000\text{ cm}^{-1}$. En este espectro se pueden observar bandas asignadas a la forma quelato enólica así como a la forma cetónica de la AcAc. La fotoquímica de ésta molécula es estudiada con el empleo de tres radiaciones láser de longitudes de onda 266 nm, 248 nm y 193 nm. Estas longitudes de onda se encuentran en la región UV. La radiación de 266 nm corresponde al cuarto armónico de un Nd:YAG, la de 248 nm a un láser excímero KrF y la de 193 nm a otro excímero ArF. Estas tres radiaciones excitan la molécula de AcAc a dos estados electrónicos diferentes. Las radiaciones de 266 nm y 248 nm la excitan a un estado S_2 mientras que la de 193 nm la excita a un estado S_3 .

I.1 Dispositivo experimental

El para-Hidrógeno (pH_2) se obtiene a partir del hidrógeno gaseoso, dentro de un criostato llamado conversor. El conversor consiste en un bloque de cobre con una cavidad cilíndrica, el cual se mantiene a temperaturas cercanas a los 19K y está previamente lleno de óxido de hierro III (Fe_2O_3). El Fe_2O_3 actúa como catalizador para la conversión del hidrógeno normal (nH_2) a pH_2 . El conversor es llenado con nH_2 , el cual entra en contacto con el campo paramagnético generado por el catalizador y se mantiene durante 1 hora y 30 minutos aproximadamente. Bajo estas condiciones el pH_2 obtenido tiene al menos una pureza del 99.9%. Para los experimentos con hidrógeno normal (nH_2) (Messer 5.5), deuterio normal (nD_2) (Alphagaz D_2-N30) y neon (Ne) (Messer 4.0), los gases pasaron a través del conversor a 19K (nH_2 y nD_2) o 40K (Ne) y luego fueron depositados.

La AcAc y los gases solventes provenientes de dos tubos diferentes son depositados en una ventana de diamante que ha sido enfriada hasta 4.2 K. La AcAc (99.5%) fue comprada en Fluka. Esta se mantuvo en un baño de hielo a 0° antes de la deposición, con el objetivo de disminuir la presión de vapor sobre el líquido y mantener las mismas condiciones de un experimento a otro. Esto permite un amplio manejo de las microválvulas y un mejor control sobre la concentración de AcAc en la matriz. La relación AcAc/solvente fue estimada a partir del espectro infrarrojo y está en el rango de 1:500 hasta 1:1000.

El espectro IR se mide en el rango de $700-5000\text{ cm}^{-1}$ utilizando un espectrómetro IR con transformada de Fourier (Nicolet) con una resolución de 0.5 y 0.125 cm^{-1} . La zona por la que pasa el rayo IR fue purgada con aire seco. Se utilizaron tres láser ultravioleta para irradiar la muestra: El cuarto armónico de un Nd:YAG que provee una longitud de onda de 266nm, un láser excímero KrF a 248nm y otro excímero ArF a 193nm. Las energías típicas de los láser fueron de 10 mJ/pulso a 10 Hz. Los tiempos de irradiación oscilan desde varios minutos hasta 10 horas.

I.2 Espectro infrarrojo del AcAc

Las estructuras y frecuencias de las formas quelato enólica y cetónica de la AcAc fueron optimizadas y calculadas respectivamente utilizando el método Teoría Funcional de la Densidad (DFT por sus siglas en inglés) con una base B3LYP/6-311++G(3df,3pd). Las frecuencias se calcularon utilizando la aproximación armónica y luego se aplicaron correcciones anarmónicas. En la figura I.2 se muestra el espectro infrarrojo de la molécula de AcAc aislada en varias matrices: (a) en matrices de pH_2 , (b) en matrices de nH_2 , (c) en matrices de nD_2 y (d) en matrices de Ne. Los asteriscos (*) representan las bandas asignadas a las moléculas de H_2O atrapadas en la matriz. Las bandas asignadas a la forma cetónica están marcadas con la letra (k). El resto de las bandas corresponden a la forma quelato

enólica de la AcAc. La asignación de estas bandas se realizó con ayuda de los espectros simulados. Los cálculos en los que se introdujeron las correcciones anarmónicas a las frecuencias resultaron tener mejor correspondencia con el espectro experimental.

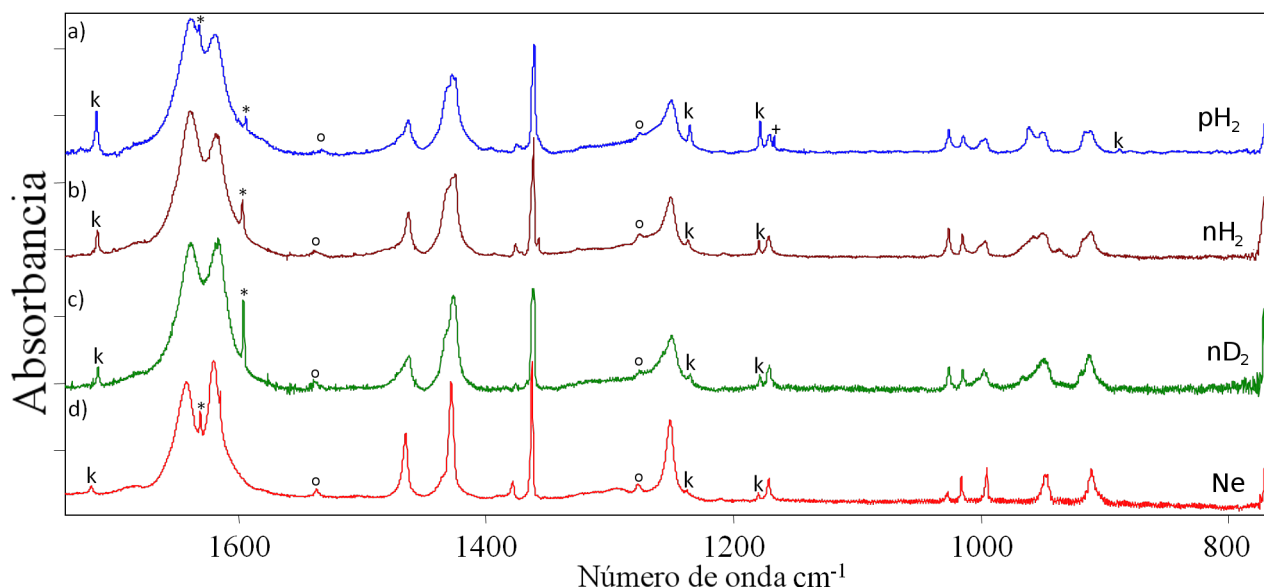


Figura I.2: Espectros de AcAc en diferentes medios: (a) en matrices de pH_2 , (b) en matrices de nH_2 , (c) en matrices de nD_2 y (d) en matrices de Ne. Las bandas que corresponden a la forma cetónica están marcadas con una (k). El (*) representa las bandas correspondientes a la molécula de H_2O y las marcas (o) se refiere a los armónicos de segundo orden de algunas bandas

Las posibles simetrías (C_{2v} y C_s) que puede presentar la distribución geométrica de la forma quelato enólica de la AcAc también fueron calculadas usando el mismo método y base antes mencionados. La comparación directa con el espectro experimental confirma una simetría C_s para la molécula de AcAc en su forma quelato enólica. A partir de los datos experimentales y con ayuda de los cálculos teóricos puede estimarse R_{ke} en las diferentes matrices. Como resultado, el mayor valor de R_{ke} se alcanza para las matrices de pH_2 . En las matrices de Ne (ver figura I.2 (d)) el espectro es muy similar al reportado en la literatura^{50,106} y se estima un valor para R_{ke} entre 1-1.5%. En las matrices de nH_2 y nD_2 los valores de R_{ke} se estiman $\sim 2\%$. Para las matrices de pH_2 , R_{ke} se estimó $\sim 4.5\%$. La abundancia de la forma cetónica de la AcAc encontrada en el presente trabajo está dentro del rango de los valores reportados en la literatura.^{51,53} Estos últimos se obtuvieron a través de estudios con NMR en fase gaseosa a 298K que conducen a valores de entre 2.5%⁵¹ y 6.7%.⁵³

Observando las regiones entre 900-1100 cm^{-1} se puede apreciar que en la matriz de pH_2 las bandas presentan una estructura de doblete mientras que en la matriz de Ne solo se observan singletes. Estas estructuras de dobletes no pudieron ser asignadas a efectos de sitios de las matrices pues se mantenía

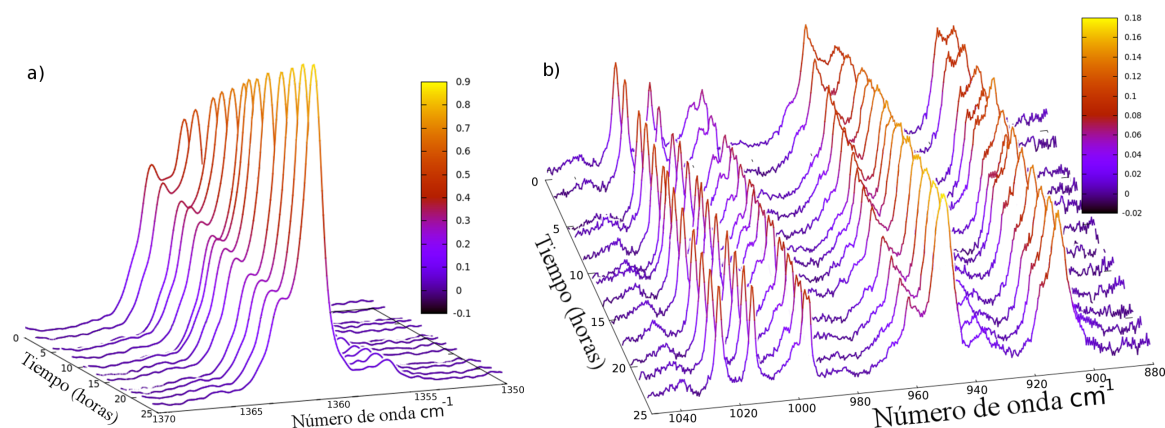


Figura I.3: Evolución temporal del espectro de AcAc aislada en matrices de pH_2 cuando la muestra es mantenida en la oscuridad. (a) región $135\text{-}1370\text{ cm}^{-1}$ (b) región $880\text{-}1050\text{ cm}^{-1}$.

la misma estructura incluso después del recocido de la matriz. Esto confirma que el efecto de sitio en la matriz de pH_2 es menos importante que en el resto de las matrices y experimentalmente imperceptible. Con el objetivo de dilucidar esta estructura la matriz se mantuvo a oscuras durante 24 horas. La evolución temporal de este proceso se muestra en la figura I.3. Aquí se puede apreciar cómo hay un grupo de bandas que disminuyen su intensidad en el tiempo mientras otro grupo siempre aumenta en el tiempo. De esta forma se pudieron separar dos espectros muy similares y se concluyó la presencia de al menos dos especies de la forma quelato enólica de la AcAc: una llamada “más estable (ms)” y otra “menos estable (ls)”. Los valores de las intensidades integradas se graficaron en función del tiempo. Los valores experimentales se ajustaron a funciones exponenciales crecientes y decrecientes. Del ajuste se estimó una constante de tiempo del orden de 0.042h^{-1} . Este valor es del mismo orden de magnitud del registrado en procesos de conversión del espín nuclear en moléculas aisladas en matrices de pH_2 que contienen un grupo metilo.^{32,113} Por ejemplo, se reporta en la literatura una constante de tiempo de 0.018 h^{-1} para la conversión del espín nuclear en el grupo metilo de la molécula de CH_3OH aislada en matrices de pH_2 ³²

El carácter poco interactivo de las matrices de pH_2 con las rotaciones del grupo metilo ya ha sido probado en el estudio de pequeñas moléculas que presentan un solo grupo metilo (metanol,³² CH_3 ¹¹³) aisladas en este tipo de matrices. El espín nuclear de un grupo metilo está completamente acoplado a su rotación por razones de simetría. El estado A está asociado a una función de onda de espín totalmente simétrica ($I=3/2$) mientras que el estado E corresponde a una función de onda no simétrica ($I=1/2$). Consecuentemente, la transferencia de población del estado E al A implica conversión de espín, el cual es un proceso muy lento comparado con la termalización.¹¹⁸ Por lo tanto, inmediatamente después de la deposición de la molécula en la matriz de pH_2 , en el caso de una diferencia grande entre los

estados A y E (rotaciones casi libres del grupo metilo) la población de los estados A y E difiere de la distribución de Boltzmann a la temperatura de la matriz (4K). De hecho una conversión lenta del espín nuclear de la AcAc aislada en el sólido pH_2 es observada a través de la evolución temporal del espectro IR de absorción. El mismo análisis puede ser usado para comparar la dinámica del estado vibracional fundamental con un estado rotacional excitado relacionado a la torsión del grupo metilo. Lo más importante en este caso es que la energía extra depositada en este estado excitado no es suficiente para sobrepasar la barrera de la transferencia de protón. Sin embargo, se deposita en un modo que puede desencadenar la reacción.

I.3 Irradiación Ultra violeta

En este capítulo se discute la irradiación de la matriz de AcAc en pH_2 con luz ultra violeta. Tres radiaciones láser fueron utilizadas para efectuar la irradiación de la muestra. Primero se discute la evolución de la matriz cuando es expuesta a un longitud de onda de 266 nm. Luego cuando se somete a una longitud de onda de 248nm. En ambos casos la molécula se excita hasta el nivel electrónico S_2 . Por último se discuten los procesos que tienen lugar en la matriz cuando la molécula es excitada al estado S_3 utilizando una longitud de onda de 193 nm.

I.3.1 Irradiación con una longitud de onda de 266nm

Tan pronto como se comienza la irradiación de la matriz con un láser a 266 nm las bandas asignadas a la forma quelato enólica de la AcAc (en lo adelante CCC) comienzan a disminuir en intensidad y nuevas bandas comienzan a aparecer. Si se continúa la irradiación por un período de tiempo prolongado se puede observar que las nuevas bandas presentan una evolución temporal diferente, lo que sugiere la presencia de nuevas especies. De forma general estas nuevas bandas se pueden separar en dos grupos: en el primer grupo están las bandas que incrementan su intensidad hasta un momento y luego comienzan a disminuir, mientras que en el segundo grupo están las bandas que aumentan su intensidad durante todo el proceso de irradiación. Las contribuciones al espectro de estos dos grupos pueden ser separadas haciendo sustracciones sucesivas de espectros a diferentes tiempos de irradiación. De esta forma se pueden obtener dos espectros puros del primer y segundo grupos.

En la figura I.4 se muestra una comparación de espectros de AcAc en pH_2 tomados en tres instantes durante la irradiación de la muestra con un láser a 266 nm. El espectro en (a) es tomado justo después de la deposición de la matriz en el que observan las bandas asignadas a la forma CCC. En (b) se muestra el espectro tomado en un punto intermedio (~ 40 min) de la irradiación y en (c) luego de un largo tiempo de irradiación (~ 300 min). El láser es apagado durante el proceso de lectura del espectro

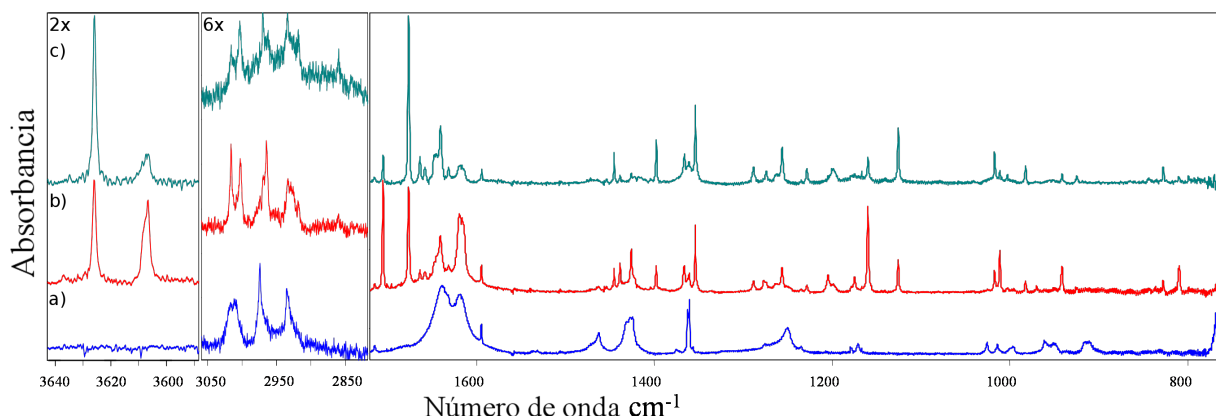


Figura I.4: Espectros IR de la AcAc aislada en matrices de pH_2 tomados en diferentes instantes durante la irradiación láser a 266nm. (a) Justo después de la deposición de la matriz. (b) En un instante intermedio (~ 40 min) donde la cantidad del isómero CTC está en su máximo. (c) Luego de una larga irradiación (~ 300 min) donde se observan fundamentalmente las bandas asignadas a los isómeros TCC y TTC

IR. Como fue mencionado anteriormente, nuevas bandas de absorción, más finas (ancho de banda ~ 2 cm^{-1}) que las asignadas a la forma CCC, aparecen en el espectro. El espectro y la distribución de intensidades de las bandas no se modifican en ausencia del láser de irradiación lo que implica que ni en la oscuridad ni bajo la luz infrarroja del espectrómetro se inducen procesos de cambio durante el experimento. Se puede observar que los espectros medidos en distintos instantes de tiempo son diferentes entre sí.

Las geometrías de todos los posibles isómeros de la forma enólica de la AcAc fueron optimizadas y las frecuencias infrarrojas fueron calculadas. Los cálculos se realizaron primero en la aproximación armónica y luego teniendo en cuenta las correcciones anarmónicas. En los mismos fue utilizado el método DFT con una base B3LYP/6-311++G(3df,3pd). Como se dijo antes, haciendo sustracciones de espectros tomados en distintos instantes de tiempo se pueden obtener los espectros puros del primer y el segundo grupo de bandas. Los espectros simulados se compararon con los espectros experimentales del primer y el segundo grupo. El primer grupo de bandas fue asignado al isómero CTC; el segundo, los isómeros TCC y TTC. Los isómeros del tipo XYT, los cuales se diferencian de los XYC sólo en la rotación del grupo OH alrededor del enlace C-O, no fueron encontrados en la matriz de pH_2 . En general los espectros simulados de los isómeros XYT son muy similares a los correspondientes XYC principalmente en la región espectral comprendida entre los 1800-800 cm^{-1} . La principal diferencia entre estos espectros está dada en la región de las frecuencias del grupo OH (3660-3600 cm^{-1}). La diferencia de energía entre los XYT y los XYC es relativamente pequeña. Dadas las características del sólido de pH_2 es posible que los XYT se isomerizan hacia los XYC más estables atravesando la barrera por efecto túnel.

Con el objetivo de comparar el efecto de la matriz sobre los cambios que sufre la molécula debido a la irradiación se realizaron experimentos similares utilizando $n\text{H}_2$, $n\text{D}_2$ y Ne como solventes para construir la matriz. Una comparación de los espectros luego de la irradiación de la AcAc en diferentes matrices se muestra en la figura I.5. En los cuatro espectros las bandas que corresponden a la forma CCC han sido sustraídas para una mejor comparación. Cuando se compara el espectro de la matriz de Ne (figura I.5 (d)) con el de la matriz de $p\text{H}_2$ mostrado en el panel (a) podemos ver que en ambos casos tenemos las mismas bandas. Sin embargo cuando comparamos con los espectros que corresponden a las matrices de $n\text{H}_2$ (b) y $n\text{D}_2$ (c) vemos que aparecen nuevas bandas. Estas nuevas bandas están señaladas con (+) en la figura I.5. Haciendo un análisis similar al anterior, se pueden separar dos grupos de bandas. Las nuevas bandas encontradas en el espectro corresponden al segundo grupo: son aquellas cuya intensidad aumenta durante todo el proceso de irradiación. Comparando con los espectros simulados y prestando especial atención a la región de vibración del grupo OH, se pueden asignar estas nuevas bandas al isómero TCT. La posibilidad de estabilizar este isómero en las matrices de $n\text{H}_2$ y $n\text{D}_2$ y no así en las matrices de $p\text{H}_2$, muestra cómo las matrices donde las interacciones son más fuertes, pueden bloquear la rotación del grupo OH por efecto túnel hacia un isómero menos energético.

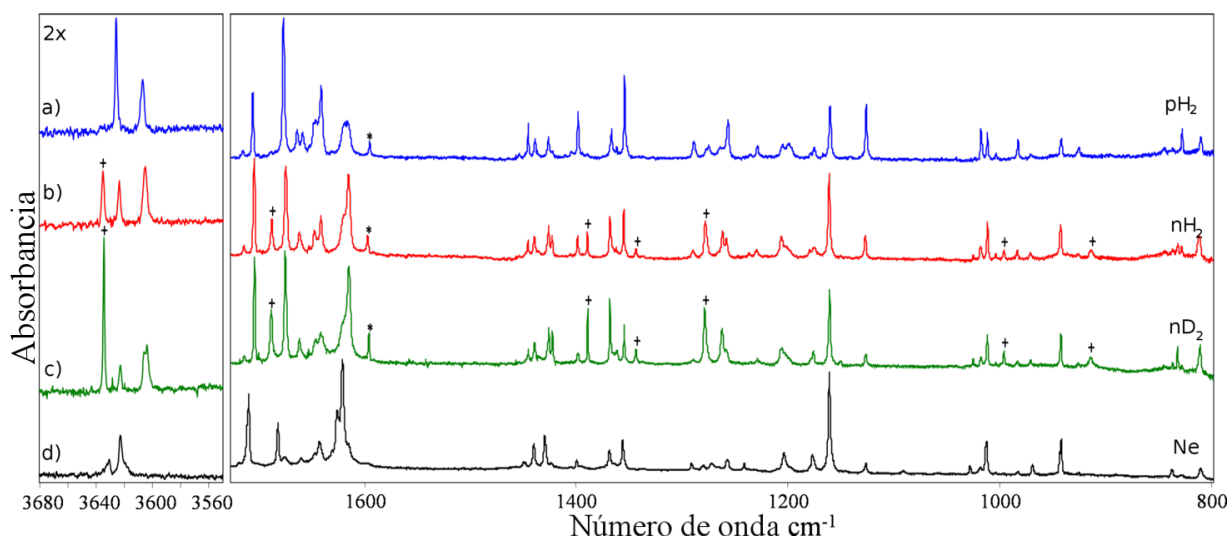


Figura I.5: Comparación de espectros del AcAc aislada en diferentes matrices después de la irradiación con laser a 266nm. (a) $p\text{H}_2$, (b) $n\text{H}_2$, (c) $n\text{D}_2$ y (d) Ne. Las bandas asignadas al isómero TCT están marcadas con un (+).

El proceso de irradiación fue monitorizado tomando espectros infrarrojos en varios instantes de tiempo. De estos espectros pudo extraerse la variación temporal de las intensidades de las bandas. Tomando bandas características de cada isómero ($\text{CTC}-1705\text{ cm}^{-1}$), ($\text{TCC}-1126\text{ cm}^{-1}$) y ($\text{TTC}-1229\text{ cm}^{-1}$) y tomando la integral sobre todo el espectro para la forma CCC se realizó un estudio cinético del

proceso de irradiación. Los isómeros formados durante el proceso de irradiación, así como los valores de las constantes de reacción se muestran en el diagrama de la figura I.6

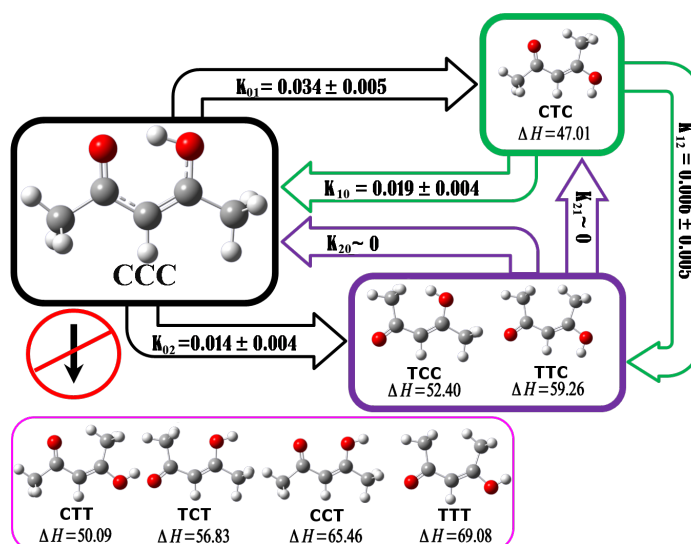


Figura I.6: Diagrama de reacción de la AcAc aislada en pH_2 bajo la acción de un laser UV a 266nm. K_{ij} son las constantes de reacción. Las energías están dadas en kJ/mol

I.3.2 Irradiación con una longitud de onda de 248nm

La irradiación de AcAc aislada en pH_2 con láser a 266 nm conduce fundamentalmente a la isomerización de la forma quelato enólica de la AcAc hacia las formas enólicas abiertas. En estudios realizados por Nagashima *et al.*⁵⁸ se muestra que la irradiación de la AcAc con una longitud de onda más corta puede incluso conducir a la tautomerización de esta molécula hacia su forma cetónica. La fragmentación de la molécula también puede ocurrir.

Con el objetivo de estudiar este fenómeno de una manera más detallada, ha sido realizada una serie de experimentos utilizando una longitud de onda más corta (248nm) como fuente de irradiación, en los cuales la AcAc se aisló en matrices de pH_2 , nH_2 , nD_2 y Ne.

Después de la deposición, la matriz de pH_2 con moléculas de AcAc es iluminada con un láser excímero a 248nm (10 mJ energía/pulso a 10 Hz). La irradiación es detenida para la mediciones del espectro infrarrojo. La figura I.7 muestra una comparación de los espectros obtenidos en dos momentos (b y c) de irradiación de la matriz con una longitud de onda de 248 nm, con un espectro IR cuando la matriz es irradiada con una longitud de onda de 266 nm (a). En los tres espectros las bandas asociadas a la forma quelato enólica de AcAc (CCC) fue sustraída para una mejor comparación. Las líneas de puntos representan las bandas asignadas a la forma cetónica de la AcAc. Durante los primeros minutos

de la irradiación a 248 nm (ver figura I.7 b) aparecen muchas bandas que ya han sido asignadas a los isómeros enólicos de la AcAc. El incremento de las bandas correspondientes a la forma cetónica comienza luego de una prolongada irradiación de la matriz.

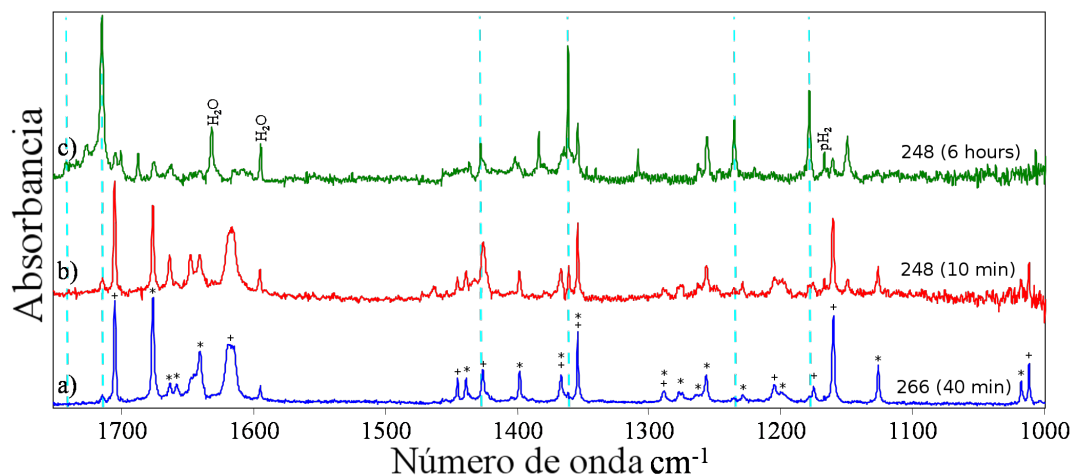


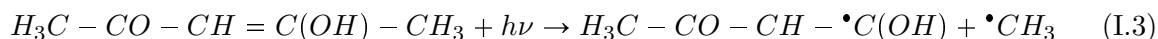
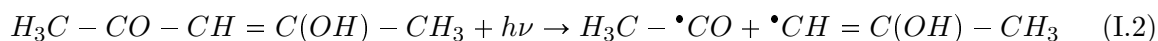
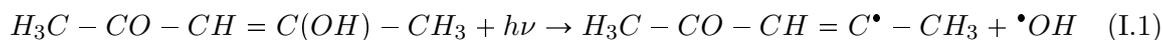
Figura I.7: Comparación de espectros IR luego de la irradiación de la AcAc aislada en matrices de pH_2 (a) Luego de algunos minutos (~ 40 min) usando una longitud de onda de 266 nm; (b) Luego de algo minutos (~ 10 min) usando una longitud de onda de 248 nm y (c) luego de algunas horas (~ 6 horas) usando una longitud de onda de 248 nm. La contribución de la forma CCC se han sustraído en todos los espectros para facilitar la comparación. Las posiciones de las bandas de la forma cetónica de la AcAc están marcadas con líneas de puntos verticales. El símbolo (+) designa a las bandas que se encuentran en el primer grupo de isómeros y el símbolo (*) designa las bandas del segundo grupo de isómeros

Luego de un período largo de irradiación fueron observadas otras bandas que no pueden ser asignadas a la forma cetónica de la AcAc. Algunas de ellas se pueden asignar a H_2O , CO y metanol. La foto-fragmentación de la AcAc también ha sido observada en las matrices de Ar⁵⁸ pero las bandas no fueron asignadas a ningún foto-producto. Los principales fragmentos observados durante estos experimentos fueron: CO, el cual muestra una banda intensa y estructurada en la región 2125-2150 cm^{-1} ¹¹³²; CH_3 que pudo ser identificado por sus modos ν_3 con un doblete a los 3170.6 y 3171.4 cm^{-1} y ν_4 con un doblete 1401.7 y 1402.9 cm^{-1} ^{127,34}; CH_4 identificado por su modo ν_3 en los 3025.3 cm^{-1} y ν_4 en los 1308.3 cm^{-1} ^{111,27} y el H_2O con su modo ν_2 en los 1631.7 cm^{-1} .³³

El decrecimiento de las intensidades de la forma quelato enólica de la AcAc y el incremento de su forma cetónica fueron monitorizados durante el proceso de irradiación con el uso de la espectroscopía FT-IR. Varios espectros fueron registrados en diferentes instantes de tiempo. Las intensidades integradas de las bandas características de la forma quelato enólica, cetónica y de algunos fragmentos como el CO se graficaron en función del tiempo. En este caso no se calcularon las constantes de reacción

pero se puede dar una explicación cualitativa del proceso de irradiación de la matriz usando el láser a 248nm.

A partir del modelo cinético se puede concluir que: bajo irradiación a 248 nm de la molécula de AcAc aislada en matrices de pH₂, en los primeros minutos se favorece la formación de isómeros enólicos abiertos. Luego, cuando continúa la irradiación sobre los isómeros enólicos abiertos, al menos dos canales de reacción compiten: la tautomerización que consiste en la transferencia del H del grupo OH hacia el carbón central y la fragmentación de la molécula dando lugar a moléculas más pequeñas tales como CO, CH₄ y radicales como CH₃. Una irradiación prolongada elimina todos los isómeros enólicos quedando solo la forma cetónica, fragmentos y moléculas más pequeñas. La dinámica de fotodisociación de la AcAc ha sido estudiada por Upadhyaya *et al.*²⁰ usando fluorescencia inducida por láser (LIF por su siglas en inglés) y técnicas “pump-probe” a temperatura ambiente. Ellos además realizaron cálculos *ab initio* de orbitales moleculares (MO) para investigar las superficies de energía potencial del estado fundamental y de los estados electrónicos excitados de la AcAc. Tres mecanismos de fragmentación fueron propuestos a partir del estado de triplete T₁ cuando la molécula es irradiada con 266 nm y 248 nm.



Aunque estos trabajos fueron realizados en la fase de gas, confirman algunos de nuestros resultados.

I.3.3 Irradiación con una longitud de onda de 193nm

Anteriormente se discutía sobre la fotoquímica de la AcAc aislada en matrices de pH₂ cuando la molécula se excita hasta un nivel electrónico S₂ utilizando dos longitudes de ondas 266 nm y 248 nm. De forma similar a los experimentos anteriores, la matriz de pH₂ con moléculas de AcAc es irradiada con un láser UV con un longitud de onda de 193nm (10 mJ energía/pulsos a 10 Hz). Esta longitud de onda excita a la molécula de AcAc hasta un estado electrónico S₃.

El primer efecto de la irradiación de la matriz es la transformación de la forma CCC en otras moléculas tales como los isómeros enólicos abiertos, la forma cetónica, radicales y moléculas más pequeñas producto de la foto-fragmentación. La aparición de fragmentos debido a la irradiación comienza desde los primeros minutos. Trazas de CO y CH₄ pueden observarse con solo 20 min de irradiación. Para tiempos más largos de irradiación, las bandas que corresponden a los isómeros enólicos y la forma cetónica también desaparecen quedando solo radicales y pequeñas moléculas.

Cuando la foto-excitación de la AcAc se realiza con una longitud de onda de 193 nm la fragmentación ocurre desde la configuración del estado fundamental o desde un estado repulsivo σ^* y no desde el estado de triplete T_1 . Sin embargo mecanismos de reacción tales como el I.1 y el I.2 son confirmados experimentalmente.²⁰

En este trabajo, al introducir la molécula de AcAc en la matriz de pH_2 los mecanismos de reacción son mucho más complejos que los propuestos en las ecuaciones (I.1, I.2, I.3). Además de las bandas que pertenecen a los isómeros de la AcAc, un gran número de bandas aparecen desde el inicio de la irradiación, mientras otras aparecen solo después de un largo período de iluminación con el láser. Los foto-fragmentos pueden reaccionar entre ellos o foto-reaccionar en las sucesivas irradiaciones a 193 nm.

Varios mecanismos de reacción pueden ser propuestos y confirmados por la data experimental para dar explicación a la formación de radicales y moléculas estables luego de la irradiación. Algunos de los fragmentos encontrados en el espectro corresponden a mecanismos de reacción que parten de las ecuaciones I.1, I.2 y/o I.3 y son los llamados “primeros productos” tales como el Propino ($CH_3-C=CH$), el monóxido de carbono (CO) y el radical CH_3 . La formación de otras moléculas dependen de procesos secundarios como la formación del H_2O y CH_4 . Este último a partir de la reacción:



seguida de la reacción¹⁴⁰:



Experimentos similares fueron realizados utilizando nD_2 como matriz. La aparición en el espectro de bandas asignadas a CH_3D , CH_2D_2 , CHD_3 y CD_4 confirman la complejidad del proceso y la posibilidad de algunos radicales de reaccionar con las moléculas de H_2 o D_2 .

Mecanismos más complejos de reacciones sucesivas como la fotólisis del acetileno o el propino, explican la formación de hidrocarburos como C_2H_2 , C_2H_4 y C_2H_6 . La formación de complejos de C_2H_2 es también confirmada por la presencia de bandas características en el espectro IR. Los complejos de C_2H_2 absorben la longitud de onda de 193nm y reaccionan para formar moléculas de C_3 . Estas moléculas también son encontradas en el espectro de absorción.

En los experimentos se observa claramente que la cantidad de moléculas de C_2H_4 es considerablemente mayor a otras, por ejemplo C_2H_6 . No existe evidencia de fotólisis del C_2H_4 o el C_2H_6 en la literatura, lo que lleva a pensar que el mecanismo de formación de C_2H_4 es más eficiente que el mecanismo de formación de C_2H_6 .

El radical HCO es también encontrado en el espectro; esto parece ser debido a la reacción del CO con los átomos de hidrógeno que a su vez son productos de reacciones similares a I.4 y que pueden

difundirse libremente por la matriz de pH_2 . La reacción de este radical con otro átomo de hidrógeno da lugar a la formación de la molécula de formaldehído (H_2CO). Otros radicales como $CCCO$ y $HCCCO$ fueron encontrados en el espectro de absorción IR luego de irradiar la matriz. Para la formación de estos radicales no se ha encontrado explicación con la data experimental que se dispone.

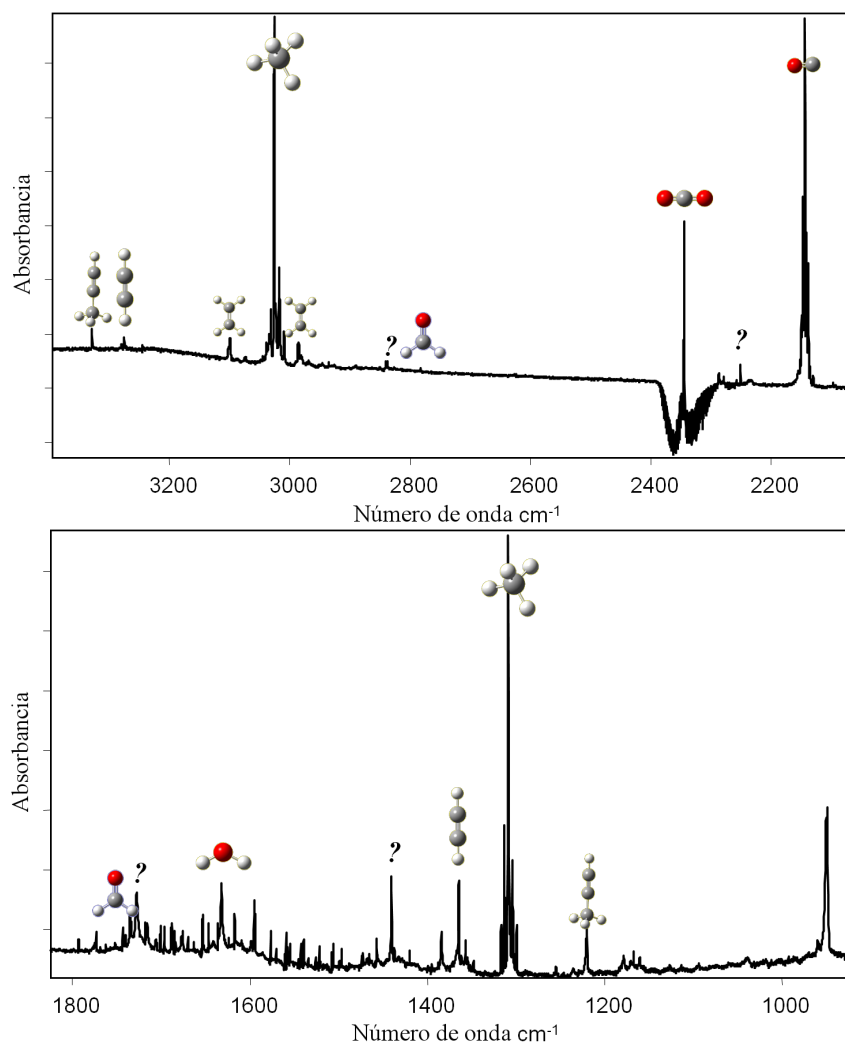


Figura I.8: Espectros infrarrojos de la molécula de AcAc aislada en matrices de pH_2 luego de un largo período de irradiación con una longitud de onda de 193 nm. Algunas de las moléculas encontradas después de la irradiación se representan con su imagen sobre las posiciones de sus bandas más intensas.

La figura I.8 muestra dos regiones del espectro infrarrojo de la molécula de AcAc aislada en matrices de pH_2 luego de un largo período de irradiación con un láser UV de longitud de onda de 193 nm. En este momento no queda rastro de alguno de los isómeros de la AcAc. Algunas moléculas asignadas luego de la irradiación están representadas por su imagen sobre la posición de sus bandas más intensas. Ellas son: el agua (H_2O), el monóxido de carbono (CO), el formaldehído (CH_2O), el metanol (CH_4),

el acetileno (C_2H_2), el etileno (C_2H_2) y el propino ($CH_3-C=CH$). Los símbolos de interrogación (?) representan alguna de las bandas que no pudieron ser asignadas.

Al final, muchas otras bandas fueron encontradas en los espectros IR producto de la irradiación y no se han podido asignar a ninguna molécula o radical. Sin embargo un estudio cinético muy sencillo logra agrupar algunas de estas bandas en tres grupos. Eso significa que además de todas las moléculas y radicales asignados se forman al menos otros tres elementos.

Conclusiones

La estructura, fotoquímica, dinámica y fotodinámica bajo irradiación con 266nm, 248 nm y 193 nm de la molécula de Acetilacetona (AcAc) aislada en matrices de hidrógeno han sido estudiadas con técnicas de espectroscopía de absorción infrarroja. Dos tautómeros de AcAc (AcAc en forma quelato enólica y cetónica) coexisten a bajas temperaturas en matrices de hidrógeno molecular y deuterio molecular. La relación ceto/enol R_{ke} es significativamente mayor en matrices de pH_2 ($\sim 4.5\%$) comparadas con los otros sólidos estudiados. Esto parece ser una característica distintiva de estos sólidos cuánticos.

El espectro infrarrojo (IR) de la AcAc en pH_2 , en el momento de la deposición de la matriz, muestra que muchas de las bandas de absorción de la forma quelato enólica son muy anchas, con anchos similares a cuando la molécula es aislada en matrices de gases nobles o nitrógeno. El ensanchamiento de las bandas es un efecto provocado por el fuerte enlace por puente de hidrógeno intramolecular que presenta la molécula de AcAc en su forma quelato enólica.

Los cálculos teóricos de la forma quelato enólica de la AcAc en las dos simetrías (C_s y C_{2v}) fueron comparados con el espectro IR de esta molécula aislada en matrices de pH_2 . El análisis del espectro vibracional muestra una buena concordancia con los de las frecuencias de los diferentes modos de vibración en la se incluyen correcciones anarmónicas a dichas frecuencias. Se confirma la simetría C_s para la forma quelato enólica de la AcAc. Los cálculos que incluyen las correcciones anarmónicas muestran además la gran influencia del enlace por puente de hidrógeno intramolecular en algunos modos vibracionales.

La fotoquímica de los isómeros de la forma quelato enólica de la AcAc (CCC) también fue estudiada. La excitación de la AcAc hasta el nivel S_2 fue investigada usando dos longitudes de ondas diferentes: 266 nm y 248 nm. La excitación usando la longitud de onda de 266 nm conduce principalmente a la isomerización hacia otras formas enólicas de la AcAc. Los foto-productos fueron identificados como conformeros no quelatos de la forma enólica del AcAc. La identificación se realizó con ayuda del espectro IR experimental, comparando con cálculos teóricos de las frecuencias IR de los diferentes isómeros, utilizando la aproximación armónica y las correcciones anarmónicas a las frecuencias. A diferencia del

caso de la forma quelato enólica, el espectro de los isómeros “abiertos” (formas ceto-enólicas en las que no hay enlace por puente de hidrógeno intramolecular) muestra bandas mucho más finas.

El carácter poco perturbativo de la molécula de pH_2 en el sólido permitió encontrar un nuevo isómero (TTC) en el espectro IR luego de la irradiación de la muestra con luz UV. En otras matrices tales como nH_2 y nD_2 en las que se formaron los mismos isómeros (CTC, TCC y TTC) que en la matriz de pH_2 y se pudo encontrar además otro isómero: TCT. El hecho de poder asignar bandas asociadas a la presencia de este nuevo isómero sugiere que la transformación desde TCT \rightarrow TCC por efecto túnel que tiene lugar en las matrices de pH_2 es bloqueada en sistemas donde las interacciones son más fuertes como la matriz de nH_2 . El hecho de bloquear procesos por efecto túnel en matrices de nH_2 y no así en matrices de pH_2 podría ser un efecto general.

La fragmentación de la molécula de AcAc atrapada en matrices cuando es irradiada con un láser con longitud de onda de 266nm es ineficiente. Ni el radical OH, ni otros productos correspondientes al rompimiento de un enlace simple han sido detectados en el espectro IR. Por el contrario fue detectada una pequeña cantidad de monóxido de carbono. Para la formación de esta molécula se necesita de una reorganización drástica de los enlaces durante el proceso de irradiación. Su aparición, luego de un largo período de irradiación, permite concluir que la isomerización de la forma quelato enólica hacia formas enólicas abiertas no proviene de procesos de disociación/recombinación. Por su parte, la excitación usando una longitud de onda de 248 nm conduce a la formación de las mismas formas enólicas abiertas que cuando se usa 266nm. La irradiación prolongada usando la longitud de onda de 248 nm hace que desaparezcan estas formas enólicas abiertas y que se incremente la forma cetónica de la AcAc. La fragmentación en este caso sí es un proceso importante. La velocidad de crecimiento de las bandas asignadas a CO es muy similar a las de la forma cetónica lo que sugiere que esta forma cetónica sí podría ser formada en procesos de disociación/recombinación, incluso en pH_2 .

La longitud de onda de 193 nm excita la molécula de AcAc hasta un estado S_3 . Durante la irradiación de la muestra usando esta longitud de onda se forman tanto los isómeros enólicos abiertos como la forma cetónica. Estos se comportan como estados intermedios para futuras reacciones. A diferencia con los resultados obtenidos en la fase gaseosa, el radical OH no pudo ser detectado en la matriz. Sin embargo las bandas asignadas a la molécula de H_2O crecieron durante la irradiación de la muestra. En los experimentos se pone en evidencia la reacción de algunos radicales con la molécula de H_2 de la matriz para formar otros radicales o especies estables. Con el objetivo de confirmar estas reacciones con las moléculas de H_2 se realizaron experimentos en los que se usó nD_2 como matriz. La presencia de moléculas estables deuteradas como es el caso de CH_2D_2 confirman la ocurrencia de las mencionadas reacciones.

El aparato experimental utilizado para realizar estos experimentos no permite mantener la muestra bajo estudio por mucho tiempo. Otros experimentos deben ser realizados con el objetivo de poder

alcanzar las condiciones estacionarias del proceso de irradiación. Esto permitiría una mejor comprensión de los mecanismos de reacción así como separar los productos finales de la irradiación de los productos intermedios. Por otro lado, algunas reacciones parecen ser dependientes del arribo de un segundo fotón para que puedan tener lugar. Un ejemplo es la reacción del radical CH_3 con la molécula de H_2 . Algunos experimentos deberán ser realizados utilizando el láser con una potencia menor para un mejor entendimiento de estos procesos.

El efecto caja muy reducido que muestran las matrices de pH_2 ha permitido aislar radicales tales como CH_3 , HCO , HCCO luego de una irradiación *in situ* de la molécula de AcAc usando longitudes de onda de 248 y 193 nm. Otras moléculas estables también fueron detectadas luego de la irradiación poniendo en evidencia la reactividad de estos radicales con la molécula de H_2 de la matriz. La estructura rotacional que presenta el espectro de la molécula de CH_4 es una prueba de su presencia en la matriz como resultado de las reacciones foto-inducidas del CH_3 con H_2 .

El pH_2 como solvente en las técnicas MIS preserva las propiedades dinámicas intrínsecas de las moléculas soluto tales como los movimientos de gran amplitud que tienen lugar en la molécula de AcAc en su forma quelato enólica. Matrices “clásicas” como el Ne bloquean, por ejemplo, los movimientos de torsión de los grupos CH_3 de la molécula de AcAc . Por su lado, el sólido de pH_2 preserva estos movimientos de torsión y revela un nuevo comportamiento del espectro vibracional que está directamente relacionado con la dinámica compleja entre la transferencia de protón intramolecular y la rotación de los dos grupos metilos de la AcAc . Teniendo en cuenta los átomos de hidrógeno de estos grupos metilos existen varios conformeros de espín de la forma quelato enólica de AcAc . Los la data experimental reportada en este trabajo es una evidencia de la presencia de estos conformeros.

Fueron presentadas evidencias experimentales de la relación que existe entre la transferencia de protón por efecto túnel y el grupo metilo casi libre y su influencia en la conversión del espín nuclear del grupo metilo. El análisis de la data experimental revela que la transferencia de protón es mediada por la torsión del grupo metilo casi libre. Esto se puso en evidencia durante el análisis del proceso de conversión del espín nuclear del grupo metilo en el cual pudieron separarse dos espectros IR correspondientes al estado vibracional fundamental de la especie más estable (ms) y el estado torsional excitado de la forma quelato enólica de la AcAc (menos estable (ls)).

Las matrices de pH_2 pueden ser usadas para estudiar los efectos de solvatación en complejos débilmente enlazados así como sistemas moleculares que tienen movimientos de gran amplitud acoplados. El presente trabajo es un modelo de estudio en el que se muestra que el proceso de conversión del espín nuclear puede ser una herramienta dedicada a la investigación espectroscópica de especies moleculares que transportan energías en las rotaciones internas de los grupos metilos. Para la AcAc aislada en matrices de pH_2 se muestra, con una mínima influencia de la matriz, qué modo vibracional está acoplado a la promoción de la transferencia de protón en forma concertada. Las posiciones y los anchos

de las bandas del espectro IR, teniendo la información necesaria de las propiedades intrínsecas de la molécula, ofrecen información cuantitativa de partida a futuros cálculos del proceso de transferencia de protón interna. Esto será ciertamente un verdadero pero realizable reto ya que deberán considerarse los modos de torsión de los dos grupos metilos y de deformación del pseudo anillo a lo largo de la coordenada de la transferencia de protón que provoca un cambio simultáneo de la configuración electrónica del sistema. Además de todas las ventajas desde el punto de vista espectroscópico de los sólidos de pH_2 expuestas en este trabajo, la fotoquímica de moléculas atrapadas en pH_2 tiene además interés astrofísico: las reacciones químicas de moléculas o radicales con la molécula de H_2 que pueden tener lugar en el espacio interestelar pueden ser controladas y estudiadas en estos sistemas criogénicos.

Otros cálculos teóricos de este sistema deberán realizarse para un mejor entendimiento de los procesos que han sido descritos. Cálculos de la molécula de AcAc rodeada de moléculas de pH_2 podrían explicar los sitios ocupados por esta en la matriz y la deformación que sufre la matriz debido a su presencia en su seno. Simulaciones de la dinámica de los procesos pueden proveer más información sobre los estados intermedios en la isomerización desde la forma quelato enólica del AcAc hacia las formas enólicas abiertas, así como la tautomerización y la fragmentación cuando la molécula es excitada al estado S_2 o S_3 . Estas dinámicas simuladas pueden ser un elemento concluyente respecto a si isomerización hacia las formas enólicas abiertas es un proceso de disociación/recombinación o se debe a rotaciones alrededor de los enlaces moleculares del anillo central. Además podría dilucidarse por qué los isómeros del tipo XYT no se estabilizan en las matrices de pH_2 y si pueden encontrarse en matrices donde las interacciones son más fuertes como el nH_2 . La influencia de la matriz en el espectro IR podría también ser explicado.

II

Résumé en Français

Introduction

La dynamique moléculaire et la photodynamique des processus moléculaires donnent accès aux informations sur des processus élémentaires tels que le transfert d'énergie ou la réactivité chimique. La photochimie, cas particulier de photodynamique, est l'étude de réactions chimiques initiées par absorption de photons permettant à la molécule d'atteindre l'"énergie d'activation" de la réaction. L'absorption de photons peut également modifier la configuration électronique de la molécule, donnant lieu à de nouveaux canaux de réaction non accessibles à l'état fondamental.

En utilisant un laser comme source de photons, il est possible d'exciter une molécule dans un état électronique et/ou vibrationnel bien défini. De même, l'émission à partir d'un état particulier peut être mesurée et on peut alors estimer la population de cet état. Pour un système moléculaire en phase gazeuse à basse pression, la distribution d'énergie des produits peut être observée avant que le système atteigne l'équilibre produit par collisions entre molécules. D'un autre côté, dans ce cas, les produits de réaction sont dispersés spatialement et ne restent pas dans la zone d'interaction. En conséquence, les réactions secondaires, comme des recombinaisons, sont peu probables. Par ailleurs, les réactifs et les produits sont en quantité très limitée dans la zone d'observation, ce qui fournit des signaux très faibles en cas de processus inefficaces. En revanche, l'utilisation des matrices cryogéniques permet de travailler avec des concentrations élevées de molécules à étudier ; de plus cette technique offre la possibilité d'étudier plusieurs processus pendant des périodes de temps relativement longues.

La technique de spectroscopie d'isolation en matrice (MIS) est largement utilisée pour analyser des propriétés moléculaires telles que la géométrie et la réactivité des espèces piégées ; elle permet en particulier l'étude d'espèces instables ou d'espèces intermédiaires dans une réaction. La technique MIS a été utilisée depuis 1954 pour piéger les molécules dans un milieu inerte.¹ De nombreuses petites

molécules telles que CO, CO₂, N₂, H₂, O₂, Cl₂, CCl₂, ainsi que les gaz nobles ont été utilisés comme milieu "inerte" pour isoler les molécules qui seront étudiées par des techniques spectroscopiques. L'utilisation de la molécule d'hydrogène (H₂) et en particulier le para-hydrogène (pH₂) présente des avantages spécifiques pour la technique MIS en raison des propriétés "quantiques" du solide. Les interactions entre la matrice et l'impureté sont très faibles, permettant aux espèces étudiées de garder des caractéristiques très proches de celles de la phase gazeuse. Nous avons mis en oeuvre des études photochimiques de molécules et complexes moléculaires présentant des liaisons hydrogène (liaisons H) dans les solides de pH₂ afin de bénéficier des propriétés particulières de ce milieu.

Les liaisons H sont des interactions moléculaires relativement faibles, mais qui jouent un rôle très important dans la réactivité des nombreux systèmes chimiques. Ces liaisons ne devraient être que très faiblement affectées par l'environnement solide de pH₂. Les études dynamiques et en particulier photodynamiques des espèces à liaison H dans ces solides pourront donner des informations pertinentes à l'échelle moléculaire, dans l'étude des effets de solvatation notamment.

Ce travail est dédié à l'étude d'une petite molécule organique présentant une liaison hydrogène interne : l'acétylacétone (AcAc). AcAc est une β -dicétone qui appartient à un groupe bien connu de composés tautomères largement utilisés en chimie organique et inorganique. Depuis de nombreuses années, les structures des formes cétone et énol (voir figure II.1) de AcAc ainsi que la nature de la forte liaison H intramoléculaire O–H \cdots O de la forme énol ont fait l'objet d'études approfondies utilisant une variété de méthodes différentes qui incluent les techniques IR, Raman, micro-ondes et autres.²⁻¹⁰

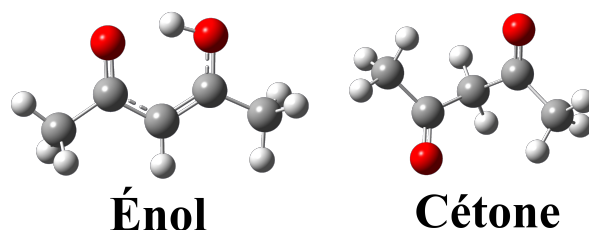


Figure II.1: Formes énol et cétone de AcAc.

L'intérêt croissant pour les composés à courte (forte) liaison d'hydrogène, comprenant les formes énols chélatés de β -dicétones, est lié à l'étude du transfert de proton d'un atome d'oxygène à l'autre le long de la liaison hydrogène. Ce processus est une des réactions les plus générales et les plus importantes en chimie. Le transfert de proton joue un rôle crucial dans nombreux processus tels que la neutralisation de réactions acide-base, l'addition électrophile, etc...¹¹ Il a également une grande importance en catalyse et dans plusieurs processus biochimiques, allant de réactions enzymatiques jusqu'à l'interconversion tautomère de bases de l'ADN.¹² AcAc est l'une des plus simples β -dicétones

présentant un transfert de proton intramoléculaire entre deux atomes d'oxygène dans sa forme énol,² ce qui en fait un système modèle pour l'étude de ce phénomène.¹³

Une attention particulière a été portée aux caractéristiques structurales des tautomères d'AcAc et au processus de tautomérisation en lui-même. L'équilibre cétone/énol dans différents milieux a été étudié pendant de nombreuses années. Ces travaux montrent que l'équilibre entre les formes énol et cétone d'AcAc dépend fortement des conditions et des caractéristiques du milieu environnant.¹⁴⁻¹⁷ Il est généralement admis qu'à des températures modérées, la forme énol prédomine, que ce soit en phase gazeuse ou en phase liquide.¹⁷⁻¹⁹

Les processus photoinduits sur la molécule d'AcAc dûs à l'irradiation avec de la lumière ultraviolette (UV) (tels que l'isomérisation, la tautomérisation et la fragmentation) ont également fait l'objet d'études à la fois expérimentales et théoriques.^{2,20,21} En phase gazeuse, l'irradiation de cette molécule conduit à une fragmentation qui libère le radical OH.²⁰ Lorsque AcAc est isolée en matrice cryogénique de gaz noble ou d'azote, une irradiation UV conduit principalement à la formation d'isomères.^{2,22,23}

Avec la technique MIS, il est extrêmement utile de se servir de la spectroscopie infrarouge (IR) comme diagnostic. En raison de la basse température ($< 70\text{K}$) ne sont peuplés que les niveaux de vibration et de rotation moléculaires les plus bas. Dans la matrice, les réactions chimiques peuvent être suivies et contrôlées dans une large mesure.²⁴⁻²⁶

Les matrices d'hydrogène, en particulier de pH_2 , constituent un milieu très intéressant pour les applications de la technique MIS.²⁷ En raison des conditions de symétrie qui doit remplir la fonction d'onde totale de la molécule d'hydrogène (H_2), la molécule existe sous deux formes dans la nature.²⁸ La molécule H_2 ayant un spin nucléaire nul ($I=0$) est appelée para-hydrogène (pH_2) et elle a un nombre quantique rotationnel J pair, alors que lorsque $I=1$, la molécule est appelée ortho-hydrogène (oH_2) et ses nombres J sont impairs. A la température ambiante, l'équilibre entre les populations de oH_2 et pH_2 donne un rapport de 3 :1. L'interconversion entre les deux états de spin ($I=0$, $I=1$) pour une molécule isolée est interdite par les règles de sélection de la mécanique quantique. Les niveaux rotationnels de la molécule de H_2 sont très éloignés en énergie les uns des autres (la transition $J=0 \rightarrow J=2$ est à 354.38 cm^{-1} et $J=1 \rightarrow J=3$ est à 587.06 cm^{-1}). A basse température ($< 20\text{K}$), seuls les niveaux $J=0$ et $J=1$ sont donc peuplés. Une molécule à l'état $J=1$ est maintenue métastable à ce niveau en raison d'une conversion vers le niveau $J=0$ extrêmement lente en l'absence de champ magnétique externe.^{28,29}

La fonction d'onde rotationnelle de H_2 dans l'état $J=0$ a une symétrie sphérique. La molécule pH_2 n'a pas de moment électrostatique permanent de tout ordre. Par conséquent, le cristal de pH_2 ($T=6\text{K}$) fournit un milieu totalement homogène pour une molécule piégée à l'intérieur. Ce solide a une structure cristallographique hcp. Ses propriétés quantiques viennent d'un déplacement "de point zéro" de la molécule de l'ordre de 20% de la distance entre plus proches voisins, ce qui rend la matrice

très "molle". Cette caractéristique liée au grand mouvement de point zéro minimise les imperfections qui peuvent exister autour de la molécule étudiée.

Grâce aux spécificités du solide de pH_2 , le spectre IR de petites molécules piégées à l'intérieur montre des bandes étonnamment fines associées aux états ro-vibrationnels de la molécule.^{11,31-33} De plus, la matrice de pH_2 est utile pour l'étude des réactions chimiques aux températures cryogéniques. Comme l'effet de cage est réduit au minimum, les produits primaires d'une réaction chimique, par exemple, devraient être plus similaires à ceux obtenus dans la phase gazeuse que dans d'autres matrices cryogéniques. C'est un avantage pour l'étude des réactions photochimiques en phase condensée.^{30,34,35} Dans les matrices de gaz rares, la photolyse *in situ* est fortement influencée par la cage matricielle, car dans la plupart des cas, les espèces résultant du processus de photolyse ne peuvent pas s'échapper de cette cage. En revanche, les photofragments produits dans le solide de pH_2 peuvent se séparer facilement en utilisant l'énergie en excès produite dans la photodissociation en raison de cet effet de cage minimal. La recombinaison *in situ* des photofragments est moins probable, ce qui permet à des réactions secondaires des photofragments d'avoir lieu pendant ou après la photolyse. Dans tous les cas, la mesure d'un spectre peut se faire après la photolyse sur une longue période de temps, ce qui permet l'observation de réactions plus lentes, après photolyse, ainsi que la détection de quantités faibles de photoproduits.³⁰

Cet travail porte sur la photodynamique de la molécule de AcAc isolée dans des matrices de pH_2 . La molécule est caractérisée par spectroscopie IR. On observe dans le spectre des bandes attribuées à la forme énol chélatée et à la forme cétone de AcAc. La photochimie de cette molécule est étudiée en utilisant trois lasers UV de longueurs d'onde différentes : 266 nm, 248 nm et 193 nm. Sous ces trois irradiations, la molécule AcAc peut être excitée dans deux états électroniques différents. L'état S_2 est atteint à 266nm et à 248nm, alors qu'avec la longueur d'onde d'irradiation 193 nm, la molécule est excitée dans l'état électronique S_3 .

II.1 Dispositif expérimental

Le para-hydrogène (pH_2) est obtenu par conversion ortho-para de l'hydrogène gazeux dans un convertisseur placé dans un cryostat. Le convertisseur est constitué d'un bloc de cuivre avec une cavité cylindrique remplie d'oxyde ferrique (Fe_2O_3), maintenu à des températures proches de 19K. Fe_2O_3 joue le rôle de catalyseur pour la conversion de l'hydrogène normal (nH_2) en pH_2 . Le convertisseur est rempli avec nH_2 , qui vient en contact avec le catalyseur et on maintient ce contact pendant 1h30. Dans ces conditions, pH_2 est obtenu avec une pureté d'au moins 99,9%. Pour les expériences complémentaires avec l'hydrogène normal (nH_2), le deutérium normal (nD_2) et le néon (Ne), les gaz passent simplement au travers du convertisseur à 19K (nH_2 et nD_2) ou 40K (Ne) avant leur dépôt pour former la matrice.

AcAc et les gaz constituant la matrice arrivent dans l'enceinte d'un second cryostat par deux tubes différents. Ces gaz se déposent sur une fenêtre de diamant qui a été refroidie à 4,2 K. AcAc a été conservée dans un bain de glace à 0 °c avant le dépôt, afin de diminuer sa pression de vapeur et de maintenir des conditions reproductibles d'une expérience à l'autre. Le flux des gaz est régulé par l'ouverture fine de vannes à pointeau, cela permet un meilleur contrôle de la concentration d'AcAc dans la matrice. Le rapport AcAc /solvant a été estimé à partir du spectre infrarouge de la matrice formée. Il varie entre 1 :500 et 1 :1000 selon les expériences.

Le spectre IR est mesuré entre 700 et 5000 cm^{-1} à l'aide d'un spectromètre infrarouge à transformée de Fourier (Nicolet) avec des résolutions de 0,5 cm^{-1} et de 0,125 cm^{-1} . La région traversée par le faisceau IR a été purgée avec de l'air sec. Les trois lasers ultraviolets utilisés pour irradier l'échantillon sont : la quatrième harmonique d'un laser Nd : YAG fournissant une longueur d'onde de 266 nm, un laser excimère KrF à 248 nm et un autre laser excimère ArF à 193 nm. L'énergie typique des impulsions laser est de 10 mJ à 10 Hz et les temps d'irradiation varient de quelques minutes à 10 heures.

II.2 Spectroscopie infrarouge de l'acétylacétone

Les structures des formes énol chélaté et cétone d'AcAc ont été calculées et optimisées en utilisant la méthode de la théorie de la fonctionnelle de densité (DFT) B3LYP avec la base 6-311++G(3df, 3pd). Les fréquences de ces formes ont été calculées par la même méthode dans l'approximation harmonique et en incluant des corrections anharmoniques. La figure II.2 montre le spectre infrarouge de la molécule AcAc isolée dans différentes matrices : (a) pH_2 , (b) nH_2 , (c) nD_2 et (d) Ne. Les (*) représentent les bandes attribuées aux molécules d'eau piégées dans la matrice. Les bandes attribuées à la forme cétone sont marquées par la lettre (k). Le reste des bandes correspond à la forme énol chélaté. L'attribution des bandes dans le spectre a été réalisée par comparaison avec les spectres simulés. Les simulations incluant les corrections anharmoniques se sont avérées en meilleur accord avec les données expérimentales.

D'après différents travaux antérieurs, la structure géométrique de la forme énol chélaté de AcAc pourrait être de symétrie C_{2v} ou C_s . La structure de cette forme a donc été calculée dans les deux symétries. La comparaison directe avec le spectre expérimental confirme la symétrie C_s pour AcAc dans sa forme énol chélaté. D'après les données expérimentales et avec l'aide des calculs théoriques, le rapport de concentrations cétone/énol (R_{ke}) a été estimé dans les différentes matrices et il s'avère que la valeur la plus élevée correspond à la matrice de pH_2 . Dans les matrices de néon (voir la figure II.2 (d)), le spectre est très similaire à celui rapporté dans la littérature,^{50,106} et R_{ke} est estimé entre 1 et 1,5%. Dans les matrices de nH_2 et nD_2 , R_{ke} prend des valeurs intermédiaires entre celles de Ne

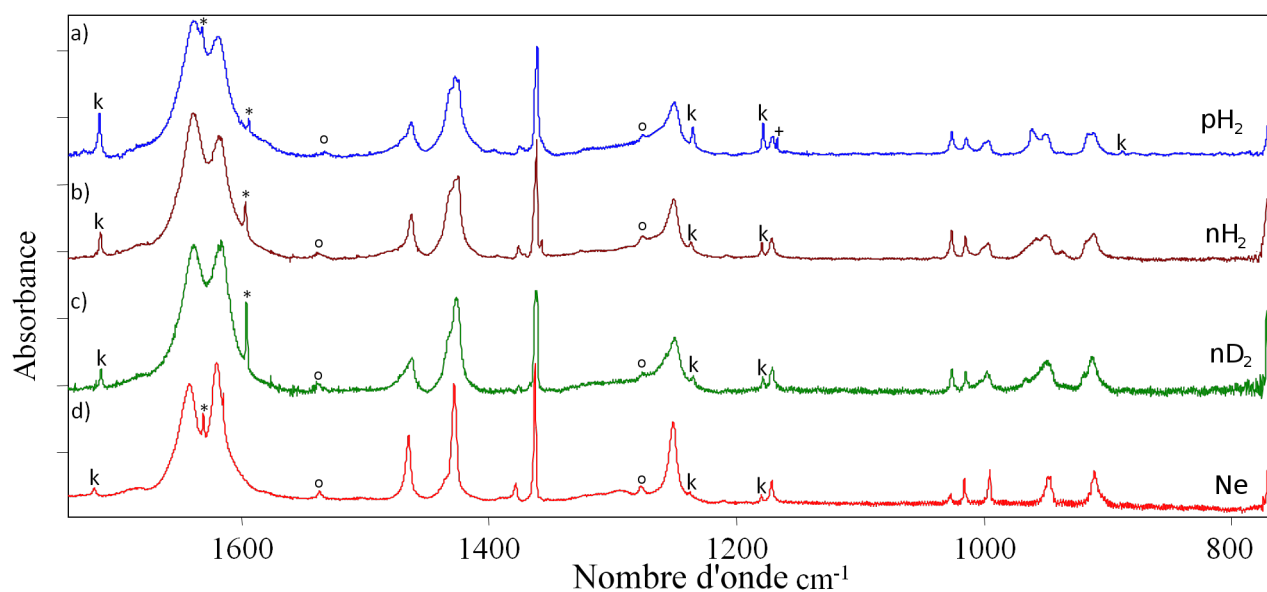


Figure II.2: Spectres IR de AcAc dans différentes matrices : (a) pH_2 , (b) nH_2 , (c) nD_2 et (d) Ne. les bandes correspondant à la forme cétone sont marquées avec un (k). Les (*) se rapportent aux bandes correspondant à la molécule de H_2O et les marques (o) se réfèrent aux harmoniques de quelques bandes.

et de pH_2 ($R_{ke} \sim 2\%$). Pour la matrice de pH_2 , cette valeur est estimée à $\sim 4,5\%$. L'abondance de la forme cétone en matrice de pH_2 est en bon accord avec les valeurs rapportées dans la littérature en phase gazeuse à 298K (entre 2,5%⁵¹ et 6,7%⁵³). La composition de la phase gazeuse semble gelée lors du dépôt dans le solide de pH_2 .

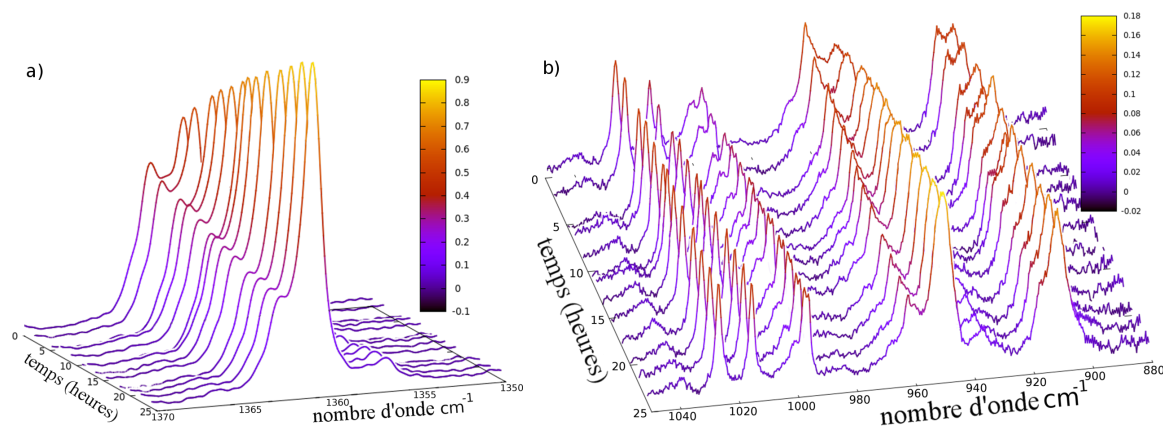


Figure II.3: Evolution temporelle du spectre de AcAc isolée dans pH_2 lorsque l'échantillon est maintenu dans l'obscurité. (a) région $1350-1370\text{ cm}^{-1}$ (b) région $880-1050\text{ cm}^{-1}$.

Le spectre de AcAc en matrice d'hydrogène est plus structuré qu'en matrice de néon (doublets particulièrement visibles dans la région $900-1100\text{ cm}^{-1}$). Aucune évolution de ces structures n'est

observée après recuit de la matrice, ces structures sont difficilement attribuables à des effets de sites. Les effets de site dans la matrice de pH_2 sont beaucoup moins importants que dans d'autres matrices et expérimentalement imperceptibles. Afin d'élucider la cause de ces structures, l'échantillon a été maintenu à froid dans l'obscurité pendant 24 heures. L'évolution temporelle des spectres est décrite dans la figure II.3. On observe au fil du temps la diminution en intensité d'un groupe de bandes, tandis qu'un autre groupe augmente en intensité progressivement. Il a été ainsi possible de décrire les spectres sous forme de deux contributions, correspondant à la présence d'au moins deux espèces de forme énol chélaté de AcAc, l'une appelée la "plus stable (ms)" et l'autre la "moins stable (ls)". Les valeurs des intensités intégrées des deux contributions ont été tracées en fonction du temps. Leurs évolutions ont été ajustées par des fonctions exponentielles, l'une croissante et l'autre décroissante respectivement. La constante de temps qu'on en déduit, similaire pour les deux fonctions, est de l'ordre de $0.042h^{-1}$, valeur du même ordre de grandeur que la constante de temps correspondant à des processus de conversion de spin nucléaire dans des molécules contenant un groupe méthyle isolées dans pH_2 .^{32,113}

Le caractère peu perturbateur de la matrice de pH_2 sur les rotations du groupe méthyle a été montré dans l'étude de petites molécules ayant un seul groupe méthyle (méthanol,³² CH_3F ¹¹³). Le spin nucléaire d'un groupe méthyle est couplé à sa rotation (ou torsion) pour des raisons de symétrie. Le niveau de symétrie A est associé à la fonction d'onde de spin totalement symétrique ($I = 3/2$) alors que celui de symétrie E est associé à la fonction d'onde non-symétrique ($I = 1/2$). Par conséquent, le transfert de population de E à A implique une conversion de spin nucléaire, ce qui est un processus très lent par rapport à la thermalisation.¹¹⁸ Dans le cas d'une différence d'énergie importante entre les états A et E (rotation pratiquement libre du groupe méthyle), la population des états A et E différera alors de la distribution de Boltzmann à la température de la matrice (4K) immédiatement après le dépôt de la molécule dans la matrice de pH_2 . En fait, c'est la conversion lente de spin nucléaire de AcAc isolée dans le solide pH_2 qui est observée à travers l'évolution dans le temps du spectre d'absorption IR. Dans AcAc, les méthyles sont en positions décalées l'un par rapport à l'autre. Le transfert de proton implique donc une rotation des deux méthyles. Les deux spectres obtenus ("ms" et "ls") peuvent alors être utilisés pour comparer la dynamique de différents modes vibrationnels de pliage et d'étirement suivant l'état de torsion du groupe méthyle et en déduire quels sont les modes les plus couplés au transfert de proton. Un point très important ici est que l'énergie supplémentaire déposée dans le niveau de torsion n'est pas suffisante pour vaincre la barrière du transfert de proton. Toutefois, l'énergie de ce niveau est déposée d'une manière qui aide au déclenchement de la réaction, les torsions des méthyles étant fortement couplées au transfert de proton.

II.3 Irradiation dans l'ultra-violet

L'irradiation de l'Acétylacétone (AcAc) dans une matrice de pH_2 par différents lasers UV provoque des isomérisations et fragmentations qui dépendent des longueurs d'onde utilisées. Nous allons d'abord discuter de l'évolution de l'échantillon lorsqu'il est exposé à un faisceau de longueur d'onde de 266 nm, puis quand il est soumis à une de longueur d'onde de 248 nm. Dans les deux cas, la molécule est excitée jusqu'à le niveau électronique S_2 . Enfin, nous discuterons des processus qui se déroulent dans la matrice lorsque la molécule est excitée à l'état S_3 en utilisant une longueur d'onde de 193nm.

II.3.1 Irradiation avec une longueur d'onde de 266nm

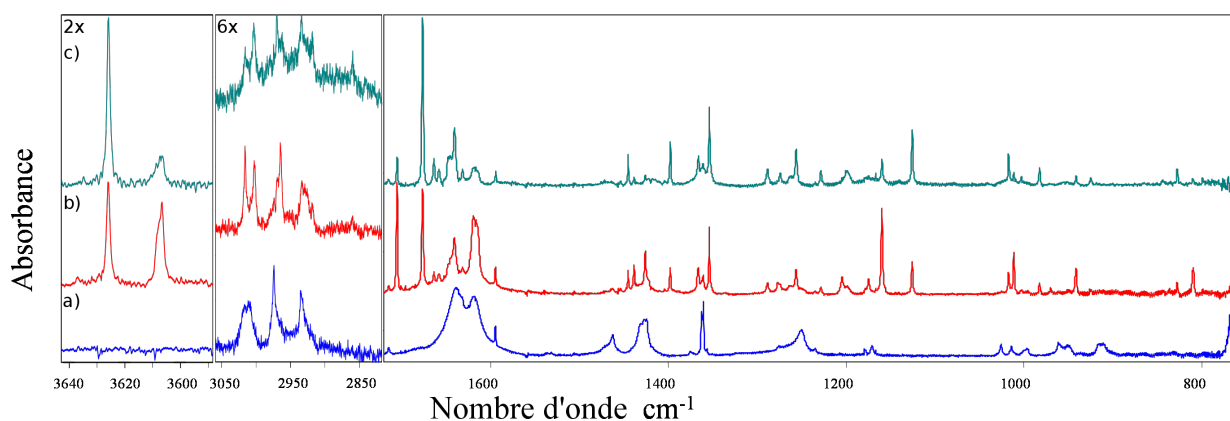


Figure II.4: Spectres IR de AcAc isolée dans une matrice de pH_2 à différents temps d'irradiation laser à 266 nm. (A) juste après le dépôt de la matrice. (B) A un temps intermédiaire (~ 40 min), la quantité d'isomère CTC est à son maximum. (C) Après une longue période d'irradiation (~ 300 min), on observe principalement les bandes attribuées aux isomères TCC et TTC

Lors de l'irradiation de la matrice avec un laser à 266nm, l'Acétylacétone présente initialement dans sa forme énol chélatée (ci-après CCC) disparaît progressivement en donnant de nouvelles espèces. Au cours de l'irradiation, ces dernières présentent des évolutions temporelles différentes. Elles sont caractérisées par leur spectre IR et peuvent être séparées en deux groupes. Le premier contient des espèces dont les concentrations augmentent puis diminuent au cours du temps, alors que celles du deuxième augmentent continuellement lors de l'irradiation. Les contributions de ces deux groupes dans le spectre IR peuvent être séparées par soustractions successives de spectres à différents temps d'irradiation. De cette manière, on obtient les spectres de chaque groupe.

La figure II.4 montre les spectres de AcAc piégée dans une matrice de pH_2 pour trois temps d'irradiation différents. Le spectre en (a) a été pris juste après le dépôt de la matrice. On observe les bandes attribuées à la forme CCC. Celui en (b) montre le spectre pris à un temps intermédiaire

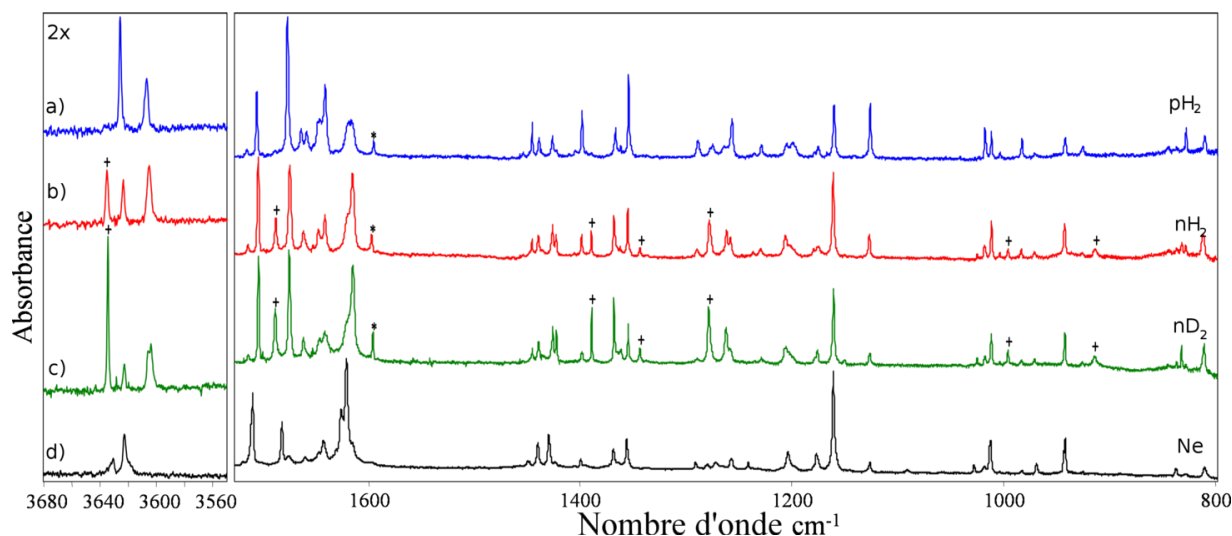


Figure II.5: Comparaison des spectres de AcAc isolée dans différentes matrices après irradiation avec un laser à 266nm. (a) pH_2 , (b) nH_2 , (c) et nD_2 (d) Ne. Les bandes attribuées à l'isomère TCT sont marquées d'un (+)

(~ 40 min) alors que (c) correspond à une longue période d'irradiation (~ 300 min). Les nouvelles bandes d'absorption sont plus fines (largeur de bande de ~ 2 cm^{-1}) que celles de CCC indiquant une ouverture de la liaison hydrogène. Elles ne sont pas modifiées en l'absence d'irradiation par laser UV. L'apparition de nouveaux produits est bien due à cette irradiation UV. Afin d'identifier les nouveaux produits, les géométries des différents isomères de la forme énol de AcAc ont été optimisées et les fréquences infrarouges ont été calculées. L'anharmonicité a été prise en compte. Une méthode DFT B3LYP avec une base 6-311++G(3df, 3pd) a été utilisée. Par comparaison des spectres simulés avec les spectres expérimentaux, il a été possible d'attribuer les produits à des isomères de AcAc. Le premier groupe correspond à l'isomère CTC, le deuxième aux isomères TCC et TTC. Les isomères de type XYT qui ne diffèrent de XYC que par la rotation du groupe OH autour de la liaison C-O n'ont pas été observés dans la matrice de pH_2 . Ils sont légèrement moins stables et compte tenu des caractéristiques du solide de pH_2 , la barrière à franchir doit être faible. Les isomères XYT peuvent donc s'isomériser vers XYC à travers cette barrière par effet tunnel.

Dans le but de comparer l'effet de la matrice sur les modifications de AcAc, des expériences similaires ont été réalisées en utilisant nH_2 , nD_2 et Ne comme matrices. Une comparaison des spectres après irradiation dans ces différentes matrices est montrée dans la figure II.5. Dans les quatre spectres, les bandes correspondant à la forme CCC ont été soustraites pour une meilleure comparaison. Les spectres en matrice de Ne (figure II.5 (d)) ressemblent à ceux obtenus en matrice de pH_2 (représentée dans la partie (a)), alors que de nouveaux groupes de bandes apparaissent dans les spectres correspondant aux matrices de nH_2 (b) et nD_2 (c). Ces nouveaux groupes sont indiqués par (+) dans la figure II.5.

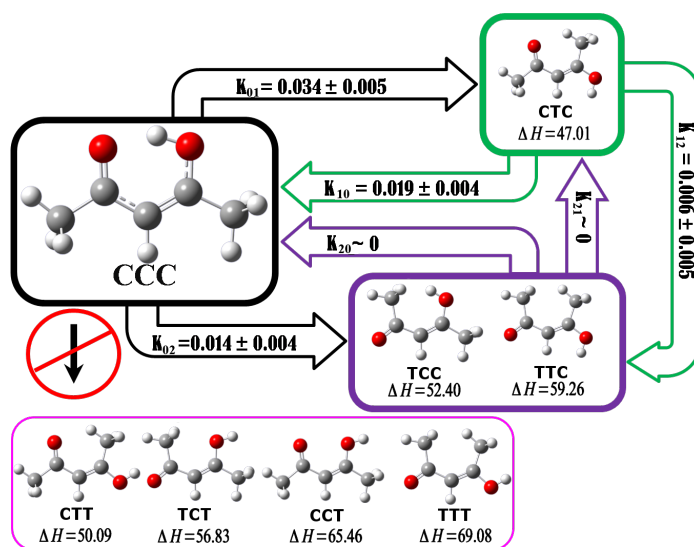


Figure II.6: Diagramme cinétique simplifié du processus d'isomérisation. ΔH [kJ/mol] représente la différence entre l'énergie calculée d'un isomère et la forme CCC de AcAc, en utilisant une méthode DFT(B3LYP/6-311++G(3df, 3pd)). Les valeurs estimées des constantes de vitesse de k_{ij} [min⁻¹] sont données pour nos conditions expérimentales (intensité laser constante à 10 Hz, quelques mJ/impulsion).

En utilisant une analyse similaire à celle qui précède, on peut séparer en deux groupes de bandes. Les nouvelles bandes se trouvent toutes dans le second groupe. Leur intensité augmente au cours du processus d'irradiation. Par comparaison avec les spectres simulés obtenus à partir des calculs ci-dessus et en accordant une attention particulière à la région de la vibration du groupe OH, il est possible d'attribuer ces nouvelles bandes à l'isomère TCT. La possibilité de stabiliser cet isomère dans les matrices de nH₂ et nD₂ et pas dans celle de pH₂ montre que des matrices avec des interactions plus fortes peuvent bloquer la rotation du groupe OH.

Le processus d'irradiation a été suivi en fonction du temps en enregistrant régulièrement des spectres infrarouges. Les variations d'intensités de bandes caractéristiques ont été extraites (1705 cm⁻¹ pour CTC, 1126 cm⁻¹ pour TCC et 1229 cm⁻¹ pour TTC) pour calculer les différentes concentrations. Pour CCC, présent au départ, l'intégrale sur tout le spectre de la forme CCC a été prise. Un modèle simple de cinétique a permis d'estimer les différentes constantes de vitesse. Les isomères formés au cours du processus d'irradiation et les valeurs des constantes de la réaction sont indiqués sur le schéma de la figure II.6. Cette cinétique montre que les deux groupes sont formés à partir de CCC et que seul le premier groupe peut donner un retour vers la forme initiale CCC. Il en résulte à long terme une disparition du premier groupe au profit du second.

II.3.2 Irradiation avec une longueur d'onde de 248 nm

L'irradiation laser à 266nm sur AcAc isolée dans la matrice de pH_2 conduit principalement à l'isomérisation de la forme CCC vers des formes énols ouvertes de AcAc. Dans les études de (Nagashima *et al.*)⁵⁸ on voit que l'irradiation de AcAc avec une longueur d'onde plus courte peut conduire à la tautomérisation de cette molécule en cétone. La fragmentation de la molécule peut également se produire. Afin d'étudier ce phénomène plus en détail, une série d'expériences dans lesquelles AcAc est isolée dans des matrices de pH_2 , nH_2 , nD_2 et de Ne ont été réalisées en irradiant avec une longueur d'onde de 248 nm.

Après dépôt, la matrice est éclairée par un laser excimère à 248 nm (10 mJ d'énergie/impulsion à 10 Hz). L'irradiation est arrêtée pendant la mesure du spectre infrarouge. La figure II.7 montre une comparaison entre deux spectres IR correspondant à deux temps (b et c) d'irradiation de la matrice à une longueur d'onde de 248nm avec un spectre IR obtenu lorsque la matrice est exposée à une longueur d'onde de 266nm (a). Dans les trois spectres, les bandes associées à la forme CCC ont été soustraites. Les lignes pointillées représentent les bandes attribuées à la forme cétone de AcAc (keto). Dans les dépôts, la forme prédominante est la forme énol CCC, mais la forme cétone est déjà présente (quelques %). Durant les premières minutes d'irradiation à 248nm (voir figure II.7 b) les isomères observés également après irradiation à 266 nm sont formés. L'augmentation de bandes correspondant à la forme cétone ne s'observe que plus tardivement, après une irradiation prolongée de la matrice, alors que les isomères créés commencent à disparaître.

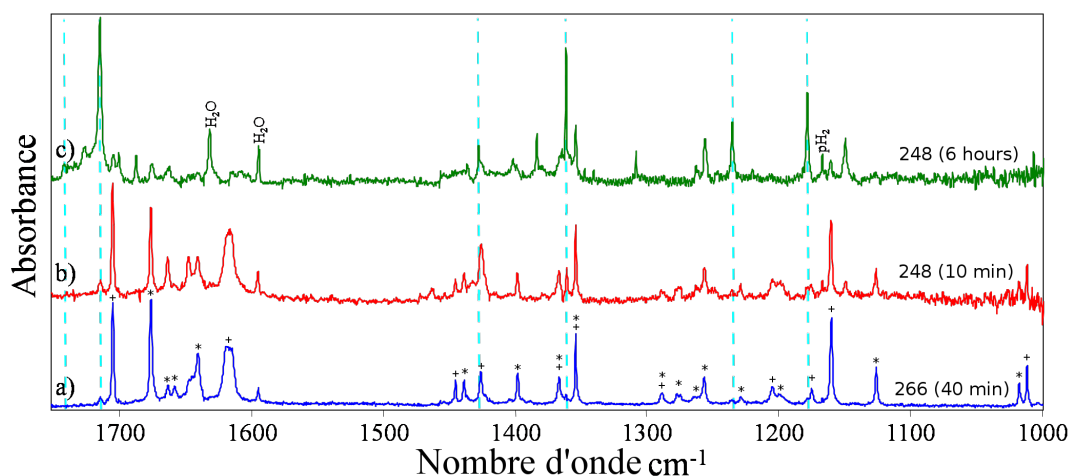


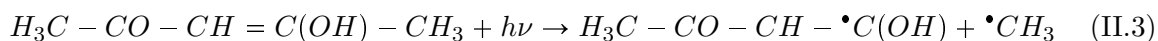
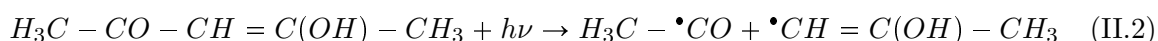
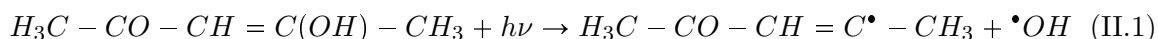
Figure II.7: Comparaison des spectres IR après irradiation de AcAc dans pH_2 (a) après quelques minutes (~ 40 min) à 266nm; (b) après quelques minutes (~ 10 min) à 248nm et (c) après quelques heures (~ 6 heure) à 248 nm. La contribution de la forme CCC a été soustraite dans tous les spectres pour faciliter la comparaison. Les positions des bandes de la forme cétone sont repérées par des lignes pointillées verticales. (+) Désigne le premier groupe d'isomères et (*) désigne le second groupe d'isomères.

RÉSUMÉ EN FRANÇAIS

Lors de cette irradiation prolongée d'autres groupes de bandes apparaissent montrant une photofragmentation de AcAc. Celle-ci a également été observée dans les matrices d'Argon par Nagashima *et al.*,⁵⁸ mais sans identification des photoproduits. Les fragments majeurs observés dans nos expériences sont : CO avec une forte bande structurée dans la région 2125-2150 cm⁻¹,¹³² CH₃ identifié par les modes ν_3 avec un doublet à 3170,6 et 3171,4 cm⁻¹ et ν_4 avec un doublet à 1402,9 et 1401,7 cm⁻¹,^{27,34} CH₄ identifié par le mode ν_3 à 3025,3 cm⁻¹ et ν_4 à 1308,3 cm⁻¹,^{11,27} et H₂O avec le mode ν_2 à 1631,7 cm⁻¹.³³

Afin de comprendre les étapes menant à cette fragmentation, les variations des intensités des spectres de la forme CCC et des produits formés ont été suivies pendant le processus d'irradiation à l'aide spectroscopie FT-IR. Les intensités intégrées des bandes caractéristiques des formes énol chélatée et cétone et des fragments comme CO, ont été tracées en fonction du temps. Aucune constante de réaction n'a été calculée, mais cela nous a permis de donner un schéma qualitatif des étapes observées par irradiation à 248nm.

Sous irradiation à 248 nm, les molécules AcAc isolées dans pH₂ s'isomérisent. La liaison hydrogène intramoléculaire se rompt. Puis, lorsque l'irradiation continue sur les énols ouverts, au moins deux canaux de réactions concurrentes s'ouvrent : La tautomérisation qui correspond au transfert de l'atome d'hydrogène du groupe OH à l'atome de carbone central et la fragmentation de la molécule qui conduit à de plus petites molécules telles que CO, le CH₄ et le radical CH₃. Une irradiation prolongée supprime tous les isomères énols ne laissant que la forme cétone, des fragments et des molécules plus petites. La tautomérisation nécessite donc au moins 2 étapes : Rupture de la liaison hydrogène intramoléculaire permettant une isomérisation de la forme énol, suivie d'une tautomérisation des isomères. La production des fragments suit une cinétique très proche de celle de la forme cétone. On peut noter également que la dynamique de photodissociation de AcAc a été étudiée par Upadhyaya *et al.*²⁰ expérimentalement par fluorescence induite par laser (LIF) et par des techniques "pompe-sonde" à la température ambiante et théoriquement par des calculs *ab initio* d'orbitales moléculaires (OM) pour visualiser les surfaces d'énergie potentielle de l'état fondamental et des états électroniques excités de AcAc. Des mécanismes de fragmentation à partir de l'état triplet T₁ ont été proposés lorsque la molécule est irradiée avec 266nm et 248 nm.



Bien que ces travaux soient menées en phase gazeuse, ils confirment certains de nos résultats.

II.3.3 Irradiation avec une longueur d'onde de 193 nm

Alors que les photons à 266 nm et 248 nm excitent la molécule AcAc vers son état S_2 , une excitation à 193 nm permet d'atteindre l'état S_3 . Il est donc intéressant de regarder l'effet d'un laser ArF émettant à 193 nm (10 mJ/impulsion à 10 Hz) sur AcAc piégée en matrice de pH_2 . Une photochimie différente de celle observée précédemment est attendue.

En effet, le premier effet de l'irradiation à 193 nm de AcAc en matrice de pH_2 est toujours de transformer la forme CCC en d'autres molécules telles que les isomères ouverts de la forme énol, la forme cétone, des radicaux ou des molécules plus petites. Mais à cette longueur d'onde, l'apparition des fragments commence dès les premières minutes d'irradiation avec des traces de CO et de CH_4 . Pour des temps plus longs, les isomères et la forme cétone disparaissent.

Mais lorsque la photoexcitation de la AcAc est réalisée avec une longueur d'onde de 193 nm, la fragmentation se produit à partir de la configuration de l'état fondamental ou d'un état antiliant σ^* et non de l'état triplet T_1 . Cependant, certains mécanismes réactionnels tels que II.1 et II.2 sont confirmés par les expériences.²⁰

En piégeant la molécule de AcAc dans une matrice de pH_2 les mécanismes réactionnels sont évidemment beaucoup plus complexes que ceux proposés par Upadhyaya *et al.*²⁰ car les fragments peuvent réagir les uns avec les autres ou réagir à l'irradiation à 193 nm.

Quelques-uns des fragments trouvés dans le spectre correspondent à des mécanismes réactionnels qui sont basés sur des équations de II.1, II.2 et/ou II.3 et sont appelés "premier produits" tels que propyne ($CH_3-C\equiv CH$), le monoxyde de carbone (CO) et le radical CH_3 . La formation d'autres molécules qui dépendent de processus secondaires telles que la formation de H_2O et CH_4 sont appelés "deuxième produits". Par exemple la formation de CH_4 à partir de la réaction¹⁴⁰ :



suivie de la réaction¹⁴⁰



Des expériences similaires ont été réalisées en utilisant de nD_2 comme matrice. L'apparition des bandes attribuées à CH_3D , CH_2D_2 , CHD_3 et CD_4 confirme la complexité du processus et la possibilité qu'ont certains radicaux de réagir avec les molécules H_2 ou D_2 .

Des mécanisme de réactions successives plus complexes, par exemple la photolyse de l'acétylène ou de propyne, peuvent expliquer la formation des hydrocarbures comme C_2H_2 , C_2H_4 et C_2H_6 .

Les expériences montrent clairement que certains processus comme la production de molécules de C_2H_4 sont plus efficaces que d'autres tels que la production de C_2H_6 par exemple. Le radical HCO est également présent, probablement formé par une réaction de CO avec des atomes d'hydrogène qui sont

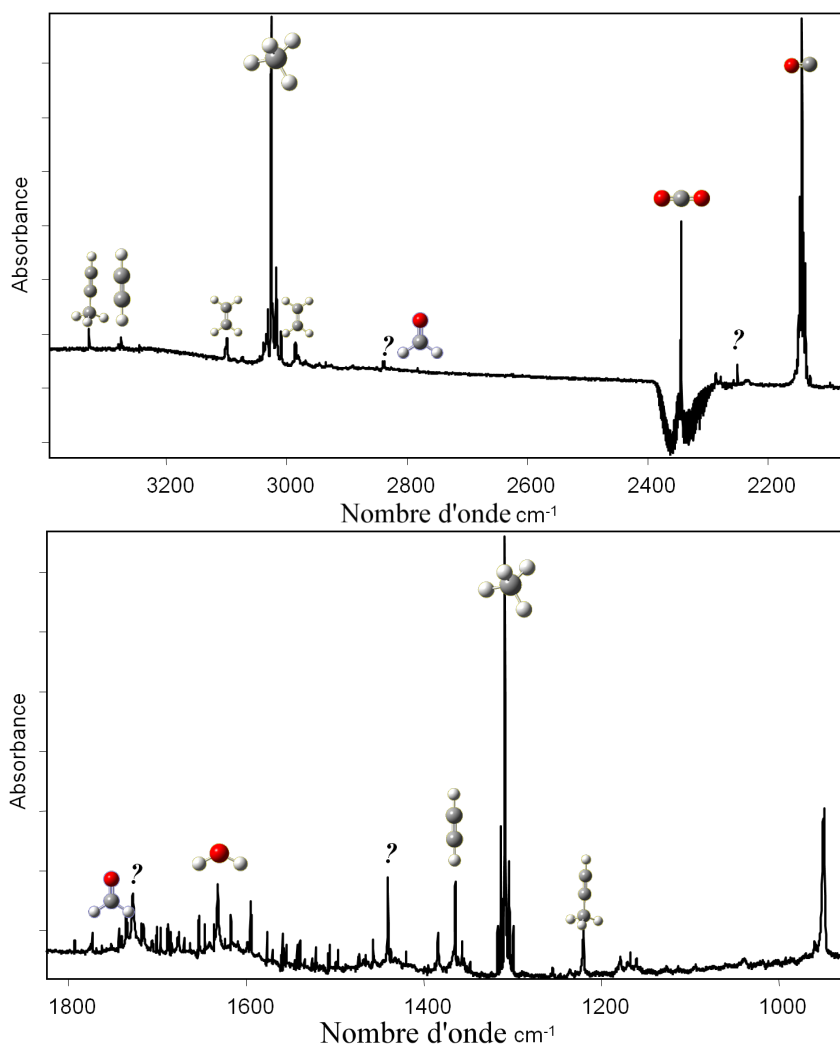


Figure II.8: Spectre infrarouge de la molécule AcAc isolée dans une matrice pH_2 après une très longue période d'irradiation UV à 193 nm. Certaines molécules obtenues par irradiation sont représentées sur la position de leurs bandes les plus intenses. Les (?) sont les bandes encore non attribuées

à leur tour des produits de réaction similaire à II.4 et peuvent diffuser librement à travers la matrice de pH_2 .¹⁴⁶ La réaction de ce radical avec un autre atome d'hydrogène résulte dans la formation de la molécule de formaldéhyde (H_2CO). D'autres radicaux comme CCCO et HCCCO existent aussi dans le spectre d'absorption infrarouge de la matrice après l'irradiation. On voit donc se produire une photochimie très riche à cette longueur d'onde avec des réactions successives entre produits plus ou moins piégés ou migrants dans la matrice de parhydrogène qui peuvent être plus ou moins efficacement excités à 193 nm.

La figure II.8 montre deux régions du spectre infrarouge de la molécule AcAc isolée dans une matrice pH_2 après une très longue période d'irradiation UV à 193 nm. Plus aucune trace de la molécule

AcAc n'est visible. Certaines molécules obtenues par irradiation sont représentées sur la position de leurs bandes les plus intenses : l'eau (H_2O), le monoxyde de carbone (CO), le formaldéhyde CH_2O , le méthane (CH_4), l'acétylène (C_2H_2), l'éthylène (C_2H_4) et le propyne ($\text{CH}_3\text{-C}=\text{CH}$). Les (?) sont les bandes encore non attribuées.

Conclusions

La structure, la photochimie, la dynamique et la photodynamique de la molécule d'acétylacétone (AcAc) isolée dans des matrices d'hydrogène ont été étudiées par spectroscopie d'absorption infrarouge. Deux tautomères de AcAc (formes cétone et énol chélaté) coexistent à basse température dans les matrices d'hydrogène et de deutérium. Le rapport des populations cétone/énol R_{ke} est significativement plus élevé dans les matrices de pH_2 ($\sim 4,5\%$) par rapport aux autres solides étudiés. Il semble que le rapport R_{ke} de la phase gazeuse soit mieux préservé dans cette matrice à cause des propriétés spécifiques de ce solide quantique.

Le spectre infrarouge (IR) de AcAc dans le pH_2 solide montre après dépôt que la plupart des bandes d'absorption de la forme énol chélaté sont très larges, avec des largeurs similaires à celles de la molécule isolée dans les matrices de gaz noble ou d'azote. L'élargissement des bandes est dû à la forte liaison hydrogène intramoléculaire qui existe dans cette forme énol.

Les calculs théoriques de la forme énol chélaté de AcAc suivant deux symétries (C_{2v} et C_s) ont été comparés avec le spectre IR des molécules isolées en matrice de pH_2 et les résultats confirment la symétrie C_s . Le spectre est analysé à l'aide des calculs anharmoniques de fréquences des différents modes de vibration et l'accord théorie-expérience est excellent. Les calculs anharmoniques montrent également la grande influence de la liaison hydrogène intramoléculaire sur certains modes de vibration.

La photochimie des isomères de la forme énol chélaté de AcAc a également été étudiée. AcAc a été excitée dans l'état S_2 en utilisant deux longueurs d'onde différentes : 266nm et 248nm. L'utilisation de 266nm conduit principalement à l'isomérisation de AcAc vers des conformères non chélatés de la forme énol. L'identification des photoproduits a été effectuée en comparant les spectres IR expérimentaux aux calculs théoriques de fréquences IR des différents isomères, dans l'approximation harmonique ainsi qu'en incluant les corrections anharmoniques. Le spectre des isomères "ouverts" (formes énol sans liaisons hydrogène intramoléculaires) montre des bandes beaucoup plus fines que celles de la forme énol chélaté.

Le caractère peu perturbateur de la molécule de pH_2 dans le solide a permis de trouver un nouvel isomère (TTC) dans le spectre IR, après irradiation UV de l'échantillon. Dans d'autres matrices telles que nH_2 et nD_2 , les mêmes isomères que ceux détectés dans la matrice de pH_2 sont formés (CTC, TTC et TCC), mais un autre isomère, TCT, est également observé. Ce résultat suggère que la transformation

RÉSUMÉ EN FRANÇAIS

de TCT→TCC peut avoir lieu par effet tunnel dans les matrices de pH₂, alors que TCT est bloqué dans les matrices plus interactives comme nH₂ solide. Le blocage de tels processus tunnel en présence de nH₂, contrairement à pH₂, pourrait être un effet général.

La fragmentation de la molécule de AcAc piégée dans des matrices de pH₂ sous irradiation à 266nm est inefficace. Ni le radical OH, ni d'autres produits correspondant à la rupture d'une liaison simple n'ont été détectés dans le spectre IR. Cela permet de conclure que l'isomérisation en matrice de la forme énol chélaté vers les formes énols ouverts ne provient pas de processus de dissociation/recombinaison. En revanche, une petite quantité de monoxyde de carbone a été observée. La formation de cette molécule nécessite une réorganisation drastique des liaisons de la molécule et elle n'apparaît qu'après une longue période d'irradiation. Par ailleurs, une excitation à 248nm conduit à la formation des mêmes formes énols ouverts que l'excitation à 266nm. Mais une irradiation prolongée à cette longueur d'onde (248 nm) fait disparaître ces formes énols et accroît l'intensité des bandes IR de la forme cétone de AcAc. La fragmentation dans ce cas devient un processus plus important. Le taux de croissance des bandes attribuées au CO est très similaire à celui de la forme cétone, ce qui suggère que cette forme cétone pourrait être formée par des processus de dissociation/recombinaison, même dans pH₂.

La longueur d'onde de 193nm excite la molécule de AcAc dans l'état électronique S₃. Lors de l'irradiation de l'échantillon à cette longueur d'onde, tous les isomères de forme énol ouvert et la forme cétone sont formés, mais ils sont également détruits dans des réactions « secondaires ». Contrairement aux résultats en phase gazeuse, le radical OH n'est pas détecté dans la matrice. Cependant, l'intensité des bandes attribuées à la molécule de H₂O a augmenté lors de l'irradiation de l'échantillon. Ces expériences mettent en évidence la possibilité de réaction entre le radical et la molécule de H₂ de la matrice pour former d'autres radicaux ou espèces stables. Afin de confirmer ces réactions avec des molécules H₂, des expériences ont été effectuées dans nD₂ solide. La présence de molécules stables deutérées telles que CH₂D₂, confirme l'existence de réactions avec la molécule hôte.

Le dispositif expérimental utilisé pour ces expériences ne permet pas de maintenir longtemps l'échantillon à étudier. D'autres expériences doivent être menées en vue d'atteindre l'état stationnaire dans le processus d'irradiation. Cela permettrait de mieux comprendre les mécanismes de réaction et de séparer les produits finaux des produits intermédiaires. D'autre part, certaines réactions sont dues à l'arrivée d'un deuxième photon. Un exemple est la réaction des radicaux CH₃ avec la molécule de H₂. Certaines expériences doivent être effectuées à l'aide d'un laser de puissance plus faible pour une meilleure compréhension des processus.

Le très faible effet de cage des matrices de pH₂ a permis d'isoler des radicaux tels que CH₃, HCO, HCCO après irradiation *in situ* de AcAc à 248nm et 193nm. D'autres molécules stables ont été détectées après irradiation, mettant en évidence la réactivité de ces radicaux avec les molécules H₂ de

la matrice. La structure du spectre de rotation de la molécule de CH_4 est une preuve de la présence des réactions photo-induites dans la matrice telles que la réaction de CH_3 avec H_2 .

Les matrices de pH_2 préservent les propriétés dynamiques intrinsèques des molécules solutées telles que les mouvements de grande amplitude. Il y en a trois dans la forme énol de AcAc : Le transfert de proton et les deux rotations gênées ou torsion des méthyles non équivalentes. Dans pH_2 , les spectres révèlent une interaction entre ces mouvements. Considérant les orientations des spins des atomes d'hydrogène des groupes méthyle, plusieurs conformères de spin de la forme CCC de AcAc coexistent. Pour des raisons de symétrie, ces états de spins sont associés à des états de torsion différents, dont le fondamental. La conversion de spin nucléaire est très lente et est observable. Elle est mise à profit pour séparer les bandes IR provenant de ces différents niveaux de torsion. La comparaison de ces spectres renseigne sur les couplages entre ces torsions et les autres vibrations. L'analyse des données expérimentales montre que le transfert de proton est favorisé par l'excitation de la torsion du groupe le plus libre (celui présentant la plus faible barrière à la rotation interne). Le présent travail est une étude modèle qui montre que la conversion des spins nucléaires peut être un outil d'aide à la spectroscopie pour les molécules comportant des groupes méthyle, ce qui est fréquent pour les molécules organiques. Il permet d'étudier des processus concertés faisant intervenir la torsion de ces méthyles. La matrice de pH_2 est le milieu adapté pour observer ces phénomènes car il préserve cette torsion. Les données des spectres infrarouge et les propriétés intrinsèques de la molécule offrent des informations quantitatives, mais des approches théoriques complémentaires seront nécessaires pour traiter le problème du transfert de proton. D'autres calculs théoriques sur la molécule de AcAc entourée par des molécules de pH_2 pourraient également permettre une meilleure compréhension des processus qui ont été décrits. Des simulations de processus dynamiques pourraient fournir plus d'informations sur les états intermédiaires de l'isomérisation de la forme énol chélaté de AcAc vers les formes énols ouverts ou cétone ou sur la fragmentation lorsque la molécule est excitée à l'état S_2 ou S_3 . La question de savoir si la formation des formes énols ouverts dans le procédé d'isomérisation vient d'un processus de dissociation /recombinaison ou de rotations/ déformations autour des liaisons moléculaires reste ouverte. D'un point de vue expérimental, les avantages des solides de pH_2 exposés dans cet travail, peut être utile dans d'autres domaines comme l'astrophysique. Les réactions chimiques des molécules ou radicaux avec la molécule de pH_2 qui peuvent se produire dans l'espace interstellaire peuvent être contrôlées et étudiées dans ces systèmes cryogéniques.